Optimisation des formulations EOR (Enhanced Oil Recovery) chimique pour les réservoirs pétroliers fissurés.

Mohammed Abdelfetah Ghriga

Université M'Hamed Bougara de Boumerdes
Faculté des Hydrocarbures et de la Chimie

Université de Pau et des Pays de l'Adour
Ecole Doctorale des Sciences Exactes
et leurs Applications (ED211)

THÉSE

En cotutelle

Pour obtenir le grade de

Docteur de l'Université de Pau et des Pays de l'Adour

Domaine : Physique

Spécialité : Physico-chimie des Matériaux

Et de

Docteur de l'Université M'Hamed Bougara de Boumerdes

Domaine : Hydrocarbures

Spécialité : Génie Pétrolier et Gazier

Présentée et soutenue publiquement le 30/06/2020 par :

Mohammed Abdelfetah GHRIGA

Optimisation des formulations EOR (Enhanced Oil Recovery) chimique pour les réservoirs pétroliers fissurés

---

Jury

M. DAOUD Kamel	Professeur	USTHB Algerie	Président
M. ZERAIBI Noureddine	Professeur	UMBB Algerie	Examinateur
M. SALHI Yacine	Professeur	USTHB Algerie	Examinateur
M. JADA Amane	HDR	CNRS-UHA France	Rapporteur
M. GIGAULT Julien	HDR	CNRS-UR1 France	Rapporteur
M. GARECHE Mourad	MCA	UMBB Algerie	Directeur de thèse
M. GRASSL Bruno	Professeur	UPPA France	Directeur de thèse

Année Universitaire : 2019/2020

This work is dedicated with pride & love to my dearest parents, grandparents, brothers & sisters...

Acknowledgement

This thesis was performed within the international doctoral co-supervision program (Cotutelle de these) between the University of Pau and the Adour countries (UPPA) in France and the University M'Hamed Bougara of Boumerdes (UMBB) in Algeria, with the financial support of Campus France through the PROFAS B+ scholarship. The work was established in the facilities of the Institute of Analytical Sciences and Physico-Chemistry for the Environment and Materials (IPREM) in France and the Laboratory of Hydrocarbons Physical Engineering (LGPH) in Algeria.

First and foremost, I would like to express my deepest gratitude to my supervisor Pr. Bruno Grassl, for his excellent guidance, support and motivation. Professor Bruno Grassl gave me a lifetime chance to work in one of the most prestigious laboratories in France and provided me with the best conditions to succeed my research. I had the privilege to learn from him, lessons in life and science. Equally, I would like to thank Dr. Mourad Gareche for accepting to co-supervise my thesis with the best scientific contributions and administrative guidance I could ever have.

I am very grateful to Pr Kamel Daoud, the president of the jury and the members of the jury Pr Noureddine Zeraibi, Pr Yacine Salhi, Dr Amane Jada, Dr Julien Gigault who showed their interest in my thesis and accepted to judge and evaluate this manuscript and contribute in its perfection.

My sincere thanks to those, without whom this work would not have been achieved: Pr. Stephanie Reynaud for facilitating my entry to the laboratory and being a part of my PhD committees. Dr. Abdelouahed Khoukh for his unconditional assistance and help in the NMR experiments, Dr. Nathalie Andreu for training me on the capillary viscosimeter. Mr. Anthony Laffore for giving me the necessary initiations in the various techniques of rheology, TGA and DSC. Mrs. Virginie Pellerin for helping me with the SEM and AFM techniques. I would like also to thank Pr Ahmed Hadjadj for his presence and endless help in the most critical moments, Pr Daniel Broseta for participating in my PhD committees, Pr Corinne Nardin for giving me a chance to work with her in my first (mini) Post Doc experience. Many thanks also to Pr. Mohamed Amara for facilitating my arrival to France. To those who I considered as my examples and mentors Dr. Wissem Khelifi and Dr. Hind El Hadri, thank you for the fruitful discussions, inspiration and encouragement.

I will always remember my friends and colleagues in France and Algeria, who assisted me and stood by my side during this long and stressful journey. I would especially thank the ones who worked closely with me: Dr. Islam Lebouachera, Dr. Hocine Ouaer, Dr. Amine Ben seghier, Dr. Menad Nait Amar, Dr. Nadjib Drouiche, and the ones who shared this adventure with me: Ahmed Sialiti, Fatima Sherry, Emna Nasr, Ghaya Elchoubassi, Hisham Driss, Maryam Zaiter, Izabela strzeminska and all the others. It is difficult to list all the names here, however, I will be always thankful for the good souls that helped me and believed in me.

Most importantly, I would like to thank my beloved parents, my brothers Dr. Ziane and Akram, my sisters Kawther, Salsabil, Hidaya, and my grandparents Ziane, Smicha, Aicha, for their endless support. A special thanks to my cousins Mohamed, Zineb & Karima and to all my uncles, aunts and the families of Ghriga and Ouled Abdallah.

Fetah GHRIGA

Abstract

Naturally fractured reservoirs occupy the first places in the world's reserves and form a very special class of hydrocarbons reservoirs. Their study is very specific and complex due to the secondary porosity and permeability of the fractures network. Fluids flow essentially through the fracture network while the large amount of oil is stored in the rock matrix, making the oil production from these reservoirs a great challenge for petroleum engineers. During secondary or tertiary recovery in severely fractured reservoirs, the injection of low viscosity fluids, such as gas or water, leads usually to the early breakthrough of these fluids (fluid channeling) into the production wells causing thereby a poor microscopic and macroscopic oil recovery efficiency. The main challenge in chemical enhanced oil recovery (cEOR) operations in fractured reservoirs is to prevent this fluid channeling phenomenon, so that the injected fluids can enter, get in touch and move the oil trapped in the matrix. These operations are known as conformance control and an improved conformance in a fractured reservoir can be achieved by reducing the fractures permeability through gel systems, foam systems or the microbial growth. The purpose of this thesis is to study the thermal gelation of a polymer gel system formed by partially hydrolyzed polyacrylamides (PHPAs) and polyethylenimines (PEIs). The gelation time, gel strength and gel thermal stability, of well characterized reactants, are investigated as function of the main physico-chemical parameters. The response surface methodology (RSM) is employed to develop a mathematical model that allows the prediction of the gelation time of PHPA/PEI systems in the temperature range between 70 to 90 °C. The crosslinking mechanisms of PHPA and PEI are then investigated and quantified using advanced techniques.

Keywords: Partially hydrolyzed polyacrylamide, polyethylenimine, thermal gelation, gelation time, response surface methodology, crosslinking mechanisms.

Résumé

Les réservoirs fracturés naturellement occupent la première place dans les réserves mondiales et forment une classe très particulière des réservoirs d'hydrocarbures. Leur étude est très spécifique et complexe à cause de l'existence de la porosité et de la perméabilité secondaires caractéristiques des réseaux de fractures. Les fluides s'écoulent essentiellement à travers un réseau de fractures tandis que la grande quantité de pétrole est emmagasinée par la matrice rocheuse, ce qui rend la production de pétrole à partir de ces réservoirs difficile et un grand défi pour les ingénieurs pétroliers. Lors de la récupération secondaire ou tertiaire dans les réservoirs fortement fracturés, l'injection des fluides de faible viscosité, tels que le gaz ou l'eau, conduit généralement à des percées précoces de fluides (canalisation de fluide ou channeling) dans les puits de production, entraînant ainsi une mauvaise efficacité, à l'échelle microscopique et macroscopique, de la récupération de pétrole. Le challenge pour les opérations de la récupération chimique améliorée du pétrole (cEOR) dans les réservoirs fracturés, c'est d'empêcher ce phénomène de canalisation des fluides « channeling », afin que les fluides injectés puissent entrer, se mettre en contact et déplacer l'huile piégée dans la matrice. Ces opérations sont connues sous le nom de « contrôle de conformance ». Dans un réservoir fracturé, la conformance peut être améliorée en réduisant la perméabilité secondaire des fractures par l'utilisation des systèmes de gels, de la mousse ou de la croissance microbienne. L'objectif de cette thèse est d'étudier la gélification d'un système de gel polymère formé par les polyacrylamides partiellement hydrolysés (PAPHs) et les polyethylenimines (PEIs). Pour des réactifs bien caractérisés, le temps de gélification, la force du gel et la stabilité thermique du gel sont étudiés en fonction des principaux paramètres physico-chimiques du système (PAPH/PEI). La méthode des surfaces de réponses (MSR) est utilisée pour développer un modèle mathématique qui permet la prédiction du temps de gélification des systèmes (PAPH/PEI) dans l'intervalle de températures compris entre 70 et 90 °C. Les mécanismes de réticulation, du PHPA avec de la PEI, sont ensuite étudiés et quantifiés à l'aide des techniques avancées.

Mots clés: polyacrylamide partiellement hydrolysé, polyethylenimine, gélification thermique, temps de gélification, La méthode des surfaces de réponses, mécanismes de réticulation.

ملخص

تحتل الخزانات المتصدعة طبيعيا المراكز الأولى في احتياطيات العالم وتشكل فئة خاصة جدًا من الخزانات الهيدروكربونية. تعتبر دراسة هذه الخزانات خاصة ومعقدة للغاية بسبب المسامية والنفاذية الثانويتين لشبكة الكسور. تتدفق السوائل بشكل أساسي عبر شبكة الكسور بينما الكمية الكبيرة من النفط تكون مخزنة في المصفوفة الصخرية، مما يجعل إنتاج النفط من هذه الخزانات تحديا كبيرا لمهندسي البترول. أثناء الاستخراج الثانوي أو العالي في الخزانات المتصدعة بشدة، عادةً ما يؤدي حقن السوائل المنخفضة اللزوجة، مثل الغاز أو الماء، إلى الاختراق المبكر لهذه السوائل لآبار الإنتاج مما يؤدي إلى ضعف مردودية استرجاع النفط المجهرية والعيانية. يتمثل التحدي الرئيسي، أثناء العمليات الكيميائية للاستخلاص المعزز للنفط في الخزانات المتصدعة، في منع ظاهرة الاختراق المبكر بحيث تتمكن السوائل المحقونة من الدخول، الاتصال وتحريك النفط المحتجز في المصفوفة. تُعرف هذه العمليات باسم التحكم في التوافق، ويمكن تحسين التوافق في خزان متصدع عن طريق تقليل نفاذية الكسور من خلال المواد الهلامية (الجل)، الرغوة أو التكاثر الميكروبي. هدف هذه الأطروحة هو دراسة التشكل الحراري لمادة هلامية (جل بقاعدة البوليمرات) المتشكلة من البولي-أكريلاميد المهدرج جزئياً والبولي-يثيلين-أمين. يتم فحص وقت التشكل، وقوة الجل، والثبات الحراري للجل، للمتفاعلات الموصوفة جيدا، اعتمادا على العوامل الفيزوكيميائية الرئيسية. تُستخدم منهجية أسطح الاستجابة لتطوير نموذج رياضي يسمح بالتنبؤ بوقت تشكل جيل أنظمة البولي-أكريلاميد المهدرج جزئياً والبولي-يثيلين-أمين في نطاق درجات الحرارة بين 70 إلى 90 درجة مئوية. يتم الفحص والتحديد الكمي لآليات التشابك بين البولي-أكريلاميد المهدرج جزئياً والبولي-يثيلين-أمين باستخدام التقنيات المتقدمة.

الكلمات المفتاحية: البولي-أكريلاميد المهدرج جزئياً، البولي-يثيلين-أمين، التشكل الحراري، وقت تشكل جيل، منهجية أسطح الاستجابة، آليات التشابك.

Table of contents

List of figures

List of tables

Nomenclature, Symbols and Abbreviations

NFRs: Naturally Fractured reservoirs.
WOC: Water-Oil Contact.
GOC: Gas-Oil Contact.
PVT: Pressure Volume Temperature.
GOR: Gas Oil Ratio.
EOR: Enhanced Oil Recovery.
IFT: Interfacial Tension.
PV: Pore Volume.
CDGs: Colloidal Dispersion Gels.
PPGs: Performed Particle Gels.
AM: Acrylamide.
PAM: Polyacrylamide.
PAA: Polyacrylate.
PHPA: Partially Hydrolyzed Polyacrylamide.
PAtBA: Polyacrylamide/tert-Butyl Acrylate.
HAP: Hydrophobically Associating Polymer.
HEC: Hydroxyethyl Cellulose.
AMPSA: Acrylamido-2-Methylpropane Sulfonic Acid.
N, N-DMA: N, N-Dimethyl Acrylamide.
NVP: N-Vinylpyrrolidone.
N-DDAM: N-dodecyl acrylamide.
PEI: Polyethylenimine.
HQ: Hydroquinone.
HMTA: Hexamethylenetetramine.
SAAP: Sodium Acid pyrophosphate.
CitAc: Citric Acid.
PEEK: Polyether Ether Ketone.
HD: Hydrolysis Degree (%).
Y: Molar concentration of the carboxylate groups (mol/l).
X: Molar concentration of the amide groups (mol/l).
BD: Branching Degree (%).
D: Dendritic units (%).
L: Secondary amine linear units (%).
PF: Polymer Flooding.
ASP: Alkaline-Surfactant-Polymer.
LCM: Loss Circulation Material.
PECs: Polyelectrolyte Complexes.
DS: Dextran Sulfate.
d-PEI: derivatized-PEI.
EA: Ethanolamine.
DEA: Diethanolamine.
TEA: Triethanolamine.
EDA: Ethylenediamine.
DETA: Diethylenetriamine.
TETA: Triethylenetetramine.
TEPA: Tetraethylenepentaamine.
Rsm: Rigid setting materials.
CFA: Coal Fly Ash.
bbls: Barrels.
BOPD: Barrel of Oil Per Day.

BWPD: Barrel of Water Per Day.
MMSCFD: Million Standard Cubic Feet per Day.
IGT: Initial Gelation Time.
FGT: Final Gelation Time.
NMR: Nuclear Magnetic Resonance.
DSC: Differential Scanning Calorimetry.
TGA: Thermogravimetric Analysis.
DLS: Dynamic Light Scattering.
PLT: Production Logging Tool.
$\bar{M}_v$: viscosity-average molecular weight (g/mol).
M_w: Molecular weight (g/mol).
[η]: Intrinsic viscosity (ml/g).
K: Mark Houwink equation constant (ml/g).
α: Mark Houwink equation constant (dimensionless).
η_R: Reduced viscosity (ml/g).
η_I: Inherent viscosity (ml/g).
η: Solution's shear viscosity (cP).
η_s: Solvent's shear viscosity (cP).
η_r: Relative viscosity.
η_{r_i}: Relative viscosity of a dilute solution "i".
η_{sp0}: zero-shear specific viscosity (cP).
η_0: zero-shear viscosity (cP).
η_∞: Infinite-shear viscosity (cP).
C: Polymer concentration (ppm or g/ml).
C×[η]: overlap parameter.
L: Length (m).
R: Radius (m).
Q: Flow rate (m^3/s or μl/s)
$\dot{\gamma}$: Shear rate (s^{-1}).
ΔP: Pressure drop (Pa or mbar).
λ: Time constant (s^{-1}).
m: cross model exponent (dimensionless)
G': Storage modulus (Pa).
G": Loss modulus (Pa).
TDS: Total Dissolved Solids (g/l).
TFT: Tin Fouyé Tabankort.
HMD: Hassi Messaoud.
REB: Rhourde El Baguel.
V_h: Hydrodynamic volume.
R_g: Radius of gyration.
t_g: Gelation time (minutes).
M: Frequency factor (minutes).
E_a: Activation Energy (kJ/mol).
R: Universal gas constant (kJ/mol.K).
T: Absolute Temperature (K).
OVAT: One Variable At Time.
RSM: Response Surface Methodology.
ANOVA: Analysis Of Variance.
DoE: Design of Experiments.
ζ_i: Independent Variables.
y: the response.
f: the unknown response function.
ε: the statistical error.

σ^2: variance.
x_i: Dimensionless Coded Variables.
β_i: Regression coefficients.
b: the vector of least squares estimators.
L: the sum of square errors.
CCD: Central Composite Designs.
CCC: Central Composite Circumscribed.
CCF: Central Composite Faced.
CCI: Central Composite Inscribed.
BBD: Box-Behnken Designs.
PBD: Plackett-Burman Design.
CMC: Carboxymethyl Cellulose.
F_{ij}: the experimental value of the factor "i" at the level "j".
X_{ij}: the value of the coded variable "i" at the level "j".
$\bar{F}_i$: the value of the factor "i" in the center of the experimental domain.
ΔF_i: the variation range of the factor "i".
θ_i: the coded value limit for each factor.
SS: Sum of Squares.
Df: Degree of freedom.
MS: Mean Square.
y_i: the experimental value of the run ''i''.
$\hat{y}_i$: the predicted value of the run ''i''.
$\bar{y}$: the overall mean of experimental values.
$\bar{y}_i$: the mean of experimental values of replicates.
n: the number of experimental runs (observations).
n_r: the number of experimental replicates.
p: the number of terms in the model.
SS_{term}: Sum of Squares of the term.
MS_{term}: Mean Square of the term.
R^2: Coefficient of determination.
R^2_{adj}: Adjusted coefficient of determination.
RMSE: Root Mean Square Error.
$d(\hat{Y}_i)$: Desirability Function.
BBFO: Broad Band Fluorine Observe.
DOSY: Diffusion Ordered SpectroscopY.
NOESY: Nuclear Overhauser Enhancement SpectroscopY.
$[R]_0$: Reactant concentration at t=0.
[R]: Reactant concentration at a given time t.
[P]: Product concentration at a given time t.
K: is the apparent reaction rate constant.
D_i: Diffusion Coefficient.

Introduction Générale

Introduction Générale

Avec l'explosion démographique et la croissance économique des grands pays émergents (Chine, Inde, Brésil et autres) sans précédentes, les besoins mondiaux en énergie ne cessent de croître depuis le début du siècle contre des exigences et des restrictions écologiques de plus en plus strictes. Dans ce contexte, de grands efforts ont été déployés pour substituer les énergies fossiles non renouvelables par d'autres sources d'énergie renouvelables et respectueuses de l'environnement, en dépit de tout cela, le pétrole reste toujours la source d'énergie la plus utilisée et la plus demandée de nos jours. Par conséquent, les compagnies pétrolières se trouvent face à un défi majeur pour maintenir et/ou augmenter la production des grands champs pétroliers matures au regard du déclin constant du nombre de nouvelles découvertes et les coûts extravagants de l'extraction des réserves non-conventionnelles.

Dans les réservoirs conventionnels, la récupération du pétrole se fait généralement en trois étapes : primaire, secondaire et tertiaire. Durant la récupération primaire, le pétrole est acheminé vers les puits producteurs à travers les forces motrices présentes naturellement dans le réservoir telles que, l'expansion des aquifères actifs et des chapeaux de gaz, l'expansion du gaz dissout, l'expansion de l'huile et de la roche réservoir ainsi que l'effet de la gravité. La récupération secondaire consiste à injecter de l'eau ou bien du gaz, dans l'aquifère ou le chapeau de gaz respectivement, pour maintenir la pression du réservoir et balayer le pétrole vers les puits producteurs. Après ces deux étapes de production, le réservoir atteint sa limite de production économique et il est considéré comme étant un réservoir « mature », si bien que le plus souvent, deux tiers du pétrole restent toujours piégés dans le réservoir.

Selon les pétroliers, l'extraction de la moitié du pétrole piégé dans les champs matures permettra de doubler les réservés mondiales exploitables. C'est dans ce contexte, que de nouvelles techniques de récupération assistée du pétrole, communément appelées en anglais « Enhanced Oil Recovery (EOR) » ont été mises en œuvre et largement développées depuis les années 1960. Tout particulièrement, les méthodes chimiques de la récupération assistée du pétrole (cEOR) consistent à réduire la tension interfaciale et les forces capillaires entre les fluides d'injection et les fluides du réservoir, et/ou l'augmentation de la viscosité du fluide déplaçant.

Dans les réservoirs fracturés naturellement, les fluides circulent essentiellement à travers un réseau de fractures. Pour l'ingénieur pétrolier, la production du pétrole se trouve dans un paradoxe relativement au double comportement observé dans les réservoirs fracturés par rapport aux réservoirs non fracturés. En effet, les fractures ouvertes jouent un rôle très important durant la récupération primaire mais peuvent poser des contraintes lors des récupérations secondaire et tertiaire. Nous pouvons citer le phénomène de channeling (canalisation de fluide) comme problème typique

rencontré lors de l'exploitation des réservoirs fracturés. Les percées précoces des fluides d'injection dans les puits producteurs entraînent de mauvaises efficacités de balayage à l'échelle microscopique et macroscopique. Le principal défi au cours des opérations EOR dans ce type de réservoirs est d'empêcher le channeling, de sorte que les fluides injectés durant la phase secondaire ou tertiaire, peuvent entrer, se mettre en contact et déplacer le pétrole piégé dans la matrice rocheuse. La réduction de la perméabilité des fractures en faveur de la matrice rocheuse est connue sous le nom « contrôle de conformance ». Dans ce contexte, l'application des systèmes de gels retardés demeure l'une des stratégies les plus efficaces.

En Algérie et après plus d'un demi-siècle d'exploitation, les grands champs pétroliers se rapprochent de plus en plus de leurs limites de productions. Cependant, les projets EOR chimique n'ont vu le jour que depuis un quinquennat et demeurent toujours en phase de recherche. C'est dans ce contexte actuel que s'inscrit cette thèse qui constitue une contribution à l'étude et à l'application de l'EOR dans les champs pétroliers algériens et tout particulièrement, l'utilisation des systèmes de gels retardés pour éventuellement les opérations de contrôle de conformance dans les réservoirs fracturés comme ceux de Tin Fouyé Tabankort (TFT), Hassi Messaoud (HMD), Rhourde El Baguel (REB)… etc. Cette étude repose sur deux critères essentiels en se basant d'une part, sur les aspects écologiques et économiques et d'autre part, sur l'aspect technique en termes d'avantages que peuvent apporter les gels formulés à partir du polyacrylamide partiellement hydrolysé et de la polyethylenimine lors de l'exploitation des réservoirs fracturés naturellement qui feront l'objet de discussion dans ce manuscrit.

Pour atteindre cet objectif, cette étude est répartie en cinq chapitres.

Le premier chapitre expose l'état de l'art actuel des grands axes faisant l'objet de cette étude réparti en trois points principaux. Il présente en premier lieu, une définition des réservoirs fracturés naturellement, leurs classifications, caractéristiques et mécanismes de récupération. En second lieu, un point sur les méthodes chimiques de la récupération tertiaire. Troisièmement, une synthèse bibliographique concernant les méthodes de caractérisation et les différents types de gels, et tout particulièrement les gels à base du polyacrylamide partiellement hydrolysé et de la polyethylenimine.

Le second chapitre est consacré à la caractérisation des matériaux et les réactifs utilisés dans cette étude en termes de masse moléculaire apparente, degré d'hydrolyse ou de branchement, température de dégradation, les concentrations de recouvrement et le comportement viscoélastique des polyacrylamides partiellement hydrolysés.

Le troisième chapitre traite la thermo-gélification des systèmes de gels à base du polyacrylamide partiellement hydrolysé et de la polyethylenimine en termes de stabilité thermique, morphologie, relations structure-propriété et comportement viscoélastique.

Le quatrième chapitre consiste à élaborer un modèle mathématique décrivant le temps de gélification en fonction des principaux paramètres physico-chimiques en utilisant la méthode des surfaces de réponses (MSR).

Le dernier chapitre aborde d'une part, l'influence du degré d'hydrolyse et du pH sur le temps de gélification. Et d'autre part, l'étude des mécanismes de réticulation entre le polyacrylamide partiellement hydrolysé et la polyethylenimine. Par ailleurs, des techniques de la résonance magnétique nucléaire classiques 1D (Proton « ^{1}H » et carbon « ^{13}C ») et avancées 2D (DOSY et NOESY), ont été utilisées pour suivre les variations chimiques sur les réactifs et quantifier la cinétique de gélification.

Enfin, ce manuscrit s'achève avec une conclusion générale où sont regroupés les résultats essentiels de cette thèse ainsi que les recommandations et les perspectives de ce travail.

Chapter I:
State of Art

1. Chapter I: State of art

1.1 Naturally Fractured Reservoirs

1.1.1 Definition

Naturally Fractured reservoirs (NFRs) are geological formations with two distinct types of porous media: a rock matrix and a fracture network, which give the reservoir a dual porosity and permeability characteristics. Formed in many depositional environments including carbonates, shales and sandstones, naturally fractured reservoirs represent more than 50 % of hydrocarbons reservoirs and contribute in a large extent to the worldwide production of oil and gas [1]. Although, the majority of the hydrocarbon reservoirs are fractured to some extent, their fractures have an ignored effect on the fluid flow and storage. In the case of naturally fractured reservoirs, the fracture network has a significant impact on fluid storage and its conductivity, the reservoir performance and oil recovery [2]. The fractures may appear in a single or multiple rock formations, due to the mechanical failures of the rock under natural geological stresses such as tectonic movements, lithostatic (overburden) pressure changes, thermal stresses, high fluid pressures, drilling activities, and even fluid extraction [3]. These fractures can have dimensions of several micrometers (micro-fissures) to several thousand kilometers (continental fractures). Neglecting or failing to determine the distribution, the orientation, the interconnectivity and the degree of mineral cementation of these fractures [4, 5], can have serious consequences on the development and production from the reservoir such as designing inappropriate wells patterns or drilling unnecessary in-fill wells. Performing a proper characterization of a naturally fractured reservoir was always a challenging task especially during the earliest stages of the reservoir history. While, the complex role of the fractures during the primary and secondary recovery phases makes the naturally fractured reservoirs a production paradox [6].

1.1.2 Classifications

The naturally fractured reservoirs can be classified based on the contributions of the porosities and permeabilities of both the fracture network and the rock matrix into the overall reservoir production. Nelson [7] introduced the most general typology considered nowadays, which classify the naturally fractured reservoirs to four types as shown in **Figure 1.1** and explained below:

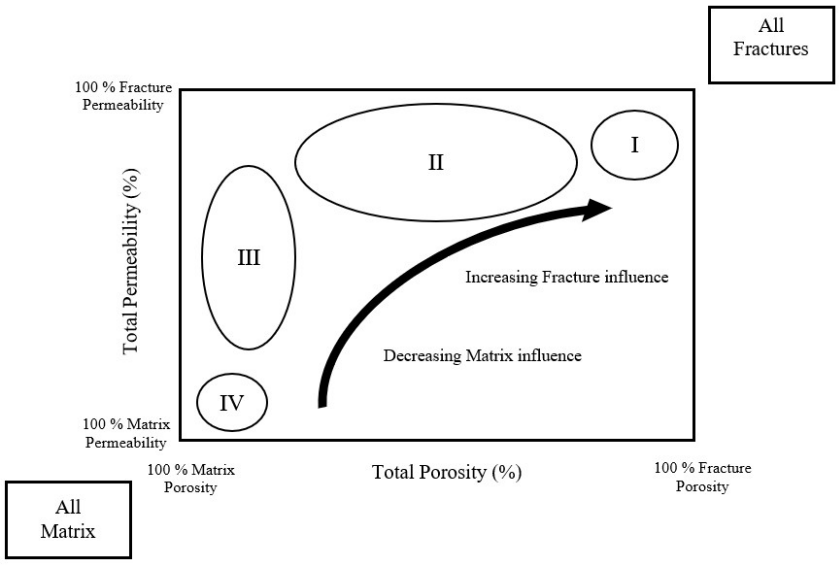

Figure 1.1 : Naturally fractured reservoirs classification system. [7]

Type I: Fractures provide the essential reservoir porosity and permeability while the matrix has little porosity and permeability. In this case, the hydrocarbons are stored in the fracture network and the fluids flows are controlled also by this network. The reserves in this reservoir type are rather low, and the development of such reservoir requires only the drilling of few wells. The latter are likely to produce at high initial rates due to the larger drainage area per well. However, the production will decline very fast and the water/gas breakthrough will occur earlier [6]. An example of this reservoir type is the Amal field in Libya.

Type II: Fractures provide the essential reservoir permeability while the matrix provides more porosity and stores a part of the hydrocarbons. The reserves in this reservoir type are substantially higher than those in Type I reservoirs thanks to the enhanced matrix porosity. The initial production rates are generally good, however during the secondary recovery, difficulties can occur if the fracture matrix communication is poor. Examples of such type are the Agha Jari and Haft Kel fields in Iran and La Paz/Mara field in Venezuela.

Type III: Fractures only assist the permeability in an already producible reservoir which has a high matrix porosity. This type represents the case of most of the largest fields in the world such as the Kirkuk field in Iraq, Gachsaran field in Iran, Hassi Messaoud field in Algeria and Dukhan field in Qatar. The reservoirs are more continuous and tend to sustain economic production rates but can have complex directional permeability relationships.

Type IV: Matrix has high porosity and permeability and governs the storage of all the hydrocarbons of the reservoir. On the other side, fractures provide no additional porosity or permeability and create only a reservoir anisotropy. Usually, these fractures are filled with minerals and tend to block the fluid flow, which renders the reservoir economically unprofitable for development and production.

1.1.3 Characteristics

During the drilling and production phases, fundamental differences between naturally fractured reservoirs and conventional non-fractured reservoirs can be observed. Van golf Racht [8] and Saidi [9] listed the biggest differences between the two types of reservoirs as follow:

- Mud losses during the drilling phase are more pronounced in fractured reservoirs due to the presence of large fractures and thief zones/voids.
- The water-oil contact (WOC) and gas-oil contact (GOC) are sharp interfaces before and during the production phase because of the rapid re-equilibration of the fluids insured by the high fracture permeabilities. In contrast, large transition zones between the water and oil, the gas and oil are observed in conventional non-fractured reservoirs.
- Thanks to the convective circulation inside the fractures, PVT properties and fluids compositions are constant with depth in fractured reservoirs. On the other side, varying bubble points as function of depth are observed in the conventional non-fractured reservoirs.
- Very high productivity indexes of around 500 Standard Barrel/Day/psi or higher are typically observed in naturally fractured wells producing under laminar flow.
- The pressure drops around producing wells (horizontal pressure gradients) are usually lower than those in conventional non-fractured reservoirs due to the high transmissibility of fluids in the fracture network. These pressure drops do not have any important role in the production phase which is more related to the fracture/matrix communication.
- The vertical communications in fractured reservoirs causes the liberated gas from the oil phase to segregate towards the top of the reservoir rather than towards the well, which result in lower Gas Oil Ratio (GOR).
- The petrophysical characteristics of the rock matrix and the PVT properties of the fluid which affect largely the breakthrough phenomenon in conventional non-fractured reservoirs, have no significant effect in the case of fractured reservoirs. The breakthrough phenomenon and the water cut depend only on the production rate.
- An artificial stimulation, by acidizing, results usually in a considerable increase in the productivity of the wells in naturally fractured reservoirs compared to conventional non-fractured reservoirs. In this case, the acids tend essentially to increase the width of the already existing fractures and channels.

1.1.4 Recovery mechanisms in naturally fractured reservoirs

In general, the oil production from a reservoir is governed by viscous, capillary and gravitational forces [10]. In the case of naturally fractured reservoirs, the recovery mechanisms are slightly different from those in conventional non-fractured reservoirs because of the low viscous forces and

the high capillarity differences between the matrix and the fracture network [11]. Depending on the displacing fluid and reservoir characteristics and conditions, four basic recovery mechanisms are usually considered in naturally fractured reservoirs namely the gravity drainage, spontaneous imbibition, fluid expansion and molecular diffusion [12] as depicted in **Figure 1.2** and discussed subsequently.

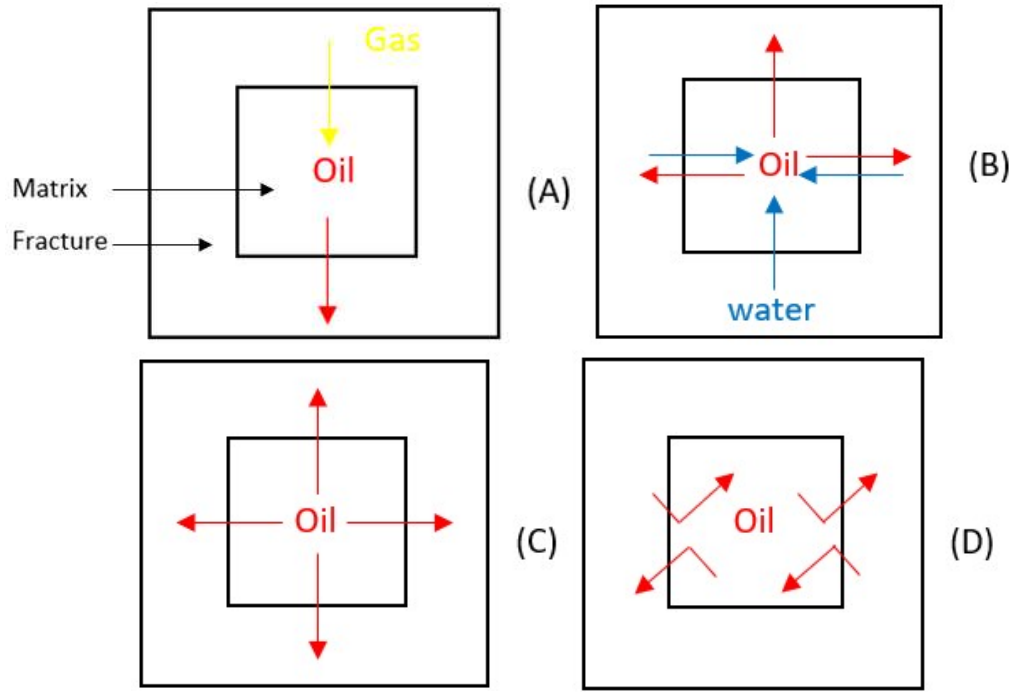

Figure 1.2 : Schematic of different recovery mechanisms in fractured reservoirs (A) Gravity drainage (B) Spontaneous imbibition (C) Fluid expansion (D) Molecular diffusion. [13]

The gravity drainage was first discussed by Cardwell and Parsons [14]. The mechanism consists on oil displacement by immiscible gas and occurs from the top of the matrix blocks when the gravity forces overcome the capillary forces in the matrix [15]. The gravity forces are determined by the density difference between the gas in the fracture and the oil in the matrix and the effective height of the matrix blocks [16]. The latter represents the height of one matrix block if there is no capillary continuity and the sum of the matrix blocks heights if a capillary continuity is established between the blocks as shown in **Figure 1.3**. The larger the effective height and the lower density difference are, the lower is the capillary threshold pressure of the matrix block and the higher is the gravity drainage mechanism.

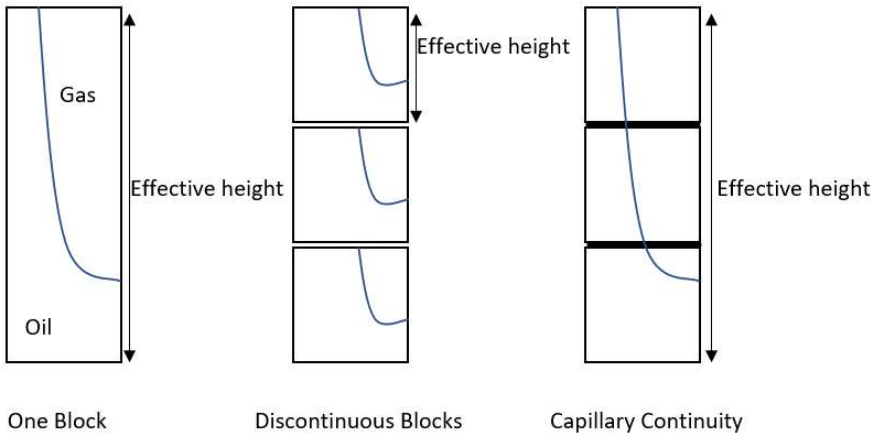

Figure 1.3 : Gravity drainage between vertical matrix blocks.[16]

The imbibition mechanism consists on oil displacement by water and can occur naturally/spontaneously if initiated by capillary forces or forcibly if caused by external forces which give rise to a pressure gradient between the fracture and the matrix [17]. An imbibition where the water enters from one matrix side (face) and the oil is recovered from the opposite side is a co-current imbibition. While an imbibition where the water enters from one matrix side (face) and the oil is recovered from the same side is a counter-current imbibition. The imbibition is governed by numerous factors including rock wettability, capillary pressure, initial water saturation, oil/water interfacial tension, pore structure, matrix block size and the surface area open to flow [18]. In water wet reservoirs, the spontaneous imbibition can result in important oil recoveries during the primary recovery phase by an active water drive process and during the secondary recovery phase by a water flooding process.

Fluid expansion mechanism occurs mainly in the primary recovery phase. As the oil production from the reservoir starts, it causes a rapid pressure drop in the fracture network compared to the matrix. Such pressure difference between the two systems initiates the oil flow to outside the matrix as it expands. Moreover and below the bubble point, gas will evolve from the oil and the expanding gas will lead to further recovery from the matrix [13].

Similarly, to the fluid expansion mechanism, the molecular diffusion mechanism occurs due to the difference in the hydrocarbon components concentrations between the gas in the fracture network and the oil in the matrix. The hydrocarbon components of the gas may diffuse into the oil and cause it to swell, reducing its viscosity and forcing it outside the matrix [13]. This mechanism is very limited and slow. However, if a miscible gas is injected, the two fluids can be easily mixed and can reach a thermodynamic equilibrium by exchanging some of their individual hydrocarbon components forming consequently a single hydrocarbon phase that can be recovered. It was reported in literature that a gas recycling process can result in a recovery of the half of condensates, from a fractured gas condensate reservoir, only through the diffusion mechanism [12].

1.2 Enhanced Oil Recovery methods in Naturally Fractured Reservoirs

Oil recovery from hydrocarbon reservoir passes by three recovery phases: primary, secondary and tertiary phases. During the primary phase, the oil is produced under the initial reservoir energy (active water drive, gas cap drive, dissolved gas) through one of the aforementioned mechanisms (imbibition, drainage, expansion, diffusion). The fracture network usually plays a positive role by conducting the oil towards the producing wells. In the secondary recovery phase, water or gas are injected to maintain the reservoir pressure and provide an additional mean to sweep the oil, in such phase, the fracture network has a complex role depending on the matrix rock wettability preferences, the fractures dimensions and orientation in regards the injection and production wells. For instance, a waterflooding operation in a water-wet fractured reservoir can be very cost efficient due to the spontaneous imbibition mechanism as observed by the increased oil production rates in the Ekofisk fractured reservoir in Norway as shown in **Figure 1.4** [19]. However, in oil-wet or neutral wet fractured reservoirs, the spontaneous imbibition mechanism is low, and the injected water tends to flow exclusively through the fracture network leaving the majority of the oil unswept [10].

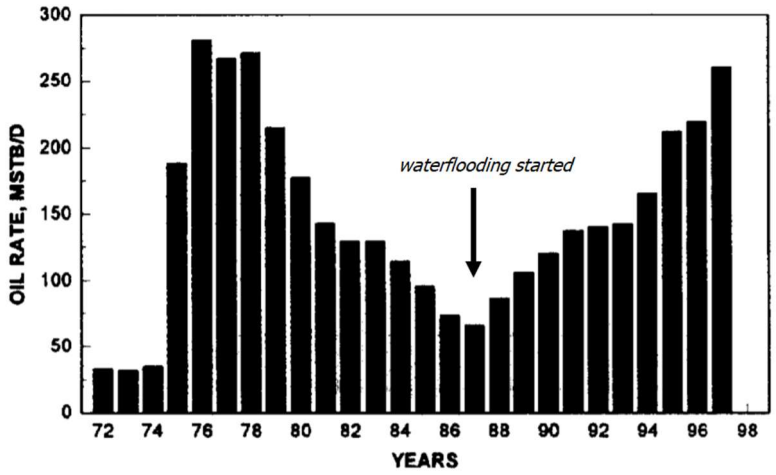

Figure 1.4 : Oil production rate response in the Ekofisk field during 25 years with a waterflooding process starting after 15 years. [19]

Allan and Sun [20] evaluated the ultimate oil recovery during primary and secondary recovery in one hundred 100 fractured reservoir around the world. In 56 oil reservoirs and 8 gas reservoirs for which reliable data were available as depicted in **Figure 1.5**, the average ultimate recovery in oil reservoirs was of 26% while in gas reservoirs was of 61%. Particularly, in Type III fractured reservoirs, the well fractured water-wet reservoirs had ultimate recovery factors ranging from 25 to 45% compared to only 5 to 25% for the well fractured oil-wet reservoirs, which confirms the pronounced efficiency of the secondary waterflooding in the water-wet reservoirs [21].

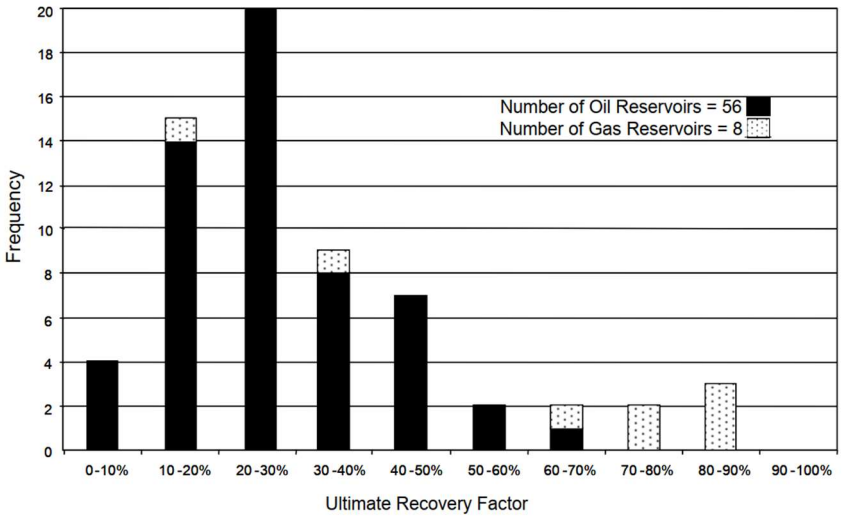

Figure 1.5 : Distribution of ultimate recovery factor for Oil/Gas fractured reservoirs of all types. [20]

Tertiary recovery or Enhanced oil recovery (EOR), which encompasses various techniques used to increase the amount of recoverable oil after the conventional (primary and secondary recoveries) strategies are no longer effective, has found its application also in naturally fractured reservoirs. Green and Willhite [22] categorized the EOR methods into five categories namely: mobility control, chemicals, miscible, thermal and others which include the Microbial EOR. More recently, Sheng [23] considered the mobility control methods as a subcategory of Chemical EOR methods. In this study, we are presenting only the main chemical EOR methods including mobility control methods employed in naturally fractured reservoirs:

1.2.1 Wettability Reversal/ Interfacial Tension Reduction

Promoting the spontaneous imbibition mechanism, by altering the wettability of an oil-wet fractured reservoir to become water-wet or reducing the interfacial tension (IFT) between the two phases, is one of the strategies that can be very efficient. The injection of cationic, anionic and nonionic surfactants was reported to alter the wettability of oil-wet carbonates towards water-wet [24]. The mechanism of the wettability reversal is not fully understood. However, some of the proposed mechanisms include the desorption of polar organic components from the originally oil-wet surfaces through ions pairing with the charged surfactants [25] and the micellar solubilization [26]. The thermal stimulation was also proposed as a method to alter the rocks wettability [27]. Schembre et al. [28] stated that high temperatures enhance the water wetness of diatomite rocks and reduce the oil to water viscosity ratio, which yields a less resistant force to water imbibition. A third technique consists on injecting smart water [29]. A smart water is a brine with optimized concentrations of calcium (Ca^{2+}), sulfate (SO_4^{2-}) and magnesium (Mg^{2+}) ions. These ions are considered as wettability influencing ions in carbonate reservoirs due to their preferential adsorption on the chalk surfaces and abilities in displacing the organic carboxylic groups responsible on the oil-wet state of the surface [30].

On the other side, if the IFT between the oil and the gas is reduced, the gravity drainage mechanism can be enhanced. Karimaie and Trorsaeter [31] observed an increased oil recovery as the IFT was decreased between the gas and oil following the re-pressurization of the injected gas.

1.2.2 Mobility/Conformance Control

In fractured reservoirs where the imbibition/drainage mechanisms are limited and the fractures are so large or highly conductive, the injected fluids will essentially flow in the fracture network leaving huge quantities of the oil trapped in the matrix. A rapid breakthrough of injection fluids into the production wells and poor oil sweep efficiencies are observed as illustrated in **Figure 1.6**. In this case, a fracture channeling phenomenon occurs, which is considered as one of the most common reservoir conformance problems [32].

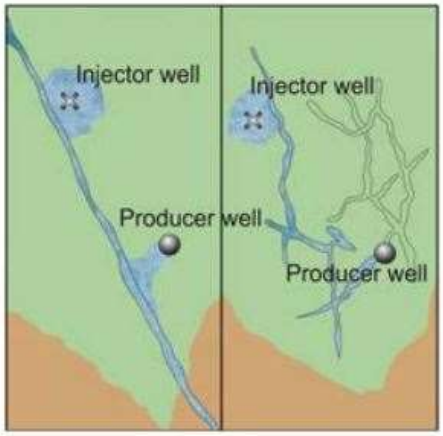

Figure 1.6 : Fracture channeling phenomenon.[33]

The main challenge is to reduce the fractures conductivity in order to force the injection fluids to enter, get in touch and move the oil trapped in the matrix. These operations are known as conformance control treatments. Three techniques employed in reducing fractures permeability namely Foam, Microbial and Gels are presented below:

1.2.2.1 Foam

Foams are liquid systems prepared by mixing gas (CO_2, N_2, CH_4 or flue gas), liquid (water) and foaming agents (surfactants) to form a discontinuous gas phase (bubbles) separated by a thin liquid films called lamellae. Based on the amount of the gas phase, dry foams/Polyederschaum or wet foams/Kugelschaum can be prepared [34]. As shown in **Figure 1.7**, dry foams are characterized by polygonal bubbles separated by thin lamellae films due to the high gas volume fractions. While, wet foams are formed by low gas volume fractions and are characterized by spherical bubbles separated by thick lenses of the liquid [35]. The bubbles size and distribution are the main indicators of a bulk foam stability. The latter is affected by many factors associated with both the physiochemical properties of the foam components (gas, liquid, surfactant) such as surfactant type and concentration,

liquid viscosity, density difference between gas and liquid, and the presence or not of detrimental components such as lower chain hydrocarbons [36].

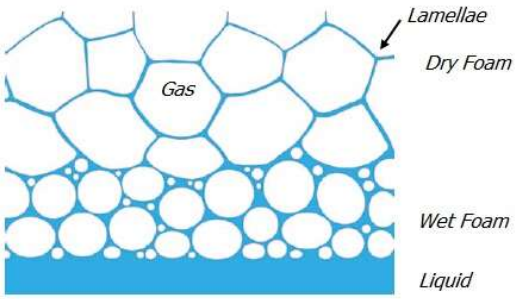

Figure 1.7 : Gas bubbles forms in dry and wet foams.

Foam injection in porous media as a potential EOR method was first proposed by Boud et Holbrook [37]. Later, Bernard and Holm [38] highlighted the effect of foam in reducing the gas relative permeability in heterogeneous reservoirs, and considered the foam as a promising agent for controlling gas mobility. In fact, foams have higher viscosities compared to water and gas [34]. When injected in a reservoir, foams exhibit both a viscosity-enhancement component and a permeability-reducing component [32]. The viscosity-enhancement component is related to the high-pressure drops needed to drive the bubbles at a constant velocity. While, the permeability-reducing component is related to the formation or the increase in the trapped residual-gas saturation, which reduces the relative permeability of the gas [39]. **Figure 1.8** shows a pore scale schematic of gas trapping function of foam in porous media, where capillary forces play an important role in immobilizing a large fraction of the foam bubbles especially in the intermediate-sized pores.

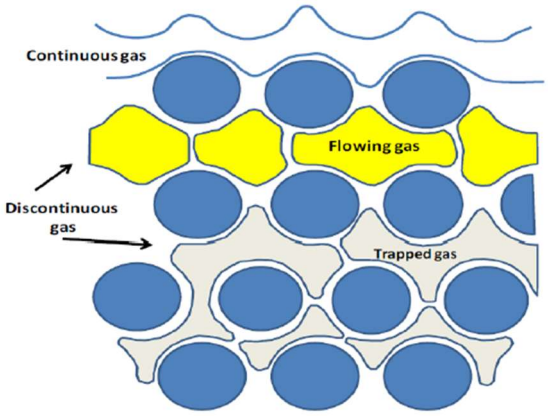

Figure 1.8 : Pore scale schematic of gas trapping function of foam in porous media.[40]

In heterogeneous reservoirs, Foams can be generated in-situ through one of the generation mechanisms namely snap-off, lamellae division and leave behind [41] as shown in **Figure 1.9**.

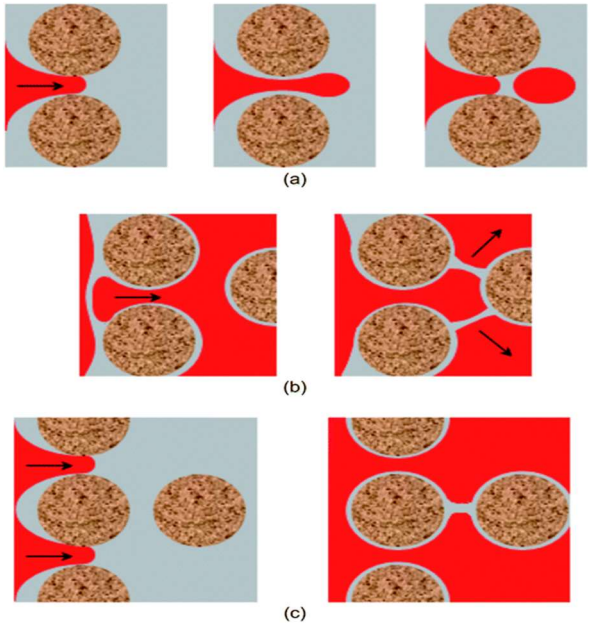

Figure 1.9 : Foam generation mechanisms (a) Snap-off (b) Lamellae division (c) Leave-behind.[42]

Foams are preferentially generated in the high permeability zones and tend to divert the subsequent flow into the low permeable zones. When capillary communications and crossflows are established between the two zones, the foam front will move uniformly at equal velocity [43]. This feature encouraged the investigations of foam injection for conformance control operations in fractured reservoirs. Kovscek et al. [35] studied experimentally the flow of nitrogen, water and foam through a transparent rough-walled rock fracture with a hydraulic aperture of 30 µm. For foam qualities ranging from 0.60 to 0.99, their results showed that foam flow resistance was 100 to 540 times higher than that of nitrogen gas. At the microscopic scale, foam injection was evaluated in fractured silicone models by Kovscek et al. [44] and Gauteplass et al. [45]. Similarly, Fernø et al. [46] evaluated the generation of foam and its behavior in a fractured network of marble blocks. Zuta and Fjelde [47] reported an important improvement in the sweep efficiency and the recovery factor when CO_2 foam was injected under reservoir conditions in a fractured core plug where the fracture was simulated by a drilled hole of 0.3 cm diameter. Recently, Haugen et al. [48] investigated the injection, in fractured rocks with different wettability preferences, of miscible CO_2, CO_2 foam and N_2 foam following a secondary water injection. The Ultimate oil recoveries were found to be higher in oil-wet cores than in water-wet cores. While the miscible CO_2 and N_2 foams were more efficient compared to the immiscible foams. The major limitation of foam injection at the field scale is the excessive pore volume (PV) needed to achieve high oil recoveries. Haugen et al. [49] obtained an 80 % recovery of the original oil in place only after injecting more than 100 PV of a pre-generated immiscible N_2 foam.

1.2.2.2 Microbial

The bacterial growth inside the fractures was investigated as an innovative method to reduce the fractures permeability [50]. *Bacillus* and *Clostridium* microorganisms have a great potential to survive under harsh conditions of hydrocarbon reservoirs. Once in the reservoirs with sufficient

nutrients, the in-situ metabolism starts producing cellular mass capable of plugging physically the fractures [51]. Soudmand-asli et al. [52] investigated two types of bacteria (Bacillus subtilis and Leuconostoc mesenteroides) to enhance the oil recovery in fractured porous media of etched-glass micromodels. They observed a considerable permeability reduction when the Leuconostoc mesenteroides bacteria were incubated in sand-packed column. However, the plugging of the matrix-fracture interfaces resulted in a poor oil recovery in the fractured porous media. Al-Hattali et al. [53] studied the plugging recovery mechanism of Bacillus licheniformis strains in fractured carbonate rocks under various nutrients such as nitrogen sources, yeast extract, peptone and urea. They obtained a total of 27–30% of the residual oil recovery within only 11 hours of incubation.

1.2.2.3 Gels

Gel systems have shown to be of great interest for the petroleum industry. Several gel systems, such as Bulk Gels [54], Weak Gels [55], Colloidal Dispersion Gels (CDGs) [56], Performed Particle Gels (PPGs) [57], Microgels [58], were developed and applied in oilfields to account for the various technical and environmental demands. By far, bulk gels were the largest applied gel technology in conformance control operations, including sweep-improvement treatments and water- and/or gas-shutoff treatments [32] overcoming the other two techniques (Foam and Microbial) thanks to their cost efficiency, controllable gelation times and adjustable strengths [59]. Bulk gels are chemically crosslinked fluid-based systems which have acquired a solid-like properties induced by a continuous 3D structure of a chemical agent [32]. Bulk gels are initially under the form of low viscosity gelant solutions which allows their injection in injection/production wells. When arriving to the targeted zone, a gelation reaction takes place under the effect of one of the activation methods such as temperature, pH, chemical precursors, transforming the mobile gelant solution to a nonmobile gel that block the targeted zone (fracture, high permeability zone). Three main characteristics of bulk gels namely, the gelation time, the final gel strength and the long-term stability, alongside their behavior and flow properties in porous media, should be well studied and controlled to guarantee the success of the gel treatment. When placed in the reservoir, bulk gels can be significantly affected by the surrounding reservoir conditions, which may alter their volumes and affect their blocking capacity. Dehydration, syneresis and swelling are the most common processes that alter gel volume with different manner and to different extents. The first two processes reduce the gel volume while the third increases the gel volume. In dehydration, the gel volume is decreased due to the expulsion of solvent from the gel by a pressure gradient imposed on the bulk gel or a spontaneous imbibition of the water from the gel to the rock matrix. Syneresis occurs when an over gelation/crosslinking takes place while swelling occurs under the effect of osmotic pressure when a salinity concentration difference between the water forming the gel and the injection or formation water is present.

A variety of bulk gels were widely studied and developed in both laboratories and oilfields since the earliest years of the 20th century. For instance, two major groups namely the inorganic sodium silicate gels and the organic polymer gels can be distinguished. Both groups are presented in the subsequent sections with an emphasis on the second group (polymer gels).

1.3 Silicate gels

Silicate gels are likely the oldest bulk gel technology in conformance-improvement treatments, with the first application reported as early as 1922 [60]. Sodium silicate gels are precipitation type gels [61] formed by lowering the pH value of a sodium silicate solution ($Na_2O.nSiO_2$) with an acidic activator such as hydrochloric acid (HCl), sulfuric acid (H_2SO_4) or citric acid, following the steps illustrated in **Figure 1.10**. Depending on the percentage of the active content in the solution and the ratio of silica (SiO_2) to sodium oxide (Na_2O), a wide range of sodium silicate gel forms can be obtained. Nevertheless, the most common sodium silicate solution, used in oilfields, has a ratio of SiO_2 to Na_2O around 3,3 to 1 with an active content of 38-40 wt% in water [62].

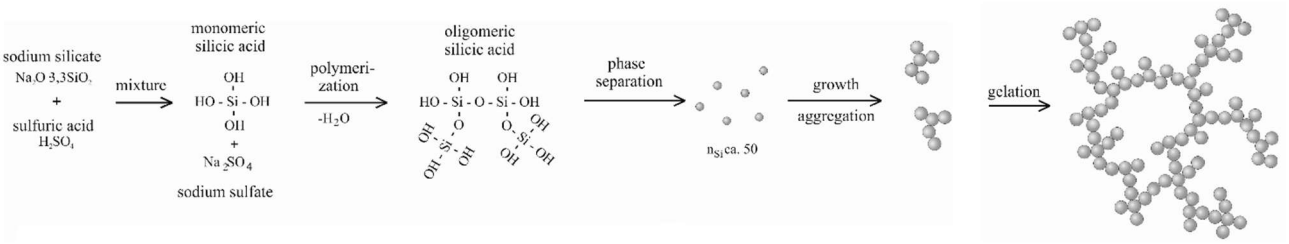

Figure 1.10 : Formation mechanism of sodium silicate gel.[63]

While the silicate portion of the gel is in itself environmentally friendly, the environmental aspect of the activator depends on the selected acid [32]. Sodium silicate gels represent also some limitations regarding their applications in fractured reservoirs such as the very low initial gelants viscosities which can invade the non-targeted zones [64], gel syneresis and brittleness that causes gels to lose its blocking efficiency very easily [65] and the hardly controlled gelation times [66]. Despite these disadvantages, the silicate gels have regained some interest during the last decade with additional enhancement on the employed chemicals. Nasr-El-Din and Taylor [67] evaluated a sodium silicate system with urea as an internal activator, as both reactants are non-toxic and readily available. Recently, Hatzignatiou et al. [68] screened and compared commercial silicate gelants for conformance control in naturally fractured carbonate reservoirs. Several activators, such as NaCl, HCl, sodium acid pyrophosphate (SAAP) and citric acid (CitAc), were tested for their ability to form rigid gels at 40 °C, 60 °C and 80 °C, considering different types of silicates and SiO_2 to M_2O ratios,. The authors proposed to incorporate polymers as additives to the standard silicate-based gelants in order to enhance the initial gelants viscosities and the final gel strength.

1.4 Polymer gels

Polymer gels are prepared by dissolving small quantities of a water-soluble polymer with a crosslinker agent, which under the effect of temperature form a gel as shown in **Figure 1.11**. A typical polymer gel is consisted of about 7000–10000 ppm polymer and 500–2000 ppm crosslinker with the remainder (99%) being water [69].

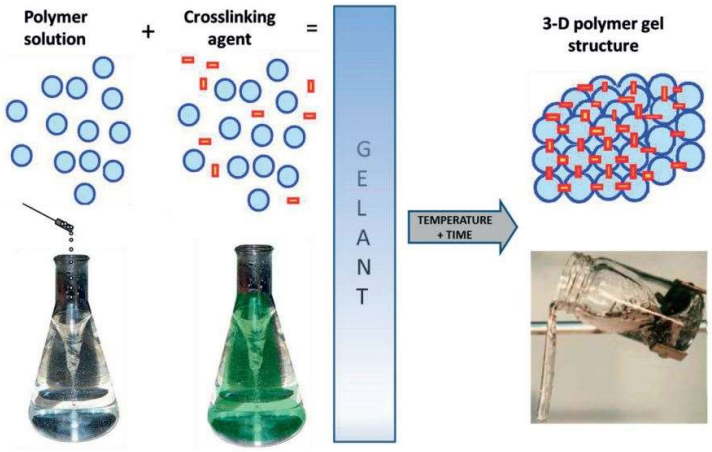

Figure 1.11: The typical scheme for preparing a polymer gel.[18]

The base-polymers used for preparing polymer gels are mainly of two types:

- **Synthetic polymers** such as Polyacrylamide (PAM) [70], Partially Hydrolyzed Polyacrylamide (PHPA) [33], Polyacrylamide/tert-butyl Acrylate (PAtBA) [71], Copolymer of acrylamide (AM) and acrylamido-2-methylpropane sulfonic acid (AMPSA) [72], Terpolymer of AM, AMPSA, N,N-Dimethyl Acrylamide (N,N-DMA) [73], Terpolymer of AM, AMPSA, N-Vinylpyrrolidone (NVP) [74], Hydrophobically Associating Polymer (HAP) [75].
- **Biopolymers** such as Xanthan gum [76], Guar gum [77] and Scleroglucan [78].

On the other hand, crosslinking agents are of three types:

- **Inorganic:** these are multivalent metal cations (chromium, aluminum, zirconium or titanium) attached to chemical complexes called ligands such as acetate, citrate, lactate, malonate and propionate… etc [79]. The ligands are mainly used to control the crosslinking rate between the polymer and the trivalent cations by releasing slowly and in controllable manner the trivalent cations according to the surrounding conditions (temperature, pH…etc.). The trivalent cations form then an ionic bond with the negatively charged groups on the backbone of the polymer [80].
- **Organic:** In this case, the crosslinking is achieved through a covalent bond between the functional groups of the polymer and an organic crosslinker such as glyoxal [81], polyethylenimine (PEI) [82], a combination of a phenol source (Phenol, Phenyl acetate, Hydroquinone (HQ), Dihydroxy-naphthalene) with a formaldehyde source (Hexamethylenetetramine (HMTA), Terephthalaldehyde, Paraformaldehyde) [33]. Two main advantages of these crosslinkers, over the

inorganic ones, are the longer gelation times and the thermal stability at higher temperatures [69] and the resistance to ionic forces [81].

- **Natural:** In an attempt to examine and promote eco-friendly crosslinkers, Reddy et al. studied the crosslinking ability of chitosan with acrylamide-based polymers such as PHPA, PAtBA and Acrylamide/AMPSA copolymer [83]. Chitosan is a low molecular weight (Mw) linear polysaccharide, thus nontoxic and biodegradable, which can crosslink with acrylamide-based polymers through covalent bonds. However, as it precipitates above pH=6, the use of this crosslinker at large scales (oilfield) was restricted.

Among all these polymers and crosslinkers, partially hydrolyzed polyacrylamide (PHPA) and polyethylenimine (PEI) as the base polymer and the crosslinker respectively, were the most promising reactants at both the laboratory and industrial scales especially during the last decade. Here below, we are presenting each one alongside their characteristics and advantages.

1.5 Partially Hydrolyzed Polyacrylamide

Partially Hydrolyzed polyacrylamide (PHPA) is a synthetic linear polymer consisted of acrylamide and acrylate monomers presented through their amide ($CONH_2$) and carboxylate (COO^-H^+/Na^+) functional groups respectively, as shown in **Figure 1.12**. PHPAs have usually high molecular weights of 4 and up to 30 $\times 10^6$ g/mol [84]. They are produced through the hydrolysis reaction of a non-ionic polyacrylamide (PAM), the copolymerization reaction of an acrylamide with an acrylic acid, and finally the aminolysis reaction of a polyacrylate (PAA) [85]. However, only the first two reactions are used for the commercial production of PHPA, which is supplied either in the powder or the emulsion form [23].

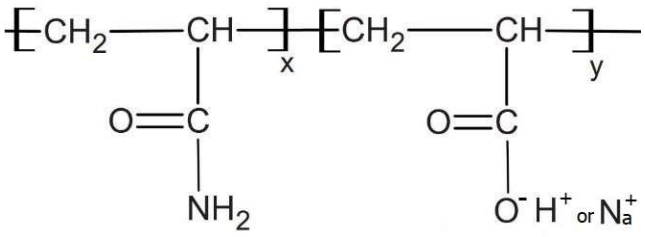

Figure 1.12 : The chemical structure of PHPA.

One of the most important parameters that describes a PHPA is its hydrolysis degree (HD) defined as the ratio of the carboxylate groups divided by the total number of the carboxylate and the amide groups [86], as given in the following equation:

$$HD = \frac{Y}{Y+X} \qquad \text{Equation 1.1}$$

Where Y is the molar concentration of the carboxylate groups in (mol/l) and X is the molar concentration of the amide groups in (mol/l).

The hydrolysis degrees of PHPA vary typically between 1 to 60 % [79] but are comprised only between 5 to 30 % for the commercial PHPA products [23]. The number of the negatively charged carboxylate groups on the PHPA backbone is so decisive regarding the stability and the rheological properties of the polymer solution in one side and the crosslinking reaction with inorganic crosslinkers in the other one. When prepared in a given aqueous solution, the electrostatic repulsion between these negatively charged groups is responsible on the conformation of the polymer and its apparent viscosity. In salt free water, the negative charges (COO^-) tend to repel each other causing the polymer flexible chains to stretch, the hydrodynamic volume to increase and the apparent viscosity to be high. In contrast, in saline water and under the effect of monovalent or bivalent cations, the negative charges are screened and neutralized, resulting in the polymer chains to be compressed, the hydrodynamic volume to decrease and low viscosity to be observed. The temperature, the presence of bivalent or trivalent cations in the aqueous solution, and oxygen were all found to affect the stability and efficiency of PHPA. For temperatures greater than 60 °C, the auto-hydrolysis of the amide groups ($CONH_2$) to carboxylate groups (COO^-) is accelerated [87] shifting the initial hydrolysis degree to very high values (> 45%) which result in viscosity drop as the polymer chains become compressed and distorted. Moreover, and in the presence of high concentration bivalent or trivalent cations, the polymer may precipitate [88]. While, the presence of oxygen, especially at high temperatures, leads to the oxidative degradation of the polymer [89], which result in quick viscosity loss with time [90]. Despite these limiting factors, PHPAs were by far the most widely employed polymer for both conformance control especially in fractured reservoirs and for enhanced oil recovery (EOR) operations including polymer flooding (PF) and alkaline-surfactant-polymer (ASP) flooding [91], thanks to their lower cost, commercial availability, greater viscoelasticity, lower adsorption to reservoir rocks and resistance to microbial degradation [23].

1.6 Polyethylenimine

Polyethylenimines (PEIs) are low molecular weight polymers (Mws varying between 0.8 to 750 × 10^3 g/mol) of variable structures such as linear, branched, comb, network and dendrimer architectures formed by the linking of ethylenimine units through different synthesis and modifications methods [92]. Usually, commercial polyethylenimines have a spherical branched structure and are synthetized by an electrophilic ring-opening polymerization of unsubstituted ethylenimine with a protonic catalyst such as Lewis acids and their salts, strong Brønsted acids, carboxylic acids, or halogens [93]. Branched PEIs are consisted essentially of three amino groups, making it a highly nucleophilic reactant: (1) primary amine end groups (NH_2), (2) secondary amine linear units (NH), (3) tertiary amine branched units (N) (i.e., dendritic units), separated by two methylene carbons (CH_2) as shown in **Figure 1.13**. They are also characterized by a branching degree (BD) defined as:

$$BD=\frac{2D}{2D+L}$$ Equation 1.2

where: D are the dendritic units and L are the secondary amine linear units [94].

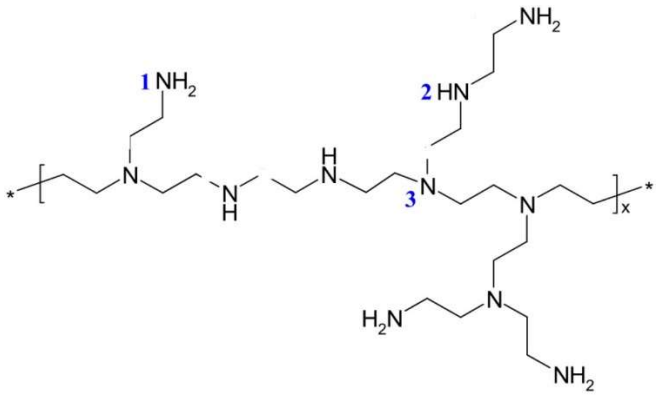

Figure 1.13: The chemical structure of a branched polyethylenimine.

Branched PEIs are amorphous and freely soluble in water, methanol, ethanol and acetone, while at room temperature, they are highly viscous and odourless liquids [92]. Most importantly, PEIs are considered as eco-friendly materials, that were approved for food contact in the United States [83]. In fact, the acute oral toxicity of branched PEIs varies with its molecular weight. For example, the median lethal dose (LD_{50}) of PEIs with a molecular weight between 0.3-30 × 10^3 g/mol, is around 0.8-3.0 g/kg (mouse) and reaches 8.0 g/kg (mouse) for a 30 wt% aqueous solution of PEI with a molecular weight between 70-100 × 10^3 g/mol [93].

Polyethylenimines have also a highly cationic character [95], since some of their primary and secondary amine groups can be protonated to ammonium ions (NH_3^+), according to the pH of the solution as shown in **Figure 1.14**:

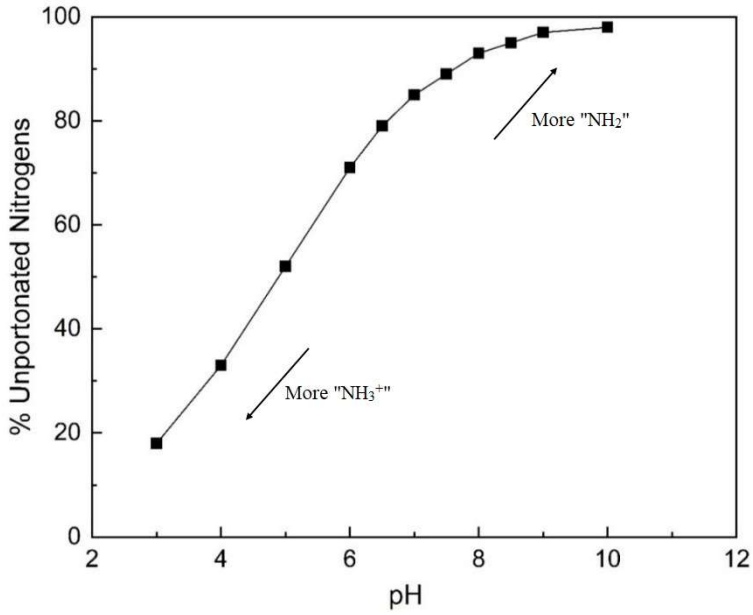

Figure 1.14 : The percentage of PEI's unprotonated nitrogens versus the solution pH.[96]

Thanks to all these attractive features (branched structure, high nucleophilicity, high ionic charge, water solubility and non-toxicity nature), PEIs were employed in a wide range of applications including but not limited to medicinal chemistry such as DNA transfection agents or drug delivery agents [97, 98], water treatment [99], carbon dioxide capture [100], cosmetics [101]. Similarly, PEIs have gained a huge interest in the oil and gas industry, especially during the last two decades, as effective crosslinkers of various acrylamide-based polymers that are presented and discussed in the subsequent parts.

1.7 Polyethylenimine crosslinked polymer gels

The first study on PEI crosslinked polymer gels was reported in a patent by Allison and Purkaple [102]. The authors stated that upon the mixing of 2.5 % Polyethylenimine with 0.1 % polyacrylamide (PAM), a viscous gel was quickly formed at room temperature. It was until 1997, when Morgan and co-workers introduced for the first time a gel system based on the crosslinking of PAtBA and PEI for the high temperature water/gas shutoff applications [82]. Since then, several acrylamide-based polymers were tested to crosslink with PEI as discussed here below and summarized in **Table 1.1** at the end of the section.

1.7.1 PAtBA/PEI

The introduction of this system was in order to overcome the problems of the rapid gelation at high temperatures and the precipitation of the crosslinker at high pH associated with the PHPA/chromium (III) acetate gels. To solve the rapid gelation problems, the initial idea consisted of controlling the hydrolysis of the polymer to delay the crosslinking between the trivalent chromium cations and the negatively charged groups of the polymer. This option was offered by controlled hydrolysis co-polymers such as Polyacrylamide/tert-butyl Acrylate (PAtBA) as shown in **Figure 1.15**:

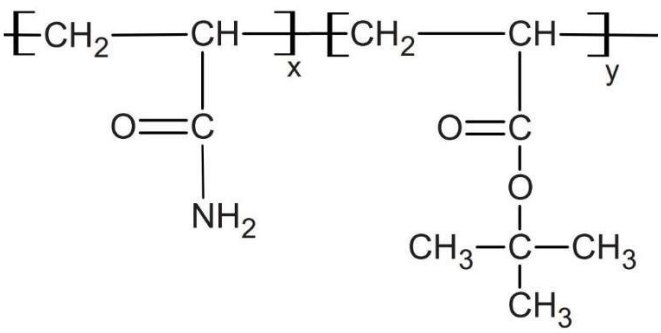

Figure 1.15 : The chemical structure of PAtBA.[103]

PAtBA was chosen based on its feed stock price and its high solubility in water [82]. However, the persistence of problems associated with the crosslinker itself, such as toxicity and precipitation in carbonate rocks, encouraged the investigations of new crosslinkers. At this stage, the PEI was selected first due to its ability to form covalent bonds with the carbonyl carbon at the PAtBA ester groups

through nucleophilic attack as shown in **Figure 1.16** and secondly due to its eco-friendly aspect compared to other nucleophilic species which can also displace the PAtBA ester groups.

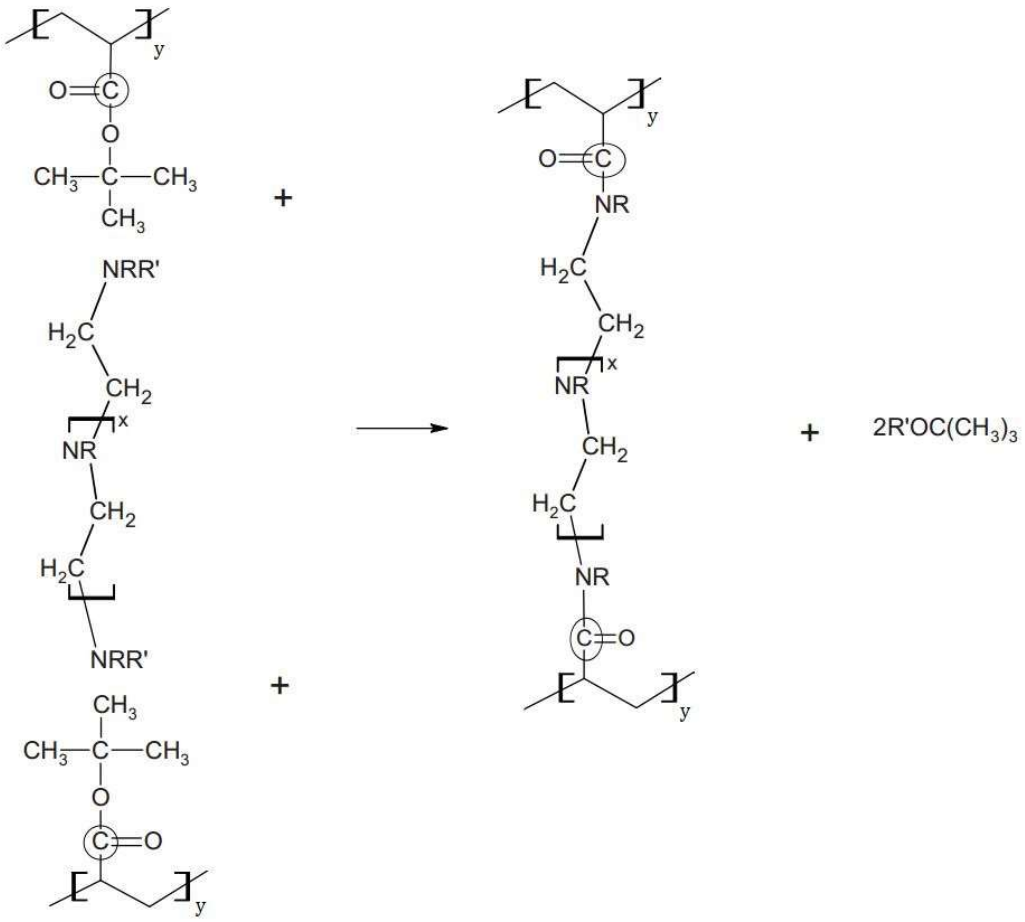

Figure 1.16 : PEI nucleophilic attack on the ester groups of PAtBA. [103]

The interaction of PAtBA with PEI formed a ringing solid gel that was stable for two months at 156 °C [82] and it was later developed for the large commercial use [71]. The crosslinking mechanism between PAtBA and PEI was an active area of research for a lot of scientists. Hardy et al. [71] proposed three possible ways of crosslinking:

- the nucleophilic attack.
- the hydrolysis of the (-tBA) groups then an ionic crosslinking.
- the thermolysis of the (-tBA) groups then an ionic crosslinking.

The hydrolysis and thermolysis were the two reaction pathways of tert-butyl acrylate (-tBA) decomposition into an acrylic acid as shown in **Figure 1.17** and **1.18**, respectively.

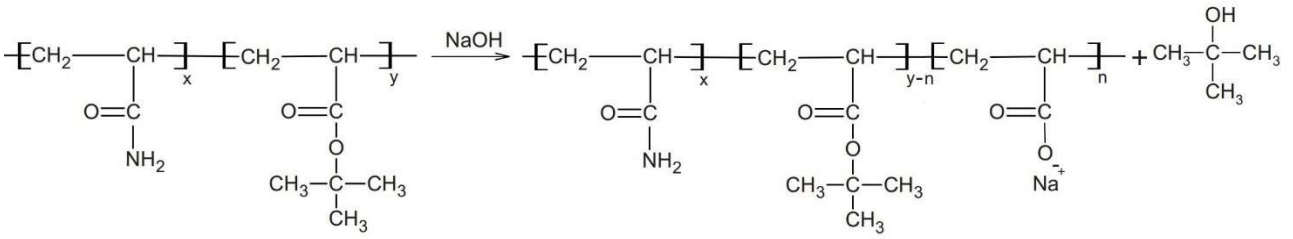

Figure 1.17 : The hydrolysis of the (-tBA) groups on PAtBA.[103]

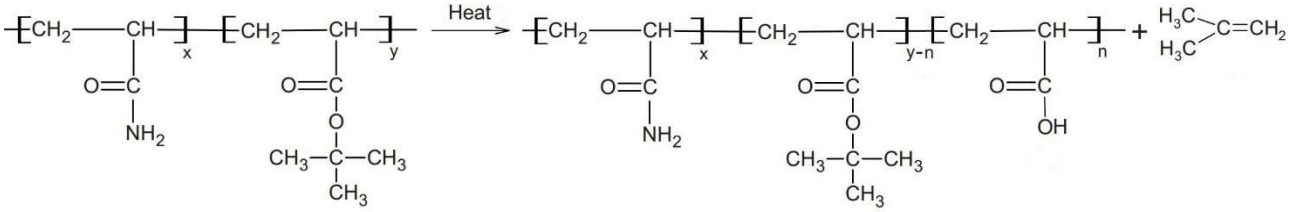

Figure 1.18 : The thermolysis of the (-tBA) groups on PAtBA.[103]

The resulted acrylic acid is then supposed to crosslink with the cationic PEI via an acid-base proton exchange: the ammonium ions (NH_3^+) of the PEI with the carboxylate groups (COO^-) of the polymer. This was especially the case for pH below 7 and temperatures below 90°C [71]. Another crosslinking mechanism was proposed by Reddy et al. [83] wherein the PEI forms covalent bonds directly with the carbonyl carbons at the amide groups of PAtBA, through a transamidation reaction as shown in **Figure 1.19**:

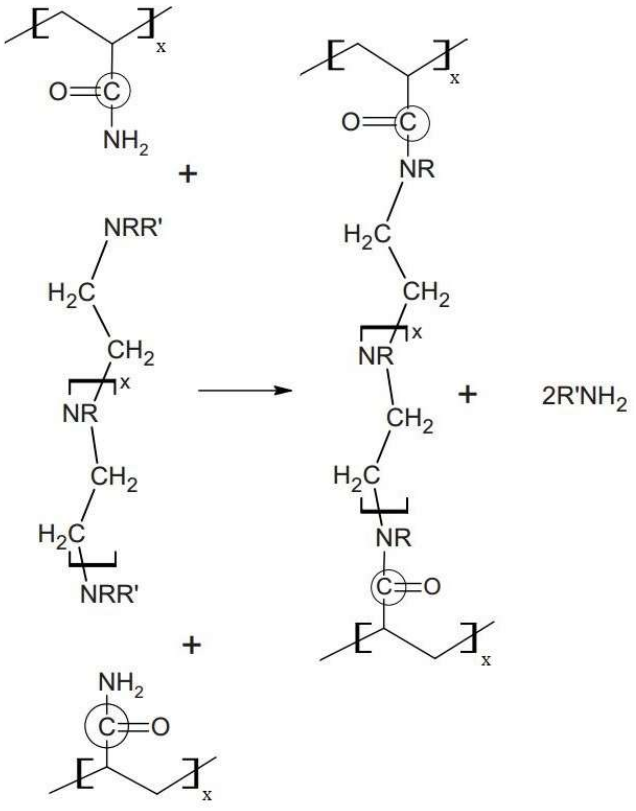

Figure 1.19 : PEI transamidation reaction with the amide groups.[103]

The transamidation reaction was confirmed by Al-Muntasheri et al. [104] who studied the gelation of a totally decomposed PAtBA with PEI. Three samples of PAtBA were heated at 80, 105 and 120 °C for sufficient times to decompose all their tert-Butyl acrylate (-tBA) groups. Then, they were mixed with PEI at the same temperature of heating. All the three decomposed PAtBA/PEI samples did form a gel confirming the transamidation reaction as one of the main crosslinking mechanisms especially in the case of 105 and 120 °C. At 80 °C, the contribution of the acid-base interaction into the crosslinking was theoretically present but no further quantification was done. Moreover, some authors considered the "nucleophilic attack" and the "transamidation reaction" to take place simultaneously and used the term "nucleophilic substitution" to describe the crosslinking mechanism of PAtBA/PEI gels [105]. As a summary, one can conclude that the PAtBA/PEI interactions are done mainly through a nucleophilic substitution for temperatures above 90°C and through a combination of nucleophilic substitution and acid-base interaction for temperatures below 90°C.

The gelation reactions, the viscoelastic properties and the performance of PAtBA/PEI gels in porous media have been also the subject of numerous studies. The effect of different controlling parameters such as polymer and crosslinker concentrations, type of mixing water, temperature, initial pH, type of inorganic salts, the presence of contaminants i.e. ferric iron, on gelation time and gel strength were thoroughly investigated [105, 106]. Gelation times reported in literature varied from 0.3 to 15 hours in the temperature range of 70 to 150 °C and for polymers loadings of 3 to 9 wt%. While, the thermal stability of PAtBA/PEI gels was reported to be up to 191°C [107]. The PAtBA/PEI gels were very strong gels confirmed by the measured storage moduli that were remarkably higher than those of inorganically gels [106]. A typical PAtBA/PEI gel, prepared with 7 wt% polymer and 0.3 wt% PEI and cured at 150 °C for 12 hours, had an elastic modulus of approximately 700 Pa compared to only 7 Pa for a typical PHPA/chromium (III) acetate gel prepared with 0.5 wt% polymer and 0.0417 wt% crosslinker and cured at 41°C for 24 hours [108]. The explanation of such behavior was the low molecular weight of PAtBA which manifest in shorter and straighter polymer chains that result in a tighter 3D structure. This was also the case in porous media, PAtBA/PEI gels showed higher resistances and higher apparent strengths in low permeability cores [109]. For example, the maximum pressure build-up reached 510 psi in a sandstone core with a permeability of 300 mD. Moreover, it was confirmed that higher intrinsic gel strength, using either higher crosslinker loadings or higher curing temperatures, will result in higher gel resistances. The PAtBA/PEI gels showed good injectivity, they went eight times farther than chromium-based systems in cores under equivalent conditions [80] thanks to their low initial gelant viscosities. A good permeability reduction of up to 88% in Oklahoma sandpacks was also maintained for one year at an extreme temperature of 176.6 °C [73]. All These good performances of PAtBA/PEI gels, whether in bulk tests where perfect gelation times and thermal stability were obtained or in corefloods where good injectivity and

permeability reductions were recorded, made the PAtBA/PEI gels the most successful PEI crosslinked polymer gels.

1.7.2 PAM/PEI

Confirming the transamidation reaction as one of the main mechanisms in the crosslinking of the PAtBA/PEI gels, encouraged Al-Muntasheri and co-workers [70] to investigate the crosslinking of polyacrylamide (PAM) shown in **Figure 1.20** with PEI. The molecular weight of the studied PAM was similar to that of PAtBA (Molecular weights comprised between 250 to 500 × 10^3 g/mol), the only reason of this choice was purely technical, as the PAM is cheaper (2 to 4 USD/Kg) compared to PAtBA (7.7 USD/Kg) [110].

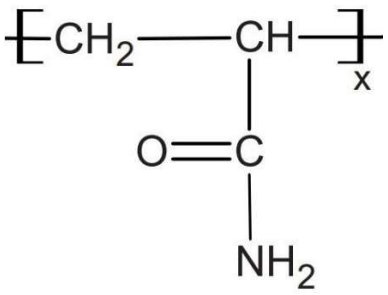

Figure 1.20 : The chemical structure of PAM.

The effect of controlling parameters on gelation reaction were fully examined using both rheological measurements and differential scanning calorimetry [111]. The PAM/PEI gel was found stable for 8 weeks at 130 °C and 30 bars [70] and gelation time did not exceed one hour at 130 °C similarly to PAtBA/PEI gels [105]. However, the activation energy of the PAM/PEI gel (71 kJ/mol) was lower than that of the PAtBA/PEI gel (120 kJ/mol), indicating a faster and easier reaction between the PAM and PEI. The viscoelastic behavior of PAM/PEI gels was also considered, El-Karsani et al. [112] studied the effect of temperature, reactants concentrations, pH and salinity on the PAM/PEI gel strength at high temperature (130 °C) and high-pressure (34.5 bars) conditions. The storage modulus of a typical PAM/PEI gel prepared using 7 wt% of polymer and 0.3 wt% of crosslinker, cured at 150 °C and 500 psi, was 1087 Pa which was higher than that of a similar PAtBA/PEI gel (700 Pa). This result confirmed that more crosslinking reactions took place between PAM and PEI compared to PAtBA and PEI, thus the stronger gel.

Moreover, several papers addressed the performance and displacement of PAM/PEI gel in porous media [113-115]. The PAM/PEI gel had an excellent permeability reduction in Berea sandstone cores, where a 100% permeability reduction was recorded over the course of three weeks at 90 °C [70]. The key point of this success was the non-adsorption of the polymer [114]. The low molecular weight and the nonionic character of the polymer were the main reasons for the absence of any mechanical retention or ionic adsorption of the polymer in Bentheimer sandstone cores. The yield of the PAM/PEI

gel in bulk and porous media had a similar trend in both cases [112]. An increased compression at pressure drops below the critical yield pressure, followed by the gel yield at this critical pressure then a lower residual gel resistance above this critical pressure. Interestingly, higher yield stresses were observed in porous media compared to bulk experiments [114].

A more recent method, which consists on using emulsified PAM/PEI gels, for selectively reducing the water permeability was introduced by Mohamed et al. [116]. In a such system, the gelant is emulsified in an oil phase using an appropriate emulsifier (surfactant) and when in porous media, the emulsion breaks up to a water phase which forms the gel and an oil phase which remains mobile. The advantage of these systems is the possibility to apply them in producer wells without the need for isolation techniques. The gelation kinetics and the viscoelastic behavior of an emulsified PAM/PEI gels prepared with 70% water phase (Gelant) and 30% hydrocarbon phase (Diesel and surfactant) were studied using differential scanning calorimetry and dynamic shear rheology, respectively [116, 117]. The emulsified PAM/PEI gels had lower characteristics in terms of crosslinking rate and gel strength compared to non-emulsified ones. This behavior was explained in one side by the limited heat transfer conducted to the emulsified gelant which slow down the reaction and consequently the number of crosslinked sites, and on the other side by the formation of isolated gel domains rather than a continuous structure, which is the case when gelation starts before the total breakage of the emulsion [117], as illustrated in **Figure 1.21**.

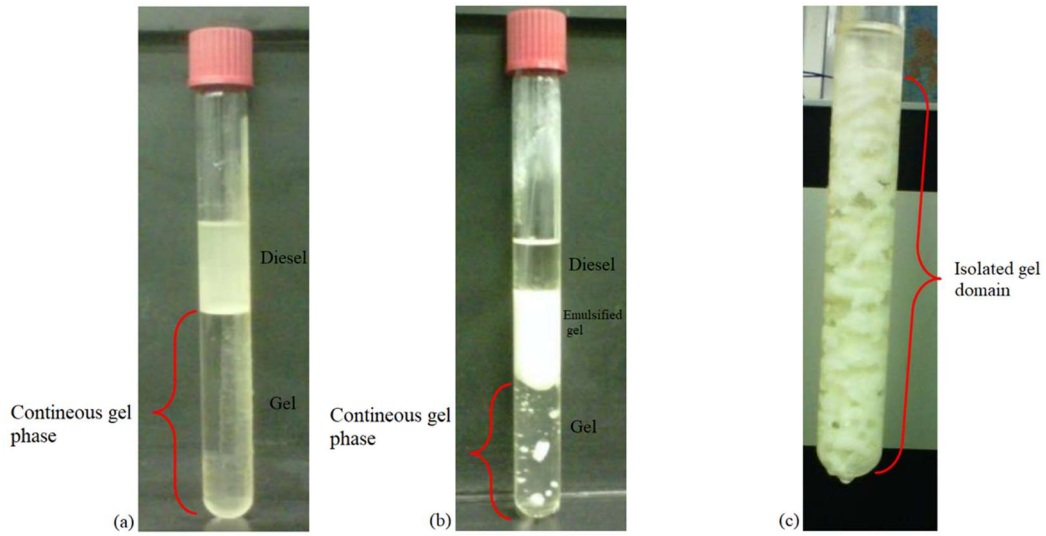

Figure 1.21 : Types of formed gels in the emulsified PAM/PEI system (a) formulation with complete separation (b) formulation with partial separation (c) formulation with no separation.[117]

1.7.3 PHPA/PEI

Partially hydrolyzed polyacrylamide (PHPA) was investigated as a good alternative for PAtBA and PAM polymers for fractures shutoff applications in the low temperature range reservoirs (<100 °C) due to its high molecular weight, which limits the gelant solution penetration to the rock matrix. The crosslinking of PHPA with PEI was documented to be mainly through a transamidation reaction of

the amide groups by the PEI's amines. Nevertheless, the interaction between the carboxylate groups (COO^-) of the PHPA and the ammonium ions (NH_3^+) of the PEI was also considered as a potential crosslinking mechanism [71, 103, 118]. For some authors, the evidence of such interaction was the lower gelation times at higher hydrolysis degrees [70].

Several studies investigated the gelation of PHPA/PEI gels mainly in the low and ultralow temperate range of 4.4 to 65 °C to address conformance control in the arctic zones, shallow water/gas zones in offshore fields and the permafrost zones in the temperature range [33, 95, 119-123]. Nevertheless, conformance control was not the only area for PHPA/PEI gels application; Hashmat et al. [124] investigated the PHPA/PEI gel as a loss circulation material (LCM) in drilling operations with temperatures of up to 100 °C.

Gelation times of PHPA/PEI gels reported in literature, varied between 0.5 hour [123] to 9 days [120] with low gelation times obtained using high polymer and crosslinker loadings of up to 7% and 2% respectively [95]. In contrast, when typical polymer and crosslinker concentrations are used, gelation time was around 15 hours at 40 °C, which was still longer than that of the commonly used PHPA/chromium (III) acetate gels (5 hours at 40°C). The performance of PHPA/PEI gels in porous media was also well-investigated. High water permeability reductions of up to 15000 were observed using PHPA/PEI gels in fractured cores [121]. The most interesting feature was the low measured fluid leakoff rates to the rock matrix, which confirmed the PHPA/PEI gels to be suitable for fractures and high permeability channels shutoff [33]. Gelation rate and gel strength were also found to improve when the gelant first flows through porous media [122], thanks to the mechanical extrusion of the long-curled polymer chains, which promotes the crosslinking between the polymer and the crosslinker.

On the other hand, the viscoelastic behavior of PHPA/PEI gels was not fully considered in literature. To the best of our knowledge, there is no systematic study on the effect of controlling parameters such as reactants concentrations, temperature, pH, salinity on the PHPA/PEI gels viscoelastic moduli. A limited investigation on the effect of hydrolysis degree on the storage modulus was reported by El-Karsani et al. [118], wherein, higher hydrolysis degrees were found to produce higher storage moduli, which was explained by the increased number of crosslinked sites when the polymer chains are fully expended at high hydrolysis degrees.

1.7.4 HAP/PEI

Hydrophobically Associating Polymers (HAPs) are synthetic polymers which contain one or more hydrophilic groups with a small fraction of hydrophobic groups as shown in **Figure 1.22**. These hydrophobic groups give the polymer an enhanced rheological behavior and a higher adsorption capacity [125].

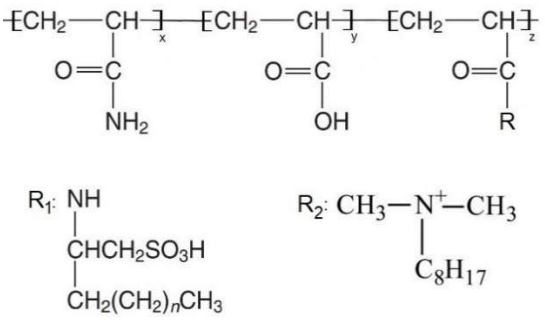

Figure 1.22 : The chemical structure of HAPs (R_1 the general radical structure reported by Sheng, R_2 the specific radical structure studied in Bai et al.).[23, 75]

HAPs were first developed and evaluated as relative permeability modifiers in sandstone reservoirs by Eoff et al. [126] and later, introduced as a base polymer for crosslinked polymer gels. The HAP/crosslinker (unknown chemical structure) gel retained 75 to 85% of its original strength, after six months of aging at 95 °C in real reservoir cores [127]. In the light of these results, it was further examined in 26 wells in the high temperature/high salinity Zhongyuan oilfield in China. The average water injection pressure increased by about 2.8 MPa and the average water injection index decreased by about 8.2 m^3/d/MPa, while over than 79% of the surrounding producer wells recorded an increase in oil production rates, indicating a huge success of the HAP/crosslinker gel. These findings encouraged a study on the crosslinking of HAP with PEI [75]. The examined HAP had a hydrophobic monomer content of 1.8% HAP with the structure shown in **Figure 1.22**.

The idea was that these hydrophobic groups associate with each other via hydrophobic interactions to further strengthen the gel. This was experimentally confirmed when low concentrations of NaCl salt were added to the gelant, a slight increase in the final gel viscosity was recorded due to the enhanced polarity of the gelant and the intensified hydrophobic associations. The gelation mechanism between the HAP and PEI was through a transamidation reaction similar to the other acrylamide-based polymers with gelation times varying between 36 to 85 hours at 80 °C. These gelation times were relatively higher than those of others acrylamide-based gels. A proposed explanation would be the reduced number of accessible amide groups. When the hydrophobic groups associate with each other, they tend to decrease the hydrodynamic volume of the polymer, which make less amide groups accessible to the PEI. The evidence of such reduction in the hydrodynamic volume was the low initial viscosity of the polymer (40 cP) despite using deionized water. The HAP/PEI gel was further tested in sandpacks cores, where it showed a very good shut-off performance of over than 98% permeability reduction and a water residual resistance factor higher than 55. Nevertheless, neither the viscoelastic properties nor the field implementations of HAP/PEI gels are reported in literature.

1.7.5 Copolymers and terpolymers/PEI

The copolymers and terpolymers of acrylamide are synthesised through incorporating monomers that give the polymer a higher thermal stability by limiting the hydrolysis of the neighbourhood amide

groups at very high temperatures [128]. In attempt to examine new acrylamide-based polymers that are thermally stable and can give relevant gelation times at extreme temperatures as high as 170 °C, Vasquez et al. [72] investigated the crosslinking of acrylamide/acrylamido-2-methylpropane sulfonic acid (AM/AMPSA) copolymer shown in **Figure 1.23** with PEI.

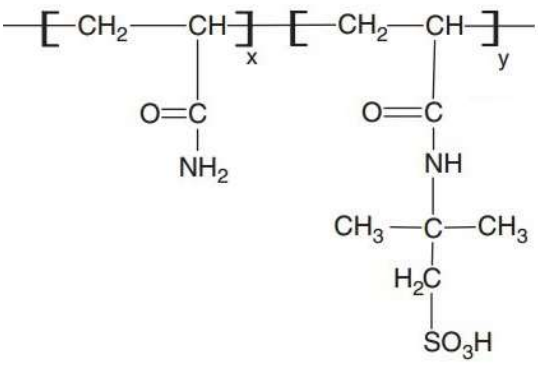

Figure 1.23 : The chemical structure of AM/AMPSA copolymer.[110]

Excellent gelation times, that vary between 2 to 20 hours, were obtained in the temperature range of 132.2 to 176.6 °C, compared to only 0.2 to 0.3 hours at 130 °C for PAtBA/PEI and PAM/PEI gels. This delayed crosslinking reaction was essentially caused by the steric hindrance provided by the methyl-propane sulfonic acid functional groups [83]. Further investigations by Vasquez et al. [73] led to the AM, AMPSA, N,N-Dimethyl Acrylamide (N,N-DMA) terpolymer shown in **Figure 1.24**.

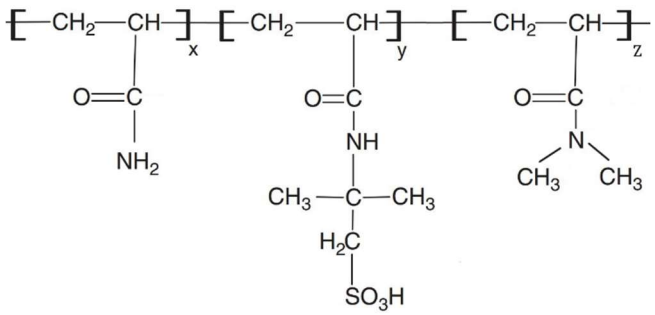

Figure 1.24 : The chemical structure of AM/AMPSA/N,N-DMA terpolymer.

The added N, N-DMA groups were incorporated to further delay the crosslinking rate via their steric hindrance. However, gelation times were very sensitive to the solution pH and the salinity of the mixing brine. For example, the gelation time decreased from 24 hours to only 2 hours when the pH of the solution passed from 11 to 8 at 135 °C. No further explanation was provided for this behavior. (AM/AMPSA/N, N-DMA)/PEI gels were then examined in sandpacks, where they maintained a 97% water permeability reduction at 176.6 °C over the course of one year.

More recently, Zhu et al. [74] studied the gelation at 150 °C of the terpolymer of AM, AMPSA, N-vinylpyrrolidone (NVP) shown in **Figure 1.25** with PEI. The crosslinking reaction was investigated using four PEIs having different molecular weights. It was found that very low molecular weight PEI

(Mw= 1.8 × 10^3 g/mol) cannot form a consistent gel, and gelation time decreases with the increase of the crosslinker molecular weight. This was explained by the length of the PEI chains and the number of the crosslinking sites on them. The gelation time was around 3.5 hours at 150 °C for a typical sample prepared with 0.8 wt% terpolymer and 0.3 wt% PEI (Mw= 70 × 10^3 g/mol), which was higher than the gelation times of PAtBA/PEI and PAM/PEI gel systems. While the gel maintained a good thermal stability over the course of 2 months.

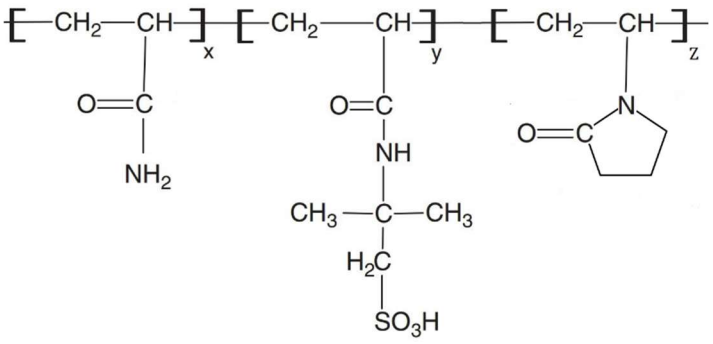

Figure 1.25 : The chemical structure of AM/AMPSA/NVP terpolymer.

One should precise that no field implementations nor viscoelastic behavior of all the above gels have been reported in literature.

Table 1.1 : Polymer/PEI gel systems reported in literature.

Polymer	Crosslinker	Temperature (°C)	Gelation Time (Hours)	solvent	Reference
10% (*) PAtBA	1% PEI	70-90	9 to 1.5	Synthetic Sea water	[82]
7% PAtBA	0.33% PEI	95	15	/	[71]
5% PAtBA	1% PEI	95	5		
3% PAtBA	1% PEI	95	7		
7% PAtBA	1% PEI	70	13		
5% PAtBA	0.5% to 2% PEI	80	3.3 to 24	2% KCl brine	[109]
		100	1.3 to 7		
		120	0.3 to 3		
350 gal/1000 gal (**) PAtBA	40 gal/1000 gal PEI	80	5	2% KCl brine	[72]
7% PatBA	1.5% PEI	85	14	7% KCl brine	[73]
7% PatBA	0.3% PEI	100	3.9	Distilled water	[105]
3.5% PatBA	1% PEI	71.1	21.3	2% KCl brine	[95]
5 to 9% PAM	0.3 to 2% PEI	130	0.25 to 0.53	Distilled water	[70]
5% PHPA	0.33 to 2% PEI	25	8 to 13	2% KCl brine	[119]
		60	1.5 to 6		
0.5 to 1.5% PHPA	0.2 to 1.5% PEI	40	15 hours to 9 days	Synthetic water Total Dissolved Solids (TDS)= 90000 mg/l	[120]
2% PHPA	0.35% PEI	65	10	Synthetic water TDS= 5000 mg/l	[121]
1 to 2% PHPA	0.2 to 0.35% PEI	65	4 to 72	Fresh water TDS= 500 mg/l	[122]
5% to 7% PHPA	1% to 2% PEI	4.4 and 23.3	0.5 to 30	2% KCl brine and Fresh water	[123]
3.5% PHPA	1% PEI	71.1	2.5	2% KCl brine	[95]

0.75% PHPA	0.41% PEI	85	3	2% KCl brine	[33]
3% PHPA (Flopaam3330S)	0.6 to 1.2% PEI	100	3.3	Distilled water	[124]
2% PHPA (Alcomer130)			3.4		
0.15% HAP	0.2% PEI	80	85	Distilled water	[75]
0.45% HAP	0.8% PEI	80	36		
410 gal/1000 gal AM/AMPSA	100 to 250 gal/1000 gal PEI	132.2	14 to 20	2% KCl brine	[72]
		176.6	2		
3 to 9% AM/AMPSA/N,N-DMA	0.5 to 2% PEI	135	2 to 41	10% KCl brine	[73]
		162.7	0.75 to 5		
0.6 to 1.2% AM/AMPSA/NVP	0.3% PEI	150	3.5 to 6	Distilled water	[74]

*: mass concentration (wt%) **: Gallons per 1000 Gallons (volume per volume ratio)

1.8 Major enhancements on polyethylenimine crosslinked polymer gels

Despite the variety of gelation times and gel strengths that can be obtained by the classical PEI crosslinked polymer gels, several techniques were employed to further enhance these two properties. Here below, we are representing and discussing some of these techniques. While **Table 1.2** summarize the gelation times obtained with these techniques.

Table 1.2 : PEI/Polymer gel systems with different additives reported in literature.

Polymer	Crosslinker**	Temperature (°C)	Gelation Time (Hours)	solvent and additive**	Refer -ence
150 gallon/1000 gallons (gpt)* PAtBA	10 gpt PEI	126.6	2	824 gpt field water+ 167 gpt KCl+ 275 lb/1000 gal **NaCl**	[129]
		140	0.9		
		150	1.5	824 gpt field water+ 167 gpt KCl+ 300 lb/1000 gal **NH_4Cl**	
7% PAtBA	2% PEI	162.7	9.6	2% KCl brine +8% **Na_2CO_3**	[130]
		176.6	6		
0.75% PHPA	0.41% PEI	85	15	2% KCl brine+	[33]

		107.2	4	15 lb/1000 gal **Na_2CO_3**	
4000 ppm PHPA	4000 ppm research grade PEI with (**DS:PEI**=1:2)	100	2.66	1% KCl brine	[131]
	4000 ppm commercial grade PEI (**DS:PEI=**1:2)		14		
4000 ppm PHPA	4000 ppm PEI+ 2000ppm **AMPSA**	100	120	1% KCl brine	[132]
5% PHPA	1.3% PEI	26.6	11.3	2% KCl brine	[123]
	1.3% PEI+ 0.5 gpt **EA**		10.1		
	1.3% PEI + 0.5 gpt **TEA**		9.9		
3.5% PHPA	1 % PEI	71.1	2.75	2% KCl brine	[95]
	1 % PEI + **TETA**		3.5		
3% PAtBA	1% PEI		22		
	1% PEI+ 1mole **TEA**		18		
	1% PEI+ 1mole **EA**		16.5		
10% PAtBA	1% PEI **chelated with zirconium**	100	5	/	[133]
7% PAtBA	0.65% PEI+ 4% **Polyamino acid**	135	21	2% KCl brine	[73]
		148.8	2.5		
	0.5 to 1.5 **d-PEI**	176.6	6.5 to 29		
		190.5	4.5 to 10		
(AM/AMPSA/*N*-DDAM) terpolymer	80% modified PEI (**PEI–GX**)	100	30	/	[134]
5% PAtBA	1% PEI	90	5.45 to 8.40	Water + **cement** + retarders	[135]
		100	2.45 to 4.55		

*: gpt (gallon per thousand gallons).

** additives are written in bold character.

1.8.1 Retarders

Various methods are used to delay the gelation of gel systems when placed in the well. These methods include cooling the near wellbore area, varying the polymers type and concentrations, adjusting the pH of the mixture. However, the use of chemical retarders, especially inorganic salts was the most economical method to delay the gelation of PEI crosslinked polymer gels. Inorganic salts such as sodium chloride (NaCl), sodium carbonate (Na_2CO_3) and ammonium chloride (NH_4Cl) act through their positive charged ions on the carboxylate groups of the polymer. This interaction reduces in one hand the number of carboxylate sites available for crosslinking with PEI and in the other hand the repulsion between these groups, which consequently decrease the hydrodynamic volume of the polymer and the number of accessible amide groups to PEI. This phenomenon is commonly known as the charge-shielding effect [118].

In literature, various studies reported the delaying effect of the above-mentioned salts. The gelation time did increase from less than one hour at 126 °C to 6 hours at 176.6 °C when sodium carbonate was added to the PAtBA/PEI gel [130] and from 3 hours to 15 hours at 85 °C for a PHPA/PEI gel [33]. The addition of sodium carbonate did not affect the thermal stability and the strength of PAtBA/PEI gel and PHPA/PEI gel when tested in sandpacks [136]. However, the main issue with sodium carbonate was the compatibility problems with field mixing water. Ammonium chloride (NH_4Cl) was reported to overcome these compatibility issues and succeeded in delaying the gelation of the PAtBA/PEI at 150 °C to 90 minutes [129]. Despite this success, it was found later that the addition of NH_4Cl resulted in weaker gels compared to NaCl-added or salt-free gel systems [118]. Sodium chloride (NaCl), on the other hand, did not have compatibility issues and did not affect the gel strength but its retardation effect was too short for field implementation. All these problems with retarders encouraged the investigation of other techniques, which affect the crosslinking rate by affecting the crosslinker rather than the polymer.

1.8.2 Nanoparticles

Nowadays, nanotechnology is gaining a huge interest in the oil industry [137, 138]. The first use of nanoparticles for gelation delay was investigated for PHPA/chromium (III) acetate gels [139]. Polyelectrolyte complexes (PECs) were used to entrap the Cr(III) ions and control their release. PECs are usually formed, through strong coulomb interactions, when two solutions of oppositely charged polyelectrolytes are mixed as illustrated in **Figure 1.26** [140]. The PECs, in that study, were formed by the electrostatic interactions of highly charged cations (PEI) and highly charged anions (Dextran Sulfate DS) which resulted in nanoparticles of 100 to 200 nm. The approach succeeded in delaying the gelation time from 30 min to 4.5 days at temperature of 40 °C.

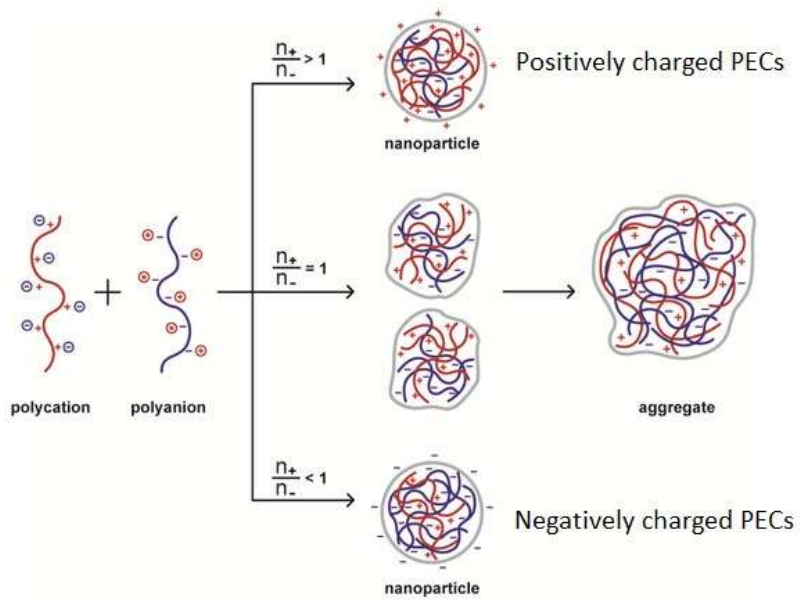

Figure 1.26 : PECs charge and size as function of the polyelectrolytes charge ratios (nanoparticles are formed when one charge of the polyelectrolytes is in excess otherwise aggregates are formed).[140]

During the investigation, the authors compared the gelation of PHPA/free PEI, PHPA/Unloaded PECs and PHPA/PECs+Cr(III). Interestingly, PHPA/Unloaded PECs elongated the gelation time to the order of several days compared to PHPA/free PEI. These findings encouraged the investigation on the gelation reaction of PHPA/Unloaded PECs [131]. The effects of various controlling factors on gelation time, mainly the effect of DS:PEI ratio, were examined. The PEI:DS mixture succeeded in delaying the onset of the gelation with up to 12 hours at 100 °C and stronger gels were formed compared to the inorganically crosslinked polymer gels. Nevertheless, and despite this success, the use of DS at the commercial scale in oilfields was impossible. Since DS is too expensive (10000 USD/kg) and is mainly used in the pharmaceutical industry as a controlled-release agent [132]. In an effort to substitute the DS with cheaper readily available chemicals, the 2-Acrylamido-2-methylpropane sulfonic acid (AMPSA) monomer, which is produced at 8 USD/kg, was investigated as a potential replacement. The AMPSA successfully delayed the gelation in a similar way to the DS. The gelation time of the PHPA/PEI+AMPSA gel was around 120 hours at 100 °C compared to only 13 hours for PHPA/PEI+DS gel at the same temperature [132].

1.8.3 Derivatives

The use of polyethylenimine derivatives such as polypropylene imine has been reported in literature as one of the most effective methods to elongate the gelation time. In a patent, Hardy reported the first use of a polyethylenimine derivative [133]. He found that the time required for the crosslinking of a PAtBA, with a polyethylenimine chelated with zirconium, was increased by a factor of two compared to a non-chelated polyethylenimine. The same delaying effect was observed when polyamino acid was used to form a complex with PEI to constrain it from attacking the PAtBA polymer [73]. In the above scenarios, chemical species are complexed permanently with the PEI's

amine groups to reduce the number of available crosslinking sites. One can see that this mechanism is similar to that of nanoparticle complexes, however the main difference between the two, is the resulted particles size and the interaction type (permanent or temporary). In other scenarios, the chemical structure of PEI is itself altered. It was the case for a derivatized-PEI (d-PEI), where some of the amine groups were converted to amides [73]. Here, the amide groups must be hydrolyzed back to free amines before the crosslinking can take place, which result in the gelation delay. The PAtBA/d-PEI gel provided an excellent gelation time of 13 hours at 149 °C compared to only 0.3 hour at 130 °C for a classic PEI. A 100% permeability reduction was also maintained at a temperature as high as 190.5 °C. Another modified PEI (PEI-GX) was also reported to delay the gelation of a terpolymer of AM/AMPSA/N-dodecyl acrylamide (N-DDAM) [134]. The gelation time of this system reached 30 hours at 100 °C for a PEI modified at 80%, which is 7.5 times higher than that when a non-modified PEI is used. The nature of PEI modification was not disclosed, however and regarding the commercially available PEIs, the modified PEI can be an ethoxylated PEI at 80%, where the some of the amine groups are converted to hydroxyethyl groups as shown in **Figure 1.27**.

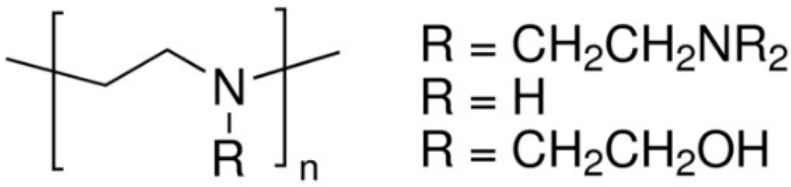

Figure 1.27 : the chemical structure of the 80 % ethoxylated PEI.

1.8.4 Accelerator

Researches on PEI crosslinked polymer gels were not limited on high temperature applications. Ultralow temperature reservoirs were also considered for gel treatments as discussed for the PHPA/PEI gels. However, the high polymer and crosslinker concentrations, used to achieve reasonable gelation times at low temperatures, are technically and economically unacceptable. Therefore, Reddy et al. [95, 123] investigated the use of chemical activators to increase the PEI reactivity and consequently decrease the reactants loadings needed to achieve the same gelation time. Theoretically, the maximum number of crosslinking sites of both the polymer and the crosslinker should be accessible and available to achieve the best gelation performance using the lowest reactants loadings. However, when the PEI's amine groups are protonated, they become less nucleophilic and unreactive [71]. They can be deprotonated and re-activated using amine-bases activators. Alkanolamines such as ethanolamine (EA), diethanolamine (DEA) and triethanolamine (TEA); olgomeric polyamines such as ethylenediamine (EDA), diethylenetriamine (DETA), triethylenetetraamine (TETA) and tetraethylenepentaamine (TEPA) were all examined to activate the PEI through one of the reaction pathways shown in **Figure 1.28**:

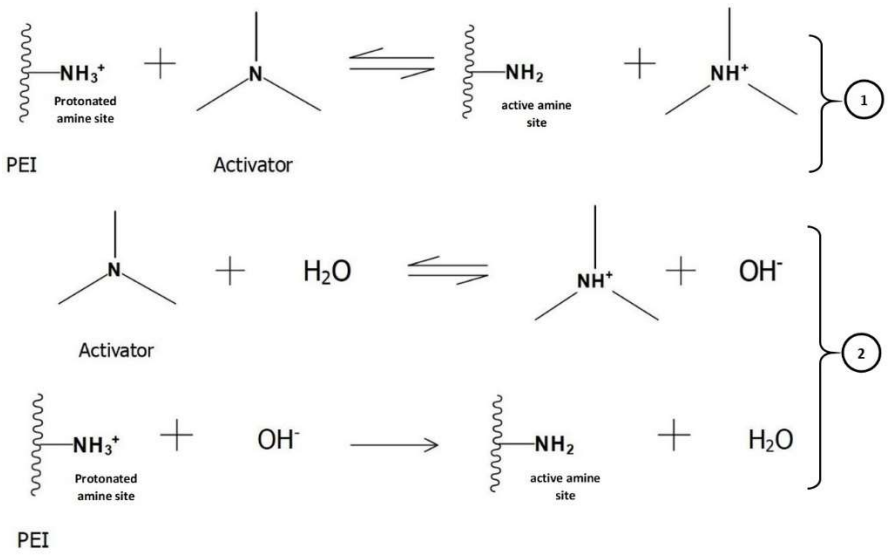

Figure 1.28 : Two potential ways for PEI activation using amine-based activators.[95].

These activators were found to effectively reduce the gelation time of the PHPA/PEI gel at 26.6 °C and of the PAtBA/PEI gel at 71.1 °C. They allowed also to reduce by 30 to 50% the needed amount of reactants to obtain a given gelation time. This was the case for a specific concentration of activators, while higher amounts acted inversely as in the case for EA and TEA [123]. Moreover, the accelerating effect of activators was found to decrease with temperature, which was explained by the lower deprotonation abilities of these activators at higher temperatures. On the other side, the effect of these activators on the final gel strength was not reported.

1.8.5 Solid particles

The PEI crosslinked polymer gels were known to form strong gels especially when low molecular weight polymers are used. “Ringing gels” were reported for the PAtBA/PEI system [141]. However, the enhancement of the final gel strength for near wellbore applications by adding solid particles such as cement, rigid setting materials (Rsm), silica flour and coal fly ash (CFA), was also reported. The cement was first added as a fluid loss agent which can form an additional barrier when it filtrates inside the matrix [142]. The gelation reaction of a PAtBA/PEI gel with “dykerhoff class-G cement” were evaluated at 90 °C and 100 °C [135]. The mixture showed an excellent shutoff behavior in laboratory experiments and withstood differential pressures of up to 180 bars. It was then applied in two production wells in a Syrian oilfield, the first well (118 °C) showed a good response and the net oil production increased initially by 2500 barrel of oil per day (BOPD) then stabilized at 1000 BOPD during one year of production, while, the water cut decreased from 63% to 25%. The production in the second well (144°C) was sadly lost. The gel/cement mixtures showed some drawbacks such as the interaction between the cement retarders and the gel, the need to drill out a part of the system from the well, the difficulty of treatment design at high temperatures. These drawbacks encouraged to replace the cement by other inert materials. The choice was rapidly fixed

on silica flour because of its inert nature, similar particle distribution, cheaper price and availability [143]. The effect of temperature, permeability, and silica flour percentage on the leakoff and sealing abilities of a gel/silica flour mixture were thus investigated [144]. The percentage of silica flour was found to have the greater effect on the leakoff percentage, while the other two parameters had no effect. Moreover, the gel/Silica flour mixture was reported to withstand differential pressure of up to 172 bars which is similar to that of the gel/cement mixture. Some authors recommended to add the cement to the gel/silica flour mixture to further strengthen the system. This new mixture was successfully employed in sealing a 186 meters interval length of a dead well with a bottom-hole temperature of 148 °C in Syria [142]. However, the main drawback of the above two systems was the use of high silica flour and/or cement loadings (50%). The solution was in rigid setting materials (Rsm) that can be added in lower percentages (<5%). These Rsm are low-viscosity metal oxychloride-type cements, which set rapidly at a given temperature and limit the gel penetration to the matrix. They were reported to develop high compressive strength of up to 275 bars in few hours and to resist temperatures of up to 204 °C. The PAtBA/PEI+ Rsm gels were mainly employed in the Cantarell Field in Mexico [107]. Other proposed inert materials such as starches and water swellable materials which offer the same leakoff rates as silica flour but using lower loadings was reported in literature [143]. Further efforts by Adewunmi et al. [145] led to coal fly ash (CFA) as a potential additive to reinforce PAM/PEI gels. CFA is an inorganic waste material constituted essentially of silica and alumina [146]. The gelation reaction and the viscoelastic behavior of the PAM/PEI+CFA gels were evaluated at 90°C, where the results showed a delayed gelation times and an improved viscoelastic behavior for these systems. More recently, Chen et al. investigated the reinforcing performance of nano-silica on PAM/PEI gels through core flooding tests in sandpack. The gel strength and stability were highly improved thanks to the hydrogen bonding between the nano-silica and PAM. As a result, the stability was increased 10 times from 18 to 180 days at 130 °C. While, the shutoff ratio was maintained above 80% (during 180 days at 130 °C) when nano-silica was incorporated compared to only 14% for a common PAM/PEI gel at the same conditions [147].

1.9 Successful applications around the world

As presented earlier, various PEI crosslinked polymer gels and improvements have been examined in laboratories. Among the different PEI crosslinked polymer gels, the PAtBA/PEI was the only system to be applied in oilfields at the large scale. Here below, we are representing some of its applications in three different regions of the world:

1.9.1 North Sea

The first application of the PAtBA/PEI gel was in the North Sea region. The B-21A well, in the Ekofisk field in Norway, was producing 60% water after three years of its drilling. A gel treatment using the PAtBA/PEI gel was implemented to seal the voids created by the early acid treatments on the well [71]. The targeted zones were at two intervals: 10953-10963 ft and 11000 -11013 ft. A cool down of the near wellbore area was first implemented to decrease the downhole temperature from 126.6 °C to 82.2 °C then 550 barrels (bbls) of the PAtBA/PEI gel were injected. The water production in the well did not decrease. However, the upper target zone which was producing 100% water was successfully sealed. Another well in the North Sea, the A-13 well in the "Åre" formation of the Heidrun field, was producing undesirable high gas quantities because of a high permeability flow channel, which connects the upper part of an open-hole gravel pack to the gas-filled sand layer. The placement of 100 m^3 PAtBA/PEI gel, at a downhole temperature of 88 °C, helped in reducing the gas oil ratio of the well from 700 to 200 Sm^3/ Sm^3 [148]. The third case is the A-01 well in the Valhall field. The well was suffering from a leak between the production tubing and the annulus that had to be re-established immediately according to the regional safety regulations [149]. This was achieved by injecting only 28 bbls of the PAtBA/PEI gel, which helped in plugging the leak and decreasing the unstable annulus pressure from 90 bars to 24 bars.

1.9.2 Middle East

PEI crosslinked polymer gels were thoroughly studied for application in Saudi Arabia oilfields [150, 151]. Al-Muntasheri et al. [129] reported the results of a successful gel treatment in a high temperature (149 °C), high-pressure (482.6 bars) horizontal gas well, that was producing at a water cut of 100%. The resistivity log analysis helped in identifying the water production zone and the laboratory work helped in evaluating the adequate gel formulations. During the execution phase, the well showed a good injectivity with injection pressure of less than 4000 psi, which allowed the use of high polymer loadings to prepare the gel. A pre-flush of 120 bbls of water +KCl was first injected to cool down the near wellbore area from 149 °C to 115 °C, followed by 150 bbls of the optimized gel and 5 bbls of the gel+ silica flour mixture. The well remained closed for 3 days and upon its opening, the water cut decreased by 42% and the gas rate increased from 2.2 to 17 million standard cubic feet per day (MMSCFD) as shown in **Figure 1.29**:

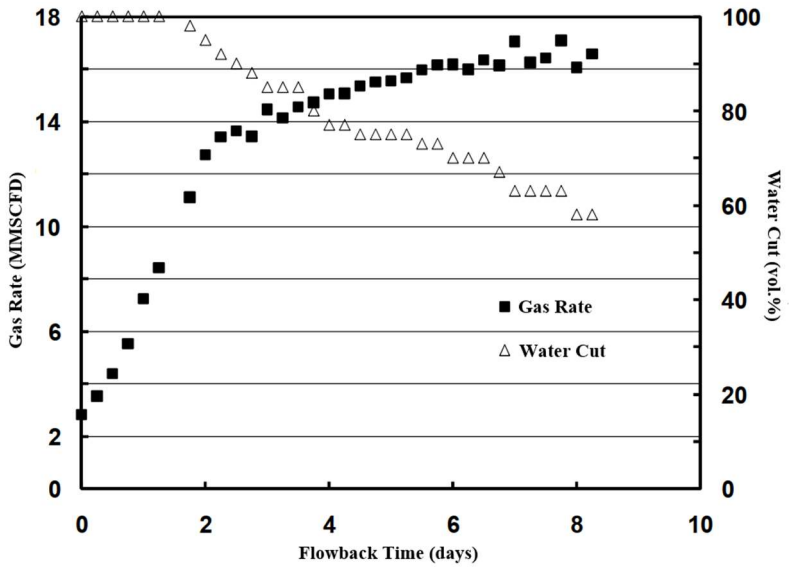

Figure 1.29 : Gas rate and water cut during the flowback in the treated horizontal gas well.[129]

Another open-hole horizontal well in the Wafra Ratawi field was the subject of the first gel treatment in Kuwait using the PAtBA/PEI gel [152]. The oil production of the well was decreasing from 794 BOPD to 680 BOPD and the water cut increased from 75% to 82% during the course of two months. The engineers decided to treat the toe side of the well using 850 bbls of the PAtBA/PEI gel. The heel side of the well was first isolated using a non-damaging gel system based on a modified Hydroxyethyl Cellulose (HEC) and a metal-oxide crosslinker. After the treatment, the oil production of the well increased by 25% from 680 BOPD to 840 BOPD and the water cut decreased to 70% from its initial value of 82%.

Recently, El-Beltagy et al. [153] reported the use of a PAtBA/PEI+ retarder gel and PAtBA/PEI +retarder+ Silica Flour gel in a high temperature (160.5 °C), high acidity (>300 ppm H_2S) offshore well in the red sea area. The Saqqara A1 well, located in the Saqqara field in the Gulf of Suez- Egypt, was producing with a water cut of 95%, after only one year of production. The production logging tool (PLT) analysis showed that the zone number 3, among the 4 productive zones, was the source of the excessive water. Thus, a gel treatment, using a PAtBA/PEI + retarder, was designed to treat the targeted zone. In order to isolate the upper zones, a PAtBA/PEI + retarder+ Silica Flour (50%) system was injected to form a temporary formation/wellbore barrier that was easily perforated and cleaned after the main treatment. Consequently, the water production decreased from 2300 barrel of water per day (BWPD) to almost zero BWPD.

1.9.3 Mexico

Mexico is the region where the greatest number of treatments using PEI crosslinked polymer gels were implemented [119, 154]. Ortiz Polo et al. [155] presented the results of 37 wells in the fractured carbonate and sandstone reservoirs in the southern region of Mexico, among a total of 93 cases treated with the PAtBA/PEI gel back to 2004. Natural fractures in these reservoirs promoted the water

conning into producer wells and caused a major challenge to handle the excessive produced water. Water shutoff treatments were the only convenient solution to treat a large number of the wells. As a result, most of the treated wells, which were producing over 80% water before treatment, experienced a 100% reduction in water cut after the treatment and in one case of them, the oil production increased from zero to 2000 BOPD.

The case of the offshore well "Abkatun-53A", in the Abkatun field in the Gulf of Mexico, was discussed in detail [130]. Water coning through high permeability streaks in the naturally fractured reservoir resulted in an excessive water production. In 2005, the well was producing around 4725 BOPD and 2196 BWPD (water cut 31.7%) with a bottom hole temperature of 141 °C. After cooling down the well with 250 bbls of seawater, about 315 bbls of the PAtBA/PEI gel were placed in the targeted zone. As a result, the water cut was decreased to 3.7%. This result was compared to a conventional cement squeezing implemented in an adjacent well having the same problem. By far, the gel treatment was better in reducing the water cut. Hernandez et al. [144] described the case histories related to the rising of the water oil contact in 3 wells in the Caan field in the Gulf of Mexico. The wells were producing with water cuts of 57, 60 and 57% respectively, and bottom hole temperatures of around 140 °C. After the treatment with the PAtBA/PEI gel, the water cuts were reduced to almost 0% as shown in **Figure 1.30**.

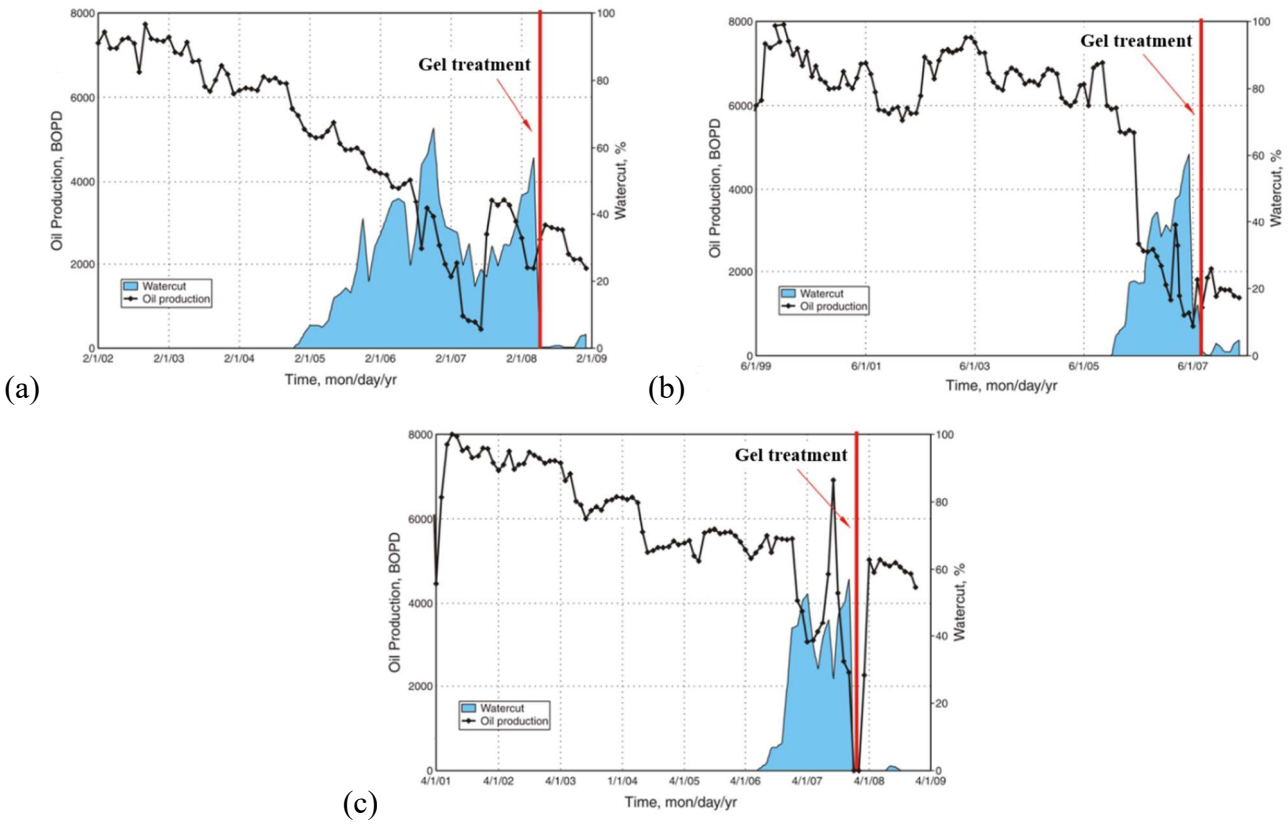

Figure 1.30 : Oil production rate and water cut before and after gel treatment in three well in the Caan field in Mexico (a) Well_1 (b) Well_2 (c) Well_3.[144]

1.10 Polymer gel evaluation methods

The success of any gel treatment depends heavily on the ability of scientists and engineers to control and adjust its gelation time and its final strength, as function of the technical requirements of the injection operation and the in-situ conditions of the reservoir. Likewise, the long-term thermal, chemical and biological stabilities of the gel, under the reservoir conditions, are critical and should be evaluated thoroughly. Gelation time is essential during gel placement in the targeted well because it determines how deep the gel can be placed in a formation. Overestimating gelation time may lead to injectivity problems such as premature gelation in the coiled tubing or in the near wellbore. In contrast, underestimating gelation time may lead to a gel washout once the well is re-opened. The gel strength and its ability to effectively block the targeted zone are important when resuming the injection of the chase fluids. While, the needed gel volumes, to completely occupy the fracture/ zone, can be estimated approximately; the gel strength must be well defined. Consequently, the gel rupture pressure, at which the gel breaks down and allows the chase fluids to pass through it, should be measured and the higher it is, the better is the gel treatment.

In a laboratory work, bulk tests and core flood experiments are usually conducted to evaluate the gel characteristics (gelation time, gel strength and gel stability) under the effect of the maximum number of controlling parameters such as reactants concentrations, reactants molecular weights, temperature, salinity, pH, presence of contaminants. Here below, we are briefly presenting the laboratory methods used to evaluate these characteristics:

1.10.1 Bottle test method

The bottle test method or the "sealed tube method" as documented also in literature [156] is the most popular method used to evaluate the gel parameters. It is an experimental method that provides a semi-quantitative measurement of gelation time, gel strength and gel stability [157]. In such method, glass bottles or tubes are filled with the specific polymer gel system to approximately one-half of their volumes and sealed with a cap. The bottles/tubes are then placed in a preheated oven or a thermostatic bath set at the test temperature and taken for periodical observations [72]. The gel flow behavior under gravity, upon inversion of the bottles, is assigned to a strength code.

Sydansk's gel code is the most commonly used code system [158], where gel flow behavior is represented through alphabets from "A" to "J" with each alphabet corresponding to a given flow behavior as summarized in **Table 1.3** and illustrated in **Figure 1.31**.

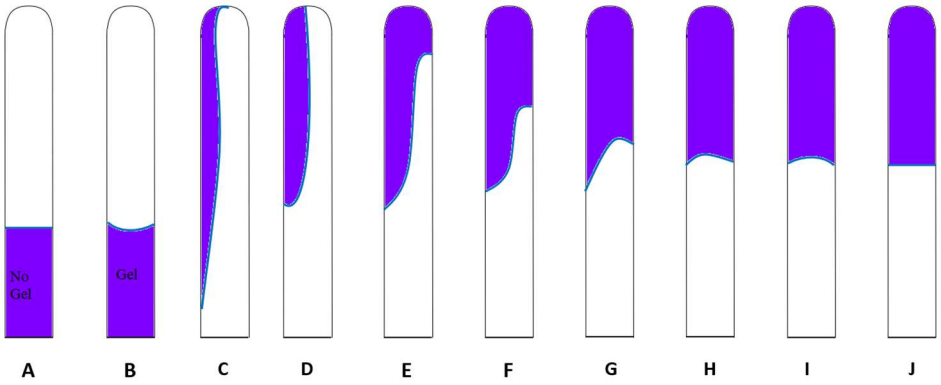

Figure 1.31 : Illustration of Sydansk's gel codes in the bottle test method.

Table 1.3 : Sydansk's gel code. [159]

Code	Observation	Description
A	No Detectable gel formed	The gel appears to have the same viscosity as the original polymer solution.
B	Highly flowing gel	The gel appears to be only slightly more viscous than the initial polymer solution.
C	flowing gel	Most of the gel flows to the bottle cap by gravity upon inversion.
D	Moderately flowing gel	A small portion (5—l0%) of the gel does not readily flow to the bottle cap by gravity upon inversion.
E	Barely flowing gel	The gel can barely flow to the bottle cap and/or a significant portion (> 15%) of the gel does not flow by gravity upon inversion.
F	Highly deformable non-flowing gel	The gel does not flow to the bottle cap by gravity upon inversion.
G	Moderately deformable non-flowing gel	The gel deforms about halfway down the bottle by gravity upon inversion.
H	Slightly deformable non-flowing gel	Only the gel surface slightly deforms by gravity upon inversion.
I	Rigid gel	There is no gel surface deformation by gravity upon inversion.
J	Ringing rigid gel	A tuning fork-like mechanical vibration can be felt upon tapping the bottle.

Stavland et al. [160] proposed a more simplified code where numbers from 0 to 3 give the state of the gel as given in **Table 1.4**. However, the authors did not provide any visual illustration of these codes. When compared to Sydansk's gel code, the following superimpositions can be accepted: (code 0 = code A), (code 1 = code B), (code 2 = code C to F) and (code 3 =code G to J).

Table 1.4 : Stavland's simplified gel code.

code	Observation
0	No gel
1	Indications for gel
2	Floating gel
3	Rigid gel

The main advantages of the bottle test method are the non-destructive nature of this method (no shear degradation), the possibility of testing a larger number of samples at the same time, and the long period of observation that can be achieved (days to months). All these advantages qualify it as the easiest, fastest and cheapest evaluation method. On the other side, this method must be considered with caution because it can lead to a subjective and mistaken characterizations [161] as the attribution of the codes using naked eyes differs from person to another.

1.10.2 Breakthrough vacuum method

The breakthrough vacuum method is an uncommon method used essentially to determine the gel strength [162] through the measurement device shown in **Figure 1.32**. The principle consists on measuring the gel strength through the pressure difference between the atmospheric pressure and the pressure in the filtering flask [163]. For that, a gel sample (approximately 25 ml) is placed in the ampoule and the vacuum pump is turned on. When the gel breaks into to the intermediate flask, the maximum pressure indicated on the pressure meter gives the gel strength [164]. This value is then corrected by considering the breakthrough vacuum value of the preparation phase alone (water or oil). A breakthrough vacuum value of 0.007 MPa for water was reported in literature [163].

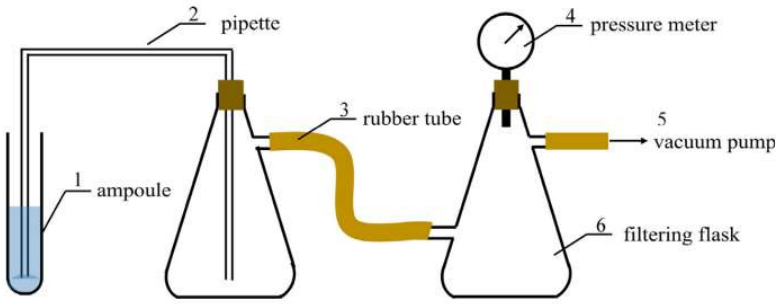

Figure 1.32 : The measurement device of the breakthrough vacuum method.[164]

1.10.3 Steady shear method

Steady shear viscosity measurements have been extensively used to determine the gelation time [86]. It is a quantitative and an accurate method for gelation time determination compared to the bottle test method [165]. The viscosity of the gelant samples is measured at a fixed shear as function of time. The gelation time correspond to the time when the viscosity starts to build up sharply or more precisely the inflection point on the curve of viscosity versus time [166] as shown in **Figure 1.33**:

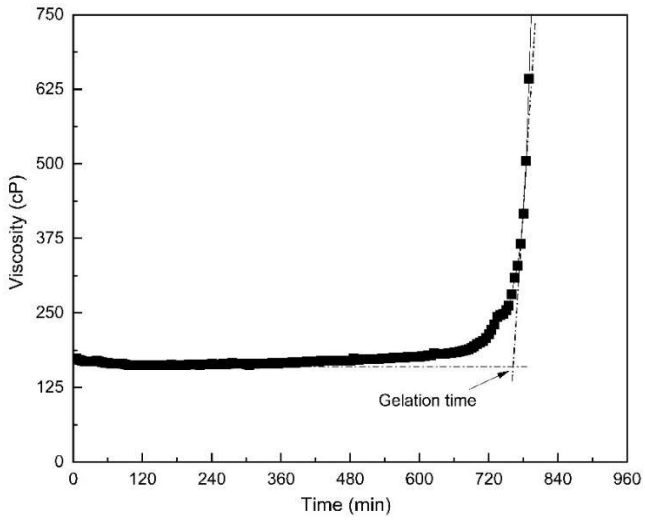

Figure 1.33 : Gelation time determination in the viscosity versus time curve.

Some authors divided gelation time into an initial gelation time (IGT) and final gelation time (FGT) when plotting viscosity versus time [167] as depicted in **Figure 1.34**. Nevertheless, defining a final gelation time is theoretically inaccurate as gel systems have infinite viscosities and not a plateau viscosity. The latter results from the degradation of the gel network under shear. Other authors considered the gelation time as simply the elapsed time from preparation to when the viscosity of the gelant reaches 1000 cP [168].

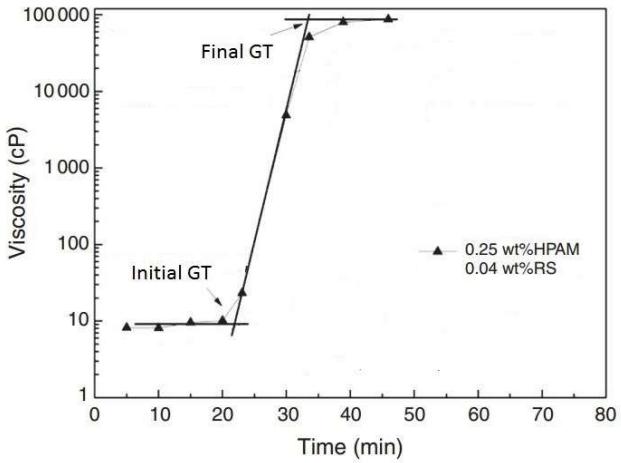

Figure 1.34 : Initial (IGT) and final (FGT) gelation time determination in the viscosity versus time curve.[169].

Despite being the simplest rheological method for gelation time determination, the steady shear viscosity has however one major drawback. The shear flow effect on the gelation reaction and gel structure, especially near the gel point, is a matter of debate between those considering a positive effect [170, 171] and those considering a negative one [172], which influence on the accuracy of this method.

1.10.4 Dynamic shear Method

Polymer gels are viscoelastic systems, which means that they exhibit intermediate properties between those of elastic solids and viscous liquids [85]. The elastic nature dominates over short periods of applied stress while the viscous nature becomes more evident over long periods [108]. The elastic and viscous responses are presented respectively by the storage modulus G' and the loss modulus G". The storage modulus G' measures the ability of the material to store elastic energy that can be recovered eventually, while the loss modulus G'' measures the amount of mechanical energy that is transformed into heat because of the viscous forces. The ratio of the loss modulus G" to the storage modulus G' defines the phase angle δ, which is equal to zero for an elastic solid and 90 degree for a newtonian liquid. The three quantities are defined below:

$$G' = \frac{\tau_0'}{\gamma_0} \qquad \text{Equation 1.3}$$

$$G'' = \frac{\tau_0''}{\gamma_0} \qquad \text{Equation 1.4}$$

$$Tan\ \delta = \frac{G''}{G'} \qquad \text{Equation 1.5}$$

Where, τ_0' is the maximum component of the elastic stress in Pa, τ_0'' is the maximum component of the viscous stress in Pa and γ_0 is the maximum strain in %.

Dynamic shear method consists on applying small sinusoidal shear deformations on the gelant or gel system and monitoring the evolution of the storage (G') and loss (G") moduli as function of time or frequency, allowing to determine both the gelation time [173, 174] and gel strength [106]. First, the

gelation time was documented in literature to be at the crossover of G' and G'' (tan δ=1) as assumed by Tung and Dynes [175]. While, Winter and Mours suggested that the gelation time should be determined at the intersection of the tangent of the shift angle (tan δ= G''/G') at several frequencies as function of time [176]. The two definitions are highlighted below in **Figure 1.35**:

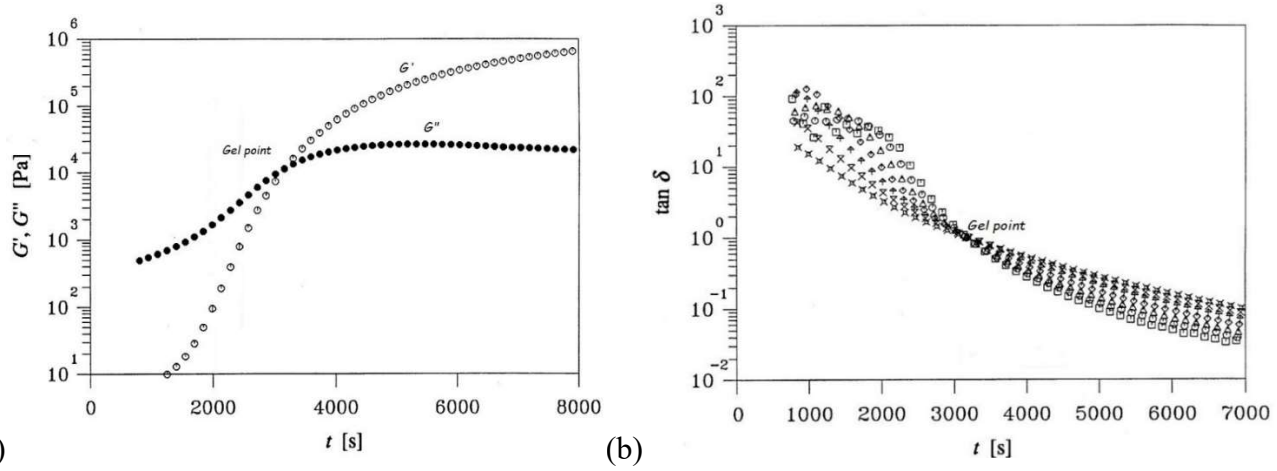

(a) (b)

Figure 1.35 : Gelation time determination as defined by (a) Tung and Dynes, (b) Winter and Mours.[176].

On the other side, the gel strength was directly correlated with the elastic or storage modulus (G') [106]. In fact, the monitoring of the storage modulus as function of time during a gelation reaction reveals three major phases [112] as shown in **Figure 1.36** : an induction phase where G' is negligible, an abrupt-increase phase where G' increases monotonically and a final phase where G' reaches an equilibrium plateau. This equilibrium value was considered as the quantitative representation of the final gel strength [177]. Moreover, when monitoring the storage modulus as function of frequency for a liquid-like gelant solution that transforms to a non-flowing gel system, the slope of the storage modulus starts to decrease from an initial value of 2 for the liquid-like non-crosslinked gelant solution to become totally independent of the applied frequency for the fully set crosslinked gel system [178] as shown in **Figure 1.37**. This plateau value is considered as the final gel strength.

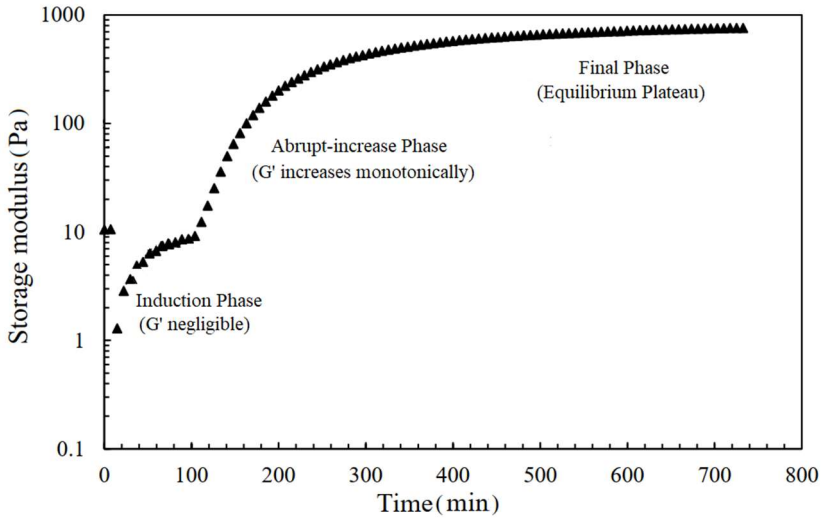

Figure 1.36 : The typical variation of the storage modulus as function of time during a gelation reaction.[117]

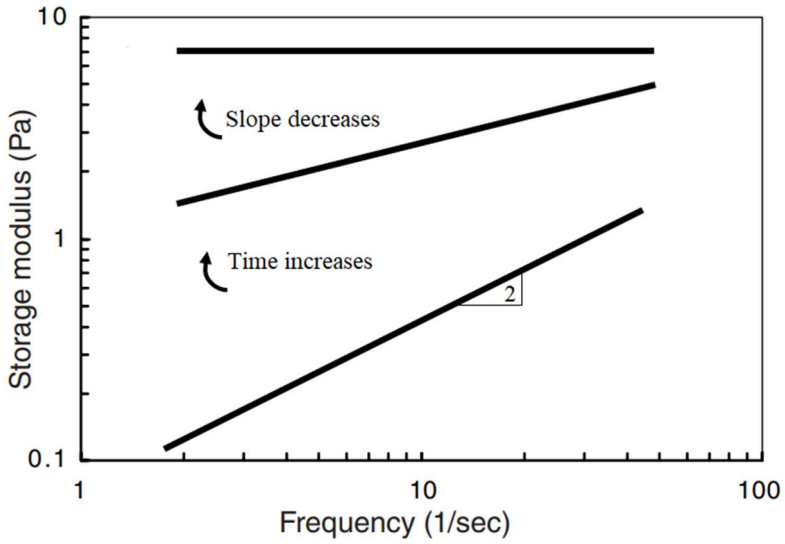

Figure 1.37 : The typical variation of the storage modulus as function of frequency from a liquid-like gelant solution to a fully set polymer gel.[106]

Although dynamic rheology provides a consistent polymer gel description, it remains a time consuming, expensive (when using high temperature and high pressure equipment) and invasive (if the investigation parameters are not well optimized) [85].

1.10.5 Low field nuclear magnetic resonance

In order to develop new methodologies that allow a practical and accurate monitoring of gelation time and gel strength characterization, Romero-zeron et al. [161] evaluated the use of low field nuclear magnetic resonance (NMR) to investigate the gelation reaction and gel states of the PHPA/chromium (III) acetate system. As the bulk relaxation rate, which is a fluid property that characterizes how easily the protons give off energy to one another, is related to the viscosity of the system through the relationship given below [179]; A low field NMR measurement was supposed to be able to track the variation of viscosity observed macroscopically.

$$\frac{1}{T_{2B}} \propto \frac{\eta}{T}$$ Equation 1.6

Where $\frac{1}{T_{2B}}$ is the bulk relaxation rate in s^{-1}, T_{2B} is the time for the signal to disappear in the reverse plane, η is viscosity and T is the absolute temperature.

The authors succeeded to represent the bulk relaxation rate as function of reaction time and extract the precise liquid/solid transition or the gelation time as illustrated in **Figure 1.38**.

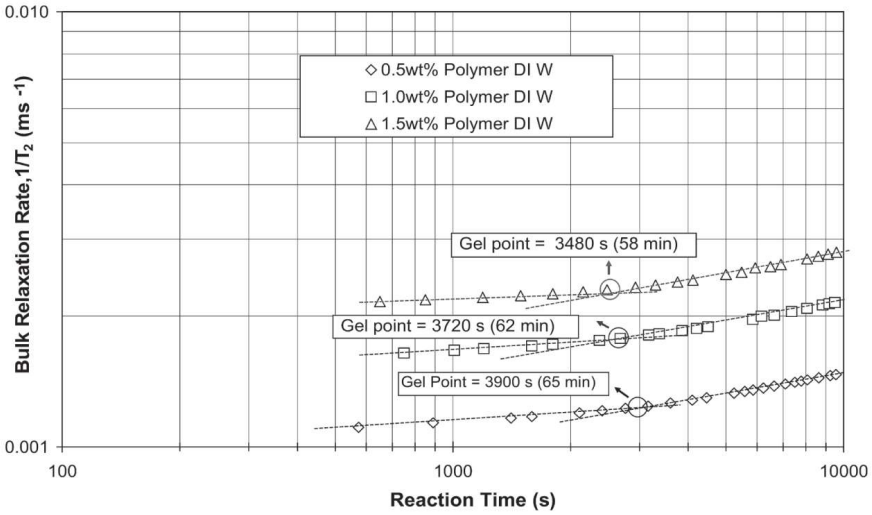

Figure 1.38 : Bulk relaxation rate obtained using low-field NMR versus reaction time for the PHPA/chromium (III) acetate system.[161].

The authors confirmed also that the low field NMR could observe shifts in gelation time as function of polymer concentration, crosslinker concentration and salinity of preparation water and was even able to detect the onset of gel degradation. On the other side, they failed to establish the relationships between the low field NMR and the dynamic rheological measurements in terms of gel strength.

The low field NMR method as an unbiased and nonintrusive technique approved to be reliable in gelation time determination. It was considered as the best alternative, to the previously discussed rheological and observation methods, to study the gelation time in porous media. Despite these promising features, no further development of this technique is reported in literature.

1.10.6 Differential scanning calorimetry

Differential scanning calorimetry (DSC) is a thermo-analytical technique which provides quantitative and qualitative information, as a function of temperature or time, about the physico-chemical variations (endothermic/exothermic processes, heat flow and changes in heat capacity) associated with materials transitions [180]. For instance, DSC has been largely used to study the kinetics of crystallization [124]. On the other side, as the stability of the polymer/crosslinker bonds or interactions depends heavily on the temperature and the energy which they can sustain [181], DSC

was employed in studying the thermal stability and degradation temperature of various polymer gels [182-184].

More recently, and since the crosslinking reactions are associated with temperature and heat release phenomenon similarly to the crystallization processes, DSC was investigated as a promising technique for studying the gelation reaction and kinetics of polymer gels [111]. The gelation kinetics of single or multi-crosslinked, emulsified or non-emulsified gel systems, during an isothermal or a non-isothermal gelation process, were reported in literature [116, 185, 186]. In such DSC experiments, the gelant samples are loaded and sealed in aluminum hermetic pans, then examined following a curing scheme wherein temperature is either fixed at a constant value (isothermal process), ramped with a constant gradient (non-isothermal process) or a combination of both schemes (non-isothermal/isothermal process). The heat released during the process is then used to calculate the fractional gelation (x_t) as function time "t" using the following equation:

$$fractional\ gelation = x_t = \frac{the\ heat\ released\ up\ to\ time\ t}{the\ total\ heat\ released\ during\ the\ process} \quad \text{Equation 1.7}$$

This allows to obtain curves of fractional gelation as function of time as shown in **Figure 1.39**. The effect of different controlling parameters can be assessed at any given fractional gelation value, while gelation time is determined when fractional gelation is equal to unity [124]. The gelation kinetics such as the gelation rate constant and the reaction order are consequently obtained by modeling the fractional gelation experimental data with kinetics models such as the Rate model, Avrami model, Jeziorny model and Mo's model [185].

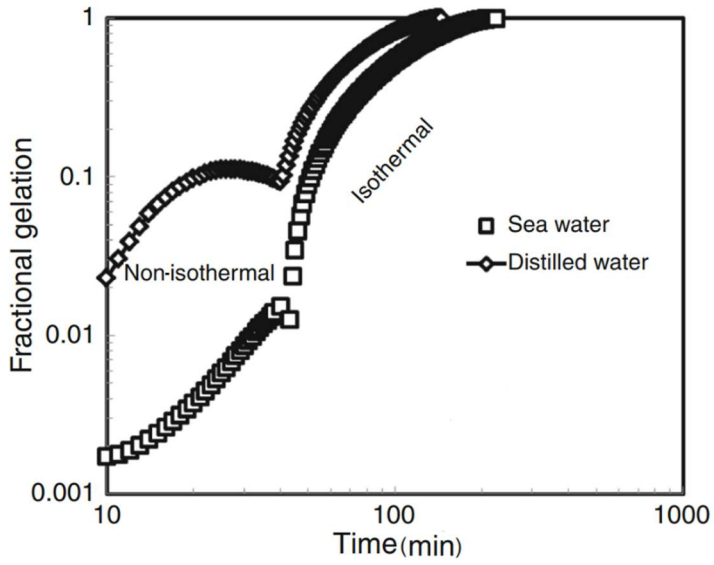

Figure 1.39 : Typical curve of fractional gelation versus time for a polymer gel system examined in a non-isothermal/isothermal process.[111]

1.11 Conclusion

The presented state of art dealt with four major axes. The first axe focused on naturally fractured reservoirs, their classifications and characteristics compared to the conventional non-fractured reservoirs alongside the four fundamental recovery mechanisms governing the oil recovery in these NFRs. The latter have atypical production/recovery behaviors that depend mainly on the wettability preference of the rock matrix, the fractures dimensions and orientation in regards the injection and production wells. The average ultimate recovery factor was only around 26 % in oil reservoirs and reached 61% in gas reservoirs after the primary and secondary phases. In type II and III fractured reservoirs, the ultimate oil recovery factor in water-wet reservoirs was comprised between 25 and 45 % compared to only 5 to 25% in oil-wet and neutral-wet reservoirs. In the second axe, we highlighted the chemical enhanced oil recovery methods employed in the fractured reservoirs with an emphasis on the three techniques used for mobility/conformance control namely foam, microbial and gels. The superiority of gel systems compared to the other two techniques was expressed through their high stability, high efficiency, low quantities needed to block the most conductive fractures and possibility of application in oil/gas reservoirs after water/gas flooding. Consequently, two major groups of bulk gel systems namely the inorganic sodium silicate gels and the organic polymer gels were presented. As the polymer gels can be formulated with a variety of base polymers (synthetic and biopolymers) and crosslinkers (inorganic, organic and natural), controllable gelation times and adjustable strengths can be designed. The third axe reviewed the different PEI crosslinked polymer gels reported in literature alongside with their latest improvements, as well as some of their successful applications around the world. As summary, PEI was tested to crosslink with different acrylamide-based polymers such as PAtBA, PAM, PHPA, HAP, AM/AMPSA copolymer, AM/AMPSA/N,N-DMA and AM/AMPSA/NVP terpolymers through nucleophilic substitutions and acid-base ionic interactions. The main reasons for testing these base polymers were the economical and/or the technical advantages of each one. Some polymers were much more cheaper and readily available in larger quantities compared to the others, as it the case for PHPA compared to PAtBA and HAP. While, some polymers reacted easily with PEI thanks to their reactive functional groups such as the PAtBA ester groups, compared to other polymers with functional groups that act inversely and delay the gelation such as the AM/AMPSA copolymer sulfonic groups; HAP polymer, for example, was investigated to benefit from the hydrophobic interactions of its functional groups to strengthen the gel. The molecular weight of the polymer played also an important role. Low molecular weight polymers (PAtBA, PAM) formed strong gels and were destined for matrix shutoff. While high molecular weight polymers (PHPA) had lower leakoff to the matrix and were intended for fractures shutoff. These PEI crosslinked polymer gels have been examined in a wide temperature application interval ranging from 4.4 °C to 205 °C, where they showed excellent gelation times at high

temperatures and could withstood differential pressures of up to 3600 psi. Despite the variety of gelation times offered by these gels, many improvements were incorporated to enhance the gelation time and gel strength. Inorganic salts such as sodium carbonate, sodium chloride and ammonium chloride were used as retarders thanks to their charge-shielding effect. However, they were found to affect the final gel strength and had some compatibility problems with mixing waters. PEI derivatives and nanoparticles, which constrain the PEI from attacking the polymer, were shown to be good alternatives for these conventional retarders. The only restriction for their large-scale application was the higher price. On the other side, for low temperature applications, chemical activators such as Alkanolamines and Olgomeric polyamines were used to activate the PEI unreactive sites, which were shown to accelerate the crosslinking rate at very specific amounts. Inert solid materials such as cement, silica flour, coal ash fly, Rsm, Starches and Water Swellable Materials were used to enhance the final gel strength for near wellbore applications and some of them were successfully applied with PAtBA/PEI gels in North Sea, Middle East and Mexico oilfields. While, for the other polymer/PEI gels, no field application is reported in literature. Finally, the fourth axe discussed the various evaluation methods used to study the gelation time, gel strength and gel stability of polymer gels. The principle of each method besides its advantages or limitations were presented. The bottle test method was the only method which allows to evaluate the three characteristics simultaneously with the possibility of testing a larger number of samples at the same time, and for long periods of observation. The steady and dynamic shear methods were the best accessible techniques to obtain consistent quantitative values of gelation time and gel strength if the shear effect is well determined and controlled. While sophisticated techniques such as NMR and DSC showed to be the most promising methods in studying the gelation time and kinetics. However, they stay time-consuming and cost-intensive methods which need to be optimized. For the case of the Algerian fractured reservoirs, where the reservoir temperatures are usually comprised between 60 and 100 °C, partially hydrolyzed polyacrylamide (PHPA) and polyethylenimines (PEI) seem to be the best base polymer and crosslinker respectively, regarding their ecological, economic and technical aspects. The PHPA is cheap and readily available and its height molecular weight makes it adaptable for fractures shutoff. While PEI is ecological with confirmed crosslinking capabilities at wide temperature ranges. On the other side, the PHPA/PEI systems were investigated only for the lower temperature conformance control applications. In those studies, the adequate characterization of the reactants was not considered, while numerous lacks still exist in terms of investigating and optimizing the thermal gelation of these systems under various physico-chemical conditions. Moreover, the crosslinking mechanisms between the two reactants were not fully investigated. Consequently, it became obvious that studying these systems for higher temperature applications while taking into account the physico-chemical characteristics of the reactants and their crosslinking mechanisms, represents a good working prospect for us.

Chapter II: Materials Characterization

2. Chapter II: Materials characterization

2.1 Products

Three partially hydrolysed polyacrylamides (PHPAs), kindly provided by "SNF Floerger-France", were employed as the base polymers. The PHPAs had different molecular weights and were provided in a powder form. Two polyethylenimines (PEIs), used as crosslinkers, were purchased from "Sigma Aldrich". They had also different molecular weights but were in a liquid form. The products are shown in **Figure 2.1** and their main physical and chemical characteristics communicated by the suppliers are summarized in **Table 2.1**. In order to obtain a more precise information on these products, a complete set of characterizations were conducted to determine their viscosity-average molecular weight ($\overline{M}_v$) using capillary viscosimetry, the PHPAs hydrolysis degrees and PEIs branching degrees using NMR, the water content and degradation temperature using thermogravimetric analysis (TGA).

(a) 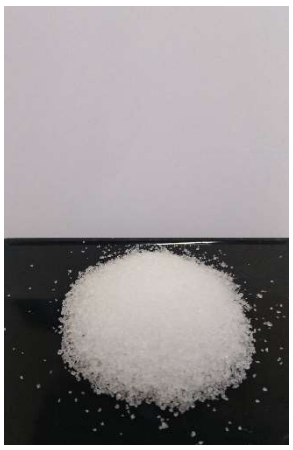 (b) 

Figure 2.1 : PHPA in a solid form provided by SNF Floerger (b) PEIs in liquid form from Sigma Aldrich.

Inorganic salts namely sodium chloride (NaCl), potassium chloride (KCl), calcium chloride ($CaCl_2$), magnesium chloride ($MgCl_2$), sodium sulfate (Na_2SO_4), sodium bicarbonate ($NaHCO_3$) were ACS (American Chemical society) grade salts purchased from "Sigma Aldrich". These salts were employed to prepare the different mixing waters. Distilled water, obtained from a milliQ system (18.2 MΩ.cm), was also employed during this study.

Table 2.1 : The main physical and chemical characteristics of the studied products as communicated by the suppliers.

Product name	Product code in this study	Average Molecular Weight (~Mw) (10^6 g/mol)	Hydrolysis or Branching degree (%)	Appearance & water content (%)	Relative density	pH	Median Lethal Dose (LD_{50}) (mg/Kg)
AN905 BPM	PHPA1	3~5	5	White granular solids (<1%)	0.6-0.9	5-9 @ 5 g/l	>5000
AN905 PG2	PHPA2	8~10	5				
AN905 SH	PHPA3	10~13	5				
Polyethylenimine, branched sigma code:408727	PEI25	0.025 by light scattering	NP	Odorless & colorless Viscous liquid (0%)	1.03	12 @ 100 g/l	>500-<2000
Polyethylenimine solution Sigma code:181978	PEI750	0.75 by light scattering	NP	Odorless & colorless viscous liquid (=50 wt% water)	1.08	~12 @ 100 g/l	500-2000

*NP: not provided.

2.2 Mixing water

The main mixing water referred in this study as "injection water", was a synthetic water prepared in the laboratory. It has similar composition and characteristics as the injection water of the Tin Fouyé Tabankort (TFT) reservoir in Algeria as summarized in **Table 2.2** and **2.3** respectively:

Table 2.2 : Injection water composition.

Salt type	Concentration (mg/l)
NaCl	820.2
KCl	75.1
$CaCl_2$	500.2
$MgCl_2$	333.6
Na_2SO_4	1422
$NaHCO_3$	253.0

Table 2.3 : Injection water characteristics at 25°C.

Parameter	Value
Total Dissolved Solids (TDS) (mg/l)	3404.1
Conductivity (ms/cm)	5.00
pH	8.34
Viscosity (cP)	0.91

2.3 Reactants molecular weights

The molecular weights of all the products (PHPAs and PEIs) were determined using capillary viscosimetry and based on the Mark-Houwink defined as follow:

$$[\eta] = K \times M_w{}^{\alpha} \quad \text{Equation 2.1}$$

Where $[\eta]$ is the intrinsic viscosity in (ml/g), M_w is the molecular weight in (g/mol), K in (ml/g) and α (dimensionless) are constants which are found experimentally for each polymer/solvent pair at a particular temperature [187]. In fact, the molecular weights determined through this method are viscosity-average molecular weights $\bar{M}_v$, in (g/mol), which are calculated using Equation 2.2 extracted from Equation 2.1:

$$\bar{M}_v = e^{\frac{1}{\alpha}(\log[\eta] - \log K)} \quad \text{Equation 2.2}$$

While K and α are reported in literature for various polymers/solvent pairs, the intrinsic viscosity should be measured. Also called the limiting viscosity number [188], the intrinsic viscosity estimates the macromolecules dimensions (hydrodynamic volume) in a solution. It is defined as the limit of the reduced viscosity (η_R) or the inherent viscosity (η_I) when the polymer concentration tends to zero as shown in the equations below [189]:

$$[\eta] = \lim_{c \to 0} \eta_I \quad \text{and/or} \quad [\eta] = \lim_{c \to 0} \eta_R \quad \text{Equation 2.3}$$

with:

$$\eta_I = \frac{ln\,(\eta_r)}{c} \quad \text{Equation 2.4}$$

$$\eta_R = \frac{\eta_r - 1}{c} \quad \text{Equation 2.5}$$

And

$$\eta_r = \frac{\eta}{\eta_s} \quad \text{Equation 2.6}$$

Where: η and η_s are the solution's and solvent's shear viscosity in (cP), η_r is the relative viscosity (dimensionless) and C is the polymer concentration (g/ml).

It is clear from the above equations that a simple measure of the relative viscosity will allow to determine the reduced and inherent viscosities. Plotting these two viscosities, measured at different polymer concentrations, versus the polymer concentration and extrapolating the two curves to the zero concentration allows to obtain the intrinsic viscosity graphically. Most importantly, dilute polymer solutions must be considered to measure an accurate intrinsic viscosity, as the polymer chains are isolated from each other at low concentrations.

The relative viscosities are usually measured using capillary viscometers, which consist on measuring the flow time of fixed volumes of the solvent and polymer solutions through a capillary tube. Ubbelohde viscometers with suspended ball level were the most known capillary viscometers used in this area [190]. However, they work only at atmospheric pressure and without control on shear rate. Rodriguez and co-workers [191] developed a new capillary viscosimeter which allows to measure the viscosity of dilute polymer solutions at controlled and very low shear rates and for temperatures even above the boiling point of the solvent.

Based on Poiseuille's law, the viscosity of the dilute polymer solutions (which exhibits a newtonian behavior) can be calculated by measuring the differential pressure between the two ends of a cylindrical capillary of length L and radius R, at flow rate Q:

$$\eta = \frac{\Delta P\, \pi R^4}{8\, Q\, L} \qquad \text{Equation 2.7}$$

The shear rate inside the cylindrical capillary can be also calculated using the following equation:

$$\dot{\gamma} = \frac{4\,Q}{\pi R^3} \qquad \text{Equation 2.8}$$

Consequently, the new capillary viscosimetry technique consists on measuring the pressure drop (ΔP) (using pressure sensors) of dilute polymer solutions that are injected at fixed flow rates (Q), using a syringe pump, inside a known internal radius and length tubing and at a fixed temperature as shown in **Figure 2.2**:

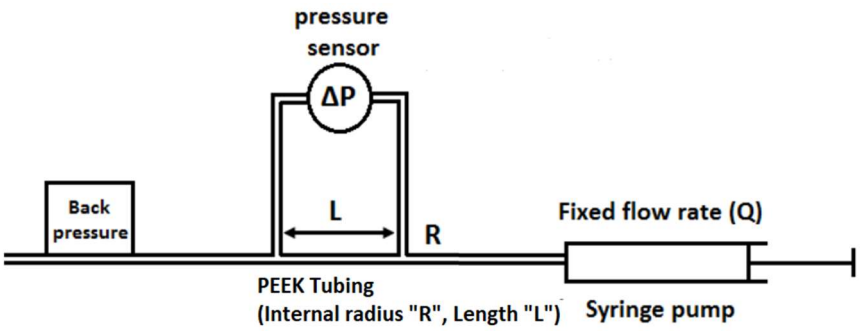

Figure 2.2 : The principle of the new capillary viscosimetry technique.[191]

Plotting the differential pressures ΔP versus the flow rates Q for the solvent and different dilute solutions should give linear curves and allows to calculate the relative viscosities:

$$\Delta P = \frac{8\,\eta\,L}{\pi R^4}\,Q \qquad \text{Equation 2.9}$$

$$\eta_{r_i} = \frac{\text{slope}_{\text{solution (i)}}}{\text{slope}_{\text{solvent}}} \qquad \text{Equation 2.10}$$

With η_{r_i} is the relative viscosity of a dilute solution (i) prepared at a fixed concentration.

The homemade capillary viscosimeter employed in this study is depicted in **Figure 2.3**. The solvent and dilute solutions were injected at fixed flow rates using a syringe pump (mid pressure neMESYS 1000N, Cetoni) inside a polyether ether ketone (PEEK) tubing having an internal radius of 254 μm and 1.3 m of length measured between the two ends of the pressure sensor. The PEEK tubing was kept inside an oven (CTO-20AC, Shimadzu) set at the test temperature, while a back pressure (Swagelok), placed at the end of the tubing, ensured no air bubbles get inside the system. The pressure drops were recorded using a pressor sensor (ABB) that can measure pressure drops comprised between 0 to 60 mbar. The data were collected via a videographic recorder (ScreenMaster 500F, ABB) and processed using the "Datamanager" software (ABB).

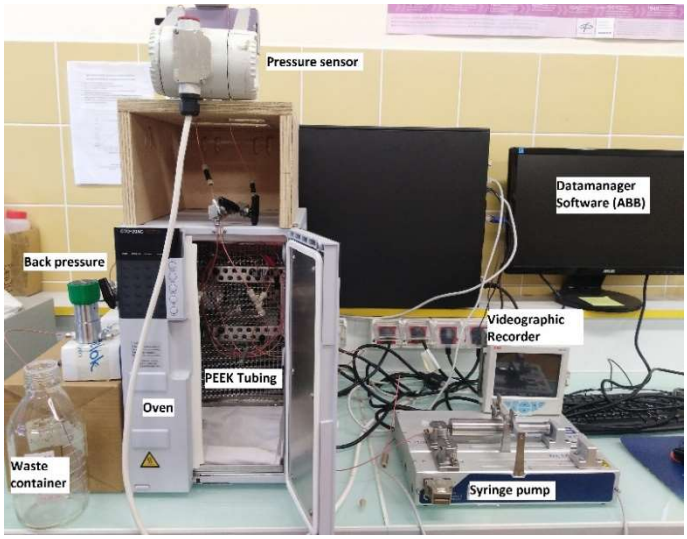

Figure 2.3 : The homemade capillary viscosimeter.

Stock solutions of PHPAs (5000 ppm) and PEIs (100000 ppm) were first prepared in 5 g/l NaCl water (solvent). For PHPAs, the powder was gently sprinkled into the vortex created by the vigorous stirring of the mixing water using a pale marine stainless-steel blade stirrer. Homogenization was kept for six hours at 500 rpm (round per minute). On the other side, the right amount of the liquid PEIs was homogenized in the 5 g/l NaCl water for only one hour using a magnetic stirrer. The stock solutions were stored at 6 °C and used when needed to prepare the diluted solutions. PHPAs dilute solutions were prepared at 100, 200, 300, 400 and 500 ppm, while PEI25 dilute solutions were prepared at 10000, 20000, 30000, 40000, 50000 ppm and PEI750 dilute solutions at 5000, 10000, 15000, 20000 and 25000 ppm. The solvent (5 g/l NaCl water) and the dilute solutions were then injected in the capillary viscosimeter at flow rates of 3µl/s ($\dot{\gamma} = 233.1\ s^{-1}$), 2.5, 2, 1.5, 1, 0.75, 0.5, 0.25µl/s ($\dot{\gamma} = 19.43\ s^{-1}$), and a fixed temperature of 25 °C.

Here below we are representing only one figure from each step of the data treatment process to finally obtain the intrinsic viscosity. First, the pressure drops recorded, using the videographic recorder, have the profile shown in **Figure 2.4**. The average value at each plateau is used to plot the pressure drop as function of the flow rate for the solvent and the dilute solutions as in **Figure 2.5**. The variations were fitted with linear functions and the ratio of the slope of a given dilute solution (i) to the slope of the solvent gives the relative viscosity as defined in Equation 2.10. The relative viscosities are then used to calculate the inherent and reduced viscosities through Equations 2.4 and 2.5. Plotting these two viscosities as function of the product concentration, as shown in **Figure 2.6**, allows to find the intrinsic viscosity (considered as the average between the two intercepts). The same procedures were repeated for the other PHPAs and PEIs solutions.

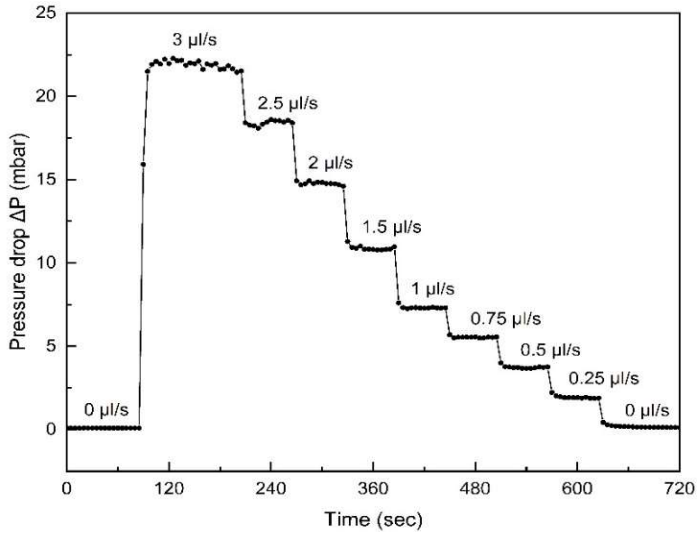

Figure 2.4 : Pressure drop profile as function of time at different flow rates for the solvent (5 g/l NaCl water) through the videographic recorder.

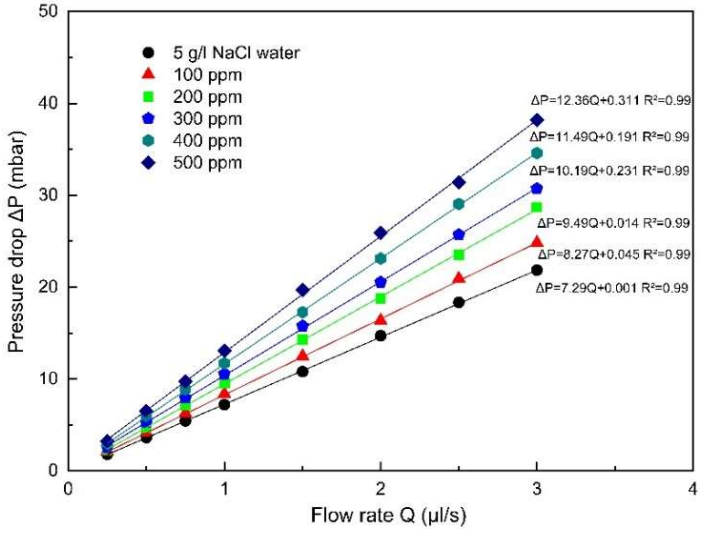

Figure 2.5 : Pressure drop versus flow rate curve for the solvent and dilute PHPA1 solutions with their corresponding linear fits.

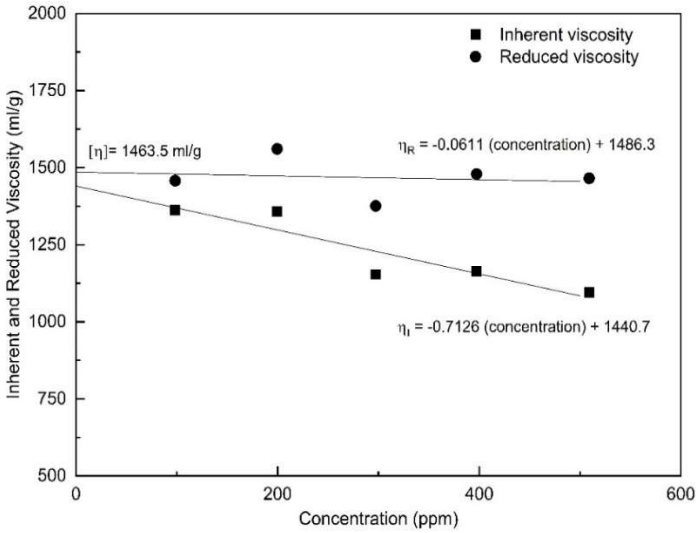

Figure 2.6 : Inherent, reduced and intrinsic viscosities of PHPA1.

The Mark-Houwink constants K and α were obtained from literature. For the three PHPAs, K was taken as 0.00631 and α as 0.80 [192], while for the two PEIs, K was taken as 1 and α as 0.26 [193]. The measured intrinsic viscosities and the viscosity-average molecular weights $\bar{M}_v$ of all the products are summarized in **Table 2.4**:

Table 2.4 : The products intrinsic viscosities and viscosity average molecular weights.

Product	Intrinsic viscosity [η] (ml/g)	Viscosity-average molecular weight ($\bar{M}_v$) (10^6 g/mol)
PHPA1	1460	5.1
PHPA2	1990	7.5
PHPA3	2560	10.2
PEI25	13.0	0.02
PEI750	32.8	0.67

2.4 Reactants hydrolysis/branching degrees

The hydrolysis degrees of PHPAs and the branching degrees of PEIs were determined using the NMR technique. The products were solubilized in deuterated water (D_2O) at a concentration of around 20 mg/ml and their proton (^1H) and carbon (^{13}C) NMR spectra were recorded at temperature of 25 °C on a Bruker AVANCE 400 MHz spectrometer equipped with a Z-gradient Bruker 5 mm BBFO (Braod Band Fluorine Observe) probe. The acquisition and processing parameters are summarized in **Table 2.5**. A TopSpin 4.0.3 software (Bruker BioSpin) was employed to analyze and process the spectra.

Table 2.5 : The acquisition parameters of the ^{1}H-RMN and ^{13}C-RMN spectra.

Parameter	^{1}H-RMN	^{13}C-RMN
Frequency (MHz)	400.13	100.61
Acquisition time AQ (s)	1.98	0.68
Spectral width SWH (Hz)	8250	24038
Fid size	32768	32768
Number of scans	32	20480

The ^{1}H-NMR spectra of PHPAs, as shown in **Figure 2.7** for the PHPA1, revealed two main peaks assigned respectively to the methylene group (CH_2) for shifts comprised between 1.5-1.7 ppm and the methine group (CH) for shifts comprised between 2.1-2.25 ppm [194]. However, these spectra do not allow any quantitative separation between the methine and methylene of the acrylamide units and those of the acrylate units. Consequently, the hydrolysis degree of PHPAs cannot be defined through proton NMR. On the other hand, the ^{13}C-NMR spectra of PHPAs allowed to separate four peaks: the methylene (CH_2) and methine groups (CH) of both acrylamide and acrylate units at shifts of around 33.8-36.7 ppm and 41.4-42.1 ppm respectively, the carbons in the amide groups ($CONH_2$) at 179.5-180.2 ppm and those in carboxylate groups (COONa) at 182.7-182.9 ppm. The use of carbonyl carbons for the quantitative determination of the hydrolysis degree of PHPAs has been reported [195, 196]. The hydrolysis degrees were thus determined using Equation 1.1, where the molar concentrations (X and Y) were taken as the integrated areas under the peaks at 180 and 182 ppm in ^{13}C-NMR spectra as shown for the PHPA1 in **Figure 2.8**.

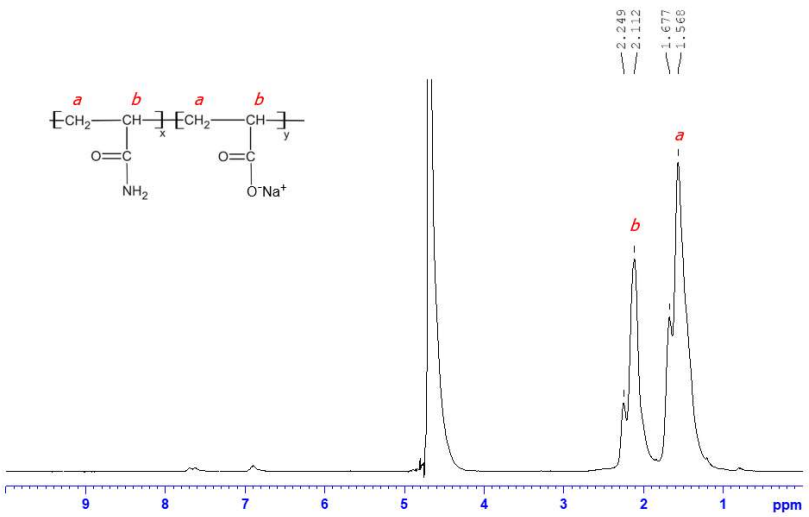

Figure 2.7 : ^{1}H-NMR spectra of PHPA1 at 25 °C.

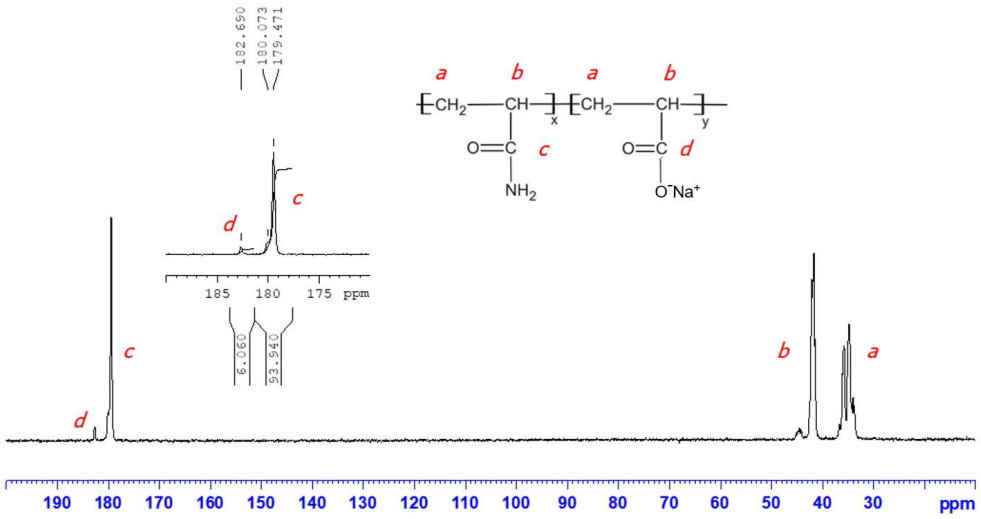

Figure 2.8 : ^{13}C-NMR spectra of PHPA1 at 25 °C.

The hydrolysis degrees of the three studied PHPAs are given in **Table 2.6**:

Table 2.6 : the hydrolysis degrees of the three PHPAs.

Product	PHPA1	PHPA2	PHPA3
Hydrolysis degree (%)	6.1	6.1	6.2

Similarly, the proton and carbon RMN spectra of PEIs were recorded to obtain the branching degrees. The ^{1}H-NMR spectra revealed only one major peak between 2.5-2.65 ppm, as shown in **Figure 2.9**, which corresponds to the methylene groups (CH_2) attached to the different amine substituents without separation between them [193]. Thus, the branching degree could have not been determined. In contrast, the ^{13}C-NMR spectra were characterized by eight major peaks as shown in **Figure 2.10**, with each set of peaks representing the methylene attached to a precise amine unit: peaks at 56.1, 53.1 and 51.1 ppm were assigned to (CH_2) attached to tertiary (N) amine units; peaks at 50.7, 47.7 and 45.7 ppm to (CH_2) attached to secondary (NH) amine units and peaks at 39.8 and 37.8 ppm to (CH_2) attached to primary (NH_2) amine units.

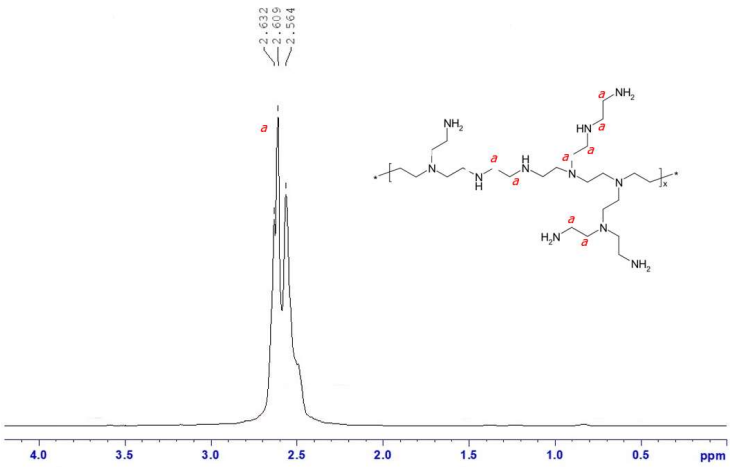

Figure 2.9 : ^{1}H-NMR spectra of PEI25 at 25 °C.

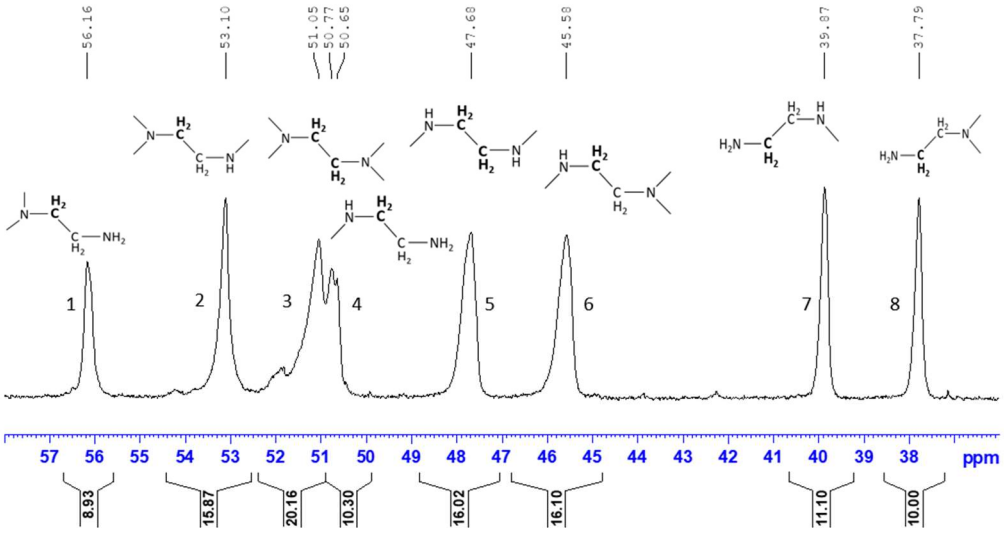

Figure 2.10 : ^{13}C-NMR spectra of PEI25 at 25 °C.

The integrated areas under the peaks (A_i) were employed to calculate the percentage of primary (NH_2), secondary (NH), and tertiary (N) amino groups in the two PEIs (PEI25 and PEI750), following the equations given below:

$$\%NH_2 = \frac{A_7+A_8}{(\frac{A_1+A_2+A_3}{3})+(\frac{A_4+A_5+A_6}{2})+(A_7+A_8)} \times 100 \qquad \text{Equation 2.11}$$

$$\%NH = \frac{\frac{A_4+A_5+A_6}{2}}{(\frac{A_1+A_2+A_3}{3})+(\frac{A_4+A_5+A_6}{2})+(A_7+A_8)} \times 100 \qquad \text{Equation 2.12}$$

$$\%N = \frac{\frac{A_1+A_2+A_3}{3}}{(\frac{A_1+A_2+A_3}{3})+(\frac{A_4+A_5+A_6}{2})+(A_7+A_8)} \times 100 \qquad \text{Equation 2.13}$$

The branching degrees were consequently calculated using the Equation 1.2, where D (dendritic units) and L (linear amine units) were substituted by %N and %NH respectively. The percentage of each amine unit and branching degrees for the two PEIs are given in **Table 2.7**:

Table 2.7 : The percentage of each amine unit (NH_2, NH, N) and the branching degrees (BD) for the two PEIs calculated from ^{13}C-NMR spectra.

Product	%NH_2	%NH	%N	Branching Degree (BD)
PEI25	36.8	37.0	26.2	58.6
PEI750	36.4	38.8	24.7	56.0

2.5 Reactants thermal degradation

The thermal degradation of the products alongside their water contents were studied using the thermogravimetric analysis (TGA). The experiments were carried out using a TA-Q50 TGA instrument. Products samples of about 5 mg were placed into an aluminum sample holder, heated

from 30 to 600 °C at a ramp rate of 10 °C/min and under a dynamic nitrogen atmosphere with a flow rate of 20 ml/min. **Figure 2.11** shows the weight percentage as function of temperature for the three PHPAs (PHPA1, 2, 3) and the two PEIs (PEI25, PEI750). The corresponding water contents of the product were calculated at 140 °C and are summarized in **Table 2.8**:

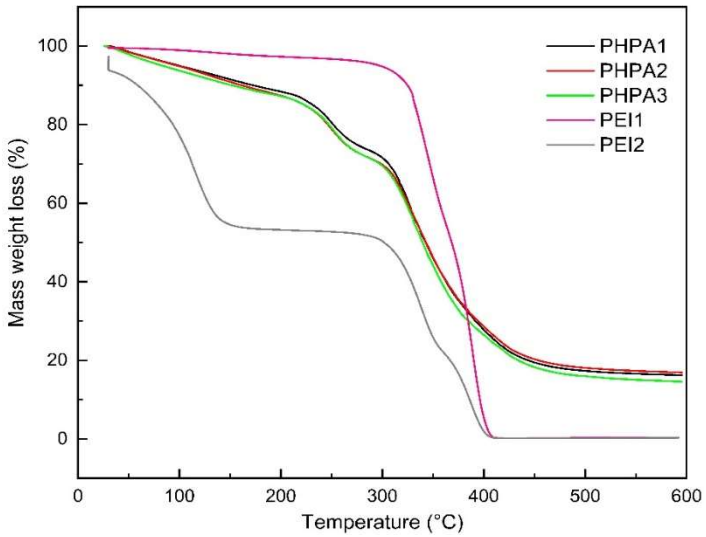

Figure 2.11 : Thermogravimetric analysis curves of the different products.

The observed thermal degradation curves of the PHPAs and PEIs were in good agreement with those documented in literature [197-199]. The PHPAs are degraded in three stages: the first one starts around 220 °C where PHPAs undergo irreversible chemical changes either through imidization reactions between the neighboring amide groups ($CONH_2$) or the dehydration of the isolated groups, which result in the formation of imides and nitriles and the release of ammonia (NH_3) and water (H_2O) respectively. The second and third degradation stages are not distinct from each other and occur at 320 °C for the second stage and above 400 °C for the third stage. The second stage is characterized by the release of CO_2 resulting from both the decarboxylation of the carboxylate groups (COONa) and the decomposition of imides, formed during the first stage. While, in the third stage, only the decarboxylation of the carboxylate groups continues to take place alongside the breakdown of the polymer backbone and the formation of paraffinic hydrocarbon materials. On the other side, the PEIs had one degradation stage comprised between 300 and 400 °C where products such as ammonia, ethylamine, pyrrole are released due to the random bond scissions.

Table 2.8 : The water content in each product.

Product	PHPA1	PHPA2	PHPA3	PEI25	PEI750
Water content (%)	7.8	8.3	9.2	1.8	44.1

2.6 Critical overlap concentration of PHPAs

In order to realize the gelation process, one of the most important parameters that should be determined beforehand is the critical overlap concentration "C*", which indicates the transition between the dilute and the semi-diluted solution regimes of the polymer as shown in **Figure 2.12**. In the dilute regime, the macromolecules behave independently because they are separated from each other, while in the semi-dilute regime, frictions are imposed on the macromolecules due to the chains overlapping and entanglement.

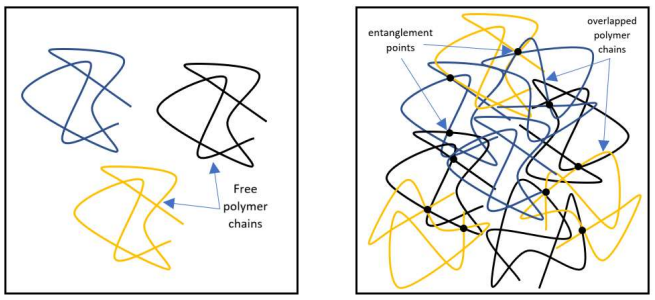

Figure 2.12 : Polymer-molecules interaction at different concentrations.

In a gelation process, the C* is the minimum concentration of the base polymer which is needed to obtain a continuous 3D structure (bulk gel) when a crosslinker is added to the polymer solution [81]. Several methods were used to determine the critical overlap concentration. Gomes and Costa [200] evaluated the use of the potentiometric titration to determine C* of a PHPA solution. Rodd et al. [201] used the Dynamic Light Scattering (DLS) to characterise the boundary between the dilute and semi-dilute regimes of xanthan solutions. However, rheological measurements were extensively employed to determine this parameter. When measuring the zero-shear specific viscosity **"η_{sp0}"** and the intrinsic viscosity **"[η]"** and plotting **"η_{sp0}"** versus the overlap parameter **"C.[η]"**, the critical overlap concentration will coincide with a slope change in this plot [202, 203]. Other recent variants of this method consist of plotting directly the zero-shear viscosity **"η_0"** versus polymer concentration **"C"** [201, 204] or the shear viscosity **"η"** at different shear rates versus polymer concentration **"C"** [205, 206].

As the determination of the C* for the three PHPAs is so extensive in terms of data points and curves, here below, we are limiting the presentation to only one example of C* determination of one of the PHPAs namely PHPA1. A stock solution of 10000 ppm of the polymer was first prepared in 5 g/l NaCl water. The powder was gently sprinkled into the vortex created by the vigorous stirring of the mixing water using a pale marine stainless-steel blade stirrer. Homogenization was kept for six hours at 500 rpm. The stock solution was then diluted to obtain polymer solutions with different concentrations ranging from the too-viscous to water-like solutions. The viscosities of the solvent (5

g/l NaCl water) and the very dilute polymer solutions were measured using the capillary viscosimeter following the same procedures presented in the subsection 2.3 of this chapter.

Figure 2.13 shows the shear viscosity of the solvent and dilute PHPA1 solutions measured at 25 °C. The viscosities and shear rates were calculated using Equation 2.7 and 2.8 respectively. Just as the solvent viscosity, the dilute polymer solutions exhibited a newtonian behavior in all the shear rate interval with constant viscosities. The intrinsic viscosity of the PHPA1 was then determined following the same procedures presented in the subsection 2.3 of this chapter ([η]=1460 ml/g).

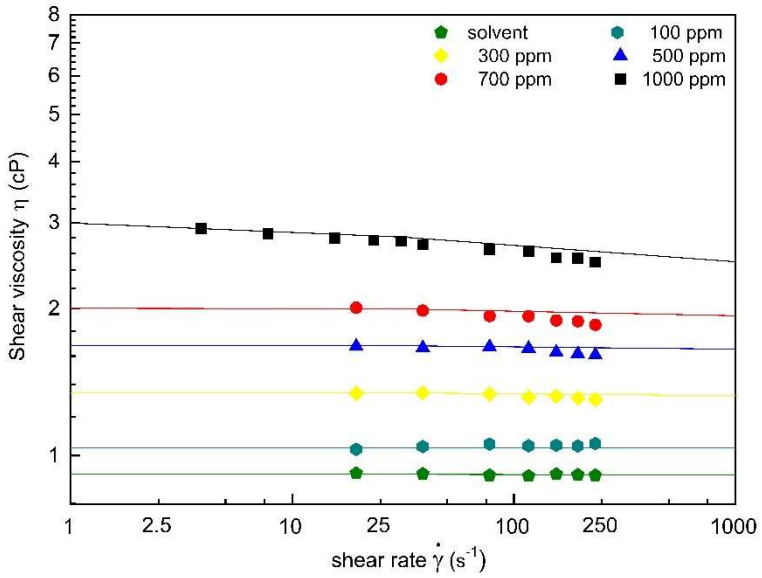

Figure 2.13 : shear viscosity of solvent and dilute PHPA1 solutions measured at 25 °C using the capillary viscosimeter.

When the pressure drops ΔP exceeded the detection limit of the pressure sensor (60 mbar) in the capillary viscosimeter, the viscosity of the polymer solution was measured using a rotational rheometer (Anton Paar, MCR 302). The latter was equipped with a coaxial cylinder that have the following dimensions (measuring bob radius, R_i=13.325 mm, measuring cup radius, R_e=14.465 mm, Gap Length, L =39.997 mm, Measuring Gap, e=1.14 mm). To ensure the exactness and repeatability of the viscosity measurements, settings in terms of measurement points per decade, measurement time per point, ascending (from 0.1 to 1000 s^{-1}) or descending (from 1000 to 0.1 s^{-1}) shear sweep were first investigated as shown in **Figure 2.14**. Consequently, the retained settings were as follow: 6 measurement points per decade, measurement time per point of 20 seconds and an ascending shear sweep from 0.1 to 1000 s^{-1}.

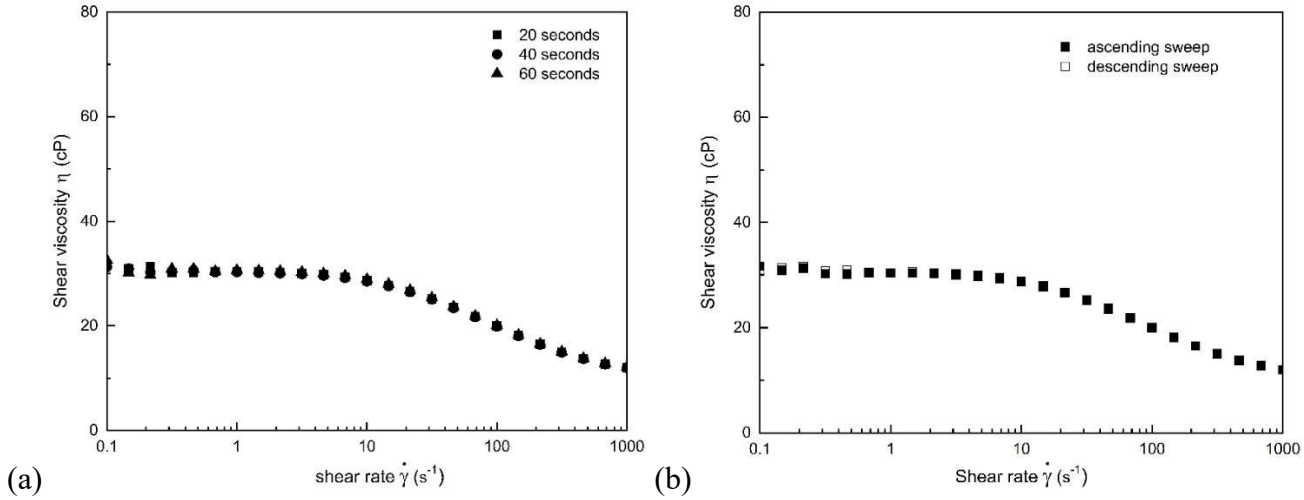

Figure 2.14 : (a) measurement time per point and (b) ascending/descending sweep effects on the measured shear viscosity.

The measured viscosities using the rotational rheometer are depicted in **Figure 2.15**. At very low shear rates, all the polymer solutions showed a newtonian behavior where viscosity remained constant up to a certain critical shear rate. Beyond this shear rate, the viscosity decreased with shear rate indicating a typical shear thinning behavior. The latter can be related to the uncoiling and the aligning of polymer macromolecules with the shear flow. When a second critical shear rate is reached, the less concentrated polymer solutions (i.e., 2000 ppm, 3000 ppm) showed a shear-thickening behavior where viscosity increased with the shear rate. This phenomenon can be related to the flow induced deformations and association of macromolecules. At high shear rates, the polymer chains may participate in the formation of clusters as the relaxation time is too short to adapt the flow geometry. Another explanation evokes the onset of the chain's dilatant behavior under the high elongational flows, which strongly deform the macromolecules and give rise to an important contribution of the polymer's elongational viscosity in the measured viscosity.

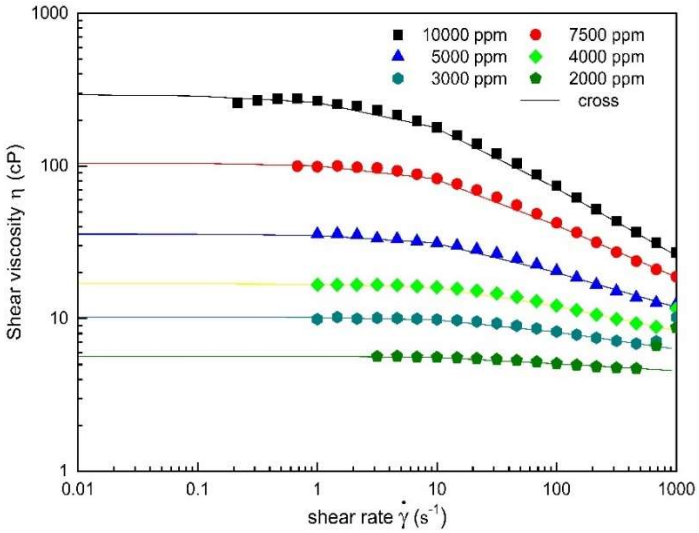

Figure 2.15 : shear viscosity of PHPA1 solutions measured at 25 °C using the rotational rheometer.

The cross model was used to fit the flow behavior of the polymer solutions with exemption of the shear thickening area. The cross model represents the data very well at both high and low shear rates, which makes it a high realistic model compared to other models:

$$\eta = \eta_\infty + \frac{\eta_0 - \eta_\infty}{(1+\lambda.\dot{\gamma}^m)} \qquad \text{Equation 2.14}$$

With η is the shear viscosity, η_∞ is the infinite-shear viscosity, η_0 is the zero-shear viscosity; λ is the time constant and m is a dimensionless exponent. The fit parameters for the different polymer concentrations are reported in **Table 2.9**:

Table 2.9 : Cross model parameters for PHPA1 solutions measured at 25 °C.

Concentration (ppm)	η_0 (cP)	η_∞ (cP)	λ (s)	m
10000	295	13.24	0.130	0.724
7500	105	13.96	0.046	0.846
5000	36	9.94	0.029	0.853
4000	17	7.54	0.013	0.945
3000	10.25	5.86	0.011	0.933
2000	5.70	4.48	0.009	1.011

When all the viscosities of the prepared polymer solutions were measured, the zero-shear specific viscosities "η_{sp0}", defined by Equation 2.15, were calculated:

$$\eta_{sp0} = \frac{\eta_0 - \eta_s}{\eta_s} \qquad \text{Equation 2.15}$$

With η_s is the solvent viscosity and η_o is the zero-shear viscosity of the polymer solution.

The zero-shear specific viscosities **"η_{sp0}"** were then plotted against the overlap parameter **"C.[η]"** as shown in **Figure 2.16**:

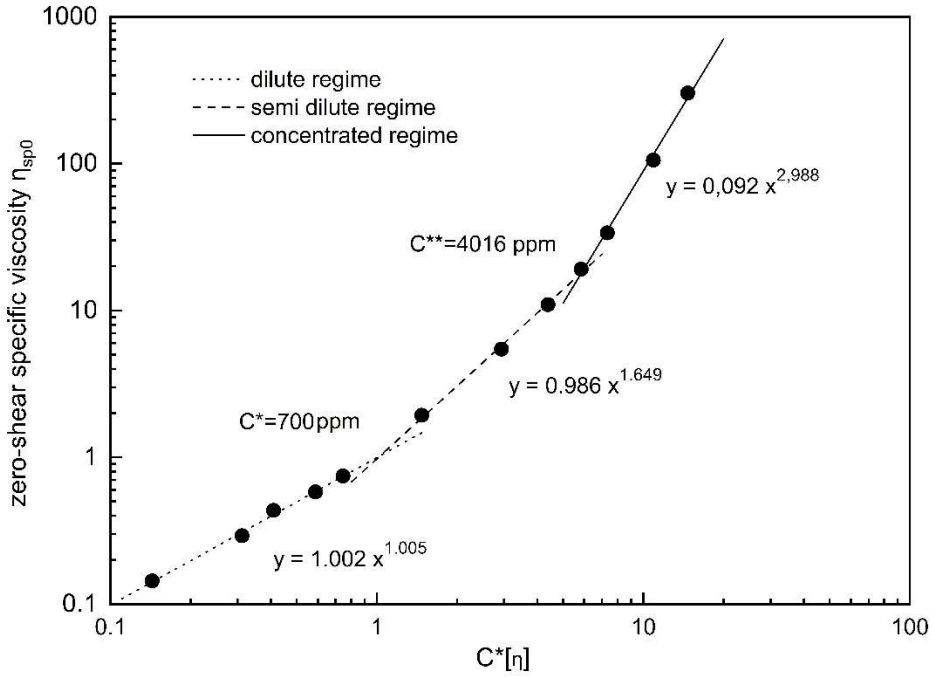

Figure 2.16 : Critical overlap concentration (C*) determination for PHPA1 prepared in 5 g/l NaCl water and at 25°C.

In the above figure, three regions were identified: the dotted line for the dilute regime, the dashed line for the semi-diluted regime and the solid line for the concentrated regime. The intersection between the three lines gave the C* and C**. The same procedures were followed for the other two PHPAs (PHPA2 and PHPA3). Stock solutions were prepared in injection water then diluted to obtain polymer solutions with different concentrations. The viscosities of very diluted were measured using the capillary viscosimeter while those of the more concentrated solutions were measured using the rotational rheometer. The intrinsic viscosities were calculated alongside the zero-shear specific viscosities **"η_{sp0}"**. The latter were then plotted against the overlap parameter **"C.[η]"** as shown in **Figure 2.17**. Interestingly, the curves of the three PHPAs superposed on each other in one single curve. This is in good agreement with previous studies suggesting the existence of a master curve for polymer solutions having a fixed conformation when prepared in good solvents [207, 208].

Table 2.10 summarizes the obtained intrinsic viscosities and the critical concentrations (C*, C**) for the three PHPAs prepared in 5 g/l NaCl water.

Table 2.10 : the intrinsic viscosities and the critical concentrations (C*, C**) measured at 25 °C for the three PHPAs prepared in 5 g/l NaCl.

polymer	PHPA1	PHPA2	PHPA3
[η] (ml/g)	1460	1994	2560
C* (ppm)	700	551	491
C** (ppm)	4016	3825	3253

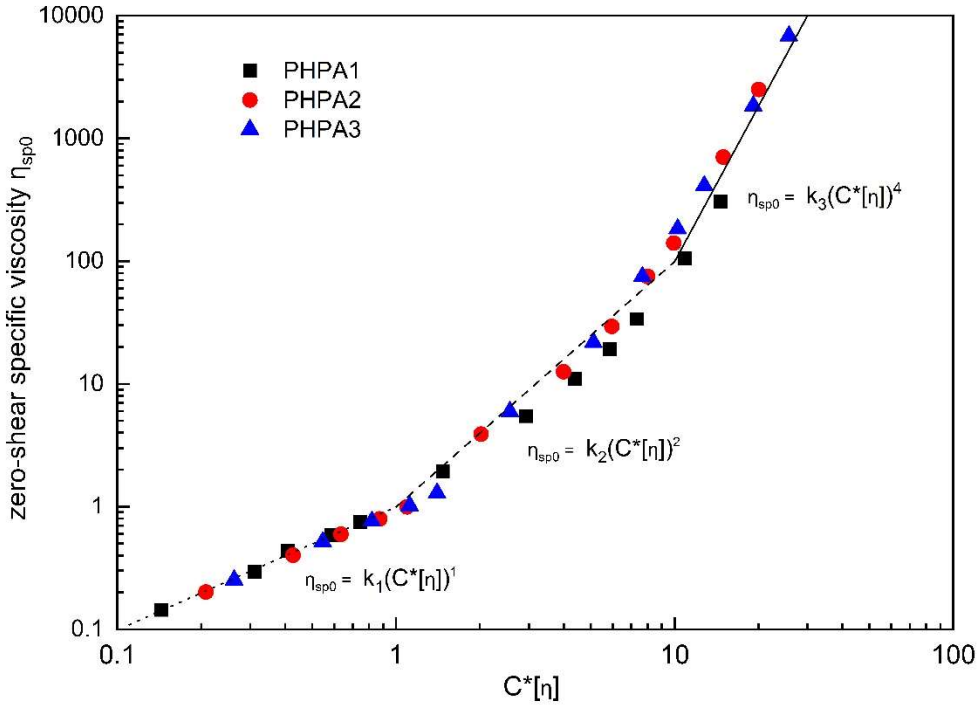

Figure 2.17 : The master curve of zero-shear specific viscosity versus the overlap parameter for the three PHPAs prepared in 5 g/l NaCl water and at 25°C.

2.7 Viscoelastic behavior of PHPAs

Understanding of the viscoelastic behavior of the base polymer is of paramount importance in the comprehension of the viscoelastic behavior of the obtained polymer gel. In this subsection, we have conducted a set of experiments to characterize the viscoelastic moduli of the three PHPAs in their non-crosslinked state, which will help afterwards in the interpretations of their viscoelastic moduli when crosslinked with PEI. Prior to that, the effect of the applied strains and frequencies on the accuracy of the measured moduli, were evaluated independently. To do so, PHPAs solutions, prepared in 5 g/l NaCl water, were loaded in the coaxial cylinder of the rotational rheometer (Anton Paar, MCR 302).

As the linear viscoelastic ranges of polymer systems are determined through strain sweep tests at fixed frequencies, the first step consisted of evaluating the effect of the chosen frequency on the measured viscoelastic moduli. Strain sweep tests were conducted at 4 different frequencies and fixed temperature of 25 °C on PHPA1 solutions prepared at fixed concentration of 10000 ppm as shown in **Figure 2.18**. In the studied strain range, the recorded loss moduli (G") were independent of the strain and were higher than the storage moduli (G') expressing the viscous behavior of the tested polymer solutions. When the frequency was increased from 0.1 to 5 Hz, the measured viscoelastic moduli were amplified by a factor of around 100. On the other side, the measured storage modulus was drastically decreased to around 2×10^{-4} Pa at a frequency of 10 Hz, indicating the beginning of the nonlinear viscoelastic range. Moreover, the viscoelastic moduli could not be measured at very high strains (strain > 600 %) which was due to the instrument limitations at these conditions. As a result,

measurements of the viscoelastic moduli in a strain sweep test were confirmed to be dependent on the chosen frequency [209, 210]. Thus and for an accurate determination of the linear viscoelastic range, strain sweep tests should be conducted at the highest frequency for which the linear domain is the shortest [211], in this case either at 1 or 5 Hz. Both very low and very high frequencies (0.1 and 10 Hz) are not recommended since the measurement in the regions of low and high strain respectively, are limited by the equipment sensitivity.

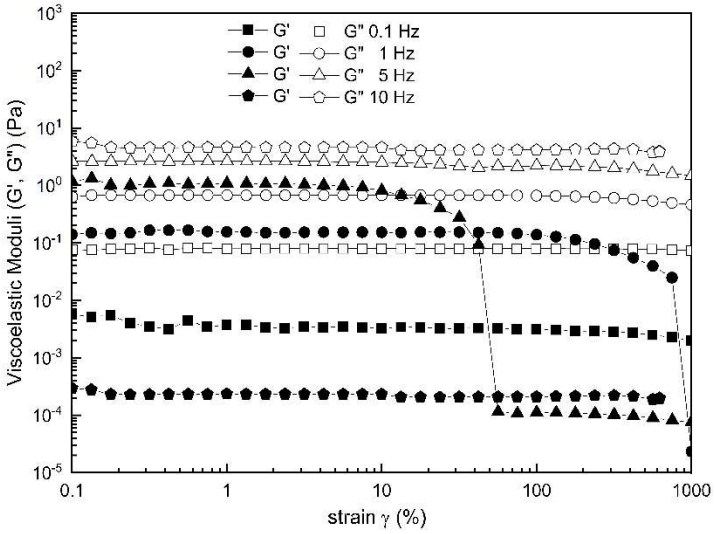

Figure 2.18 : The frequency effect on viscoelastic moduli in a strain sweep test (PHPA1 concentration=10000 ppm).

Inversely, the effect of the strain on the measured viscoelastic moduli during a frequency sweep test was evaluated. In all cases, the applied strain should be within the linear viscoelastic range. Three descending (from 10 to 0.01 Hz) frequency sweep tests at fixed strains of 0.1, 1 and 10 % were realized as shown in **Figure 2.19**. The loss and storage moduli were totally independent of the applied strain aligning with the observations from **Figure 2.18** and previous reports in literature [212]. Nevertheless, the variation of the storage modulus at low frequencies was better captured when higher strains were applied.

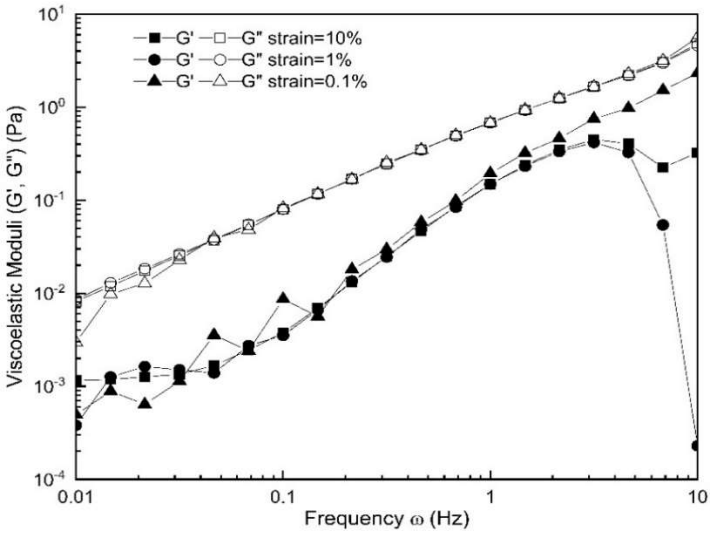

Figure 2.19 : The strain effect on viscoelastic moduli in a frequency sweep test (PHPA1 concentration=10000 ppm).

The effect of polymer concentration, temperature and polymer's molecular weight on the viscoelastic moduli of PHPA prepared in 5 g/l NaCl water were then evaluated through frequency sweep tests at a fixed strain of 10 % as shown in **Figures 2.20**, **2.21** and **2.22**, respectively. For all the studied parameters and in all the investigated frequency range, the loss modulus (G") was higher than the storage modulus (G'), with no crossover between them, indicating the predominance of the viscous behaviour over the elastic one for all polymer solutions and in all test conditions. Both viscoelastic moduli decreased when frequency decreased and the gap between them became larger at low frequencies. As illustrated in **Figure 2.21**, the loss moduli G" were very close at higher frequencies (around 10 Hz) but then the G" slopes were around 1 in the low frequency range (0.01-1 Hz). Meanwhile, the storage moduli (G') slopes were around 2 in the frequency range (0.1-1 Hz), which is in good agreement with the theoretical slope of log G' versus log ω for a non-crosslinked polymer solution (theoretical slope= 2) [176]. Experimentally, this can be explained by the decreased measurement time at high frequencies which allows less time for polymer chains to relax and thus the polymer solutions will tend to behave as rigid materials and show higher viscoelastic moduli, mainly high storage moduli at high frequencies. At low frequencies, the measurement time starts to increase compared to the relaxation time and the viscous behavior becomes more dominant. Polymer concentration and molecular weight had a proportional effect on the value of the measured viscoelastic moduli in contrast to the temperature that had a negative effect. However, for the less concentrated solutions (PHPA1 solutions prepared at 3000 and 5000 ppm) and for high temperatures (60 and 80 °C), the storage modulus could not be measured or was too low at high frequencies. In fact, the polymer solutions are crowded at high concentrations and molecular weights which results in an increased number of entanglements and a decreased motion of the polymer chains. Consequently, the relaxation time of these polymer chains becomes longer because of the restricted intramolecular motion [213]. With higher relaxation times, the polymer solutions exhibit higher

viscoelastic moduli at low measurement times (high frequencies). Inversely, the enhanced chains movement at high temperatures result in less entangled network and shorter relaxation times thus the observed low viscoelastic moduli at high temperatures. When the polymer solutions are too dilute and their network is insufficiently entangled, the elastic response (storage modulus) becomes so small and cannot be measured accurately at high frequencies as it was the case for low polymer concentrations and high temperatures.

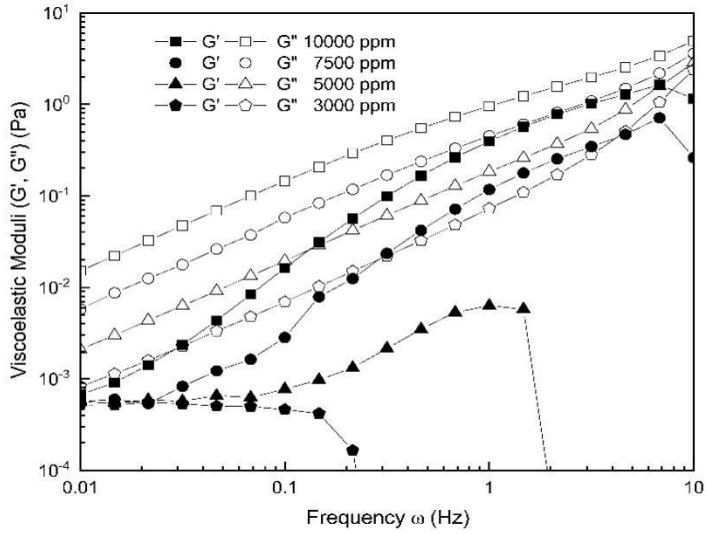

Figure 2.20 : Viscoelastic moduli at different concentrations of PHPA1 solutions prepared in 5 g/l NaCl water (strain= 10 %, T= 25 °C).

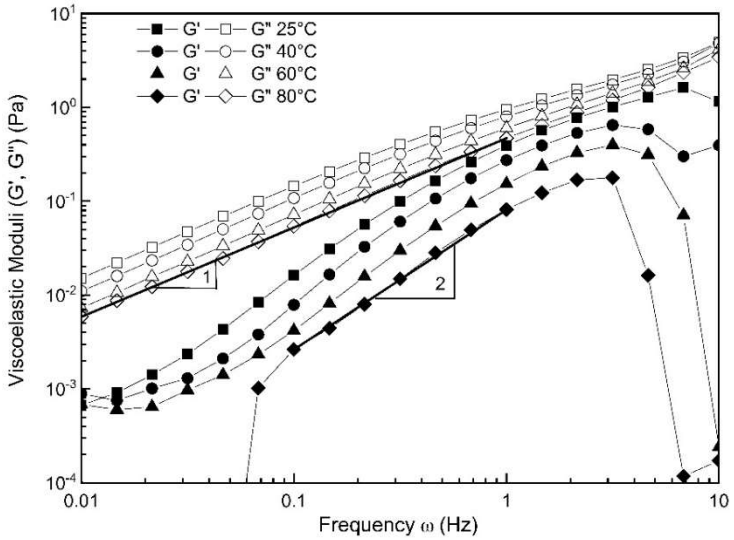

Figure 2.21 : Viscoelastic moduli at different temperatures of PHPA1 solutions prepared at 10000 ppm in 5 g/l NaCl water (strain= 10 %).

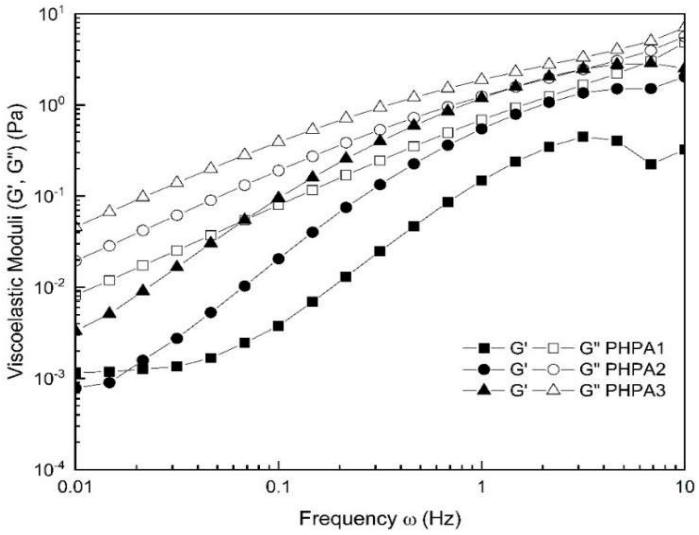

Figure 2.22 : Viscoelastic moduli at different PHPA molecular weights (polymer concentration= 10000 ppm in 5 g/l NaCl water, strain =10 %, T= 25 °C).

2.8 Conclusion

In this chapter, a complete characterisation methodology of the reactants used in the thesis (three PHPAs and two PEIs) was conducted. A new homemade capillary viscosimeter was employed to measure the viscosities of the solvent and dilute reactant solutions, which allowed afterwards to calculate the intrinsic viscosities and the viscosity-average molecular weights based on the Mark-Houwink equation. The PHPAs hydrolysis degrees and PEIs branching degrees (which are usually neglected in studies on PEI based polymer gels) were determined based on the carbon (^{13}C) NMR spectra of the reactants. The thermogravimetric analysis (TGA) gave access to the water content of the reactants and their thermal degradation. The critical concentrations (C* and C**) of the three PHPAs, which are important to the gelation reaction, were determined through the plot of the zero-shear specific viscosity versus the overlap parameter. To do so, the flow curves of concentrated polymer solutions were fitted using the cross model while the dilute polymer solutions exhibited only a newtonian behavior. The curves of zero-shear viscosity versus the overlap parameter of the three PHPAs were found to superimpose confirming the polymer to be solubilized in a good solvent. Finally, the viscoelastic behavior of the non-crosslinked PHPA solutions was investigated. The effect of the applied frequencies in strain sweep tests and inversely the effect of the applied strain in frequency sweep tests were first evaluated. It was found that the frequency had a greater impact compared to the strain. All the polymer solutions exhibited a dominant viscous behaviour over the elastic one in all the test conditions. However, and due to the equipment limitations, reliable measurements of the storage moduli were only obtained in a limited frequency range.

Chapter III:

The thermal gelation of PHPA/PEI mixtures

3. Chapter III: The thermal gelation of PHPA/PEI mixtures

3.1 Introduction

In this chapter, the thermal gelation of partially hydrolyzed polyacrylamide (PHPA) and polyethylenimine (PEI) mixtures were studied under realistic conditions of temperature (80°C) and salinity (Total Dissolved Solids, TDS= 3.4 g/l) of the Algerian reservoir of Tin Fouyé Tabankort (TFT). The thermal stability, the degradation temperature, the morphology, the structure-property relationships and the viscoelastic behavior of the PHPA/PEI mixtures were investigated as function of the main controlling parameters namely reactant concentrations, reactants molecular weights, temperature and inorganic salts presence. All experiments were conducted in the semidilute and concentration regimes of the polymer (c>c*) while maintaining practical initial gelant viscosities. Various techniques were employed such as the bottle test method, the steady shear method, the dynamic shear method, differential scanning calorimetry (DSC) and scanning electron microscopy (SEM). The obtained results were discussed and compared to the literature reported PHPA/PEI gels or PEI based gel polymers characteristics.

3.2 Materials and methods:

The three PHPAs and the two PEIs, presented in the materials characterization chapter, were investigated in this section. PHPA1, which had a medium Mw (5×10^6 g/mol) and low HD (6%), developed the lowest gelant viscosities (~12 cP at 5000 ppm in TDS =3.4 g/l water). It was consequently chosen as the main base polymer. While PHPA2 and PHPA3, having the same HD (6%) but higher Mw, were used to study the effect of the polymer's molecular weight. The main crosslinker was PEI25, while PEI750 was used to study the crosslinker's molecular weight effect at the same BD (56-59).

Prior to preparation of gelant solutions, PHPAs stock solutions of 10000 ppm (10 g/l) were prepared in injection water (**see section 2.2 of materials characterization chapter**). The polymer powder was gently sprinkled into the vortex created by the vigorous stirring of mixing water using a pale marine stainless-steel blade stirrer. Homogenization was conducted for six hours at 500 rpm. The stock solutions were stored at 6 °C. Gelant solutions were then prepared by adding the appropriate amount of crosslinker to the polymer solutions and stirring using a magnetic stirrer for an additional 5 minutes. For all the prepared gelant solutions, the pH, measured using a wtw/pH-3310 pH meter, was varying between 9.5 and 10.5 because of the crosslinker (PEI) that has a strong buffering capacity.

For the bottle test method, the gelant solutions were loaded in glass tubes that were aged in an oven at 80±1 °C. The glass tubes were taken for periodical observations of gelation time, gel strength and

gel long-term stability. In contrast, the gelant solutions were loaded directly in a rotational rheometer (Anton Paar, MCR 302) for steady shear measurements. The latter were conducted at 80 °C using a coaxial cylinder that had the following dimensions (Measuring Bob radius, R_i =13.325 mm, Measuring Cup radius, R_e =14.465 mm, Gap Length, L =39.997 mm, Measuring Gap, e=1.14 mm), which acquired a gelant sample volume of approximately 19.3 ml. In the case of dynamic shear measurements, gelant solutions were first filled in small glass flasks and cured in the oven at 80±1 °C for 48 hours. After that, the gel samples were carefully loaded into a parallel plate geometry on the same rotational rheometer (Anton Paar, MCR 302). The plates had a radius of 12.49 mm and were separated by a 1 mm gap. The viscoelastic moduli (G' and G") were measured at 25 °C set using a temperature controlling cell.

Differential scanning calorimetry (DSC) was performed with the Q1000 DSC instrument (TA Instruments) to study the degradation temperature of PHPA/PEI gel. About 5 mg of a fully formed PHPA/PEI gel (20000 ppm PHPA1/ 10000 ppm PEI25 prepared in distilled water) was placed in aluminum hermetic pan, sealed with a pressing tool and loaded into a DSC instrument, where an empty pan was used as a reference. The temperature was equilibrated at 25 °C, then ramped at 2 °C/min to 200 °C under a constant nitrogen flow of 20 ml/min.

Scanning Electron Microscope (SH3000, Hirox, South Korea) was used to examine the microstructure (morphology) of the PHPA/PEI gel. First, a gelant solution, prepared with 20000 ppm PHPA1 and 10000 ppm PEI25 in distilled water, was cured at 80 °C overnight. A small portion of the formed gel was then frozen with liquid nitrogen and cutted with razor blade to obtain ultrathin films that were placed on a copper-plate and coated with gold in a sputter coater (Denton Vacuum). SEM images were collected using a field source emission of 20 kV accelerating voltage.

3.3 Results and discussions:

3.3.1 Thermal gelation through the bottle test method

The thermal gelation of PHPA/PEI mixtures was first evaluated using the bottle test method. The semi-quantitative method allows to evaluate the gelation time and gel strength simultaneously and to observe the gel thermal stability for long periods. Sixteen gelant solutions were prepared in injection water using four PHPA1 concentrations of 3000, 5000, 7500 and 10000 ppm (all above the critical overlap concentration C* =700 ppm), and four PEI25 concentrations of 500, 1000, 2000 and 3000 ppm. The gelant solutions were loaded into glass tubes and aged at 80 °C. The qualitative evaluation of the gel samples using Sydansk's gel code was conducted over the course 3 months as summerized in **Table 3.1**:

Table 3.1 : Summary of the gelation performance of the PHPA1/PEI25 mixtures at 80 °C and TDS=3.4 g/l according to Sydansk's code.

Gel Formulation		Gel Strength according to Sydansk's Code										
PHPA1 Concentration (ppm)	PEI25 Concentration (ppm)	Time (Hours)										
		1	2	3	4	6	8	24	48	10 days	1 month	3 months
3000	500	A	A	A	A	A	A	D	E	C	B	A
	1000	A	A	A	A	C	E	F	F	F	F	A
	2000	A	A	A	B	F	F	I	I	I	S*	S*
	3000	A	A	A	C	F	F	I	S*	S*	S*	S*
5000	500	A	A	A	A	A	A	E	E	D	B	A
	1000	A	A	A	B	E	F	G	G	G	G	A
	2000	A	A	B	E	G	G	I	I	I	I	I
	3000	A	A	C	F	G	H	I	I	S*	S*	S*
7500	500	A	A	A	A	A	B	F	G	F	B	A
	1000	A	A	B	E	F	G	I	I	I	F	E
	2000	A	A	D	F	H	I	I	I	I	I	I
	3000	A	B	E	F	H	I	I	I	I	I	I
10000	500	A	A	A	A	B	D	H	H	F	D	A
	1000	A	A	B	D	G	F	I	I	I	E	B
	2000	B	D	F	G	H	I	I	I	I	I	I
	3000	A	D	G	H	I	I	I	I	I	I	I

*syneresis.

In literature, the gelation time was considered at various Sydansk's codes. Jia et al. [214] considered the gelation time at the moment when a gelant solution of code A turns to a flowing gel of code C. Others considered code D as the gelation point [165, 215]. While, You et al. [163] defined it at the time when a gelant solution reaches code G. However, the most accepted and accurate definition, and

the one retained here, was when the gelant solution passes from code A to code B [132]. The first observation extracted from the table was that the high reactant concentrations led to lower gelation times and higher gel strengths which reached the code "I" in Sydansk's gel code, comparably to the low molecular weight acrylamide-based/PEI gels [115]. Such observation can be explained by the enhanced interactions and crosslinking reactions between the polymer and the crosslinker at high concentrations, which result in an inverted variation of gelation time and gel strength (faster reaction and more crosslinked sites) as function of reactants concentrations. The second observation was that syneresis, where water is expelled from the 3D structure of the gel as shown in **Figure 3.1**, occurred rapidly for all gelant solutions prepared with crosslinker/polymer ratio higher than ½. Syneresis is generally caused by the overcrosslinking induced by the excessive crosslinker loadings [216]. Finally, the studied PHPA/PEI gel samples were relatively stable over the observation period of 3 months. Almost all gel samples, prepared with crosslinker concentrations higher than 1000 ppm and crosslinker/polymer ratios of less than ½, maintained their strength throughout all the period. While those samples prepared with low crosslinker concentration (500 or 1000 ppm) lost their strength. In such case, the low crosslinking density reduce the ability of the gel 3D structure to retain the water inside it.

Figure 3.1 : Syneresis phenomenon observed after only 3 days for the gel sample prepared with a PHPA1/PEI25 ratio of 1/1.

3.3.2 Structure-property relationships and viscoelastic behavior

In this part, the structure-property relationships and the viscoelastic behavior of the PHPA/PEI gel system are investigated as function of reactant concentrations, reactants molecular weights, temperature and inorganic salts presence using both steady and dynamic shear methods. For the steady shear method, the effect of shear rate on gelation time determination was first evaluated in order to choose the appropriate shear rate for all the subsequent steady shear viscosity measurements. While, for the dynamic shear method, strain sweep tests were conducted to determine the linear viscoelastic range of the PHPA/PEI gel.

3.3.2.1 Shear rate effect on gelation time

The viscosity evolution versus time, for gelant solutions prepared with 10000 ppm PHPA1 and 3000 ppm PEI25 in injection water, was determined at different shear rates of 1, 5, 10, 30 and 50 s^{-1}. As shown in **Figure 3.2**, the gelation time was identified at the intersection of a horizontal line that shows the initial gelant viscosity with a diagonal line that shows the viscosity evolution after the gelation point. At low applied shear rates, the viscosity evolution was sharp and rapid after the gelation point, contrary to higher shear rates where gelation times were slightly delayed and viscosity evolution was less pronounced.

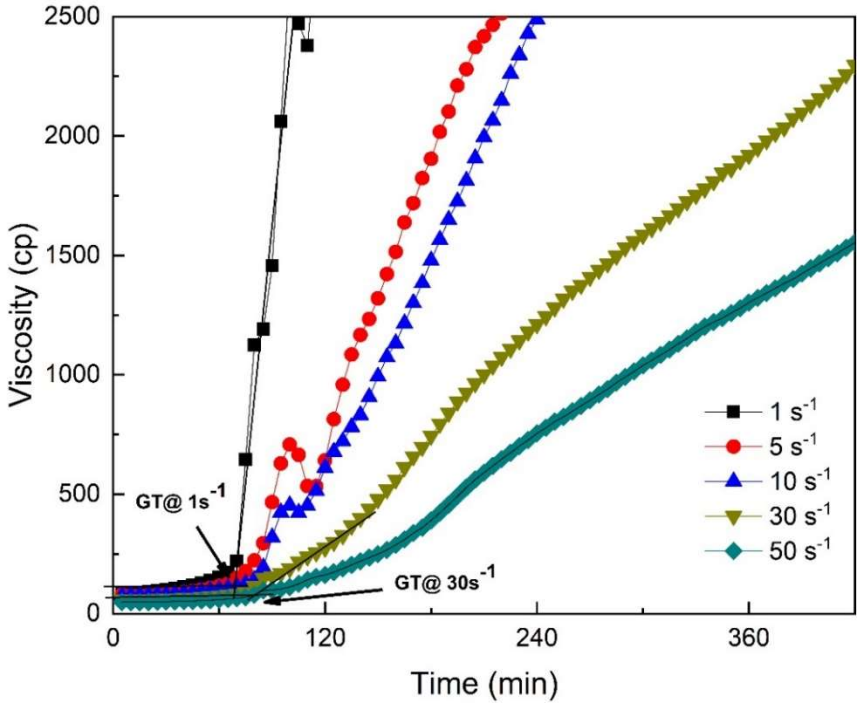

Figure 3.2 : Shear rate effect on gelation time.

In order to confirm this trend, the slopes of the viscosity variation after the gelation point (Slope $P=\frac{\text{viscosity}\,(t_2)-\text{viscosity}\,(t_1)}{t_2-t_1}$ with t_1 and t_2 higher than the gelation time) as function of the applied shear rates were plotted in a log-log curve as shown in **Figure 3.3**:

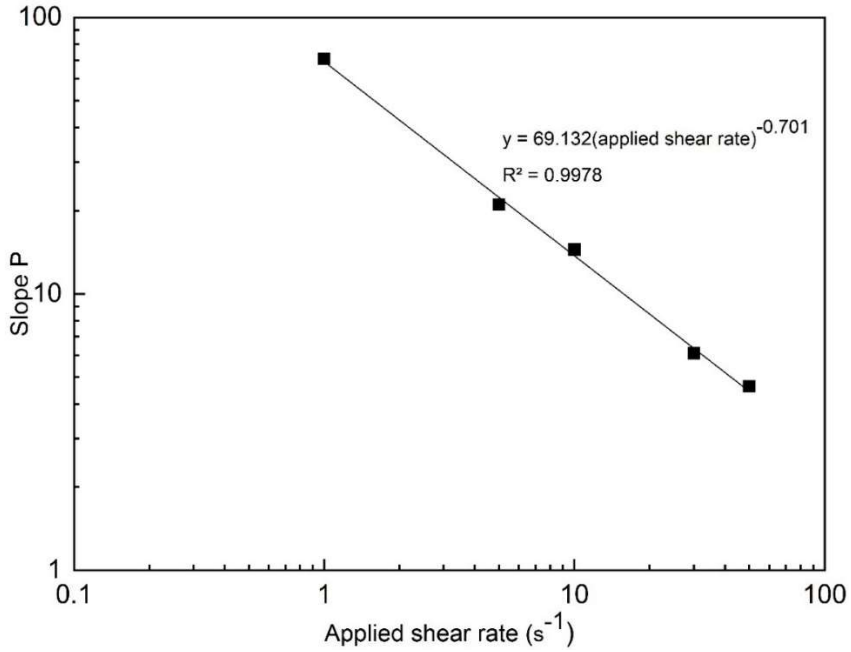

Figure 3.3 : Slope of viscosity evolution after the gelation point versus the applied shear rate.

Interestingly, the variation was found to follow a power law relationship which corresponds to a shear thinning effect of the three-dimensional structure being formed. As reviewed in the state of art, the effect of shear flow on the gelation reaction, especially near the gel point, was a matter of debate. Here, the negative effect of shear flow on the gelation reaction and gel structure was confirmed. This was clear for shear rates of 5 and 10 s^{-1}, where the viscosity drops slightly after the gelation point before resuming its increase. Previous studies reported that the shear rate destroys the aggregates formed by intermolecular bonds and limits the formation of a continuous gel structure [217]. Based on this result, we decided to consider a shear rate of 1 s^{-1} for all the subsequent steady shear viscosity measurements.

3.3.2.2 Linear viscoelastic range

The dynamic oscillatory measurements are generally consisted of two types of tests: strain or stress sweep tests where the strain/stress is varied at a constant frequency and frequency sweep tests where the frequency is varied at a constant strain/stress. In order to determine the linear viscoelastic range of the PHPA/PEI gel systems, a strain sweep test was first performed on gel samples prepared in injection water with different PHPA1 and PEI25 concentrations, and which were cured at 80 °C for 48 hours. At a fixed frequency of 1 Hz, the storage modulus remained constant within the strain range of 0.1 to 100% but largely decreased beyond that as shown in **Figure 3.4**. Based on this result and other literature reported strain sweep tests on similar gel systems tested with parallel plates geometries [218, 219] a fixed strain of 1% was chosen to perform the frequency sweep tests.

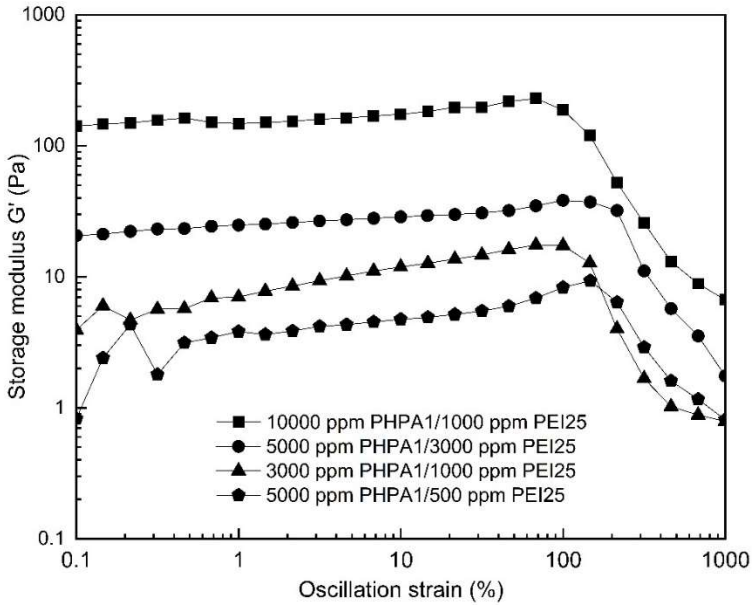

Figure 3.4 : Strain sweep test on gel samples prepared with different PHPA1 and PEI25 concentrations (Frequency= 1 Hz).

3.3.2.3 Polymer and crosslinker concentration effect

To study the effect of polymer and crosslinker concentrations on gelation time, a set (matrix) of 16 gelant solutions were prepared in injection water using four PHPA1 concentrations of 3000, 5000, 7500 and 10000 ppm and four PEI25 concentrations of 500, 1000, 2000 and 3000 ppm. The gelant solutions were directly loaded into the rheometer equipped with a coaxial cylinder, where their viscosities were monitored versus time at a fixed shear rate of 1 s^{-1} and a fixed temperature of 80 °C. Moreover, the effect of polymer and crosslinker concentrations on the viscoelastic moduli (gel strength) was also considered. For the polymer concentration effect, gelant solutions were prepared in injection water using a fixed PEI25 concentration of 1000 ppm and variable PHPA1 concentrations of 3000, 5000, 7500 and 10000 ppm. Inversely, for the crosslinker concentration effect, gelant solutions were prepared at a fixed PHPA1 concentration of 5000 ppm and variable PEI25 concentrations of 500, 1000, 2000 and 3000 ppm. In both cases, gelant solutions were first cured at 80 °C for 48 hours, then the obtained gel samples were loaded carefully into the rheometer equipped with a parallel plate geometry. Frequency sweep tests were conducted between 0.1 and 10 Hz at a fixed strain of 1% and a fixed measurement temperature of 25 °C.

Figure 3.5 shows the variation of gelation time as a function of polymer and crosslinker concentrations, respectively.

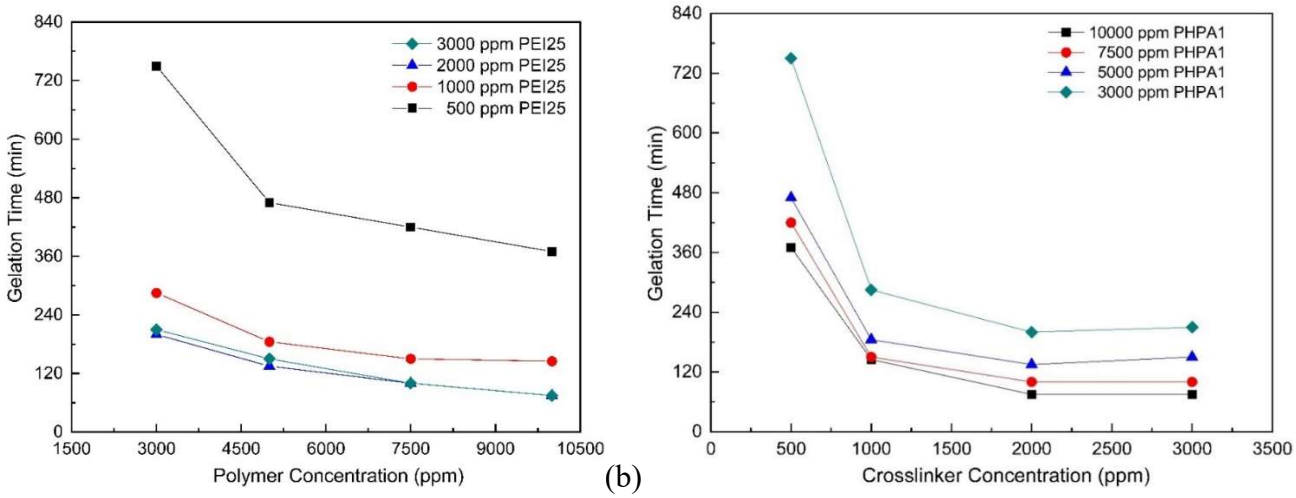

Figure 3.5 : (a) Polymer and (b) crosslinker concentrations effect on gelation time.

It was clear that higher polymer and crosslinker concentrations led to lower gelation times in correspondence to the bottle test observations. For example, gelation time decreased by a factor of 10, from 750 minutes (12 hours and 30 minutes) when 3000 ppm PHPA1/500 ppm PEI25 were used, to only 75 minutes (1 hour and 15 minutes) when 10000 ppm PHPA1/3000 ppm PEI25 were used. When comparing the measured gelation times with those reported for similar PHPA/PEI systems as summarized in **Table 3.2**, one can notice the superiority of our PHPA/PEI system in terms of lower reactants concentrations and lower initial gelant viscosities while covering a wider range of gelation times. Furthermore, from the curve profiles in **Figure 3.5 (a-b)**, it appears that the crosslinker concentration effect was more pronounced compared to that of the polymer concentration (in fact, when polymer concentration increased almost 4 times, gelation time decreased by 2 times compared to a decrease of 4 times for the same increase in the crosslinker concentration). However, gelation times remained constant above 2000 ppm (i.e., 3000 ppm). Another important observation was that the variation of gelation time versus both polymer and crosslinker concentration did not follow an exponential relationship, as reported in previous studies [105, 120, 122].

Table 3.2 : PHPA/PEI gelation times reported in literature and this study.

Polymer	Crosslinker	Initial gelant Viscosity (cp)	T (°C)	Solvent	Gelation Time (Hours)	Reference
5% PHPA	0.33 - 2% PEI	NP*	25	2% KCl brine	8-13	[119]
			60		1.5-6	
0.5 – 1.5% PHPA	0.2 – 1.5% PEI	NP	40	Synthetic water TDS= 90 g/l	15hrs – 9 days	[120]

2% PHPA	0.35% PEI	409	65	Synthetic water TDS= 5 g/l	10	[121]
1 – 2% PHPA	0.2 -0.35% PEI	617	65	Fresh water TDS= 0.5 g/l	4 – 72	[122]
3.5% PHPA	1% PEI	NP	71.1	2% KCl brine	2.5	[95]
0.75% PHPA	0.41% PEI	33	85	2% KCl brine	3	[33]
3% PHPA (Flopaam 3330S)	0.6 – 1.2% PEI	NP	100	Distilled water	3.3	[124]
2% PHPA (Alcomer130)		NP	100		3.4	
7% PHPA	0.3% PEI	NP	120	Salt free water	0.5-0.75	[118]
0.3% to 1% PHPA	0.05 – 0.3% PEI	12.5	80	Synthetic water TDS= 3.4 g/l	0.25-12.5	This study

*NP=Not Provided.

Figure 3.6 shows an example of the storage and loss moduli variations in a frequency sweep test for gel samples prepared in injection water at different polymer concentrations and fixed crosslinker concentration. For all the tested gel samples (including those prepared at fixed polymer concentration), frequency sweep tests revealed that the storage modulus (G') is totally independent of the applied frequency and is largely higher than the loss modulus (G"). Such results confirm the formation of a 3D crosslinked structure as reviewed and explained in the state of art (**see section 1.10.4**). Consequently, the variation of the storage and loss moduli at a fixed frequency of 1.36 Hz were correlated with the polymer and crosslinker concentrations through mathematical relationships as presented in **Figure 3.7**.

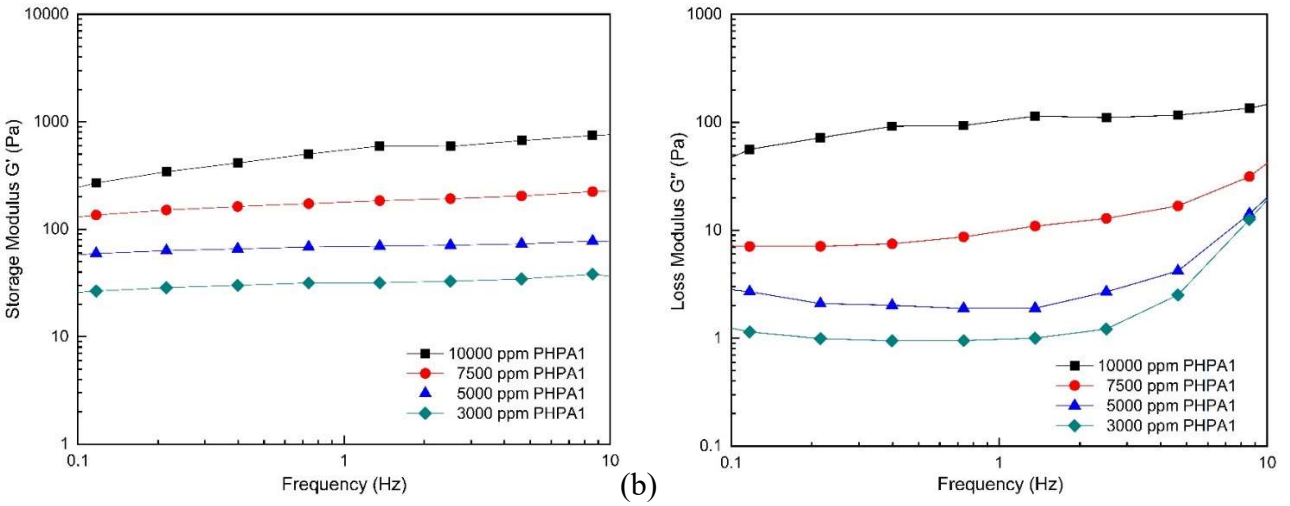

(a) (b)

Figure 3.6 : (a) storage and (b) loss modulus variations in a frequency sweep test for gel samples prepared at different polymer concentrations and fixed crosslinker concentration (strain= 1%).

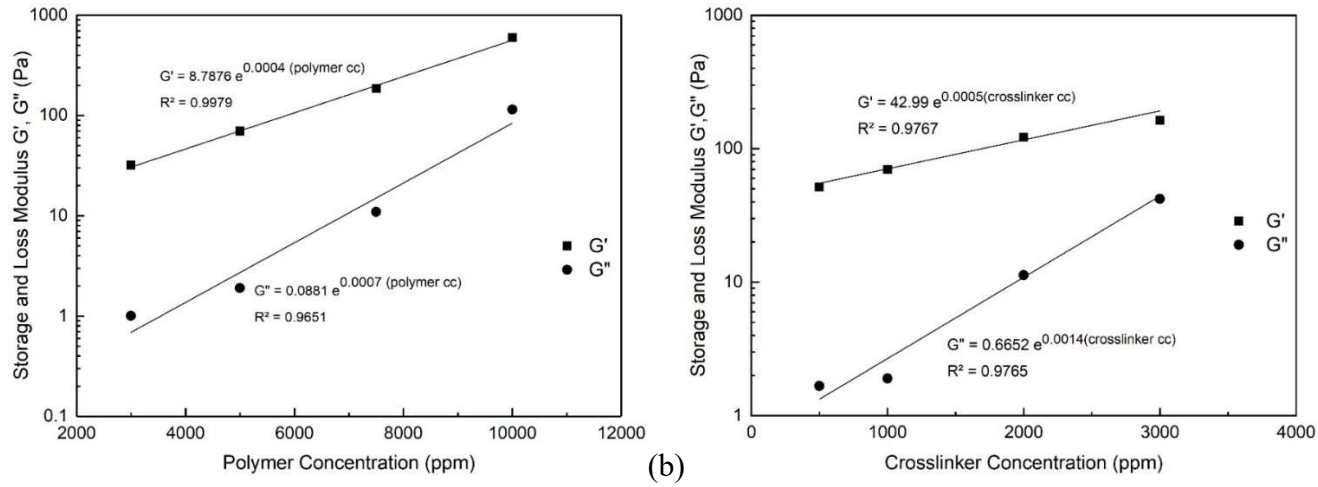

(a) (b)

Figure 3.7 : (a) polymer concentration effect (at fixed PEI25 concentration= 1000 ppm) and (b) crosslinker concentration effect (at fixed PHPA1 concentration= 5000 ppm) on the viscoelastic moduli G' and G" (Strain= 1%, Frequency= 1.36 Hz).

Both storage and loss moduli varied proportionally with polymer and crosslinker concentrations following exponential relationships $y = a * e^{b}$. In literature, Al-Muntasheri et al. [106] reported exponential variations of the storage and loss moduli of a PAtBA/PEI gel system under the respective effect of polymer concentration: $G' = 22.7 \times e^{0.49\ (PAtBA\ concentration\ in\ wt\%)}$, $G'' = 0.45 \times e^{0.73\ (PAtBA\ concentration\ in\ wt\%)}$ and crosslinker concentration: $G' = 487.56 \times e^{1.53\ (PEI\ concentration\ in\ wt\%)}$. Moreover, El-karsani et al. [112] presented the following two relationships for the storage modulus of PAM/PEI gel system as function of polymer and crosslinker concentrations: $G' = 168 \times e^{0.22(PAM\ concentration\ in\ wt\%)}$ and $G' = 931 \times e^{0.23\ (PEI\ concentration\ in\ wt\%)}$. Given the differences between the studied systems in terms of reactants concentration ranges, molecular weights, and other controlling parameters (curing and measurement temperatures, salinity... etc), a quantitative comparison between the obtained relationships (constants a and b) of this study and those reported in literature seems impossible. However, it is acceptable to consider the increase rate in comparing between the different effects. El-karsani et al. [112] stated

that when the polymer (PAM) concentration increased three times, the storage modulus increased by a factor of three compared to only a factor of 1.1 when the crosslinker (PEI) concentration increased by the same factor (3 times). Similarly, an increase of PAtBA concentration by a factor of 2.33 resulted in an increase of the storage modulus by a factor of 7, while an increase of PEI concentration by a factor of 3 resulted in the storage modulus increase by a factor of 4.3 as extracted from [106]. In this study, when considering the same PHPA and PEI concentrations increase (three times: from 3000 to 10000 ppm for PHPA and from 1000 to 3000 ppm for PEI), the storage modulus increased by a factor of 19 with polymer concentration and a factor of 2 with crosslinker concentration. This result means that the PHPA concentration effect on the storage modulus is more pronounced compared to both the PEI concentration effect and other polymers concentrations effect (i.e., PAM, PAtBA). **Table 3.3** summarizes the reported storage moduli of PEI crosslinked polymer gels. Our PHPA/PEI gel system had comparable strength with other PEI crosslinked polymer gels. Nevertheless, when considering a typical gel sample prepared with 5000 ppm PHPA and 1000 ppm PEI, having an initial gelant viscosity of 12 cP and a gelation time of 3 hours, the gel strength was only around 10% of that of typical PAM/PEI or PAtBA/PEI gels.

Table 3.3 : Storage moduli reported in the literature for PEI crosslinked polymer gels.

The system	T_{Curing} (°C)	T_{Measur} (°C)	Mixing water	G' (Pa)	Reference
PAtBA (70000 ppm)/PEI (3000 ppm)	150	23.5	Field water TDS= 1.18 g/l	675	[106]
PAM (70000 ppm)/ PEI (3000 ppm)	130	130	Field water TDS= 0.98 g/l	725	[112]
Non-emulsified PAM (90000 ppm)/ PEI (10000 ppm)	120	120	Field water TDS= 0.98 g/l	885	[117]
Emulsified PAM/PEI Completely separated				746	
Emulsified PAM/PEI Non-separated				344	
AM/AMPS/NVP terpolymer (12000 ppm)/PEI (3000 ppm)	150	150	Deionized water + 0.1 % Na_2CO_3 + 0.05 % thiourea	27.8	[74]
PHPA (10000 ppm)/PEI (1000 ppm)	80	25	Synthetic water TDS= 3.4 g/l	594.2	This study
PHPA (5000 ppm)/ PEI (1000 ppm)				69.5	

Experimentally, the lower gelation times and the higher gel strengths can be explained by the greater number of available crosslinking sites when high polymer or crosslinker concentrations are employed and by the more entangled network when high polymer concentrations are used. The gelation speed is mainly dependent on the number of PEI entities in the solution which are the initiators of the crosslinking reaction. However, this is only true to a certain extent as the crosslinking reaction speed depends also on other limiting parameters such as the temperature and salinity. Hence the gelation time was observed to become invariant starting from a given PEI saturation concentration (i.e., 2000 ppm). For PHPA, the saturation concentration was not observed in the studied concentration range. In contrast, the gel strength was more dependent on the polymer concentration. In fact, and at high PHPA concentrations, the polymer chains overlap between each other and create entanglement points which present additional crosslinking sites in one hand and on the other one favorize the intermolecular crosslinking (between sites of different chains) rather than intramolecular crosslinking (between sites on the same polymer chain). Both mechanisms render the formed 3D structure stronger. Moreover, the pronounced effect of PHPA polymer concentration on the gel strength (storage modulus) compared to PAM and/or PAtBA concentrations, is explained by the longer PHPA chains which as stated before offer a more entangled network, thus a similar PHPA concentration increase as PAM or PAtBA result in higher effect.

3.3.2.4 Molecular weight effect

One of the main reasons for studying PHPA/PEI gels is to address conformance control problems in fractured reservoirs. PHPAs have high molecular weights, which make them suitable for fractures shutoff because of their low penetration into the matrix. In this subsection, the effects of both polymer and crosslinker molecular weights on gelation time are investigated, while the gel strength is assessed only under the effect of polymer's molecular weight. **Figure 3.8** shows the viscosity evolution versus time of three gelant solutions prepared in injection water with 5000 ppm of three PHPAs having the same HD (6%) and different molecular weights (Mw_{PHPA1}= 5.1×10^6 g/mol, Mw_{PHPA2}= 7.5×10^6 g/mol, Mw_{PHPA3}= 10.2×10^6 g/mol), and crosslinked with 1000 ppm of the low Mw PEI25 (Mw_{PEI25}= 2×10^4 g/mol). Similarly, the storage (G') and loss (G") moduli of the same three gelant solutions, which were first cured in an oven at 80 °C for 48 hours, were measured and correlated with the polymers molecular weights as shown in **Figure 3.9**. Two key points can be retained from the two figures: both the initial gelant viscosities and the viscoelastic moduli (G' and G") varied proportionally with the polymer's molecular weight while the gelation times varied unproportionally and were shorter for the samples prepared with PHPA2 and PHPA3 compared to PHPA1.

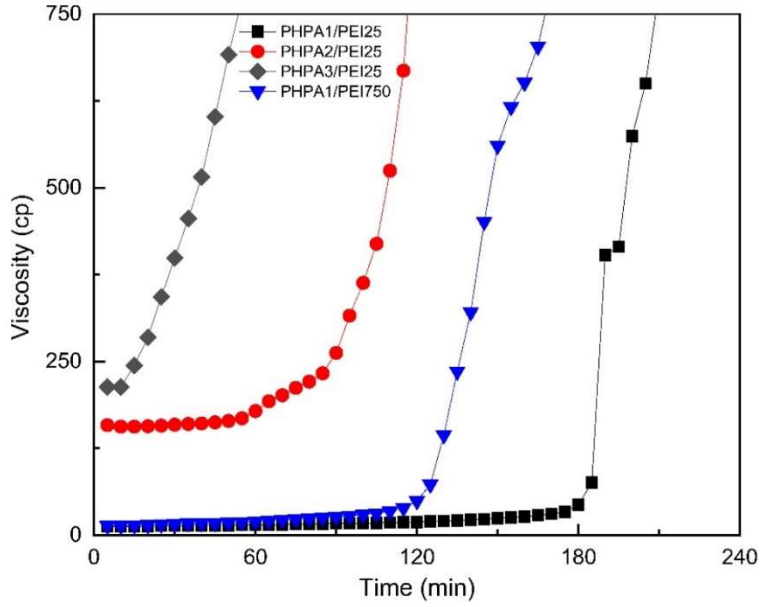

Figure 3.8 : Reactants molecular weight effect on gelation time.

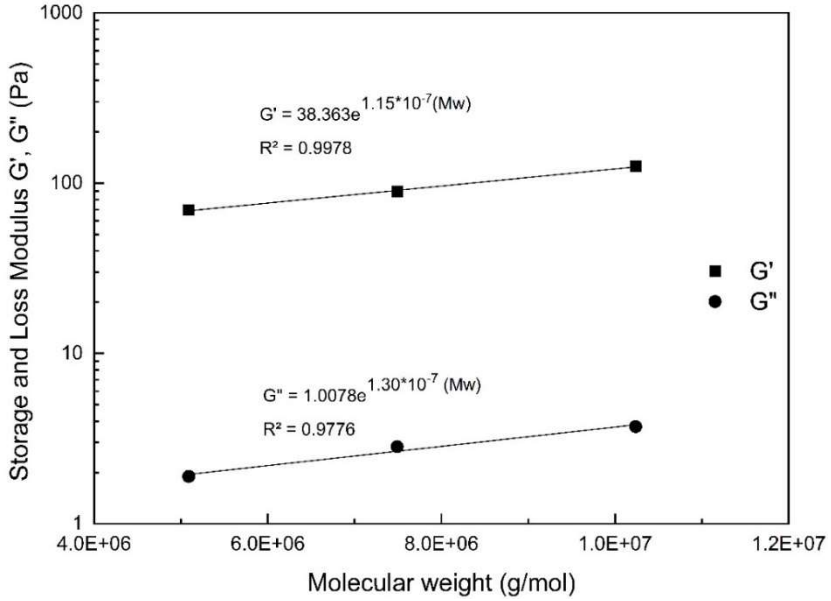

Figure 3.9 : Polymer's molecular weight effect on the storage (G') and loss (G") moduli (strain=1%, Frequency=1.36 Hz).

The effect of the polymer's molecular weight on the initial viscosity of a polymer solution was previously discussed and is well-documented in literature. Nevertheless, the explanation reported in literature for the observed shorter gelation times was the availability of additional crosslinking sites in the high molecular weight polymers [120, 122]. Such explanation is inaccurate, especially when the same polymer mass concentrations are examined. In fact, when polymers with the same hydrolysis degree but different Mws are tested at the same mass concentration (i.e., 5000 ppm = 5 g/l), the number of amide and carboxylate groups remains constant. The only difference is the number of polymer chains. Thus, the best explanation would invoke the hydrodynamic volumes of the polymers. Assuming that the conformation of the PHPA is a random coil, the hydrodynamic volume "V_h" can be calculated using the molecular weight and the radius of gyration:

$$V_h = \frac{4\pi}{3} \times {R_g}^3 \quad \text{Equation 3.1}$$

Where:

$$R_g = A \times {M_w}^{\omega} \quad \text{Equation 3.2}$$

with A=2.94×10^{-5} µm/(g/mol), and ω=0.586 [220].

In this case, PHPA2 and PHPA3 had hydrodynamic volumes greater than PHPA1 by a factor of 2 and 3.5, respectively. The longer polymer chains and the higher hydrodynamic volumes result in more entangled polymer networks. These intermolecular entanglements facilitate the crosslinking reactions as the crosslinking sites are close to each other and some nodes are already formed. This can also explain the higher storage and loss moduli recorded for the high molecular weight polymers especially that the same trend was observed for the viscoelastic moduli when polymer solutions of the three PHPAs, prepared in 5 g/l NaCl water, were tested alone without the presence of a crosslinker. It is worth noting that very high molecular weights are not recommended for conformance control operations, neither during the injection phase (high initial viscosities), nor during the deep placement in the reservoir (shorter gelation times). It may be possible to decrease the concentration of the high molecular weight polymers in order to decrease the initial gelant viscosity and to increase the gelation time. However, and as discussed earlier, the polymer concentration effect on gelation time is less significant.

Furthermore, the viscosity evolution versus time of two gelant solutions prepared in injection water with 5000 ppm of PHPA1 crosslinked with 1000 ppm of two PEIs having the same BD but a different Mws (Mw_{PEI25}= 2×10^4 g/mol and Mw_{PEI750}= 67×10^4 g/mol), was shown in **Figure 3.8**. Despite increasing the crosslinker molecular weight up to 33 times, the gelation time was affected only slightly; it decreased from 185 minutes for the gel sample prepared with PEI25, to 125 minutes for the sample prepared with PEI750, which represents a 30% reduction in gelation time. In a general scheme where PEI macromolecules are dispersed in an entanglement of polyacrylamide chains, the crosslinking appears to be governed by the number of macromolecules (concentration) and the number of NH_2 groups that are present. In our case, the two PEIs had the same BD (BD=56-59), but with a molecular weight ratio of 34. This molecular weight ratio can also be expressed in terms of a hydrodynamic volume ratio of 94 and a surface ratio of 20 that were obtained from equations 3.1 and 3.2 (where A= 7.53 × 10^{-5} µm/(g/mol) and ω=0.43 [221]). As the two crosslinkers were employed at the same mass concentrations, the number of PEI750 macromolecules was lower by a factor of 34, which was supposed to delay the gelation. However, as the PEI750 macromolecules had higher dimensions (gyration radius and a surface area higher by a factor of 4 and 20 respectively), the reaction was accelerated thanks to the higher number of NH_2 groups on the larger surface and the crosslinking which can take place even between the more distant polymer chains. The compensation

of the lower number of macromolecules by the higher number of functional NH_2 units and the larger macromolecules dimensions, can explain the slightly affected gelation time observed when the higher molecular weight PEI750 was employed.

3.3.2.5 Temperature effect

Temperature is one of the most influential parameters for any chemical reaction. For gel systems in oilfields, it is important to quantify the effect of temperature on gelation time, as a small change in reservoir temperature can severely affect the gelation time. **Figure 3.10** shows the viscosity evolution at various temperatures (from 60 to 90 °C) of gelant solutions prepared in injection water with 5000 ppm PHPA1 and 1000 ppm PEI25. The initial viscosity of the gelant solution decreased from 17 cP at 60°C to 12 cP at 90°C, while the gelation time decreased significantly with an increase of temperature, from 11 hours at 60°C to only 1.75 hour at 90°C.

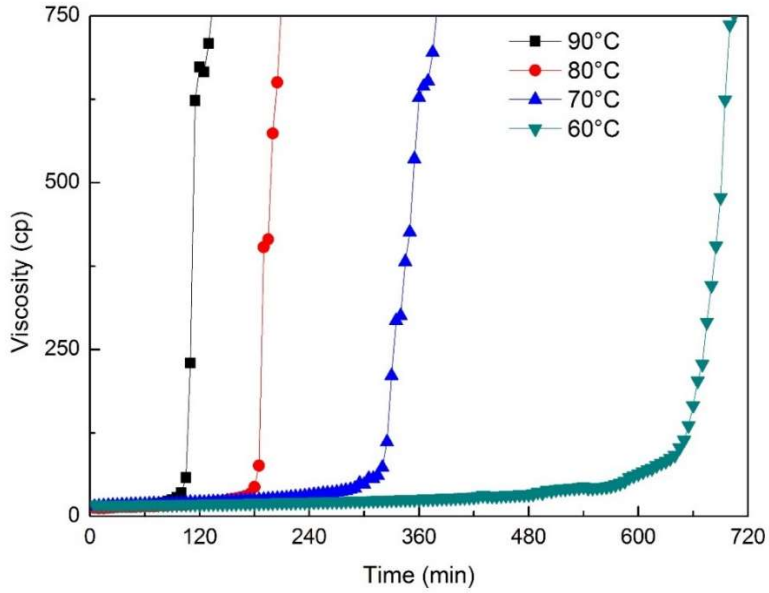

Figure 3.10 : Temperature effect on gelation time.

The enhanced mobility of the polymer and crosslinker at high temperature decreases in one hand the solutions initial viscosities and on the other hand increases the rate of interactions between the two reactants which reduces the gelation time. Most studies, reported in the literature, related the temperature effect on the gelation time of acrylamide-based polymers with PEI to the endothermic nature of the crosslinking reaction [75, 105]. More recently, some authors confirmed that the crosslinking of acrylamide-based polymers with PEI during a non-isothermal gelation, to be associated with both endothermic and exothermic processes. During the crosslinking of PAM with PEI, El-karsani et al. related the endothermic process to the hydrolysis of the polymer (PAM) while the exothermic process was related to the onset of the crosslinking with PEI [111]. When the simultaneous crosslinking of an acrylamide based polymer with two crosslinkers (inorganic "Cr^{3+}" and organic "PEI") was investigated, the endothermic process was linked to the onset of the crosslinking of the inorganic crosslinker (Cr^{3+}) and the exothermic process to the onset of the

crosslinking of the organic crosslinker (PEI) [185]. In order to investigate the exothermic or endothermic nature of the crosslinking reaction between the PHPA and PEI, a neat polymer solution of 20000 ppm PHPA1 and a gelant solution of 20000 ppm PHPA1 and 4000 ppm PEI25 both prepared in distilled water, were loaded into two hermetic pans and placed in the DSC instrument. The temperature was first equilibrated at 30 °C, increased at a rate of 1 °C/min to 80 °C, and then maintained at this temperature for 30 minutes. As depicted in **Figure 3.11**, both the polymer solution and the gelant solution showed an endothermic peak which started immediately with temperature ramp, while only the gelant solution had exhibited an exothermic peak that start at 50°C. The exothermic process is, in this case, translated by the onset of the crosslinking between the PHPA and PEI which is shown to release heat.

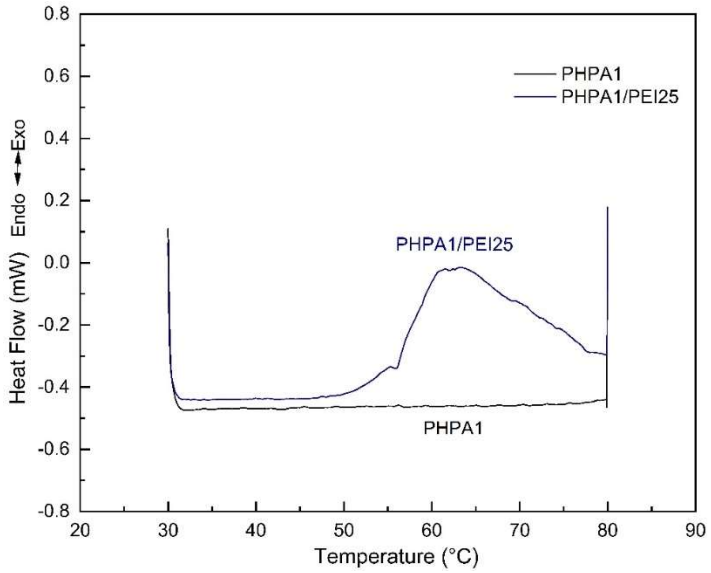

Figure 3.11 : DSC curve of polymer solution (PHPA1) and gelant solution (PHPA1/PEI25) prepared in distilled water.

Furthermore, the effect of temperature on gelation time was correlated using an Arrhenius-type equation:

$$t_g = M.exp\,(\frac{E_a}{RT}) \qquad \text{Equation 3.3}$$

where t_g and M are the gelation time and frequency factor in minutes, respectively. E_a is the activation energy in kJ/mol, R is the universal gas constant in (kJ/mol.K) and T is the absolute temperature in K.

Figure 3.12 shows an Arrhenius-type plot for two gelant solutions prepared with 5000 ppm PHPA1 and 1000 ppm PEI25 in distilled water and injection water.

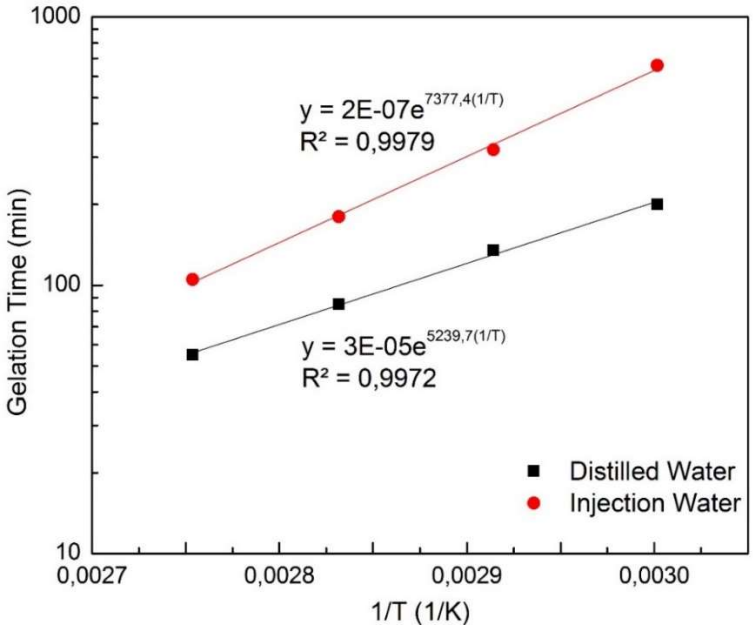

Figure 3.12 : Arrhenius-type plot for gelant solution prepared in distilled and injection water.

A good fit was obtained for both solutions using equation 3.3, which yielded activation energies of 43.6 kJ/mol and 61.4 kJ/mol for distilled and injection water, respectively. The activation energy was always considered as a good indicator of gelation reaction sensitivity to temperature [222] and the easiness or difficulty of the gelation reaction [182]. Higher activation energies indicate that the reaction is more difficult to proceed and is more sensitive to temperature, while lower activation energies indicate that the reaction can proceed more easily and is less sensitive to temperature. Based on these definitions and the activation energies obtained, it is clear that the gelation reaction occurs easier in distilled water (43.6 kJ/mol) compared to injection water (61.4 kJ/mol). Furthermore, when comparing the obtained activation energies with those reported in the literature for other PEI-based polymer gels as summarized in **Table 3.4**. We can see the good agreement, with lower values being obtained for our PHPA/PEI gels. Al-Muntasheri et al. reported activation energies of 120 and 71.3 kJ/mol for their PAtBA/PEI gel system (T=100-140 °C, TDS=0.02 g/l) [105] and PAM/PEI gel system (T=100-140 °C, distilled water) [70] respectively, compared to only 43.6 kJ/mol for our PHPA/PEI gel (T=60-90 °C, distilled water). In addition to the difference between the studied temperature ranges and the crosslinkers molecular weights (their PEI had a Mw of 70×10^4 g/mol), the most critical parameter that can result in such disproportion between our and their activation energies, would be the polymers molecular weights. Higher molecular weight polymers as it is the case for our PHPA (Mw=5×10^6 g/mol), result in more entangled polymer network compared to shorter polymers, as was the case for PAM and PAtBA (both had a Mw=0.25-0.5$\times10^6$ g/mol). Such entangled network, as discussed earlier, renders the crosslinking reaction more easier thus the lower activation energies are observed.

Table 3.4 : Activation energies reported in the literature for PEI crosslinked polymer gels.

Gelling system	Mixing water	Temperature range (°C)	Activation energy (kJ/mol)	References
PAtBA/PEI	TDS=0.02 g/l	100-140	120	[105]
	TDS=1.19 g/l		115	
	TDS=58.35 g/l		92	
PAM/PEI	Distilled water	100-140	71.3	[70]
	10 g/l NaCl water	120-140	88	
HAP/PEI	Distilled water	50-90	41.6 in bottle	[75]
		70-90	60.9 in core	
(AM, AMPSA, NVP)/PEI	Distilled water + 0.1 % Na_2CO_3 + 0.05 % thiourea	50-160	89.14	[74]
PHPA/PEI	Injection water TDS=3.4 g/l	60-90	61.4	This study
	Distilled water		43.6	

In regard to the gel strength under the effect of temperature, studies in literature were scarce. To assess this point, gelant solutions prepared with 5000 ppm PHPA1 and 1000 ppm PEI25 in injection water, were cured at different temperatures of 60, 70, 80 and 90 °C for 48 hours to account for the effect of temperature on the viscoelastic moduli of the formed gels. **Figure 3.13** shows the storage and loss moduli as function of the curing temperature. The storage modulus was found to slightly increase with temperature following an exponential relationship:

$$G' = 12.605e^{0.0215\,(T)} \qquad \text{Equation 3.4}$$

While the loss modulus remained almost constant. This result suggests that the number of crosslinked sites increased with temperature. As the concentrations of both reactants remained constant, such trend can be only explained by the higher interactions due to the enhanced mobility of the polymer and crosslinker at high temperatures.

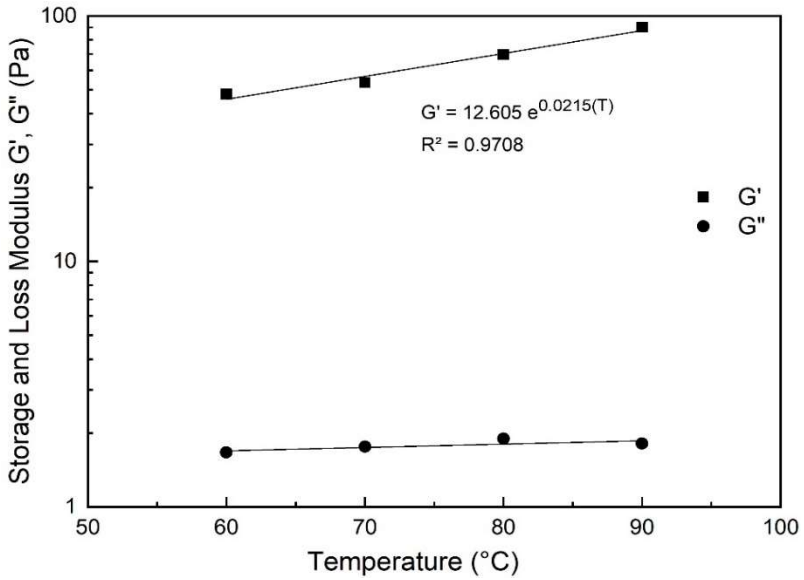

Figure 3.13 : Temperature effect on the storage (G') and loss (G") moduli.

3.3.2.6 Inorganic Salts effect

Polymer gels are usually prepared with field injection waters which represent up to 99% of their total composition. These injection waters are charged with monovalent and bivalent cations. In this subsection, we wanted to quantify separately the effects of monovalent and divalent cations on PHPA/PEI gelation time and gel strength. To accomplish this, various amounts (5, 10, 15 g/l) of NaCl and $CaCl_2$ were added to gelant solutions prepared with 10000 ppm PHPA1 and 2000 ppm PEI25 in distilled water. Each gelant solution was separated in two samples, the first sample was directly loaded to the coaxial cylinder to evaluate its viscosity evolution with time (gelation time) while the second sample was first cured for 48 hours at 80 °C and then loaded to the parallel plates geometry for the viscoelastic moduli determination. **Figure 3.14** and **Figure 3.15** show the gelation time and the storage modulus (gel strength) respectively as function of inorganic salts (NaCl and $CaCl_2$) concentrations.

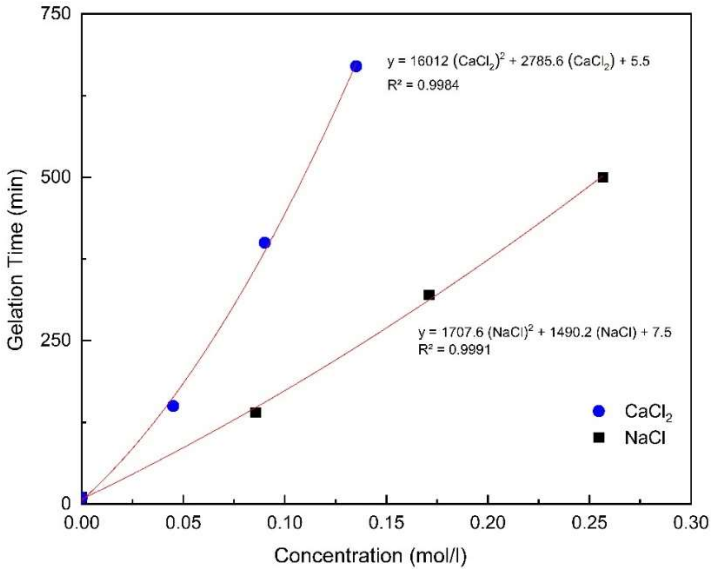

Figure 3.14 : Inorganic salts (NaCl and $CaCl_2$) effect on gelation time.

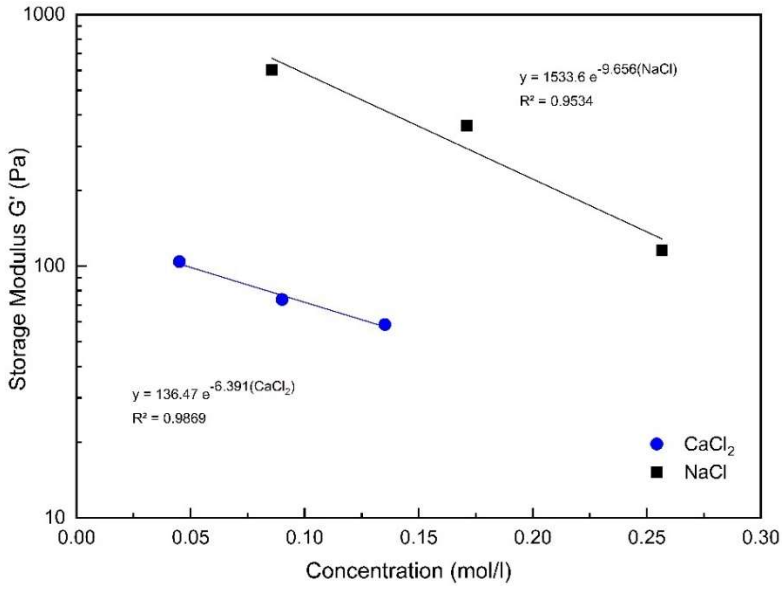

Figure 3.15 : Inorganic salts (NaCl and $CaCl_2$) effect on the storage modulus (G').

At higher salt concentrations, lower gelant viscosities, higher gelation times and lower gel strengths were recorded. Gelation times were successfully correlated with a second-degree polynomial [123] while the storage moduli were correlated with exponential relationships. Cations affect negatively on anionic polymer gels through a charge-shielding effect [84]. The crosslinking rate and its extent were limited due to the occupied carboxylate groups which represent possible crosslinking sites and the lower hydrodynamic volume of PHPA, which renders the polymer network less entangled and the crosslinking sites (either the amide or carboxylate groups) less accessible. Although the two salts have approximately the same ionic radius, and considering the same molar concentration, calcium chloride ($CaCl_2$) had a higher negative effect than sodium chloride (NaCl) because of its greater ionic charge. In order to further highlight this difference, the DSC technique was employed. DSC was recently used to study the retardation mechanism of inorganic salts (NH_4Cl and NaCl) on the gelation kinetics of PAM/PEI gels [116, 118]. In our study, two gelant solutions were prepared with 20000 ppm PHPA1 and 4000 ppm PEI25 in 10 g/l NaCl and 10 g/l $CaCl_2$ water, respectively. A sample of around 5 mg from each gelant solution was loaded in hermetic pans and placed in the DSC instrument. The same temperature program as the one employed in the temperature effect subsection was followed. **Figure 3.16** shows the heat flow variations versus temperature of the two samples. It is clear that the onset of the crosslinking temperature was higher (70.06 °C), and the exothermic heat (99.09 J/g) was lower for the sample prepared in $CaCl_2$ water. This result demonstrates that the crosslinking reaction is more difficult (higher gelation times), and the crosslinked sites are fewer (weaker gels) in the presence of calcium chloride ($CaCl_2$) compared to sodium chloride (NaCl), confirming the higher charge shielding effect of $CaCl_2$.

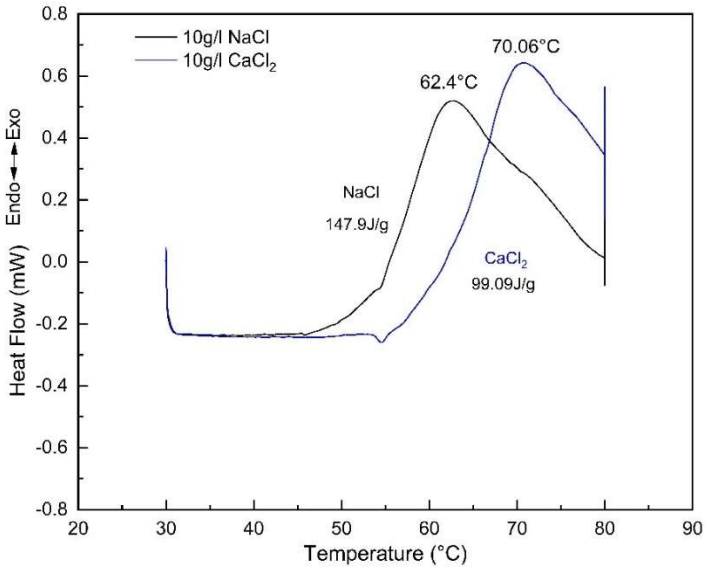

Figure 3.16 : DSC curves of gelant solution prepared in 10 g/l ($NaCl/CaCl_2$) water.

3.3.3 Gel degradation temperature

Alongside the long-term thermal stability evaluated through the bottle test method, the thermal degradation of the PHPA/PEI gel was examined using differential scanning calorimetry (DSC). The degradation temperature, at which the crosslinking bonds starts to break down, coincides with a high endothermic peak [181]. For the PHPA/PEI gel, it was found to be around 122°C as shown in **Figure 3.17**. This temperature was higher than those of similar inorganic and organic crosslinked polymer gels (temperatures from 100 to 111 °C were reported for gels prepared with an acrylamide/AMPSA copolymer crosslinked with chromium (III) acetate, aluminium nitrate, PEI and Hexamethylenetetramine) [223]. Such high degradation temperature is also an indicator on the presence of covalent bonds between the polymer and the crosslinker [69].

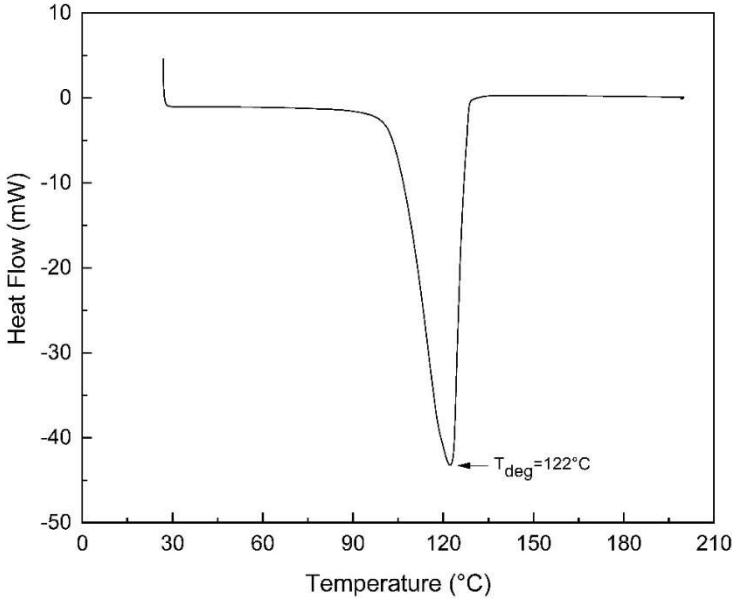

Figure 3.17 : Degradation temperature of PHPA/PEI gel.

3.3.4 Gel morphology

The microstructure of a PHPA/PEI gel, prepared with 20000 ppm PHPA and 10000 ppm PEI in distilled water and cured overnight at 80°C, was examined using the SEM technique as shown in **Figure 3.18**. SEM images magnified at ×500, ×1000, ×2000 and ×5000 revealed the dense and homogeneous morphology of the formed 3D structure. Bai et al. [75] reported a honeycomb structure which contains a connected skeleton and disconnected cavities for a hydrophobically associated polymer (HAP) crosslinked with PEI. Similarly, Zhu et al. [74] observed a more porous gel structure with grid sizes of 33.5 to 50.6 µm for their terpolymer P(AM/AMPS/NVP) crosslinked with PEI. In both cases, the structure voids were explained by the presence of intermediates groups (hydrophobic groups of HAP and AMPS/NVP of the terpolymer) which do not react with the crosslinker and only separate the amide groups that were considered as responsible on the crosslinking reaction with the amine groups of PEI. In our case, we couldn't observe any voids in the PHPA/PEI structure which can be explained by the absence of intermediate non-reactive groups. Moreover, the crosslinking reaction can take place between both the amide or carboxylate groups of the PHPA with the amine groups of PEI, which means higher number of crosslinked sites and thus a compact gel structure. However, one should not exclude the possible structure damages that could have been occurred during the freeze-drying and gold coating process related to the SEM samples preparations [224]. In any case, and despite the data provided in the literature, the interpretation of a structure of the sample in solution based on a two-dimensional microscopic visualization of the dried sample seems to us to be very controversial.

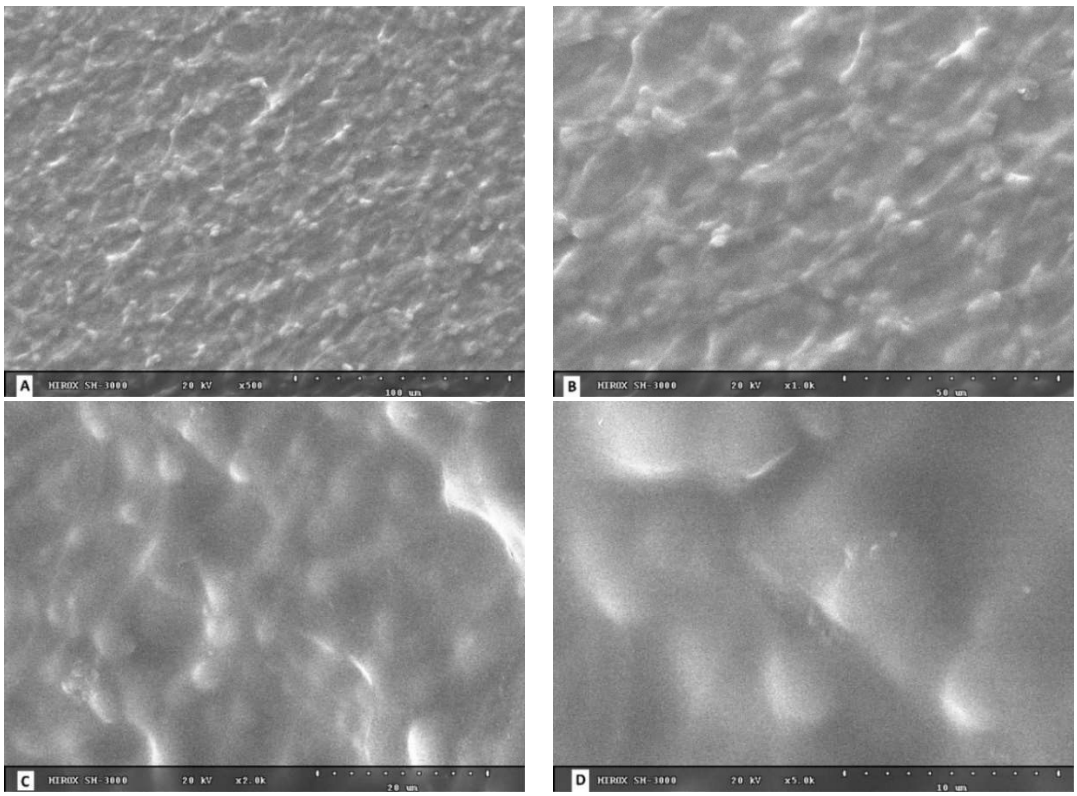

Figure 3.18 : SEM images of PHPA/PEI gel cured at 80 °C magnified at (A) ×500 (B) ×1000 (C) ×2000 (D) ×5000.

3.4 Conclusion

The proper characterization of the thermal gelation of any gel system under reservoir conditions is very important to the succeful of the gel treatement. This can be obtained through a better understanding of the thermal stability, the structure-property relationships and viscoelastic behavior of the targeted system as function of the reactant concentration ratios, the reactants structure (molecular weights) and the initial physicochemical conditions (temperature and mixing water salinity).

In this chapter, the thermal gelation of well charcterized PHPA and PEI polymers was evaluated under the effect of some controlling paramters by modifying a single parameter at a time in order to adress a gel treatement in an algerian oilfield (T= 80 °C and TDS= 3.4 g/l). First, the choice of the concentration regime is important to obtain a continuous gel structure but also to have reasonable initial gelant viscosites; thus, all the experiments were conducted above the diluted regime of the polymer ($c>c^*$) with initial gelant viscosities of around 10 cP using the main selected PHPA polymer namely PHPA1 (Mw= 5×10^6 g/mol and HD= 6%). A qualitative evaluation of the PHPA/PEI system through the bottle test method was conducted. High reactants loadings resulted in lower gelatin times and stronger gels that reached code “I” in sydansk’s gel code comparably to previous PEI based crosslinked polymer gels. The gel samples were shown to be stable at 80 °C over the course of 3 months of observations. However, samples prepared with crosslinker/polymer ratio higher than ½ suffered syneresis while those prepared with low crosslinker concentrations (500 or 1000 ppm) lost their strength over the period of 3 months. A quantitative evaluation of gelation time and gel strength was then realized using steady and dynamic shear measurements. The investigation on the effect of shear rate on the gelation time showed the negative effect of shear flow on the gelation reaction and gel structure. The viscosity increase after gelation point was found to follow a power law relationship which corresponds to a shear thinning effect of the three-dimensional structure being formed. On the other side, frequency sweep tests revealed that the viscoelastic moduli were totally independent of the applied frequency and the storage modulus (G’) is largely higher than the loss modulus (G”). confirming the formation of a 3D crosslinked structure. We demonstrated also the antagonistic effect on the gelation time and the viscoelastic moduli between reactants concentrations, reactants molecular weight and temperature in one hand, and mixing-water salinity in the other one. Contrary to what was reported in literature, the gelation time was found to not follow an exponential variation with reactants concetrations while gel strength followed this exponenetial trend with regards to reactants conentrations. The lower gelation times and the higher gel strengths obtained at high reactant concentrations were explained by the greater number of available crosslinking sites at these conditions. The gelation time was mainly affected by the crosslinker concentration whereas the gel strength by the polymer concentration. At high polymer concentrations, the polymer chains overlap

between each other and create entanglement points which favorize the intermolecular crosslinking reaction. The same explanation was evoked for the molecular weight effect on gelation time and gel strength instead of the common explanation given in literature which relates this trend to the availability of additional crosslinking sites in the high molecular weight polymers. The PHPA/PEI reaction was found to be exothermic in nature and the system activation energies were of 43.6 kJ/mol for distilled and of 61.4 kJ/mol for injection water indicating that the interaction is easier in distilled water. In fact, the presence of monovalent and bivalent cations in the mixing water reduces the gel characteristics (gelation time and gel strength) through a charge shielding effect. The cations screen the negatively charged carboxylate groups at the polymer backbone reducing consequently the hydrodynamic volume of the polymer (less entangled polymer network) and the number of possible crosslinking sites (carboxylate groups). A quantification of the effect of monovalent and bivalent cations namely sodium chloride and calcium chloride on the gelation time and gel strength was conducted. Particularly, the calcium chloride presence resulted in very high gelation times and very low storage modulus compared to the sodium chloride because of the higher ionic charge of calcium ions. Furthermore, the PHPA/PEI system showed interesting features in terms of degradation temperature which reached 122 °C and gel morphology that was homogeneous and compact.

Chapter IV:

Gelation time optimization using RSM

4. Chapter IV: Gelation time optimization using response surface methodology

4.1 Introduction

As discussed in the previous chapters, the gelation time is the most important parameter during the gel injection operations in the oilfield. For a selected polymer gel system, the gelation time can be controlled either by varying the reactants concentrations, increasing the salinity of the mixing water by adding monovalent inorganic salts or changing the temperature of the targeted reservoir zone by injecting large quantities of hot/cold water prior to the gel placement operation. In the previous chapter, the effects of four controlling parameters (polymer concentration, crosslinker concentration, temperature and salinity) were assessed using the one variable at time (OVAT) approach. In this chapter, a statistical analysis and an optimization of the gelation time of PHPA/PEI system under the effect of the aforementioned parameters were conducted using the response surface methodology (RSM). The aim was to develop a mathematical model which is able to predict the gelation time of PHPA/PEI system for temperatures between 70 to 90 °C which represent the usual reservoirs temperatures in some of the biggest Algerian fractured reservoirs. A four factor doehlert matrix was employed to design the experiments and evaluate the gelation time as function of water salinity (NaCl concentration from 0 to 8 g/l), polymer concentration (4000 to 10000 ppm), crosslinker concentration (500 to 2500 ppm), temperature (70°C to 90°C) and their corresponding combinations. The statistical analysis of the obtained experimental responses and the mathematical model fitting were next proceeded using the JMP Pro 13 software. While, the statistical significance of the proposed mathematical model and its terms was assessed using the analysis of variance (ANOVA), the determination coefficient, the adjusted determination coefficient and the root mean square error. Moreover, the effect of each parameter and the interactions between the parameters were presented and discussed through 3D response surface plots. Finally, the optimal parameters, to obtain an adequate gelation time in fixed reservoir conditions of temperature and depth, were determined using the desirability approach. Prior to the experimental part, a literature review on the Response Surface Methodology (RSM), Design of Experiments (DoE) principle, the most famous designs and the application of DoE on gel systems, was presented.

4.2 Response Surface Methodology

Introduced in the early 50s by Box and Winter [225], the response surface methodology (RSM) represents a collection of mathematical and statistical techniques which allows (1) modelling engineering problems with several controllable factors (independent variables) and responses (dependent variables), (2) analyzing the effect of these factors and the interactions between them, and

finally (3) finding the best values of the factors which optimize these problems [226, 227]. A general workflow in RSM is consisted of five steps as reported by Bezerra et al. [228]:

- Selecting the major independent variables, which effect on the system, through screening studies and delimitating the experimental region, based on the objective of the study and the experience of the researcher.
- Choosing the experimental design and carrying out the experiments according to the selected experimental matrix.
- Fitting a nonlinear mathematical model using the obtained experimental data.
- Evaluating the model's fitness.
- Obtaining the optimum values for each studied variable.

In RSM, the aim is to develop the best approximative relationship between the "k" independent variables "ζ_i" and the response "*y*" as defined below [229]:

$$y = f(\zeta_1, \zeta_2, \dots \zeta_k) + \varepsilon \qquad \text{Equation 4.1}$$

Where f is the unknown response function, ε is the statistical error which represents the other sources of variability not accounted for in *f*, including measurement error on the response, the effect of other non-considered variables. Usually ε is assumed to have a normal distribution with mean zero $E(\varepsilon) = 0$ and variance σ^2:

$$E(y) = \eta = E\big(f(\zeta_1, \zeta_2, \dots \zeta_k)\big) + E(\varepsilon) = f(\zeta_1, \zeta_2, \dots \zeta_k) \qquad \text{Equation 4.2}$$

As the independent variables "ζ_i" have different measurement units, it is more convenient to transform them to dimensionless coded variables "x_i". Consequently, the true response function can be written as:

$$\eta = f(x_1, x_2, \dots x_k) \qquad \text{Equation 4.3}$$

Based on the number of the inputs and the variation of the output, either a first-order (Equation 4.4) or a second-order (Equation 4.5) model is used to fit the independent variables to the response. By far, the second-order model was preferred in RSM because of its flexibility and easy determination of its regression coefficients (β_i) [227] :

$$\eta = \beta_0 + \sum_{i=1}^{k} \beta_i \, x_i + \sum_{i=1, j=i+1}^{k} \beta_{ij} \, x_i x_j \qquad \text{Equation 4.4}$$

$$\eta = \beta_0 + \sum_{i=1}^{k} \beta_i \, x_i + \sum_{i=1}^{k} \beta_{ii} \, x_i^2 + \sum_{i=1, j=i+1}^{k} \beta_{ij} \, x_i x_j \qquad \text{Equation 4.5}$$

The regression coefficients of the chosen model are determined using the least square method, which consists on finding the vector of least squares estimators, b, that minimizes the sum of square errors "L" as given below [230]:

$$L = \sum_{i=1}^{n} \varepsilon_i^2 = \varepsilon^T \varepsilon = (y - X\beta)^T (y - X\beta) \quad \text{Equation 4.6}$$

Equation 4.6 is minimal when its derivative is null. Thus, after calculation and simplification, the vector of the least square is given as:

$$b = (X^T X)^{-1} + X^T Y \quad \text{Equation 4.7}$$

4.3 Design of Experiment (DOE)

In RSM, the choice of the experimental design is the most critical step which affects the accuracy of the mathematical model and the cost of constructing the response surface. Design of Experiments (DoE) represents the various techniques of choosing the best combinations of the independent variables or inputs (samples) inside the design space (the intervals of theses variables) to maximize the amount of information using the lowest number of samples. The basic principles in the design of experiments encompasses the replication, the randomization and the blocking defined as follow [231]:

- Replication: consists of repeating the experiments in order to obtain a more precise result (sample mean value) and to estimate the experimental error (sample standard deviation).
- Randomization: refers to the random order of performing the experimental runs in order to rule out the dependency between the conditions of a given run from those of the previous runs and those of the subsequent runs.
- Blocking: consists of arranging the experiments in groups that are similar to one another in order to reduce the sources of variability and improve the precision.

In literature, different ways of choosing the optimal arrangement of the sampling do exist. The most famous designs are presented below:

4.3.1 Factorial Design

Factorial designs represent the basis of all most common designs. The idea of these designs is simple and consists on making all the possible combinations between the different levels of the factors [232] which results in L^k experimental points for k factors with L levels. The factorial designs allow to assess the effect of each factor over the response variable independently, that to say, they are orthogonal. Moreover, each factor combination appears equally many times which is the property of balanced designs [232]. Factorial designs with only two or three levels for all design factors are the most frequently documented designs. In the case of three-level factorial designs (3^k factorial designs), the number of the experiments increases largely with the number of the studied factors. For problems with 4 and 5 factors, the number of experiments is of 81 and 243 experiment, respectively. Thus, the 3^k factorial design had just a limited application in RSM [228], and was mainly employed for problems with only two or three factors. On the other side, the two-level factorial designs (2^k factorial design) were the most used factorial designs, thanks to their adaptability for both qualitative and quantitative factors, lower number of experiments compared to other factorial designs with more

levels (>2), comparable efficiency to other sophisticated designs such as the central composite design. **Figure 4.1** shows the location of the experimental points in the two and three-factors 2^k and 3^k factorial designs, respectively.

Another type of the factorial designs, which was developed to overcome the problem of the high number of experiments in the 2^k and 3^k factorial designs, is the fractional factorial design. In such design, only a fraction of the experiments of either the 2^k or 3^k full factorial designs is realized. This fraction can be one-half, one-quarter or more of the full factorial design. The number of experiments is thus equal to L^{k-v} with v= 1, 2, 3… and the fraction of the full factorial is calculated as $1/2^v$ [233]. for example, in a two-level fractional factorial design (2^{k-1} fractional factorial design) with 5 factors (2^{5-1}), only 16 experiments are realized instead of 32 in a ($2^k = 2^5$) full factorial design. Some information is always lost when a fractional factorial design is performed, for instance not all main and interaction effects can be estimated separately [233].

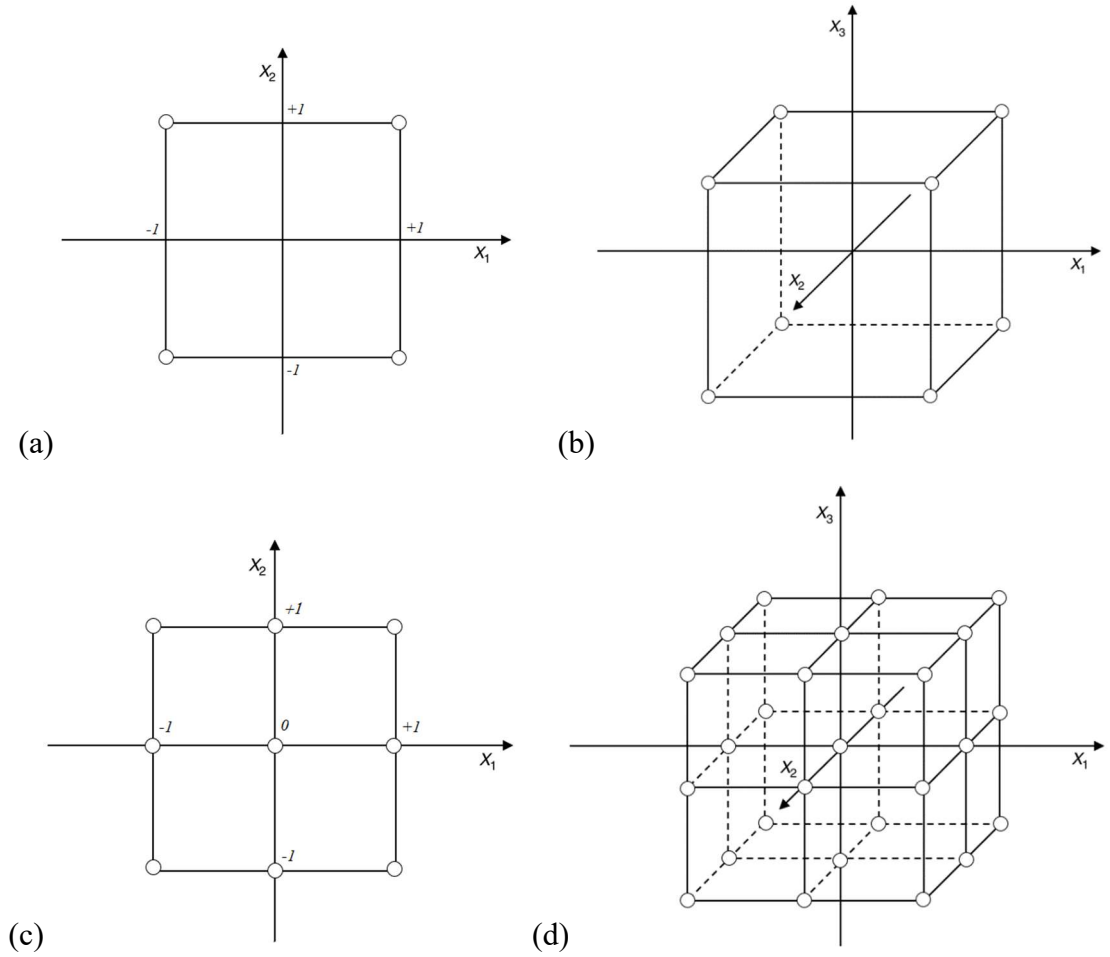

Figure 4.1 : The location of the experimental points in (a) two factors 2^k factorial design (b) three factors 2^k factorial design (c) two factors 3^k factorial design (d) three factors 3^k factorial design.

4.3.2 Central Composite Design

The central composite designs (CCD) were first introduced by Box and Wilson [225]. As their name suggests, the central composite designs are composed of three designs namely a 2^k full factorial

design, a star design in which 2×k experimental points are set at an α distance from the center and a central point [232]. Consequently, the total number of the experimental runs in CCD are equal to 2^k + 2k +1. Based on the α value, various types of CCD do exist [231] as shown in **Figure 4.2**:

- A central composite circumscribed (CCC) design with α>1, it is the original form of the CCD [234] and the most employed design in literature. In such design, the factors are studied at five levels (−1, −α, 0, +α, +1), the points at the levels −1 and +1 are those of the full factorial design, the points at the level 0 are the central points while the points at the levels −α and +α are those of the star design. The value of *α* depends on the number of factors and it is calculated as 2×k/4. For two, three, and four variables, *α* equals to 1.41, 1.68, and 2 respectively. **Figure 4.3** shows the location of the 9 and 15 experimental points for the two and three factors central composite circumscribed designs respectively.
- A central composite faced (CCF) design with α = 1, in this case the factors are studied only at three levels (−1, 0, +1).
- A central composite inscribed (CCI) design is a scale down of the CCC design, which is employed in specific situations where the limits of the factors cannot be violated [231]. In this case, the α values are taken at the limits and scaled to 1, while the factorial design points are scaled to 1/α.

While the added star points increase the ability of CCD to perceive the response behavior with a higher accuracy [235], the number of the experimental run in CCD increases rapidly with the number of factors because of the incorporated factorial design.

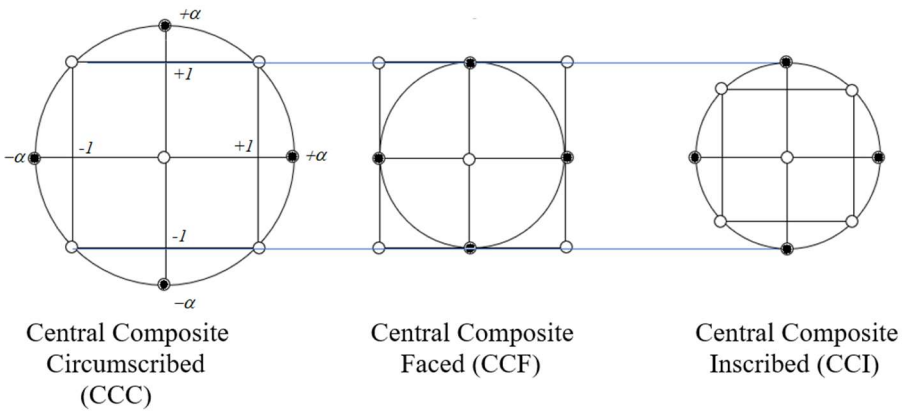

Figure 4.2 : Central composite design types.

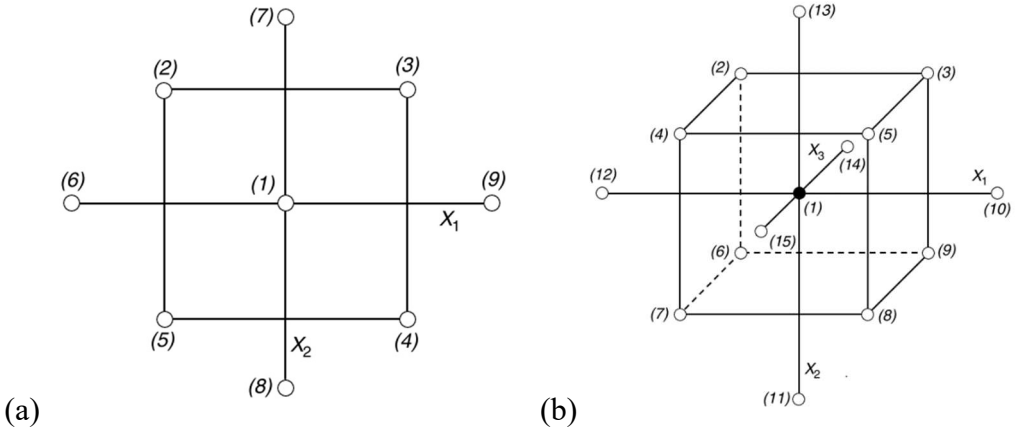

Figure 4.3 : The location of the experimental points in (a) two factors central composite circumscribed design (b) three factors central composite circumscribed design.

4.3.3 Box-Behnken Design

For problems with a number of factors strictly higher than two, the Box-Behnken designs (BBD) are built by combining two-levels factorial designs between each two factors while maintaining the other factors at zero [231]. In this case, all the factors are adjusted only at three levels (−1, 0, +1) [228]. The main idea of the Box-Behnken designs is to limit the sample size as the number of factors increases. This is obtained by maintaining only a sufficient sample size for the estimation of the coefficients in a second-degree least square approximating polynomial [236]. The number of the experimental runs in BBD, for a given number (k) of the studied factors, is thus equal to $2k^2 - 2k + 1$ [233]. **Figure 4.4** shows an example of the thirteen experimental points location in a three factors Box-Behnken design. In comparison to a full factorial design (27 experiments for three factors), the BBD is clearly more economical. However, the BBD do not cover well the experimental space and as consequent studying the combination of the factors at their extreme conditions (i.e., the corner of the cube in **Figure 4.4**) is not possible.

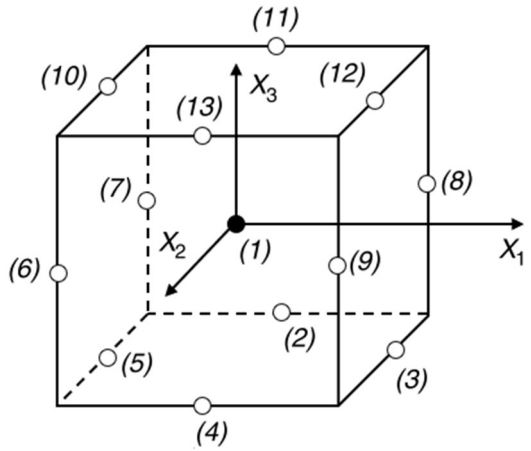

Figure 4.4 : The location of the experimental points in a three factors Box-Behnken design.

4.3.4 Doehlert Design

The Doehlert design, first proposed by Doehlert in 1970 [237], is a uniform shell design that was widely employed in the experimental design in various science fields especially in analytical chemistry [238]. Doehlert designs fill the experimental space in a regular way by choosing uniformly the sampling points at constant distances [232]. For two factors, the doehlert design is a hexagon with a central point, while for three factors, the doehlert design represents a cuboctahedron as shown in **Figure 4.5**:

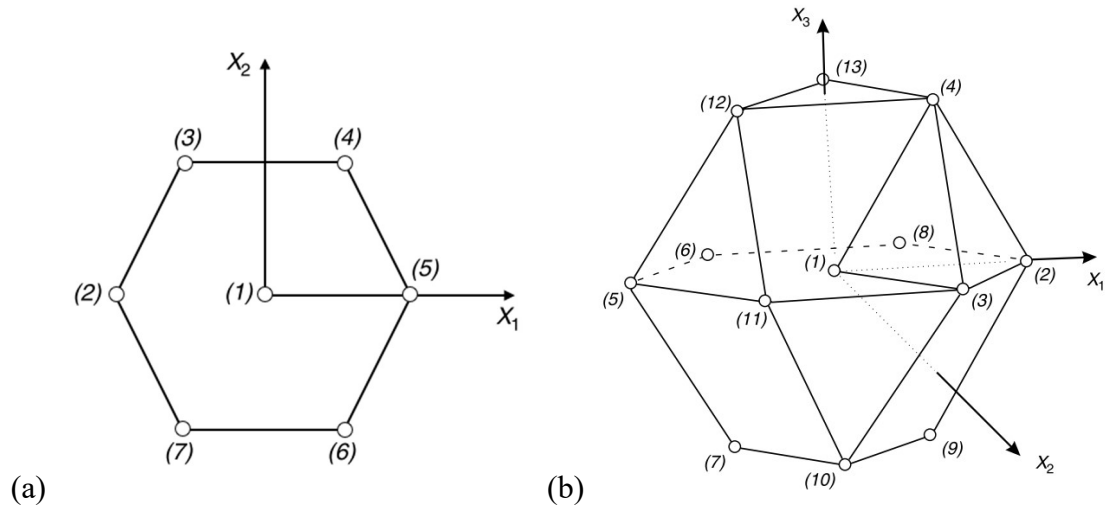

Figure 4.5 : The location of the experimental points in (a) two factors doehlert design (b) three factors doehlert design.[239]

Compared to other designs, the doehlert designs require only a few number of the experimental runs equal to k^2+k+1 where k is the number of the studied factors. These factors can be explored at different number of levels (e.g., 3, 5 and 7). In a two-factors doehlert design, one factor is studied at three level and the other one at five levels, while in the three-factors doehlert design, one factor is studied at three level, the second one at five, and last one at seven levels [233]. There is no general rule on how to assign the factors with the number of levels, however, it is preferable to study the strongest factors with the larger number of levels [238]. The doehlert matrices are not orthogonal nor rotatable as previous designs, but they allow the extension of the domain by adding another factor or displacing the design towards a new experimental domain without having to repeat all initial experiments [240].

4.4 Application of DoE on gel systems

In literature, several studies were reported on the use of DoE in evaluating the characteristics of different gel systems employed for conformance control treatments. Here below, we are reviewing those studies conducted exclusively during the last decade. Moghadam et al. [241] reported the use of the fractional factorial design to investigate the effect of eight factors namely pH, NaCl and $CaCl_2$

concentrations, crosslinker/copolymer ratio, polymer concentration and presence or absence of sodium lactate, nanoclay, and thiourea, on the gelation time of sulfonated polyacrylamide/chromium (III) acetate system. They found that sodium lactate presence, copolymer concentration, nanoclay presence, thiourea presence, and crosslinker/copolymer ratio were the main affecting factors. Salehi et al. [235] studied the effect of NaCl concentration and pH on the gelation time of a similar sulfonated polyacrylamide/chromium (III) acetate system using central composite design (CCD) and found that the gelation time was more dependent on the pH value than the salinity. In another study, Salehi and coworkers [242] employed the Plackett-Burman Design (PBD) to screen a larger number of factors namely the concentration of polymer and crosslinker, pH, temperature and presence or absence of NaCl, KCl, $CaCl_2$, $MgCl_2$, thiourea, sodium lactate and nanoclay on the gelation time of the same polymer gel (sulfonated polyacrylamide/ chromium triacetate). Since the PBD allowed to assess the effect of each parameter separately, they used the CCD to investigate the interactions between the most influencing parameters which were the temperature, pH and $CaCl_2$ concentration. The gelation time, of a grafted carboxymethyl cellulose-g-polyacrylamide copolymer (PAM-g-CMC) crosslinked to chromium acetate, was also investigated in terms of polymer concentrations and polymer/crosslinker ratios using CCD [243]. It was found that the gelation time was more affected by the polymer concentrations rather than the crosslinker concentrations. Furthermore and using CCD, Lenji et al. [244] studied the gelation time of sulfonated polyacrylamide/ Hexamethylenetetramine (HMTA) system under the effects of the polymer and crosslinker concentrations, and hydrochloric acid (HCl) concentration which was added as an activator. Similarly, CCD was used to compare the gelation and syneresis times of polymer gels prepared with a sulfonated polyacrylamide and different crosslinkers, including chromium triacetate, aluminum nitrate, PEI and HMTA [223]. The investigations on the gelation time, the viscoelastic behavior and the thermal stability of the four prepared polymer gels showed that the PEI crosslinked polymer gel had the optimum characteristics in terms of lower gelation times, delayed syneresis times and higher resistance to deformation using only low reactants concentrations. More recently, Amir et al. [245] investigated the effects of polymer and crosslinker concentrations on the gelation time and initial viscosity of PAM/PEI gel system at 95 °C using CCD. The reactants concentrations had an opposite effect on the two responses (gelation time and initial viscosity), while the polymer concentration effect was more pronounced compared to the crosslinker concentration.

4.5 Materials and methods

Partially hydrolyzed polyacrylamide (PHPA1) and polyethylenimine (PEI25), presented in the materials characterization chapter, were used in this chapter as the base polymer and crosslinker respectively. The PHPA1 had a molecular weight (Mw) of 5×10^6 g/mol and a hydrolysis degree (HD) of 6% and was chosen based on its low initial gelant viscosities, which are recommended for field

injection operations. On the other side, the PEI25, which had a molecular weight (Mw of 20000 g/mol) and a branching degree (BD) of 59% , was chosen preferentially because of its higher active content. Distilled water obtained from a milliQ system (18.2 MΩ.cm) and an ACS grade sodium chloride (NaCl) purchased from Sigma Aldrich were used to prepare the mixing water with variant salinities.

Gelant solutions, with a volume of approximately 20 ml, were prepared by sprinkling the right amount of the polymer powder inside the vortex created by the vigorous stirring of the mixing water using a magnetic stirrer. Homogenization was kept for two hours, then the appropriate amount of the crosslinker was added and the stirring was continued for additional 5 minutes. The gelant solutions were directly loaded into the coaxial cylinder of the rotational rheometer (Anton Paar, MCR 302). Viscosity evolution of each gelant solution was monitored versus time at a shear rate of 1 s^{-1} to avoid any shear effect interference.

4.6 Results and discussions:

4.6.1 Experiment implementation:

To implement the doehlert design, the experimental values of the four factors and for each experimental run, were first calculated using the following relationship:

$$F_{ij} = (X_{ij} \times \Delta F_i) + \bar{F}_i \qquad \text{Equation 4.8}$$

where F_{ij} is the experimental value of the factor "i" (i=1, 2, 3, 4) at the level "j" (j=1, 2,…,3 or 5 or 7), X_{ij} is the value of the coded variable "i" at the level "j" as given in **Table 4.1**. $\bar{F}_i$ is the value of the factor "i" in the center of the experimental domain, and ΔF_i is the variation range of the factor "i" defined as:

$$\bar{F}_i = \frac{high\ level\ of\ F_i + low\ level\ of\ F_i}{2} \qquad \text{Equation 4.9}$$

$$\Delta F_i = \frac{high\ level\ of\ F_i - low\ level\ of\ F_i}{2\theta_i} \qquad \text{Equation 4.10}$$

with θ_i the coded value limit for each factor. In a doehlert design with four factors, θ_i are taken as θ_1 = 1; θ_2 = 0.866; θ_3 = 0.816; θ_4 = 0.791. The four factors (k=4) were donated as "F_1" for NaCl concentration (salinity), "F_2" for PHPA1 (polymer) concentration, "F_3" for PEI25 (crosslinker) concentration and "F_4" for temperature. The NaCl concentration was studied at five levels (j= 1, …5), both polymer and crosslinker concentrations were investigated at seven levels (j= 1, …7) while temperature was studied at three levels (j= 1, 2, 3). The independent factors with their low/high experimental levels, central values and variation ranges are summarized in **Table 4.2**:

Table 4.1 : Possible X_{ij} values in a four factors doehlert design.

X_{ij}	j= 1	j= 2	j= 3	j= 4	j= 5	j= 6	j= 7
i= 1	-1	-0.5	0	0.5	1	/	/
i= 2	-0.866	-0.577	-0.289	0	0.289	0.577	0.866
i= 3	-0.816	-0.612	-0.204	0	0.204	0.612	0.816
i= 4	-0.791	0	0.791	/	/	/	/

Table 4.2 : Independent factors and their levels.

Independent Factors	Coded variable	Levels of factors		$\bar{F}_i$	ΔF_i
		Low level	High level		
F_1: NaCl concentration (ppm)	X_1	0	8000	4000	4000
F_2: polymer concentration (ppm)	X_2	4000	10000	7000	3464.2
F_3: crosslinker concentration (ppm)	X_3	500	2500	1500	1225.5
F_4: temperature (°C)	X_4	70	90	80	12.6

In a doehlert design, a total number of $k^2 + k + 1$ experimental run are needed. In the case of four factors (k=4), 21 experimental runs should be conducted. However, two replications of the center point were added to estimate the experimental error. Consequently, the complete doehlert matrix consisted of 23 experimental runs and the calculated experimental values of the independent factors are presented in **Table 4.3**:

Table 4.3 : Doehlert matrix and the corresponding experimental values.

No.	Doehlert matrix				Actual values of independent factors			
	X_1	X_2	X_3	X_4	NaCl concentration (ppm)	polymer concentration (ppm)	crosslinker concentration (ppm)	temperature (°C)
1	0	0	0	0	4000	7000	1500	80
2	1	0	0	0	8000	7000	1500	80
3	0.5	0.866	0	0	6000	10000	1500	80
4	-0.5	0.866	0	0	2000	10000	1500	80
5	-1	0	0	0	0	7000	1500	80
6	-0.5	-0.866	0	0	2000	4000	1500	80
7	0.5	-0.866	0	0	6000	4000	1500	80
8	0.5	0.289	0.816	0	6000	8000	2500	80
9	-0.5	0.289	0.816	0	2000	8000	2500	80
10	0	-0.577	0.816	0	4000	5000	2500	80
11	0.5	-0.289	-0.816	0	6000	6000	500	80
12	-0.5	-0.289	-0.816	0	2000	6000	500	80
13	0	0.577	-0.816	0	4000	9000	500	80
14	0.5	0.289	0.204	0.791	6000	8000	1750	90
15	-0.5	0.289	0.204	0.791	2000	8000	1750	90
16	0	-0.577	0.204	0.791	4000	5000	1750	90
17	0	0	-0.612	0.791	4000	7000	750	90
18	0.5	-0.289	-0.204	-0.791	6000	6000	1250	70
19	-0.5	-0.289	-0.204	-0.791	2000	6000	1250	70
20	0	0.577	-0.204	-0.791	4000	9000	1250	70
21	0	0	0.612	-0.791	4000	7000	2250	70
22	0	0	0	0	4000	7000	1500	80
23	0	0	0	0	4000	7000	1500	80

4.6.2 Mathematical model Fitting

Twenty-three gelant solutions were prepared following the procedure stated in the materials and methods section. The experimental measurements were performed in a random sequence to minimize the effects of uncontrolled factors [243]. For each experimental run, the response (gelation time) was determined at the inflection point in the viscosity versus time plot as previously explained in section 3.3.2.1 of chapter I. The gelation times of the 23 gelant samples varied between 10 to 540 minutes. The statistical analysis of the obtained experimental responses was next conducted using the JMP Pro 13 software (from SAS "Statistical Analysis System" Institute Inc, Copyright © 2016). The experimental responses (gelation times) were first fitted using the second order model (Equation 4.5). However, some of the model predicted responses were negative indicating the gelation time is not directly correlated to the studied factors through a polynomial model. Consequently, we decided to use an exponential model where the logarithmic of gelation time (ln GT) is inserted and fitted in the JMP software instead of the gelation time. **Table 4.4** presents the predicted responses of the polynomial and exponential models while **Figure 4.6** compares between the normalized predicted to experimental results of both models for each run. From the figure, it was clear that the predicted responses using the exponential model were fairly close to the unit compared to those obtained using the polynomial model. The obtained exponential model in terms of coded variables is given in Equation 4.11, where the regression coefficients (a_i, a_{ii}, a_{ij}) were estimated using the method of least squares:

$$\ln(GT) = 4.8923 + 1.4504X_1 - 0.6763X_2 - 0.1094X_3 - 0.8424X_4 - 0.4948{X_1}^2 + 0.0758{X_2}^2 + 0.2889{X_3}^2 - 0.0919{X_4}^2 + 0.2090X_1X_2 + 0.3518X_1X_3 - 0.0109X_1X_4 - 0.0257X_2X_3 - 0.2140X_2X_4 - 0.3397X_3X_4. \quad \text{Equation 4.11}$$

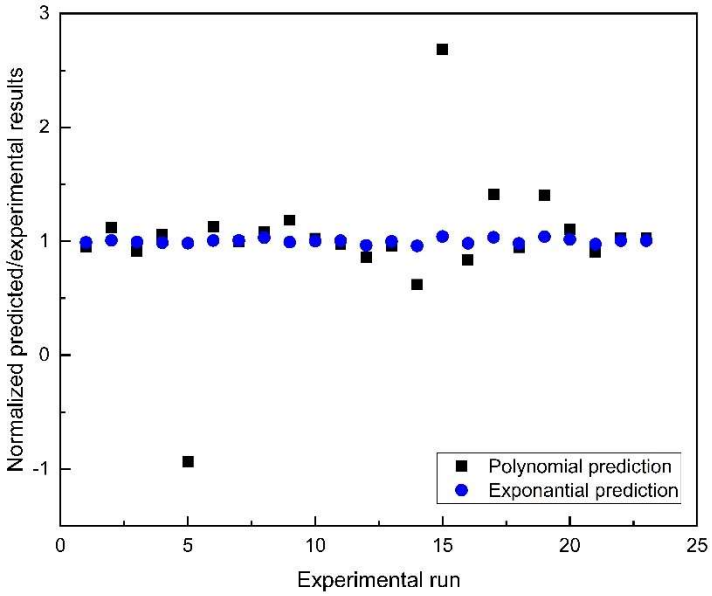

Figure 4.6 : normalized predicted/experimental results for each experimental run using the polynomial and the exponential models.

Table 4.4 : Experimental and predicted responses obtained by the polynomial and exponential models.

Run No.	Experimental response (min)	Predicted response by polynomial model* (min)	Predicted response by exponential model* (min)
1	140	133.3	133.3
2	330	368.7	346.5
3	162	147.5	156.9
4	32	33.8	30.7
5	20	-18.7	19.1
6	115	129.5	118.7
7	405	403.2	422.4
8	222	240.5	263.9
9	45	53.3	43.7
10	225	230.5	226.6
11	320	311.7	329.4
12	130	111.5	109.3
13	125	119.5	124.1
14	112	69.3	92.5
15	17	45.6	19.2
16	110	91.8	101.5
17	78	110.3	90.8
18	540	511.4	479.1
19	105	147.7	127.1
20	170	188.2	184.3
21	350	317.7	300.9
22	130	133.3	133.3
23	130	133.3	133.3

* polynomial predictions are obtained by modelling the experimental results (GT) directly to a second order equation, exponential predictions are obtained by modelling the logarithm of experimental results Ln (GT) to a second order equation.

The logarithm of the experimental responses and the predicted responses using the exponential model were plotted in **Figure 4.7**. The predicted and experimental responses were essentially aligned with the diagonal indicating the two responses to be very close.

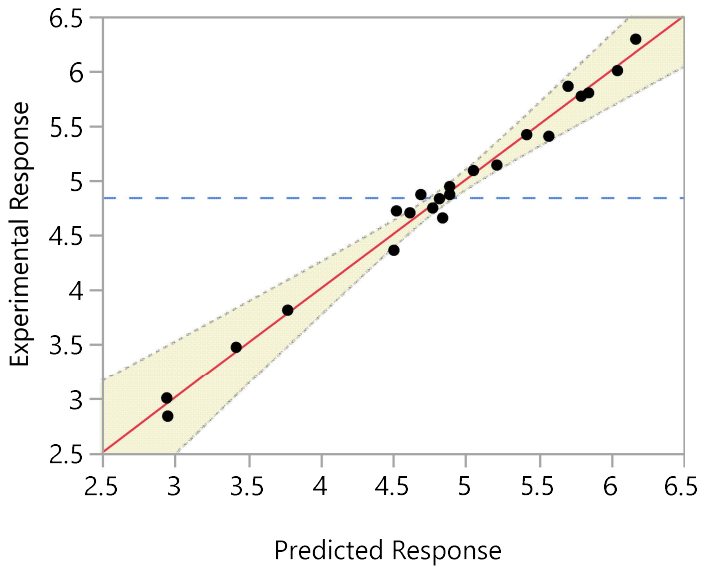

Figure 4.7 : Experimental response versus predicted response plot.

4.6.3 Statistical significance

To assess the statistical significance of the model as well as the model terms (the four factors and their interactions) on the response, the Analysis of Variance (ANOVA) was conducted. The ANOVA consists on comparing the variation due to the treatment (change in the combination of variable levels) with the variation due to random errors associated with the measurements of the experimental responses [246]. In such analysis, the evaluation of these variations is made by calculating the different deviations of the observations or their replicates, the sum of squares, the degree of freedom and the mean squares for each source (model, model terms, residuals, lack of fit and pure error) as defined in the **Table 4.5**:

Table 4.5 : The mathematical relationships of the sum of squares, the degree of freedom and the mean squares for each source used in ANOVA.

Source	Sum of squares (SS)	Degree of freedom (Df)	Mean square (MS)
Model	$SS_{model} = \sum_{i}^{n} (\hat{y}_i - \bar{y})^2$	$p - 1$	$MS_{model} = \frac{SS_{model}}{p - 1}$
Residuals	$SS_{res} = \sum_{i}^{n} (y_i - \hat{y}_i)^2$	$n - p$	$MS_{res} = \frac{SS_{res}}{n - p}$
Lack of fit	$SS_{lof} = \sum_{i}^{n} (\hat{y}_i - \bar{y}_i)^2$	$n - n_r - p + 1$	$MS_{lof} = \frac{SS_{lof}}{n - n_r - p + 1}$
Pure error	$SS_{pe} = \sum_{i}^{n_r} (y_i - \bar{y}_i)^2$	$n_r - 1$	$MS_{pe} = \frac{SS_{pe}}{n_r - 1}$
Total	$SS_{total} = \sum_{i}^{n} (y_i - \bar{y})^2$	$n - 1$	/

Where, y_i is the experimental value of the run ''i'', $\hat{y}_i$ the predicted value of the run ''i'', $\bar{y}$ the overall mean of experimental values, $\bar{y}_i$ the mean of experimental values of replicates, n the number of experimental runs (observations); n_r the number of experimental replicates, p the number of terms in the model.

For the model terms, the same quantities (sum of squares of the term "SS_{term}", degree of freedom and mean square of the term "MS_{term}") are calculated for each term by assuming that the term is null. The statistical significance of the model and its terms can be then evaluated using both the F-ratio and the p-value. The F-ratio compares the model/term variance with the residuals variance by dividing the model/term mean square (MS_{model}/MS_{term}) on the residuals mean square (MS_{res}) while the p-value gives the probability of obtaining a greater F-ratio than the actual one if the null hypothesis is true (no factor effect) [247]. The higher F-ratio values means the model/term variance is more significant than the residual variance and thus the model or the term is statistically significant. Likewise, the lower p-values (generally <0.05 is considered as a reference) indicates the null hypothesis is rejected (there is at least one factor effect). Other statistical indicators, which include the coefficient of determination (R^2), the adjusted coefficient of determination (R^2_{adj}) and the root mean square error (RMSE) defined by equations 4.12, 4.13 and 4.14, can be also used to assess the performance of the proposed model.

$$R^2 = \frac{SS_{model}}{SS_{total}} = 1 - \frac{SS_{res}}{SS_{total}} \quad \text{Equation 4.12}$$

$$R^2{}_{adj} = 1 - \frac{(1-R^2)(n-1)}{(n-p)} \quad \text{Equation 4.13}$$

$$RMSE = \sqrt{MS_{res}} \quad \text{Equation 4.14}$$

As illustrated in **Table 4.6**, a high F-ratio of 42.4457 and a P-value of <0.0001 were obtained for the model confirming its significance at a 95% confidence level. Such significance was also confirmed through the highest values of the determination coefficient (R^2 = 0.9867) and the adjusted determination coefficient (R^2_{adj} = 0.9635) with the lowest RMSE value (RMSE = 0.1718).

Table 4.6 : The ANOVA results of the model and its terms.

Source	Sum of squares (SS)	Degree of freedom (Df)	Mean square (MS)	F-ratio	p-value
X_1	10.5183	1	10.5183	356.1987	<.0001*
X_2	2.2870	1	2.2870	77.4472	<.0001*
X_3	0.0597	1	0.0597	2.0227	0.1928
X_4	3.5520	1	3.5520	120.2864	<.0001*
X_1X_2	0.0328	1	0.0328	1.1094	0.3230
X_1X_3	0.0742	1	0.0742	2.5116	0.1517
X_1X_4	0.00007	1	0.00007	0.0023	0.9632
X_2X_3	0.0004	1	0.0004	0.0134	0.9108
X_2X_4	0.0255	1	0.0255	0.8626	0.3802
X_3X_4	0.0641	1	0.0641	2.1710	0.1789
X_1^2	0.2938	1	0.2938	9.9505	0.0135*
X_2^2	0.0069	1	0.0069	0.2337	0.6418
X_3^2	0.1110	1	0.1110	3.7584	0.0885
X_4^2	0.0124	1	0.0124	0.4191	0.5355
Model	17.5475	14	1.2534	42.4457	<0.0001*
Pure error	0.0035	2	0.0017	-	-
Lack of fit	0.2327	6	0.0388	21.8317	0.0444*
Residuals	0.2362	8	0.0295	-	-
Total	17.7837	22	-	-	-

*p<0.05

For the model terms, it can be seen that the p-values of the majority of terms are greater than the significance level of 0.05; hence, they are considered to have a negligible effect on the model. Only X_1 (NaCl concentration), X_2 (Polymer concentration), X_4 (temperature) and X_1^2 (quadratic effect of NaCl concentration) had p-values lower than 0.05 and thus had a significant effect on the model. Consequently, the final mathematical model, after eliminating the insignificant terms and fitting the experimental response once more is given below:

$$\ln(GT) = 4.9765 + 1.4504X_1 - 0.6763X_2 - 0.1094X_3 - 0.8424X_4 - 0.4948{X_1}^2 \quad \text{Equation 4.15}$$

The NaCl concentration was the only factor that had a proportional effect with gelation time, where the latter increases when NaCl concentration increases. The other factors (temperature, polymer concentration and the quadratic effect of salinity) had negative coefficients (-0.6763, -0.8428, -0.4948 respectively) which mean that their effect is inversely proportional with gelation time (when they increase, the gelation time decreases).

4.6.4 3D response surface plots

To further illustrate and discuss the effect of each factor and the interactions between these factors we were referred to the 3D response surface plots.

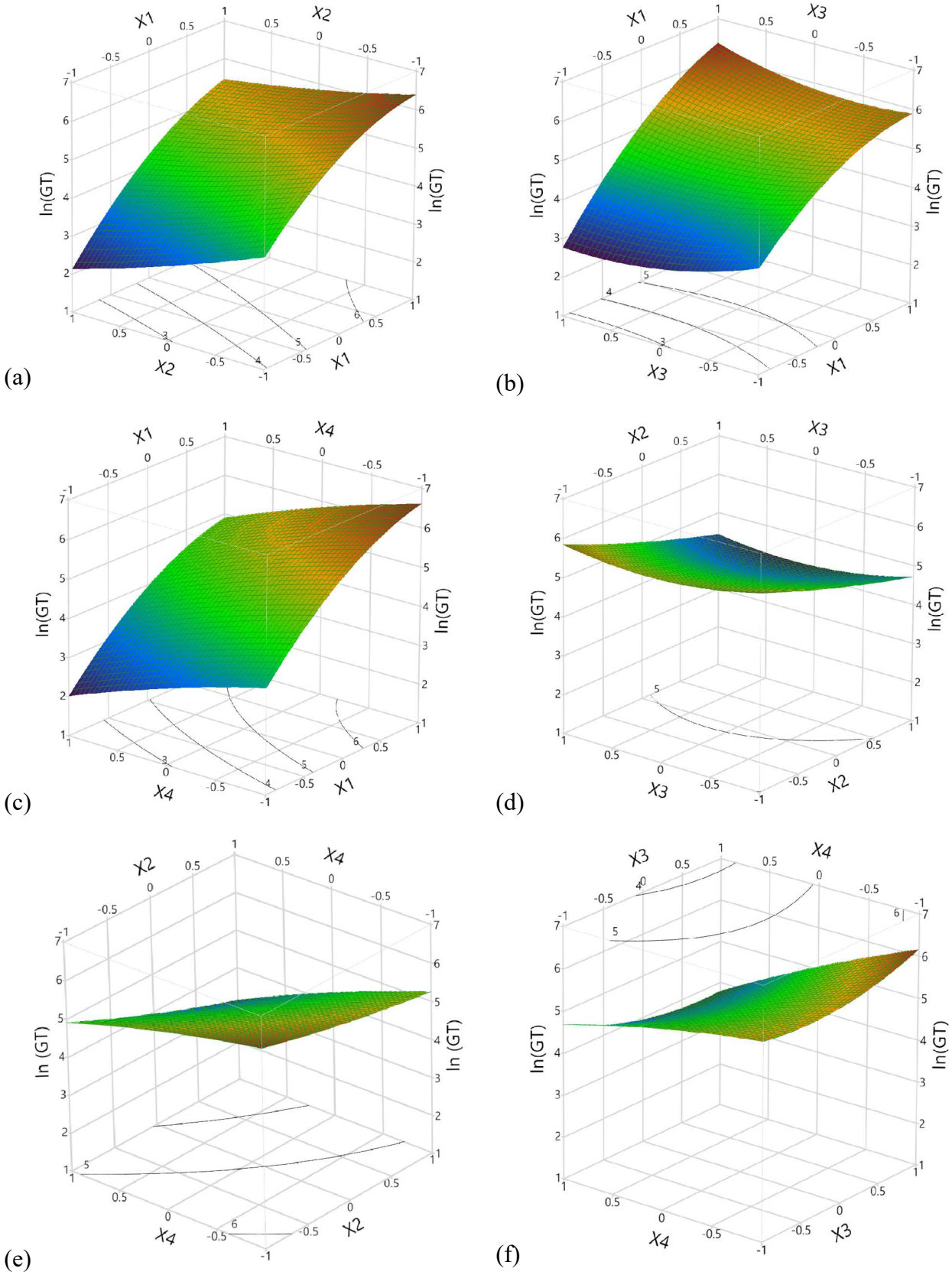

Figure 4.8 : 3D response surface plots of ln (GT) showing combined effect of NaCl concentration "X_1", polymer concentration "X_2", crosslinker concentration "X_3" and Temperature "X_4".

Figure 4.8 shows the 3D Response surface plots of ln(GT) as function of the combined effect of the four studied factors. From **Figures 4.8 (a-b-c)**, it is clear that the response (gelation time) increases when the NaCl concentration (X_1) increases despite the effect of the second combined factor. Furthermore, the effect of NaCl concentration is more pronounced compared to the effect of the second factor. In this case, the presence of sodium ions (Na^+) affects the gelation reaction through a charge shielding effect [118] which screen the negatively charged carboxylate groups (COO^-) and reduce consequently the hydrodynamic volume of the polymer. A lower hydrodynamic volume means a less entangled polymer network and less accessible PHPA crosslinking sites. Both temperature (X_4) and polymer concentration (X_2) had an inversely proportional effect on gelation time (when they increase the gelation time decreases) as shown in **Figures 4.8 (a-d-c-e-f)**. The effect of temperature is explained by the enhanced movement of molecules that promotes the interactions between the PHPA and PEI [214]. While the higher polymer concentrations bring more crosslinking sites and render the polymer network more entangled which make the gelation reaction faster. Surprisingly, the crosslinking concentration (X_3) had the least effect on gelation time in contrast to the result obtained in **chapter I**. Mainly, high crosslinker concentrations result in lower gelation times as more PEI amine groups are available to the crosslinking reaction. However, this is not always the case as shown in **Figure 4.8 (b)** and **Figure 4.8 (f)** at high NaCl concentrations (X_1=1) and low temperatures (X_4=-1) respectively. A possible explanation could be related to a pH value shifting for the PHPA/PEI mixture. This contradictory result constitutes a working prospect to investigate the interaction mechanisms between the PHPA and PEI.

4.6.5 Optimization using the desirability approach

For gel injection operations in the oilfield, the polymer and the crosslinker are usually mixed in the surface facilities, pumped downhole using a coiled tubing unit, and injected for a sufficient time until reaching the targeted depth inside the formation [161]. Some of the main operating conditions in the oilfield, which interfere in the gelation time determination, are the gelant injection rate, the diameter of the coiled tubing and the depth of the treated formation. In the literature reported conformance control operations, injection rate of 1 bbl/min (158.99 liter/min) [129, 142] and 2-inches (5.08 cm) coiled tubing diameter [136], were approved and largely employed. By considering these two operating conditions and an average reservoir depth of 6560 ft (2000 m), which is the reservoir depth of the Algerian fractured reservoir of Tin Fouyé Tabankort "TFT" [248], the estimated injection time needed to reach the reservoir is 25 minutes. Consequently, and to ensure a sufficient gel penetration inside the reservoir, the gelation time must be higher of at least five times this injection time (i.e, 125 minutes). Finding the optimum parameters to obtain this gelation time, for the studied PHPA1/PEI25 gel system, is now possible through the fitted mathematical model and a desirability function approach implemented in the JMP software.

Initially proposed by Derringer and Suich [249], the desirability function approach has become one of the most widely used methods in the industry for optimizing multiple response processes. The method consists on finding the optimal operating conditions (x_i) for which the "most desirable" response values are obtained [234]. A desirability function $d(\hat{Y}_i)$ is assigned for each estimated model response $\hat{Y}_i(x)$ and can takes values only between 0 and 1, with $d(\hat{Y}_i) = 0$ is the completely undesirable value and $d(\hat{Y}_i) = 1$ is the most desirable value of $\hat{Y}_i$. In an optimization, one can maximize, minimize or set a targeted value for the response $\hat{Y}_i$, and in each case, a different desirability function should be defined. In the case of a targeted value, the desirability function is defined as follow [234]:

$$d(\hat{Y}_i) = \begin{cases} 0 & if \quad \hat{Y}_i(x) < L_i \\ \left(\dfrac{\hat{Y}_i(x) - L_i}{T_i - L_i}\right)^s & if \quad L_i \le \hat{Y}_i(x) \le T_i \\ \left(\dfrac{\hat{Y}_i(x) - U_i}{T_i - U_i}\right)^t & if \quad T_i \le \hat{Y}_i(x) \le U_i \\ 0 & if \quad \hat{Y}_i(x) > U_i \end{cases}$$

With U_i, L_i, T_i are the upper, lower and the targeted values respectively and the exponents "s, t" determine the importance of reaching the target. For s=t=1, the desirability function develops linearly towards T_i, for s < 1 and t < 1 the function is convex while for s > 1 and t > 1 the function is concave.

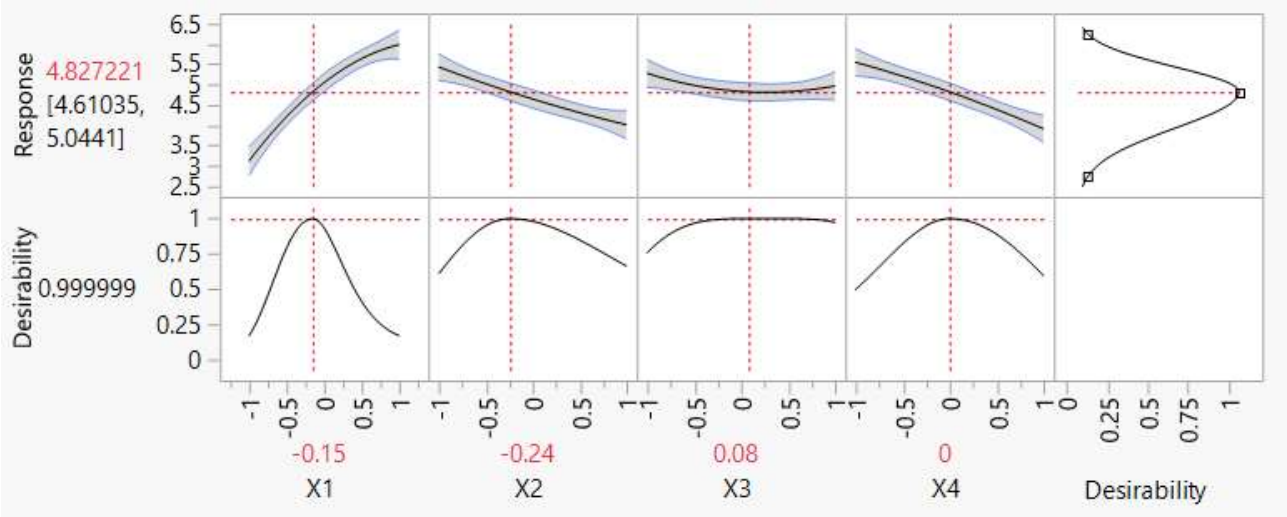

Figure 4.9 : Desirability function and the optimum parameters at the targeted response.

Figure 4.9 shows the prediction profiles of the desirability function and the response ln(GT) according to the variations of the four studied parameters. A desirability value of 1 was assigned to the targeted response of ln(125) = 4.8283. The temperature X_4 was fixed at 0, which is the reservoir temperature of the TFT reservoir (80°C), while the salinity was fixed at -0.15, which represents a mixing water with 3.4 g/l NaCl. The polymer and crosslinker concentrations were than varied to

maximize the desirability value. The optimum concentrations were obtained at -0.24 for the polymer concentration X_2 and 0.08 for the crosslinker concentration X_3, for which the desirability has reached a value of 0.999999. Using the equation 4.8, the optimal experimental concentrations were 6186 ppm and 1598 ppm for the PHPA1 and PEI25 respectively.

To validate these optimal conditions, a laboratory experimental test was conducted. A gelant solution, prepared in 3.4 g/l NaCl water using a PHPA1 concentration of 6186 ppm and PEI25 concentration of 1598 ppm, were loaded into the coaxial cylinder of the rotational rheometer. The test temperature was set at 80 °C and the viscosity evolution was monitored against time. The corresponding gelation time was of 110 minutes which is very close to the targeted gelation time (125 minutes). Based on this result, it can be concluded that the mathematical model validity was established, and the optimization was successful.

4.7 Conclusion:

In this chapter, the statistical investigation on the gelation time of the PHPA/PEI gel system using the response surface methodology (RSM) was achieved. The four parameters namely NaCl concentration (0 to 8 g/l), polymer concentration (4000 to 10000 ppm), crosslinker concentration (500 to 2500 ppm) and temperature (70 to 90 °C) were considered at five, seven, seven and three experimental levels respectively using the robust doehlert matrix. A set of 23 experimental run including two replicates to determine the pure error, were conducted. A nonlinear mathematical model was then used to fit the experimental response (gelation time) as function of the four parameters and their interactions. The polynomial model failed to fit the experimental responses thus an exponential model was considered. The latter presented the highest values of determination coefficient (R^2 = 0.9867) and adjusted determination coefficient (R^2_{adj} = 0.9635) with the lowest RMSE value (RMSE = 0.1718). The analysis of variance (ANOVA) was also employed to assess the statistical significance of the model and its terms. The sum of squares, the degree of freedom, the mean squares, the F-ratio and p-value of each source (model, model terms, residuals, lack of fit and pure error) were calculated and only sources with p-values of less than 0.05 were considered as significant. Consequently, four model terms had a significant effect on the model namely X_1 (NaCl concentration), X_2 (Polymer concentration), X_4 (temperature) and X_1^2 (quadratic effect of NaCl concentration). The effects of these factors and their interactions were then discussed through the 3D response surface plots. The NaCl concentration had a negative and the major effect on the gelation time among all the studied parameters. This was explained by the charge shielding effect which screen the negatively charged carboxylate groups (COO^-) and reduce consequently the number of polymer entanglements and available crosslinking sites. Both temperature and polymer concentration had a proportional effect on the gelation time thanks to the enhanced movement of molecules and the higher number of

crosslinking sites and entanglements. In contradiction to our previous observations, the effect of the crosslinker concentration was more complex especially when the other parameters are set to make crosslinking reaction slower (lower temperature and higher salinity). This result encourages further investigation to understand the interaction mechanisms between the PHPA and PEI, which will be the subject of the next chapter. Finally, the experimental validity and the optimization of the gelation time using the obtained mathematical model were approved. For a set of real operating conditions in the oilfield, namely the injection rate (1 bbl/min), the coiled tubing diameter (2 inches), the reservoir depth (6560 ft), the reservoir temperature (80 °C) and the injection water salinity (3.4 g/l), the estimated injection time and the minimal gelation time needed were calculated. A desirability function was then defined and the optimal concentrations to match the targeted gelation time were determined and validated experimentally.

Chapter V:

The crosslinking mechanisms of PHPA with PEI

5. Chapter V: The crosslinking mechanisms of PHPA with PEI

5.1 Introduction

Since the introduction of the PEI/acrylamide-based polymers gel systems in the late 90's, most of the literature studies considered the formed gels as covalently crosslinked gels and referred the works of Hardy et al. [71] and Reddy et al. [83] in explaining the crosslinking mechanisms between the different polymers and the PEI crosslinker as reviewed in the state of Art. Hardy et al. considered the interaction to be either through a nucleophilic attack or an ionic interaction between the cationic crosslinker and the anionic polymer. On the other side, Reddy et al. proposed the transamidation reaction between the PEI's amine groups and the amide groups of the acrylamide-based polymer. In both works, the authors did not show any evidence on the existence of such crosslinking mechanisms nor a quantification of them. Their propositions were built only on observations and comparisons of gelation times and gel strengths with other metallic crosslinked polymer gels. Furthermore, and in the case of PHPA/PEI gel systems, the effect of the hydrolysis degree and the initial gelant pH value on the gelation time were not previously addressed. In order to respond to these points, we are studying in this chapter the interaction mechanisms between PHPA and PEI, using advanced techniques such as 1D and 2D nuclear magnetic resonance (NMR), which give access to the chemical structure variations in both reactants. The effect on the gelation time of varying the anionicity of the PHPA through the hydrolysis degree or the cationcity of PEI through the solution's pH is also investigated and discussed.

5.2 Materials and methods

The three PHPAs (PHPA1, PHPA2, PHPA3) having the same HD (6%) but different molecular weights were used as the base polymers. While the crosslinker was the PEI25, having a molecular weight of 20000 g/mol and BD of 59%. Low molecular weight polymers, purchased from Sigma Aldrich, namely Polyacrylamide (PAM) in a powder form, Polyacrylic Acid (PAA) (35 wt% in water) and very low Mw PEI (PEI1300) (50 wt% in water) were employed during the NMR experiments. In the pH effect study, concentrated HCl and NaOH solutions (1 mol/l) were used to vary the initial pH value of the mixtures. The main mixing water was the injection water described in the materials characterization chapter while deuterated water (D_2O) was employed to prepare the NMR samples.

Just as the high molecular weight reactants (PHPAs and PEI25), the low molecular weight reactants (PAM, PAA and PEI1300) were characterized in terms of viscosity-average molecular weight and hydrolysis or branching degree. The characteristics of all the reactants are listed in **Table 5.1**:

Table 5.1 : Reactants characterizations in terms of viscosity-average molecular weight and hydrolysis or branching degree

Reactant/variable	PHPA1	PHPA2	PHPA3	PAM	PAA	PEI25	PEI1300
$[\eta]$ (ml/g)	1460	1990	2560	114.9	46.4	13.0	7.8
α*	0.81			0.755		0.26	
κ*	0.0062			0.031		1	
$\bar{M}_v$ (10^3 g/mol)	5100	7500	10200	52.9	15.9	19.4	2.7
HD or BD (%)	6.1	6.1	6.2	0	100	58.6	42.3

* α and κ are the Mark–Houwink equation constants issued from literature [187, 192, 193]

The three high molecular weight PHPAs were hydrolyzed to obtain PHPAs with at least four more hydrolysis degrees (HD_1= 15%, HD_2= 25%, HD_3= 35%, HD_4= 45%). The experimental procedure, to realize this, was the one reported by Feng et al. [196]: the three PHPAs were first dissolved into 0.1M (5.844 g/l) NaCl aqueous solutions at polymer concentrations of 0.1M (7.108 g/l in three different round-bottom flasks). Solid NaOH was then added to obtain final NaOH concentrations of 0.25M (10 g/l). Under constant stirring, the mixtures were heated at 50 °C and at time intervals of 15, 45, 120 and 240 minutes, samples were taken from each reaction medium and precipitated in an acetone/ethanol mixture (50/50 by volume). The samples were washed several times with acetone then dried under vacuum at 40°C for at least 24 hours [250].

For the NMR measurements, a Bruker AVANCE 400 MHz spectrometer equipped with a Z-gradient Bruker 5 mm BBFO probe was employed. The products were solubilized in deuterated water (D_2O) and their proton (^1H) and carbon (^{13}C) NMR spectra were recorded using the same acquisition and processing parameters listed in Table 2.5 in the materials characterization chapter. For the DOSY (Diffusion ordered spectroscopy) and NOESY (Nuclear Overhauser Enhancement SpectroscopY) experiments, the classic Bruker sequences **ledbpg2s** et **noesygpph** were used.

5.3 Results and discussion

5.3.1 Hydrolysis degree effect

To examine the effect of the hydrolysis degree on gelation time, three PHPAs (PHPA1, PHPA2 and PHPA3) with the same initial hydrolysis degree of 6 % were hydrolyzed to obtain a total of five different hydrolysis degrees for each PHPA. Gelant solutions prepared in injection water using 5000 ppm of each PHPA and 1000 ppm PEI25 were loaded into the rheometer set at 80 °C, where the viscosity evolution was monitored as function of time. **Figure 5.1** shows the variation of the initial gelant viscosity and the gelation time for the three PHPAs as function of their hydrolysis degrees. From **Figure 5.1 (a)**, it is clear that, for a given PHPA, the initial gelant viscosity increased with the

hydrolysis degree until reaching a maximum at HD=25% then started to decrease beyond that. Kulicke and Horl [251] reported a similar viscosity behavior with the viscosity maximum observed at HD= 40%, while, Rabiee et al. [252] observed the viscosity maximum at HD= 20%. Such behavior can be explained by the polymer chains being progressively extended and stretched as the number of the negatively charged carboxylate groups increases. When reaching a given limit, the additional negatively charged groups will not contribute in stretching the polymer chains but will rather promote the complexation with the divalent cations present in the mixing water, resulting in the shrinkage of the polymer chains and consequently in the viscosity drop. It should be reminded that high gelant viscosities are not recommended for gel injection operations in the oilfield as they increase the required pump capacities.

An inverted behavior was found in the case of gelation time as depicted in **Figure 5.1 (b)** where, gelation time decreased with hydrolysis degree until reaching a minimum at HD= 25% then resumed its increase beyond that. Al-Muntasheri et al. [141] found that the gelation time of PAM/PEI gels decreased from 2 hours to 0.55 hour when the neat PAM was hydrolyzed to 4.7% and 7.2% at 100°C. El-karsani et al. [118] observed also the lower gelation times at higher HDs for the PAM/PEI gels and succeeded in fitting the variation of gelation time as function of the hydrolysis using an exponential relationship. Furthermore, the authors explained their result by the enhanced stretching of PAM chains due to the repulsive forces between the carboxylate groups, which allows more amide/carboxylate groups to be accessible for the crosslinking with PEI. The first part of our results agrees with these results, however the second part when gelation time starts to increase with hydrolysis degree is contradictory. A possible explanation for this controversial result would evoke the reduced hydrodynamic volume of the polymer at high hydrolysis degrees which was also expressed by the lower initial gelant viscosities. Another explanation would be that the main crosslinking reaction is through the transamidation reaction between the PHPA's amide groups and the PEI's amine groups. In such case, when the hydrolysis increases, the number of the available amide groups decreases, and the reaction is consequently delayed. To further investigate this crosslinking mechanism, additional experiments were conducted as presented and discussed below.

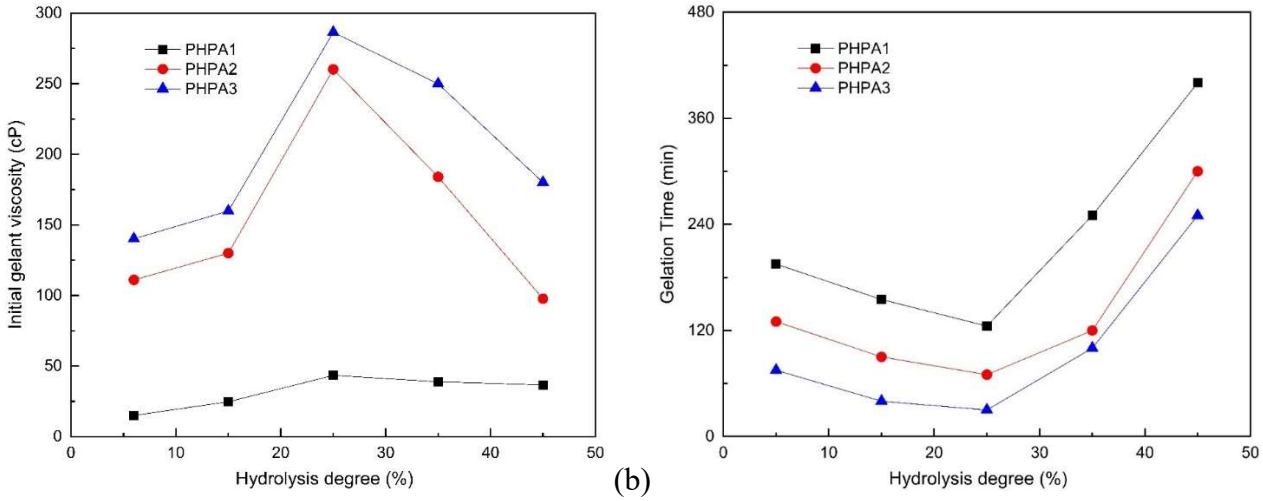

(a) (b)

Figure 5.1 : Hydrolysis degree effect on (a) initial gelant viscosity (b) gelation time.

5.3.2 Initial pH effect

Despite being one of the most influential parameters on both PHPA and PEI, the effect of pH on PHPA/PEI gel systems has, to the best of our knowledge, not been previously investigated. In this part, gelant solutions prepared with 10000 ppm PHPA1 and 2000 ppm PEI25 in injection water and having initial pH values of around 10 were titrated with concentrated HCl and NaOH solutions (1 mol/l) to account for the effect of raising or lowering the initial pH value of the gelant on the gelation time. **Figure 5.2** shows the gelation times obtained at different initial pH values for the PHPA1/PEI25 mixtures cured at 80 °C.

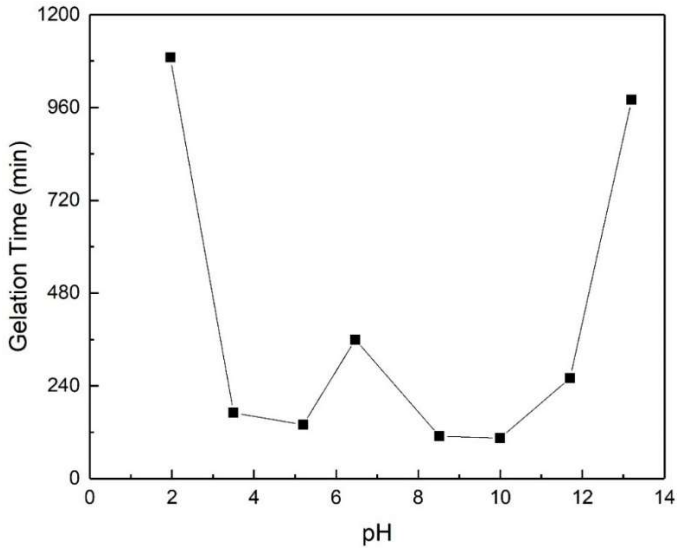

Figure 5.2 : pH effect on gelation time.

The gelation time was the lowest in mildly basic environments (8.5<pH<11), followed by mildly acidic environments (3.5<pH<6). It increased then at neutral pH and was very high in extremely high basic (pH> 12) and acidic (pH<3) environments. To explain these results, one should first identify the effect of pH on PHPA and PEI alone. For PEI, when the pH is decreased, the amine groups are protonated to ammonium ions and become less nucleophilic, and at high pH, these amines are deprotonated and become more nucleophilic as was shown in Figure 1.14 in the state of art chapter.

With PHPA, the addition of HCl or NaOH is known to accelerate the hydrolysis of amides groups, especially at high temperatures. In the PHPA1/PEI25 system, when the pH was increased from the initial value of 10 to 11.7 and 13.2 by adding NaOH, the gelation time increased from 105 minutes to 205 and 980 minutes, respectively. In this case, the NaOH is supposed to accelerate the hydrolysis of amide groups to carboxylate groups and deprotonating all the PEI amines groups. Furthermore, the added NaOH will bring additional sodium ions (Na^+) to the solution which will tend to screen the negatively charged carboxylate groups of the polymer, thereby reducing the hydrodynamic volume of the polymer. As a result of these three effects, no ionic interactions between the PHPA and PEI can take place (PEI's amine groups are uncharged), while less PHPA amide groups are available for the transamidation reaction with the PEI's amine groups thus the retardation effect that was observed. Alternatively, when HCl was added, the pH was decreased from 10 to 8.5, 6.5, 5.2 and 3.5. An instant increase in the viscosity was observed visually, even before the gelant solution was loaded to the rheometer. A similar observation was previously reported by Al-Muntasheri et al. for the PAtBA/PEI gels [105]. A possible explanation is that some of the newly protonated PEI amine groups (ammonium ions NH_3^+) react instantly with the negatively charged carboxylate groups through ionic interactions resulting in the instant increase of the viscosity. When loaded into the rheometer, a slightly delayed gelation times were observed compared to the basic conditions, which can be due to the reduced nucleophilicity of PEI amine groups. At very low pH values of around 2, the gelation was further delayed. Here, the excess hydrogen ions (H^+) will screen the negatively charged carboxylate groups, thereby reducing the polymer's hydrodynamic volume and allowing fewer amide groups to be accessible to the PEI. In contrast, the gelation was just slightly delayed at neutral pH. In neutral conditions, both the hydrolysis of PHPA is slow and the nucleophilicity of the PEI's amine groups is reduced while the added H^+ ions tend to screen the PHPA's carboxylate groups, resulting in the polymer shrinkage. All these effects render the crosslinking reaction unfavorable at this pH value.

5.3.3 Reaction mechanisms through NMR techniques

In this section, we were interested in studying the interaction mechanisms between PHPA with its two functional groups (amides and carboxylate) and PEI with its three amines (primary, secondary and tertiary) and the chemical variations that may occur on both reactants. To do so, we suggest the use of ^1H e ^{13}C NMR and 2D NMR techniques including the DOSY and NOESY techniques in studying the short distance interchain interactions. Nuclear magnetic resonance as a well-known characterization tool has found lately its application in monitoring chemical reactions progression as well as providing practical insights into the structure-property relationships [253-255]. Nevertheless, NMR was only limitedly investigated on polymer gel systems. Romero-zeron et al. [161] studied the gelation reaction and gel states of the PHPA/chromium (III) acetate system through bulk relaxation rates. Bait et al. [256] employed the proton (^1H) NMR in monitoring the polymerization-reticulation

process of hydrogel nanocomposites based on polyacrylamide and poly(acrylamide-hydroxyethyl methacrylate).

First, a mixture with a ratio of 1:1 of 20 mg PHPA1 and PEI25 was solubilized in deuterated water (D_2O), loaded in an NMR tube and then to the NMR spectrometer. The proton (^1H) and carbon (^{13}C) NMR spectra were recorded at 25 °C at an initial time (t=0) and after curing the mixture for 1 hour at 80 °C. **Figure 5.3 (a, b)** show the recorded proton (^1H) and carbon (^{13}C) NMR spectra at both conditions. At the initial time (25°C), the chemical shifts of both reactants were easily separated and identified, however, the spectra of the cured mixtures were largely broadened and overlapped over one another as observed in the shift ranges of 30 to 60 ppm and 179 to 185 ppm in the carbon spectrum. This can be attributed to the extremely accelerated interaction because of the very high concentrations of reactants which were employed in the first place to record good carbon (13) NMR spectrum. Consequently, it seems that following the reaction kinetics and the chemical variations using these high molecular weight reactants is impossible.

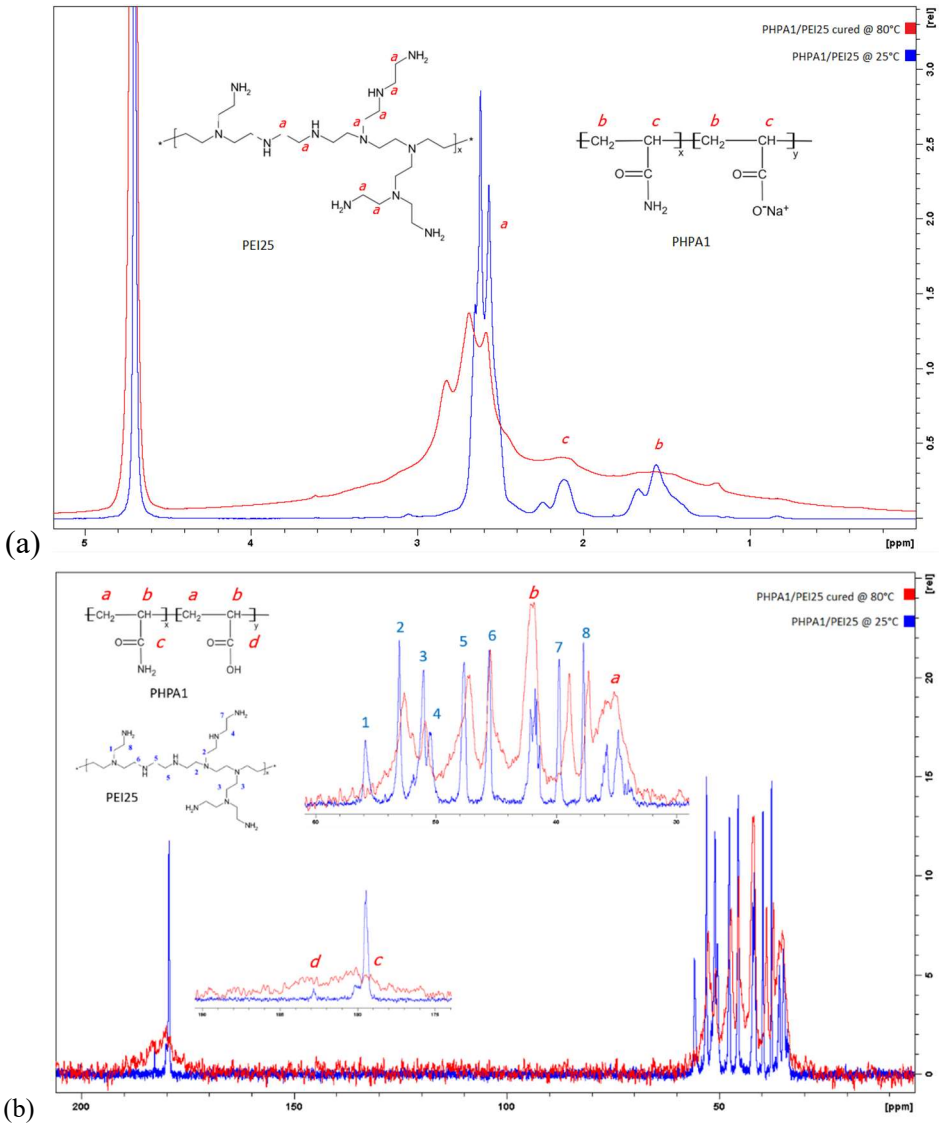

Figure 5.3 : (a) the proton "^1H" and (b) carbon "^{13}C" spectra of PHPA1/PEI25 mixture at 25°C at an initial time (t=0) (blue curve) and after curing at 80°C for one hour (red curve).

To overcome this, we were referred to the low molecular weight reactants. PAM and PAA were selected respectively to study separately the interaction of the amides and carboxylates groups of PHPA. While the PEI1300 substituted the higher molecular weight PEI25.

The NMR Diffusion ordered spectroscopy (NMR-DOSY) experiments were then conducted. The DOSY technique is a two-dimensional (2D) NMR experiment which allows a virtual chromatographic separation of different components in a mixture by correlating the conventional chemical shifts with the diffusion coefficients of these components [257-259]. As the diffusion behavior of a given specie depends on its size, shape, mass, charge and surrounding environment [260], the measurements of the ^{1}H-NMR signal attenuations during a pulsed field gradient give access to the diffusion coefficients. When representing the chemical shifts and the diffusion coefficients in a 2D map, both physical and chemical information, on the composition and the interactions between the components of the studied mixture, can be obtained. The DOSY technique was reported to have a higher accuracy when applied on low molecular weight species and diluted mixtures [261].

Before recording the DOSY spectra of the mixtures (PAM/PEI1300 and PAA/PEI1300), the diffusion coefficients of sole components (PAM, PAA and PEI1300) were recorded separately as shown below in **Figure 5.4**.

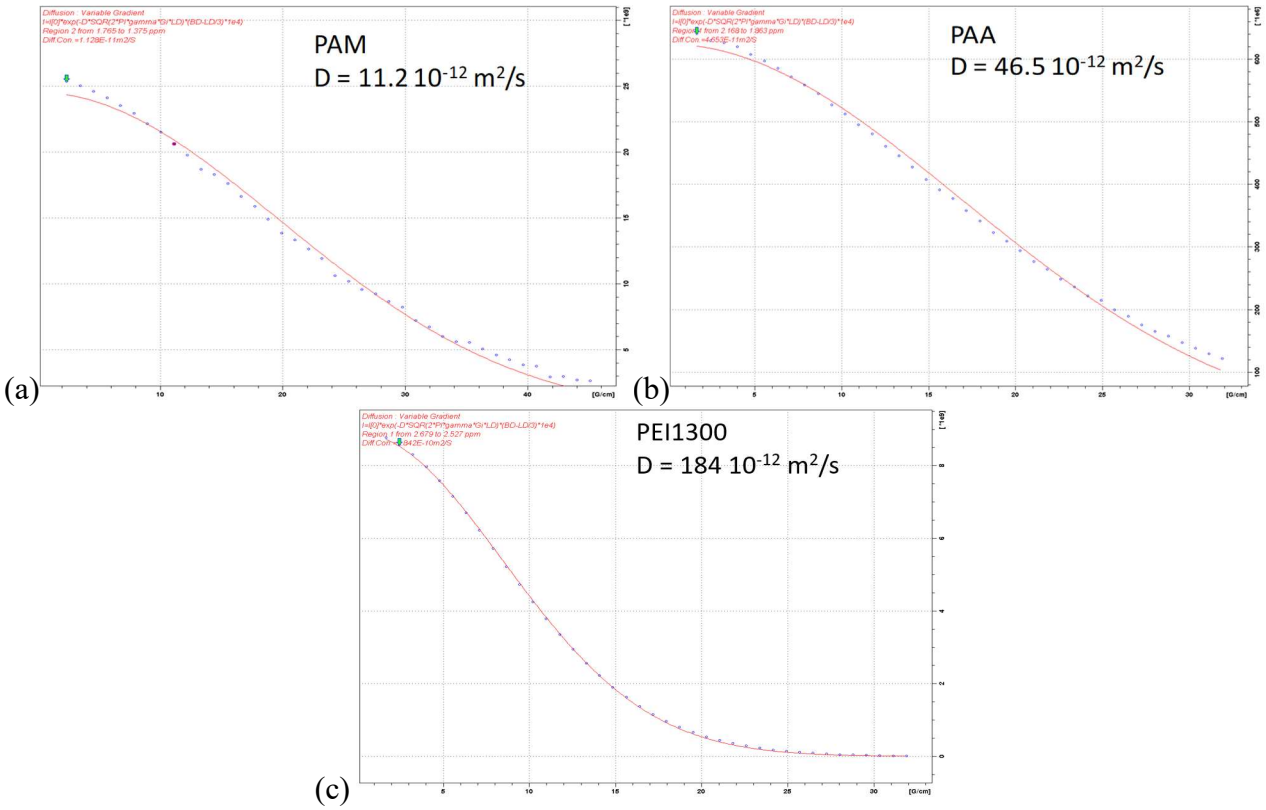

Figure 5.4 : Diffusion Coefficients of single components (a) PAM (b) PAA (c) PEI1300 at 25°C.

It was evident that the diffusion coefficients of the sole components decreased with the increase of their molecular weights. PAM had the lower diffusion coefficient (D_{PAM}=11.2×10^{-12} m^2/s) compared to PAA (D_{PAA}=46.5×10^{-12} m^2/s) and PEI1300 ($D_{PEI1300}$=184×10^{-12} m^2/s). These results were in good

agreement with diffusion coefficients reported in literature for similar reactants and also in agreement with the Stokes–Einstein equation which stipulates that high molecular weight molecules with higher hydrodynamic volumes have lower diffusion coefficients [261-264].

Following that, two diluted mixtures of PAM/PEI1300 and PAA/PEI1300 were prepared in deuterated water (D_2O) at a ratio of 3:1 and allowed to interact for a sufficient time (48h hours) before recording their proton (^1H) spectra at 25 °C as shown in **Figure 5.5**.

The PAM/PEI1300 mixture exhibited one diffusion coefficient of 5×10^{-12} m^2/s which was lower than those of PAM and PEI alone which confirms the presence and formation of a higher molecular weight component. On the other side, the PAA/PEI1300 mixture exhibited two different diffusion coefficients. The first diffusion coefficient ($D_{1(PAA/PEI1300)}$=46.4×10^{-12} m^2/s) was the same as that of PAA alone (D_{PAA}=46.5×10^{-12} m^2/s), while the second diffusion coefficient ($D_{2(PAA/PEI1300)}$=109×10^{-12} m^2/s) was slightly lower than that of PEI1300 alone ($D_{PEI1300}$=184×10^{-12} m^2/s). These results suggest that the two reactants (PAA and PEI1300) were still free and separated from each other in the mixture. The lower diffusion coefficient observed for the PEI1300 can be explained by its constrained movement caused by the presence of the larger PAA molecules in the mixture compared to PEI1300 alone. From these DOSY results, one can assume that the PEI amine groups are preferentially interacting with the amide groups rather than the carboxylate groups even at room temperature.

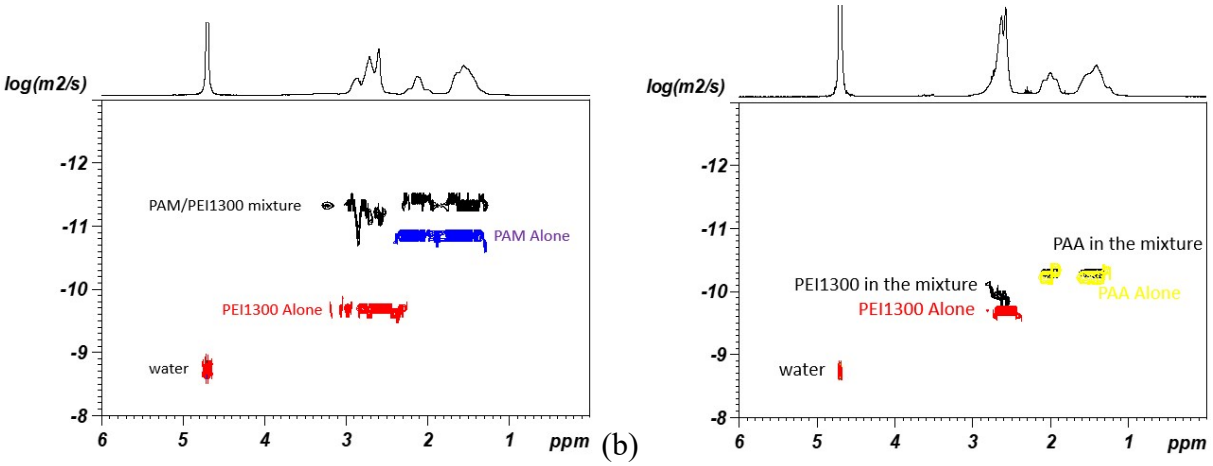

Figure 5.5 : NMR DOSY spectra at 25°C of (a) PAM/PEI1300 and (b) PAA/PEI1300 mixtures with their initial sole reactants.

To further investigate the DOSY results, we were referred to the NMR NOESY (Nuclear Overhauser Enhancement SpectroscopY) technique. This 2D NMR sequence, which was mainly employed in studying the phenomenon of encapsulation, and release of active agent carried by polymers [265], is able to reveal the spatial proximity between protons of different molecules in close proximity to each other due to the dipole interactions (^1H-^1H). The existence of correlations spots on the NOESY 2D spectrum indicates that the distance between protons is smaller than 5 Å [266]. **Figure 5.6** shows the

NOESY spectra of PAM/PEI1300 and PAA/PEI1300 mixtures taken at two different temperatures of 25 and 60 °C.

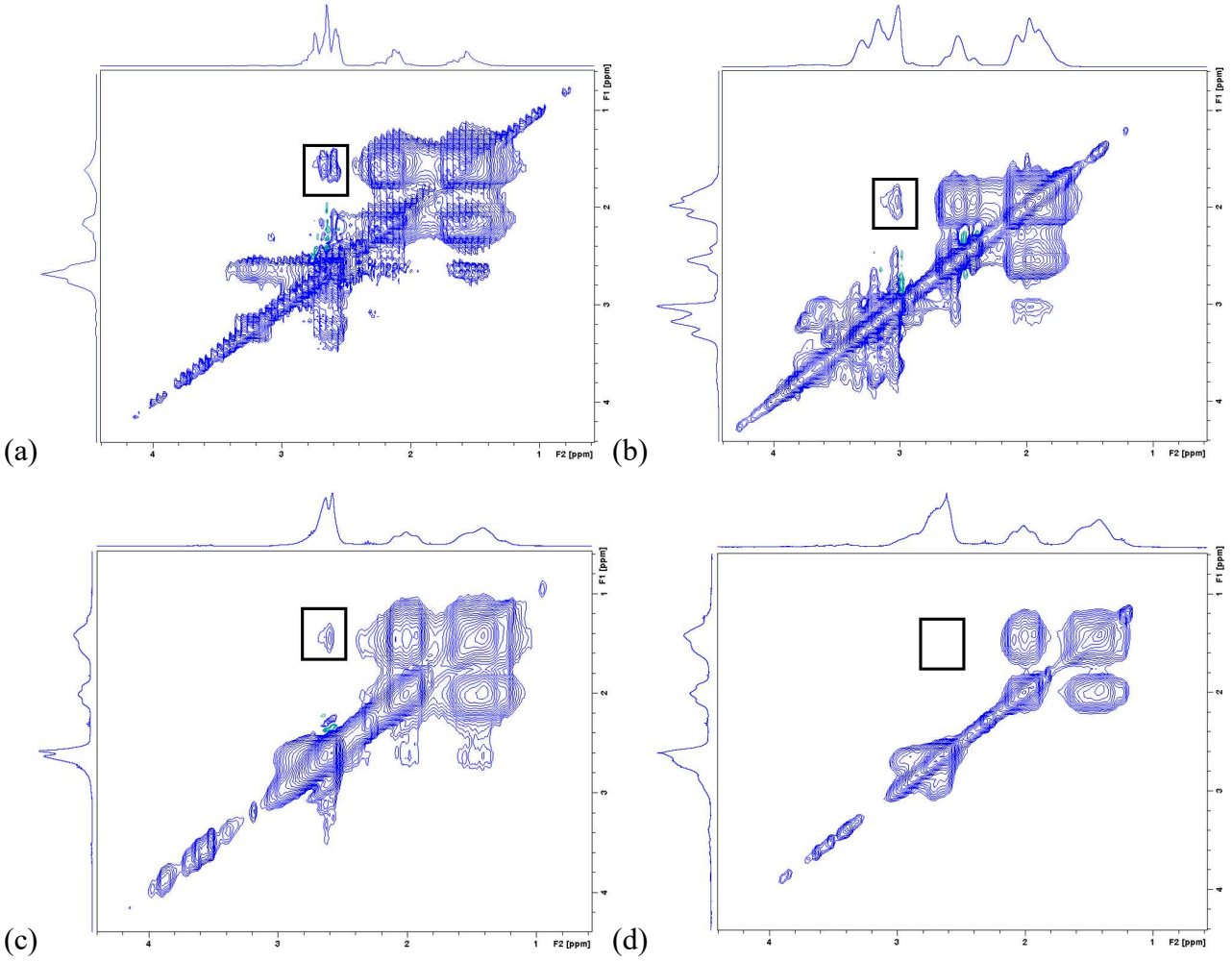

Figure 5.6 : NMR NOESY spectra of (a) PAM/PEI1300 at 25°C, (b) PAM/PEI1300 at 60°C, (c) PAA/PEI1300 at 25°C and (d) PAA/PEI1300 at 60°C.

For instance, the NOESY spectra of both mixtures recorded at 25 °C, show the existence of correlation spots (highlighted by the small black box) between the hydrogens of PAM or PAA in one hand and those of PEI1300 on the other one. While, at 60 °C, only the correlation spot of PAM/PEI1300 persisted and that of PAA/PEI1300 disappeared. This confirms that the PAM and PEI1300 are either interacting chemically or physically, but their interaction is strong and independent of the temperature. On the other side, the PAA and PEI1300 are in close proximity to each other at room temperature but are totally separated when the temperature increases. Such result is perfectly in line with the observed diffusion coefficients of PAA and PEI1300 in the mixture obtained through the DOSY experiments. When the proton and carbon spectra of a PAA/PEI mixture were recorded at 25 °C at an initial time t=0 and after curing the mixture for 24 hours at 80°C as shown in **Figure 5.7**, no chemical variations or shifts at the corresponding peaks of PAA and PEI1300 were observed, confirming no interaction between the two reactants at the study conditions.

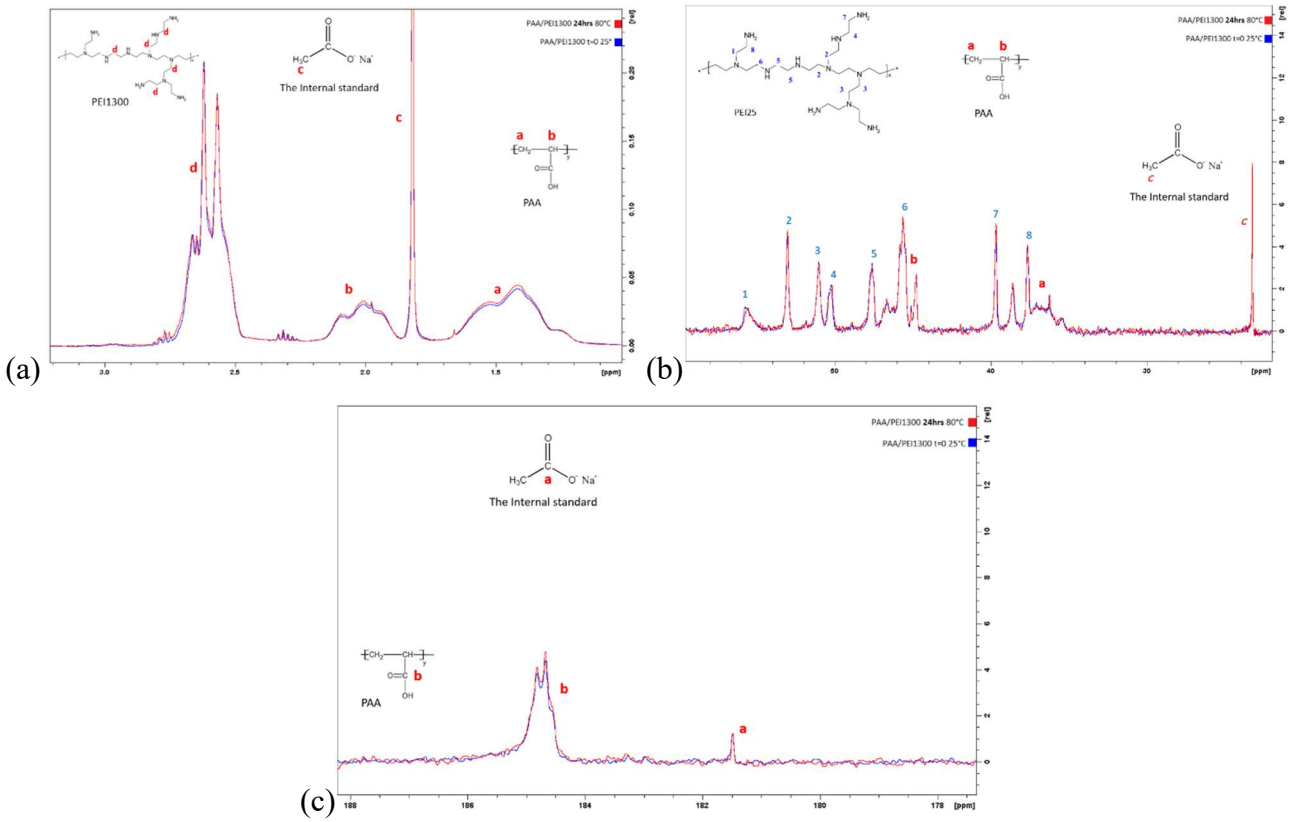

Figure 5.7 : (a) Proton "^{1}H" and (b-c) Carbon "^{13}C" NMR spectra of PAA/PEI1300 mixture recorded at t=0 (25°C) and at 24 hours (after curing at 80 °C).

In the case of PAM and PEI1300, the interaction kinetics were also investigated by tracking the chemical variations and peak shifts on the proton and carbon spectra of PAM/PEI mixtures cured at 80 °C at different reaction times. To record good NMR spectra, the concentrations of PAM and PEI1300 were of 15 mg/ml and 5 mg/ml respectively, while sodium acetate (5mg/ml) was employed as an internal standard. **Figure 5.8** highlights the proton and carbon spectra of the PAM/PEI1300 mixtures cured at 80°C for different reaction times of 1, 2, 4, 8 and 36 hours. In both proton and carbon spectra, the corresponding peaks of PAM, namely those of methylene group (CH_2) and the methine group (CH), were identical and did not shift with the increased curing time. In contrast, the shift at 179 ppm characterizing the PAM amides groups, in the carbon spectrum, decreased with the curing time, and gave raise to two other peaks at 180 and 183 ppm. The peak at 183 ppm was the shift corresponding to the carboxylate groups, which indicates the onset of the hydrolysis. While that at 180 ppm could be attributed to the amide groups neighbored to carboxylate groups or primary amine (NH_2) converted to secondary (NH) or tertiary (N) amines. For PEI, the peaks in the region of 2.5 to 3 ppm on the proton spectrum and in the region 35 to 60 ppm on the carbon spectrum, did shift with the increased curing time indicating a change in the chemical environment of the PEI's methylene carbons (CH_2) attached to the different amines groups. While the observed shift in the proton spectrum do not allow an accurate separation between the neighboring amine groups, we were more interested in the 8 characteristic peaks of PEI in the carbon spectrum. As shown in **Figure 5.8 (b)**,

the peaks number 2, 3, 5 and 6 were identical and did not shift in contrary to the four other peaks namely 1, 4, 7 and 8. It is worth noting that peaks 2, 3, 5 and 6 correspond to the methylene groups neighbored from both sides either by tertiary (N) or secondary amines (NH), while peaks 1, 4, 7 and 8 correspond with the methylene groups neighbored in at least one side by a primary amine group (NH_2). Consequently, it becomes evident that the primary amine groups are the only PEI's groups reacting with the amide groups of the PAM.

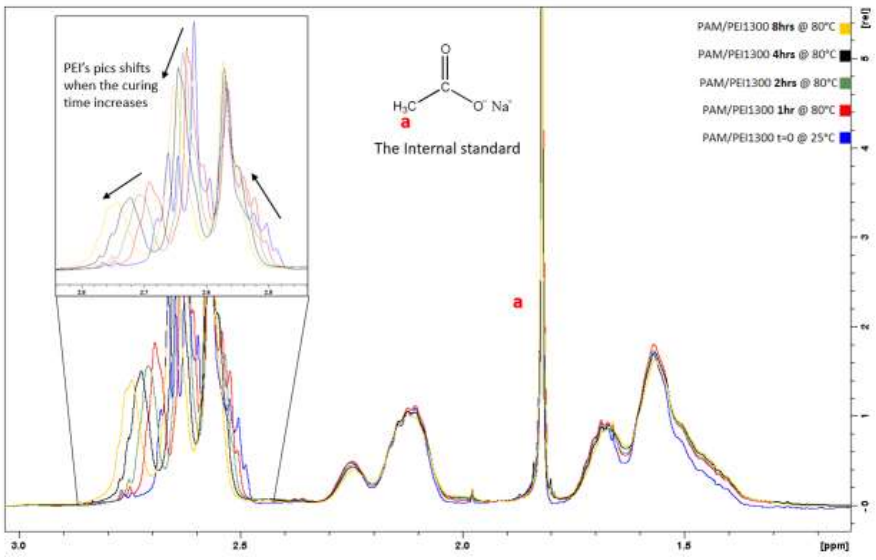

(a)

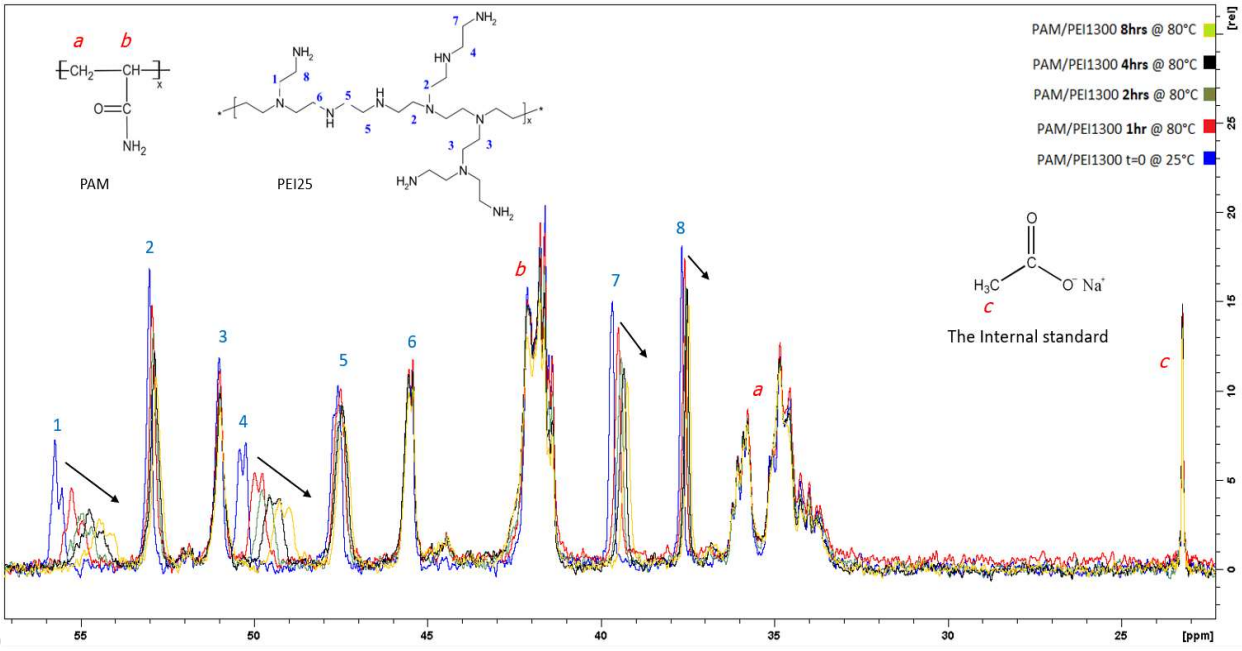

(b)

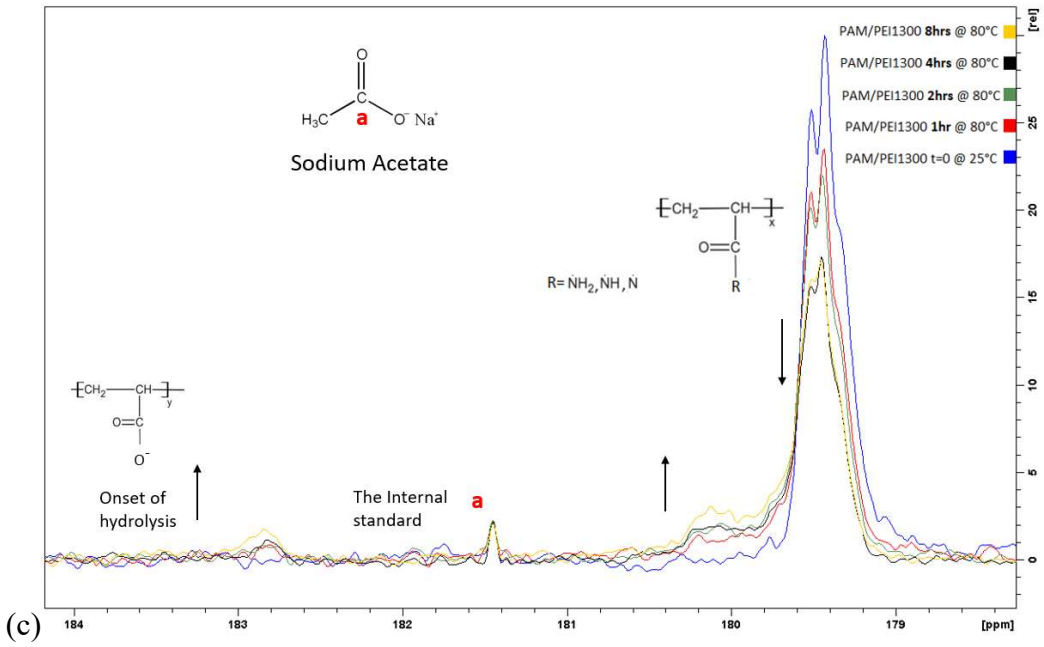

Figure 5.8 : (a) Proton "^{1}H" and (b-c) Carbon "^{13}C" NMR spectra of PAM/PEI1300 mixture cured at 80 °C for different reaction times.

Theoretically, when the primary PEI's amine groups react with the PAM amides groups, they would lose one hydrogen and convert to secondary (NH) amide groups. This would result in shifting the peak number 1 towards peak number 2, the peaks number 4 and 7 toward peak number 5 and the peak number 8 towards peak number 6. However, it was clear that only the peaks 1 and 4 shifted in the right direction towards peak 2 and 5 respectively, while the peaks 7 and 8 shifted in an opposite direction. The latter can be explained by the more pronounced effect of C=O groups on the methylene groups that are close to the primary PEI's amine groups (peak 7-8) compared to the methylene groups that are away from the primary groups (peak 1-4) as highlighted in **Figure 5.9**.

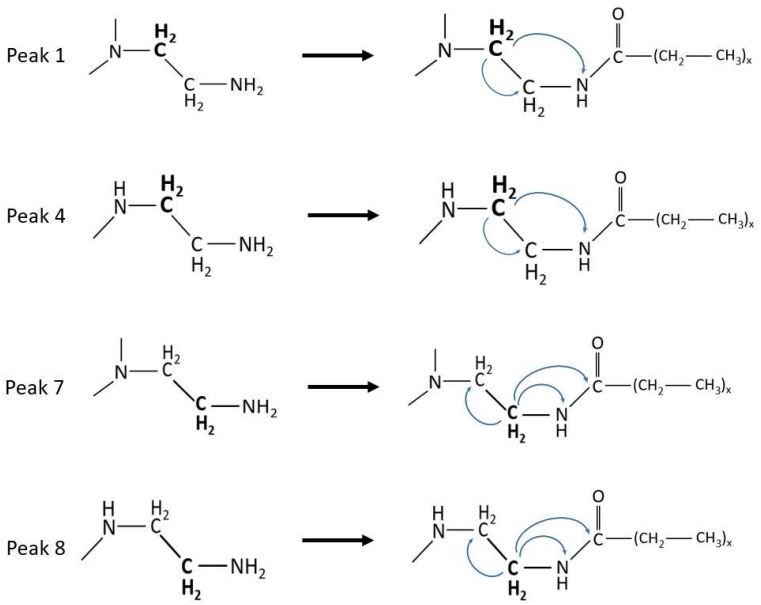

Figure 5.9 : The modified chemical environment of the methylene carbons (CH_2) of PEI1300 in Peaks 1, 4, 7 and 8 when interacting with PAM.

In literature, it was considered that the NMR peak shifts can be linearly correlated with the concentration of reactants inside a mixture [266, 267], as given in equation 5.1:

$$Peak\ shift = A \times C + B \qquad \text{Equation 5.1}$$

Where A, B are constants and C is the concentration of a given reactant.

Consequently, the peak shifts, in this study, were considered to quantify the conversion of the primary amine groups attached to the methylene groups ($CH\text{-}NH_2$) into secondary amide (CO-NH). The shifts of the 1st and 4th peaks alongside the hydrolysis degree (defined in Equation 1.1 in the state of art and section 2.4 in the materials characterization chapter) were then plotted against the curing time as shown in **Figure 5.10**.

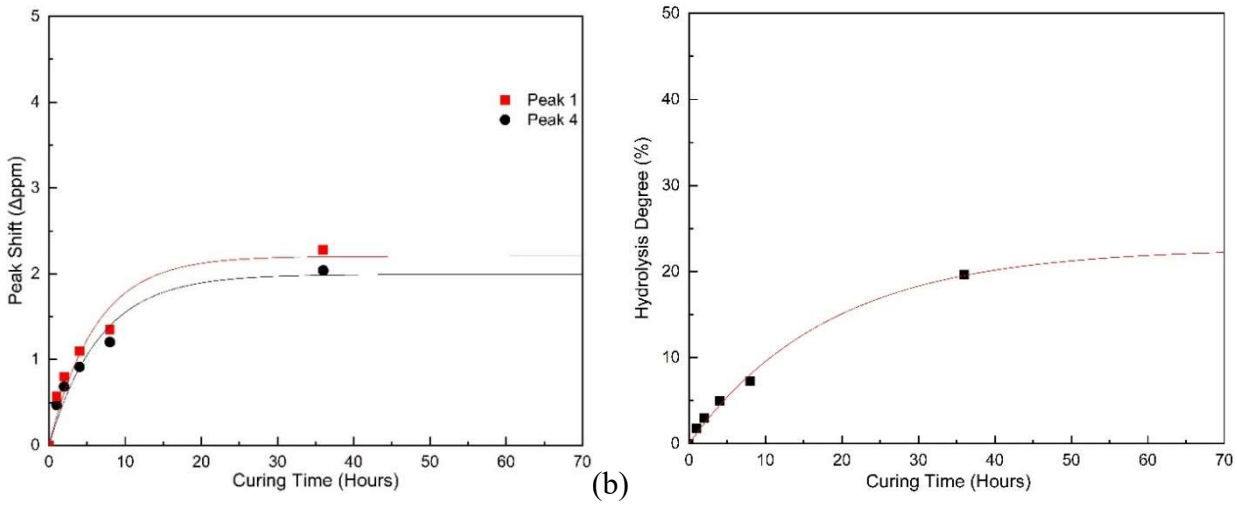

(a) (b)

Figure 5.10 : (a) The shifts of the 1st and 4th peaks and (b) the hydrolysis degree variations as function of curing time at 80 °C.

Studying the chemical reactions kinetics involves quantifying the reaction rates in order to infer about the kinetic mechanisms for chemical conversion of reactants (R) into products (P) [268]. The equations describing the pseudo first-order reactions are defined as follow:

$$[R] = [R]_0 e^{-kt} \qquad \text{Equation 5.2}$$

$$[P] = [R]_0 (1 - e^{-kt}) \qquad \text{Equation 5.3}$$

Where $[R]_0$ is reactant concentration at t=0, [R], and [P] are reactant and product concentrations respectively at a given time t, k is the apparent reaction rate constant.

In order to compare the kinetics of both reactions (transamidation and hydrolysis), the curves were fitted using the exponential relationship given below:

$$y = M(1 - e^{-kt}) \qquad \text{Equation 5.4}$$

Where, y is the peak shift or the hydrolysis degree, t is the curing time and M, k are constants. **Table 5.2** summarizes the obtained fit constants.

Table 5.2 : The fit constants and their respective determination coefficients of the hydrolysis and transamidation reactions kinetics.

	Peak 1	Peak 4	Hydrolysis
A (ppm)	2.2 ± 0.2	2.0 ± 0.2	23 ± 2
B (1/hour)	0.16 ± 0.04	0.15 ± 0.03	0.05 ± 0.01
R^2	0.945	0.957	0.994

Despite it is almost impossible to verify that the total conversion of the primary amine groups to secondary amide groups would result in peaks 1 and 4 shifting to the exact positions of peak 2 and 5 respectively, we are considering in this study that the theoretical shifts separating peak 1 from 2 and peak 4 from 5 are the maximum values indicating the end of the reaction, i.e. the total conversion. The plateau values, reached by the two peak shifts, were identical but slightly lower than the theoretical values separating peak 1 on peak 2 (2.7 ppm) and peak 4 on peak 5 (2.6 ppm), respectively. In fact, the conversion values reached 80% and 76% for peaks 1 and 4 respectively. These results suggest that a total conversion of the primary amine groups to secondary amide groups was not obtained. On the other side, the hydrolysis degree was of 23% ±2%. Moreover, and in terms of reaction rate constants, the reaction constants in respect to the transamidation reaction were three times higher than that of the hydrolysis reaction. These results explain perfectly the obtained final conversion rates and hydrolysis degree.

5.4 Conclusion

The literature knowledge on the crosslinking mechanisms between PHPA and PEI was only limited to observations and comparisons of gelation times and gel strengths with other gel systems. In this chapter, we were interested in understanding the crosslinking mechanisms and the chemical variations on the reactants. NMR techniques including 1D proton "^{1}H" and carbon "^{13}C" and 2D DOSY and NOESY techniques were thus employed. The effect of both the anionicity of PHPA and cationcity of PEI on the gelation time, which are in direct relationship with the prevailing crosslinking mechanism, were considered, for the first time, in this chapter.

As a result, the PHPA's hydrolysis and the PEI's protonation degrees were found to positively affect the gelation time to a certain extent, but beyond it an inverted affect can be observed. The positive effect of the hydrolysis degree of PHPA was related to the enhanced hydrodynamic volume of the polymer under the repulsive forces of the higher number of the negatively charged carboxylate groups. The results also demonstrate the huge dependency of the crosslinking reaction on the initial pH value of the gelant solution. At acidic conditions, an instant viscosity increase was observed visually because of the faster ionic interactions between the anionic polymer and the cationic crosslinker. Consequently, the initial pH value of gelant solutions and its variation inside the reservoir should be considered carefully, especially if the gel is to be applied in acidic environments, such as in carbonate reservoirs.

On the other side, and out from the six possible crosslinking options existing between the PHPA with its two functional groups (amides and carboxylates) and PEI with its three amines groups (primary, secondary and tertiary), we showed that the crosslinking reaction takes place preferentially between the amides groups of the polymer and the primary amines groups of the crosslinker. Interestingly, the crosslinking reaction was found to be also accompanied with a hydrolysis reaction. With the transamidation reaction rate constants calculated in respect to the methylene groups that were away from the primary amine groups, these reaction rate constants were found to be identical regardless of the amine type (secondary or tertiary) attached from the other side of the methylene. They were found also to be three times higher than the hydrolysis reaction.

While, the 1D proton "^{1}H" and carbon "^{13}C" NMR did not allow to accurately follow the reaction kinetics using the high molecular weight reactants, the DOSY and NOESY techniques alongside the 1D proton "^{1}H" and carbon "^{13}C" NMR on low molecular weight reactants were successfully employed. The DOSY experiments showed the presence and formation of a higher molecular weight components even at room temperature when PAM and PEI were mixed for a sufficient time. The NOESY experiments confirmed the spatial proximity between protons of the amide groups of the polymer and the amine groups of the crosslinker independently of the applied temperature revealing a strong interaction between the two. In contrast, the interaction of the carboxylate groups with the amine groups was neglectable.

Conclusion Générale

Conclusion Générale

Le contrôle de conformance représente l'une des méthodes les plus efficaces pour la récupération assistée des hydrocarbures par voie chimique pour les réservoirs fracturés. Il consiste à bloquer et à colmater les fractures conductrices de façon à forcer les fluides d'injection d'entrer, se mettre en contact et déplacer l'huile piégée dans la matrice rocheuse. Cependant, pour le cas des réservoirs fracturés algériens qui se rapprochent de leurs limites économiques, l'étude et l'application du contrôle de conformance n'ont pas été prévues auparavant. C'est dans cette optique, que les travaux de cette thèse ont porté sur l'étude des systèmes de gels retardés à base du polyacrylamide partiellement hydrolysé (PAPH) et de la polyethylenimine (PEI) sous les conditions de salinité et de température réelles, en vue de la mise en œuvre du contrôle de conformance dans les réservoirs fracturés algériens.

Une revue bibliographique nous a permis de faire le point sur les réservoirs fracturés, leurs taux de récupération obtenus après la récupération primaire et secondaire ainsi que les méthodes chimiques de la récupération assistée du pétrole employées. Nous nous sommes intéressés particulièrement aux systèmes organiques de gels réticulés vu les avantages en termes de disponibilité commerciale, caractéristiques contrôlables et stabilité dans les conditions de fond du réservoir. En effet, la littérature rapporte de nombreux systèmes mais les plus promoteurs sont ceux à base du polyacrylamide et de la polyethylenimine. Ainsi les différents polymères, les améliorations et les applications des gels réticulés à base de PEI ont été revus. A notre connaissance, les travaux antérieurs ont révélé que la caractérisation physico-chimique des réactifs ainsi que les paramètres optimaux et pratiques tels que les concentrations des réactifs et les viscosités initiales n'ont pas été pris en considération. Par ailleurs, l'application des systèmes (PAPH/PEI) s'est limitée aux réservoirs à faible température ($T < 60°C$). De plus, les investigations sur ces systèmes en termes de stabilité, morphologie, comportement viscoélastique, mécanismes de réticulations ainsi que l'influence de quelques paramètres de contrôle primordiaux, tels que le pH initial des solutions et le degré d'hydrolyse du polymère n'ont pas fait l'objet d'études auparavant. Pour bien cerner les problèmes posés dans la pratique, il nous a semblé très intéressant d'examiner l'application de ces systèmes (PHPA et PEI) pour les réservoirs fracturés dans une gamme de température plus élevée allant de 70 °C à 90 °C.

La première contribution de ce travail consiste à l'étude de la gélification thermique des mélanges de polyacrylamide partiellement hydrolysé (PAPH) et de la polyethylenimine (PEI), conduite principalement à une température de 80 °C et une salinité de l'eau à 3.4 g/l en quantité totale de matière dissoutes (TDS), en considérant trois caractéristiques principales: le temps de gélification, la force et la stabilité thermique du gel. Les effets, sur le temps de gélification et les modules viscoélastiques, du cisaillement [1 ; 50]s^{-1}, de la concentration du PAPH [3000 ; 10000]ppm et de la

PEI [500 ; 3000]ppm, de la masse moléculaire du PAPH [5.1×10^6 ; 10.2×10^6]g/mol et de la PEI [2×10^4 ; 67×10^4]g/mol, de la température [60 ; 90]°C et de la salinité de l'eau de préparation [0 ; 15]g/l (NaCl ou $CaCl_2$), ont été mis en évidence. Nous avons montré que les concentrations et les masses moléculaires des réactifs ainsi que la température ont un effet proportionnel, contrairement à la salinité de l'eau de préparation et le cisaillement qui ont un effet disproportionnel. Ces effets ont été expliqués essentiellement à travers le changement du volume hydrodynamique du polymère en fonction du paramètre considéré. Les temps de gélifications ont varié globalement entre 0.25 à 12.5 heures alors que la force du gel a atteint le code « I » sur l'échelle des codes de Sydansk comparablement aux autres systèmes de gels à base de la PEI. A titre illustratif, pour une formulation typique de 5000 ppm de PAPH ($Mw_{PAPH}= 5.1\times10^6$ g/mol) et 1000 ppm de PEI ($Mw_{PEI}= 2\times10^4$ g/mol), la viscosité initiale de la solution gélifiante était de 12 cP seulement donnant un temps de gélification de 3 heures et un module élastique (G') de l'ordre de 70 Pa. Sur un intervalle d'observation de 3 mois, le gel de PAPH/PEI a montré une stabilité thermique parfaite, sauf pour des rapports de polymère/agent réticulant supérieur à 0,5 ou des concentrations d'agent réticulant très faibles (500 à 1000 ppm), ou le gel a souffert de la synérèse.

La deuxième contribution de cette thèse consistait à développer un modèle mathématique permettant de prédire le temps de gélification du système PAPH/PEI en fonction de quatre paramètres clés : la salinité de l'eau de préparation, la température, la concentration du polymère et celle de l'agent réticulant. Pour cela, la méthode des surfaces de réponses basée sur la matrice de doehlert a été utilisée. L'ajustement des points expérimentaux a été réalisé par un modèle exponentiel au lieu du modèle polynomiale largement utilisé dans les études antérieures. La signification statistique du modèle et ses termes a été évaluée à travers l'analyse de la variance (ANOVA) et les coefficients de détermination et de détermination ajusté ($R^2 = 0,9867$; $R^2_{adj} = 0,9635$) ainsi que l'écart quadratique moyen (RMSE = 0,1718). La salinité, la concentration du polymère et la température étaient les plus influents sur le temps de gélification par ordre décroissant alors que la concentration de l'agent réticulant n'a pas eu d'effet significatif sur le temps de gélification. Ce dernier a été par la suite optimisé par ce modèle mathématique en considérant les conditions réelles rencontrées sur le champ (température, débit d'injection, profondeur), alors que les mesures expérimentales en laboratoires ont permis de vérifier la validité du modèle proposé.

La troisième contribution de ce travail a porté sur les mécanismes de réticulation. Deux paramètres importants ont été évalués à savoir l'anionicité du polymère et la cationicité de l'agent réticulant. Un effet proportionnel des deux paramètres a été observé jusqu'à une valeur critique, au-delà de laquelle un effet inverse apparaissait : l'anionicité du polymère était en relation directe avec le volume hydrodynamique alors que la cationicité de l'agent réticulant favorisait les interactions ioniques. La technique RMN a révélé que la réticulation du PHPA et de la PEI est effectuée essentiellement à

travers les groupes amides du PHPA et les amines primaires de la PEI. La présence de la PEI n'a pas initié seulement la réticulation mais aussi l'hydrolyse de certains groupes amides du PHPA.

Au terme de cette étude, nous pouvons affirmer que nos trois contributions (L'étude de la gélification thermique en fonction des principaux paramètres physico-chimiques, le développement d'un modèle mathématique permettant la prédiction du temps de gélification, l'étude des mécanismes de réticulation) ainsi que la revue bibliographique rapportée permettent une meilleure compréhension des systèmes gels polymères pour répondre aux besoins pratiques réels des réservoirs fracturés. Les résultats obtenus confortés, dans d'autres cas moins satisfaisants, par rapport à ceux de la littérature ont été discutés et critiqués. Cependant, pour que cette étude soit complète et valorisée, il faudra prévoir le test de ses formulations proposées sur des échantillons de milieux poreux et mettre en œuvre des essais pilotes avant de procéder à l'utilisation à grande échelle.

List of Scientific Contributions

List of Scientific Contributions

Publications

1. **Ghriga, M.A.**, Grassl B., Gareche M. et al. Review of recent advances in polyethylenimine crosslinked polymer gels used for conformance control applications. Polymer Bulletin (2019), 76 (11): 6001-6029. https://doi.org/10.1007/s00289-019-02687-1
2. **Ghriga, M.A.**, Gareche, M. et al. Structure-property relationships of the thermal gelation of partially hydrolyzed polyacrylamide/ polyethylenimine mixtures in a semidilute regime. Polymer Bulletin (2020), 77 (3): 1465-1488. https://doi.org/10.1007/s00289-019-02817-9
3. **Ghriga, M.A.**, Hasanzadeh, M. et al. Thermal gelation of partially hydrolysed polyacrylamide/polyethylenimine mixtures using design of experiments approach. Materials Today Communications (2019), 21: 100686. https://doi.org/10.1016/j.mtcomm.2019.100686
4. **Ghriga, M.A.** et al. Assisted History Matching using Evolution Strategy Algorithm. Petroleum & Coal (2019), 61(1): 64-73.
5. Nait Amar, M., **Ghriga M.A.** et al. Modeling Viscosity of CO_2 at High Temperature and Pressure Conditions. Journal of Natural Gas Science & Engineering (2020), 103271. https://doi:10.1016/j.jngse.2020.103271
6. Nait Amar, M., **Ghriga M.A.**, Ben Seghier M. E. A., Ouaer, H. Prediction of Lattice Constant of A2XY6 Cubic Crystals Using Gene Expression Programming. The Journal of Physical Chemistry B (2020), 124 (28): 6037-6045 https://doi.org/10.1021/acs.jpcb.0c04259
7. Lebouachera, S.E.I., Pessoni L., **Ghriga M.A.** et al. Rheological behaviour and adsorption phenomenon of a polymer-particle composite based on hydrolysed polyacrylamide/ functionalized poly (styrene-acrylic acid) microspheres. Soft Matter (2019), 15: 5449-5454. https://doi.org/10.1039/C9SM00844F
8. Xu, C., Nait Amar M., **Ghriga M. A.**, Evolving support vector regression using Grey Wolf optimization; forecasting the geomechanical properties of rock. Engineering with Computers (2020). https://doi.org/10.1007/s00366-020-01131-7
9. Lebouachera, S.E.I., Chemini R., Khodja M., Grassl B., **Ghriga M.A.**, Drouiche N. Experimental design methodology as a tool to optimize the adsorption of new surfactant on the Algerian rock reservoir: cEOR applications. European Physical Journal Plus (2019), 134: 436. https://doi.org/10.1140/epjp/i2019-12821-9
10. Ouaer, H., Hosseini A. H., Nait Amar M., Ben Seghier M. E. A., **Ghriga M.A.** et al. Rigorous Connectionist Models to Predict Carbon Dioxide Solubility in Various Ionic Liquids. Applied Science (2020), 10 (1): 304; https://doi.org/10.3390/app10010304

Communications

1. Poster at the first edition of the Arab Conference on Mechanical Engineering (**ARCME'17**), December 10-11th, 2017 Biskra, Algeria.
2. Poster at the Eleventh Scientific and Technical days of SONATRACH (**JST11**), April 16-19th, 2018 Oran, Algeria.
3. Poster at ExxonMobil European Research & Development Days 2018 (**ExxonMobil ER&D**), October 1-4th, 2018 Brussels, Belgium.
4. Poster at the eighth International Symposium on Hydrocarbons and Chemistry (**ISHC8**), April 8-10th, 2019 Boumerdes, Algeria.

References

References

1. Ahmed, T., *Reservoir engineering handbook*. 2018: Gulf Professional Publishing.
2. Fernø, M.A., *Enhanced oil recovery in fractured reservoirs.* Introduction to Enhanced Oil Recovery (EOR) Processes and Bioremediation of Oil-Contaminated Sites, 2012. **89**(110): p. 89-110.
3. Tiab, D. and E.C. Donaldson, *Petrophysics: theory and practice of measuring reservoir rock and fluid transport properties*. 2015: Gulf professional publishing.
4. Agarwal, B., et al. *Reservoir characterization of Ekofisk field: a giant, fractured chalk reservoir in the Norwegian North sea—history match*. in *SPE Reservoir Simulation Symposium*. 1999. Society of Petroleum Engineers.
5. Stowell, J., S. Laubach, and J. Olson. *Effect of modem state of stress on flow-controlling fractures: a misleading paradigm in need of revision*. in *DC Rocks 2001, The 38th US Symposium on Rock Mechanics (USRMS)*. 2001. American Rock Mechanics Association.
6. Bratton, T., et al., *The nature of naturally fractured reservoirs.* Oilfield Review, 2006. **18**(2): p. 4-23.
7. Nelson, R., *Geologic analysis of naturally fractured reservoirs*. 2001: Elsevier.
8. van Golf-Racht, T.D., *Fundamentals of fractured reservoir engineering*. Vol. 12. 1982: Elsevier.
9. Saidi, A.M., *Reservoir Engineering of Fractured Reservoirs (fundamental and Practical Aspects)*. 1987: Total.
10. Steinsbø, M., *Enhanced Oil Recovery by CO2 Injection in Fractured Reservoirs. Emphasis on Wettability and Water Saturation.* 2016.
11. Firoozabadi, A., *Recovery mechanisms in fractured reservoirs and field performance.* Journal of Canadian Petroleum Technology, 2000. **39**(11).
12. Haugen, K.B. and A. Firoozabadi. *Measuring Molecular and Thermal Diffusion Coeffi cients in Multicomponent Mixtures by the Beam Deflection Technique*. in *SPE Annual Technical Conference and Exhibition*. 2006. Society of Petroleum Engineers.
13. Lu, H., *Investigation of recovery mechanisms in fractured reservoirs*, 2008, Department of Earth Science and Engineering, Imperial College London.
14. Cardwell Jr, W. and R. Parsons, *Gravity drainage theory.* Transactions of the AIME, 1949. **179**(01): p. 199-215.
15. Hagoort, J., *Oil recovery by gravity drainage.* Society of Petroleum Engineers Journal, 1980. **20**(03): p. 139-150.
16. Haugen, Å., *Fluid flow in fractured carbonates: wettability effects and enhanced oil recovery.* 2010.
17. Qasem, F.H., et al., *Recovery performance of partially fractured reservoirs by capillary imbibition.* Journal of Petroleum Science and Engineering, 2008. **60**(1): p. 39-50.
18. Brattekås, B., *Conformance Control for Enhanced Oil Recovery in Fractured Reservoirs.* PhD Thesis, 2014.
19. Hermansen, H., et al. *Twenty five years of Ekofisk reservoir management*. in *SPE annual technical conference and exhibition*. 1997. Society of Petroleum Engineers.
20. Allan, J. and S.Q. Sun. *Controls on recovery factor in fractured reservoirs: lessons learned from 100 fractured fields*. in *SPE Annual Technical Conference and Exhibition*. 2003. Society of Petroleum Engineers.
21. Bourbiaux, B.J. *Understanding the Oil Recovery Challenge of Water Drive Fractured Reservoirs*. in *International Petroleum Technology Conference*. 2009. International Petroleum Technology Conference.
22. Green, D.W. and G.P. Willhite, *Enhanced oil recovery*. Vol. 6. 1998: Henry L. Doherty Memorial Fund of AIME, Society of Petroleum Engineers ….
23. Sheng, J., *Modern chemical enhanced oil recovery: theory and practice*. 2010: Gulf Professional Publishing.
24. Gupta, R. and K.K. Mohanty. *Wettability alteration of fractured carbonate reservoirs*. in *SPE Symposium on Improved Oil Recovery*. 2008. Society of Petroleum Engineers.
25. Standnes, D.C. and T. Austad, *Wettability alteration in chalk: 2. Mechanism for wettability alteration from oil-wet to water-wet using surfactants.* Journal of Petroleum Science and Engineering, 2000. **28**(3): p. 123-143.
26. Kumar, K., E.K. Dao, and K.K. Mohanty. *Atomic force microscopy study of wettability alteration*. in *SPE International Symposium on Oilfield Chemistry*. 2005. Society of Petroleum Engineers.

27. Al-Hadhrami, H.S. and M.J. Blunt. *Thermally induced wettability alteration to improve oil recovery in fractured reservoirs*. in *SPE/DOE Improved Oil Recovery Symposium*. 2000. Society of Petroleum Engineers.
28. Schembre, J., G.-Q. Tang, and A. Kovscek, *Wettability alteration and oil recovery by water imbibition at elevated temperatures.* Journal of Petroleum Science and Engineering, 2006. **52**(1-4): p. 131-148.
29. Karimi, M., et al., *Wettability alteration and oil recovery by spontaneous imbibition of low salinity brine into carbonates: Impact of Mg2+, SO42− and cationic surfactant.* Journal of Petroleum Science and Engineering, 2016. **147**: p. 560-569.
30. Zhang, P., M.T. Tweheyo, and T. Austad, *Wettability alteration and improved oil recovery by spontaneous imbibition of seawater into chalk: Impact of the potential determining ions Ca2+, Mg2+, and SO42−.* Colloids and Surfaces A: Physicochemical and Engineering Aspects, 2007. **301**(1-3): p. 199-208.
31. Karimaie, H. and O. Torsæter, *Low IFT gas–oil gravity drainage in fractured carbonate porous media.* Journal of Petroleum Science and Engineering, 2010. **70**(1-2): p. 67-73.
32. Sydansk, R.D. and L. Romero-Zeron, *Reservoir conformance improvement*. 2011: Society of Petroleum Engineers Richardson, TX.
33. Crespo, F., et al. *Development of a Polymer Gel System for Improved Sweep Efficiency and Injection Profile Modification of IOR/EOR Treatments*. in *IPTC 2014: International Petroleum Technology Conference*. 2014.
34. Sheng, J., *Enhanced oil recovery field case studies*. 2013: Gulf Professional Publishing.
35. Kovscek, A., et al., *Foam flow through a transparent rough-walled rock fracture.* Journal of Petroleum Science and Engineering, 1995. **13**(2): p. 75-86.
36. Osei-Bonsu, K., N. Shokri, and P. Grassia, *Foam stability in the presence and absence of hydrocarbons: From bubble-to bulk-scale.* Colloids and Surfaces A: Physicochemical and Engineering Aspects, 2015. **481**: p. 514-526.
37. Boud, D.C. and O.C. Holbrook, *Gas drive oil recovery process*, 1958, Google Patents.
38. Bernard, G.G. and L. Holm, *Effect of foam on permeability of porous media to gas.* Society of Petroleum Engineers Journal, 1964. **4**(03): p. 267-274.
39. Talebian, S.H., et al., *Foam assisted CO2-EOR: A review of concept, challenges, and future prospects.* Journal of Petroleum Science and Engineering, 2014. **120**: p. 202-215.
40. Adebanjo, F.O. and O. Olusegun, *Evaluating the application of foam injection as an enhanced oil recovery in unconsolidated sand.* Journal of Petroleum and Gas Engineering, 2015. **6**(2): p. 22-37.
41. Chen, M., Y.C. Yortsos, and W.R. Rossen, *Pore-network study of the mechanisms of foam generation in porous media.* Physical Review E, 2006. **73**(3): p. 036304.
42. Liontas, R., et al., *Neighbor-induced bubble pinch-off: novel mechanisms of in situ foam generation in microfluidic channels.* Soft Matter, 2013. **9**(46): p. 10971-10984.
43. Bertin, H., et al. *Foam flow in heterogeneous porous media: Effect of crossflow*. in *SPE/DOE Improved Oil Recovery Symposium*. 1998. Society of Petroleum Engineers.
44. Kovscek, A., G.-Q. Tang, and C. Radke, *Verification of Roof snap off as a foam-generation mechanism in porous media at steady state.* Colloids and Surfaces A: Physicochemical and Engineering Aspects, 2007. **302**(1-3): p. 251-260.
45. Gauteplass, J., et al., *Pore-level foam generation and flow for mobility control in fractured systems.* Colloids and Surfaces A: Physicochemical and Engineering Aspects, 2015. **468**: p. 184-192.
46. Fernø, M.A., et al., *Experimental study of foam generation, sweep efficiency, and flow in a fracture network.* SPE Journal, 2016. **21**(04): p. 1,140-1,150.
47. Zuta, J. and I. Fjelde, *Transport of CO2-foaming agents during CO2-foam processes in fractured chalk rock.* SPE Reservoir Evaluation & Engineering, 2010. **13**(04): p. 710-719.
48. Haugen, Å., et al., *Miscible and immiscible foam injection for mobility control and EOR in fractured oil-wet carbonate rocks.* Transport in porous media, 2014. **104**(1): p. 109-131.
49. Haugen, Å., et al., *Experimental study of foam flow in fractured oil-wet limestone for enhanced oil recovery.* SPE Reservoir Evaluation & Engineering, 2012. **15**(02): p. 218-228.
50. Han, C., J. Kang, and J. Choe. *Monte Carlo simulation on the effect of fracture characteristics on reduction of permeability by in-situ bacteria growth*. in *SPE Asia Pacific Improved Oil Recovery Conference*. 2001. Society of Petroleum Engineers.

51. Zekri, A.Y. and R. Almehaideb, *Microbial and waterflooding of fractured carbonate rocks: an experimental approach.* Petroleum science and technology, 2003. **21**(1-2): p. 315-331.
52. Soudmand-asli, A., et al., *The in situ microbial enhanced oil recovery in fractured porous media.* Journal of Petroleum Science and Engineering, 2007. **58**(1-2): p. 161-172.
53. Al-Hattali, R.R., et al. *Improving sweep efficiency in fractured carbonate reservoirs by microbial biomass*. in *SPE EOR Conference at Oil and Gas West Asia*. 2012. Society of Petroleum Engineers.
54. Aldhaheri, M.N., et al. *A Roadmap to Successfully Select a Proper Gel Treatment Technology*. in *SPE Kingdom of Saudi Arabia Annual Technical Symposium and Exhibition*. 2016. Society of Petroleum Engineers.
55. Han, M., et al. *State-of-the-art of in-depth fluid diversion technology: enhancing reservoir oil recovery by gel treatments*. in *SPE Saudi Arabia Section Technical Symposium and Exhibition*. 2014. Society of Petroleum Engineers.
56. Al-Assi, A.A., et al., *Formation and propagation of gel aggregates using partially hydrolyzed polyacrylamide and aluminum citrate.* SPE Journal, 2009. **14**(03): p. 450-461.
57. Qiu, Y., et al. *Lessons learned from applying particle gels in mature oilfields*. in *SPE Improved Oil Recovery Symposium*. 2014. Society of Petroleum Engineers.
58. Dupuis, G., et al. *Mechanical and thermal stability of polyacrylamide-based microgel products for EOR*. in *SPE International Symposium on Oilfield Chemistry*. 2013. Society of Petroleum Engineers.
59. Zhao, G., et al., *Experimental study and application of gels formed by nonionic polyacrylamide and phenolic resin for in-depth profile control.* Journal of Petroleum Science and Engineering, 2015. **135**: p. 552-560.
60. Van Auken, M.R., *Process of excluding water from oil and gas wells*, 1922, Google Patents.
61. Burns, L.D., et al. *New generation silicate gel system for casing repairs and water shutoff*. in *SPE Symposium on Improved Oil Recovery*. 2008. Society of Petroleum Engineers.
62. Al-Dhafeeri, A.M., H.A. Nasr-El-Din, and A.M. Al-Harith. *Evaluation of rigless water shutoff treatments to be used in Arab-C carbonate reservoir in Saudi Arabia*. in *CIPC/SPE Gas Technology Symposium 2008 Joint Conference*. 2008. Society of Petroleum Engineers.
63. Wilhelm, S. and M. Kind, *Influence of pH, temperature and sample size on natural and enforced syneresis of precipitated silica.* Polymers, 2015. **7**(12): p. 2504-2521.
64. Hatzignatiou, D.G., et al. *Laboratory testing of environmentally friendly chemicals for water management*. in *SPE Bergen One Day Seminar*. 2015. Society of Petroleum Engineers.
65. Hatzignatiou, D.G. and N.H. Giske, *Sodium silicate gelants for water management in naturally fractured hydrocarbon carbonate formations.* Chemical Engineering Research and Design, 2018. **132**: p. 40-56.
66. Pham, L.T. and D.G. Hatzignatiou, *Rheological evaluation of a sodium silicate gel system for water management in mature, naturally-fractured oilfields.* Journal of Petroleum Science and Engineering, 2016. **138**: p. 218-233.
67. Nasr-El-Din, H. and K. Taylor, *Evaluation of sodium silicate/urea gels used for water shut-off treatments.* Journal of Petroleum Science and Engineering, 2005. **48**(3-4): p. 141-160.
68. Hatzignatiou, D.G., N.H. Giske, and D. Strand, *Water-soluble silicate gelants: Comparison and screening for conformance control in carbonate naturally fractured reservoirs.* Journal of Non-Crystalline Solids, 2018. **479**: p. 72-81.
69. Moradi-Araghi, A., *A review of thermally stable gels for fluid diversion in petroleum production.* Journal of Petroleum Science and Engineering, 2000. **26**(1-4): p. 1-10.
70. Al-Muntasheri, G.A., H.A. Nasr-El-Din, and P.L. Zitha, *Gelation kinetics and performance evaluation of an organically crosslinked gel at high temperature and pressure.* SPE Journal, 2008. **13**(03): p. 337-345.
71. Hardy, M., et al. *The first carbonate field application of a new organically crosslinked water shutoff polymer system*. in *SPE International Symposium on Oilfield Chemistry*. 1999. Society of Petroleum Engineers.
72. Vasquez, J., et al. *Laboratory Evaluation of High-Temperature Conformance olymer Systems*. in *SPE production and operations symposium*. 2003. Society of Petroleum Engineers.
73. Vasquez, J., et al. *Development and evaluation of high-temperature conformance polymer systems*. in *SPE International Symposium on Oilfield Chemistry*. 2005. Society of Petroleum Engineers.

74. Zhu, D., et al., *Evaluation of Terpolymer-Gel Systems Crosslinked by Polyethylenimine for Conformance Improvement in High-Temperature Reservoirs.* SPE Journal, 2019.
75. Bai, Y., et al., *Gelation study on a hydrophobically associating polymer/polyethylenimine gel system for water shut-off treatment.* Energy & Fuels, 2015. **29**(2): p. 447-458.
76. Avery, M., L. Burkholder, and M. Gruenenfelder. *Use of crosslinked xanthan gels in actual profile modification field projects*. in *International Meeting on Petroleum Engineering*. 1986. Society of Petroleum Engineers.
77. Chakravarthy, D., et al. *Mitigating oil bypassed in fractured cores during CO2 flooding using WAG and polymer gel injections*. in *SPE/DOE symposium on improved oil recovery*. 2006. Society of Petroleum Engineers.
78. Nagra, S., et al. *Stability of waterflood diverting agents at elevated temperatures in reservoir brines*. in *SPE Annual Technical Conference and Exhibition*. 1986. Society of Petroleum Engineers.
79. Borling, D., et al., *Pushing out the oil with conformance control.* Oilfield Review, 1994. **6**(2): p. 44-58.
80. Bai, B., J. Zhou, and M. Yin, *A comprehensive review of polyacrylamide polymer gels for conformance control.* Petroleum Exploration and Development, 2015. **42**(4): p. 525-532.
81. Han, M., G. Muller, and A. Zaitoun, *Gel formation of polyacrylamide in the presence of glyoxal for water control application.* Polymer Gels and Networks, 1998. **5**(6): p. 471-480.
82. Morgan, J., P. Smith, and D. Stevens. *Chemical adaptation and development strategies for water and gas shutoff gels*. in *RSC Chemistry in the Oil Industry, 6th International Symposium, Charllotte Mason College Ambleside, UK*. 1997.
83. Reddy, B., et al., *A natural polymer-based cross-linker system for conformance gel systems.* SPE Journal, 2003. **8**(02): p. 99-106.
84. Thomas, A., N. Gaillard, and C. Favero, *Some key features to consider when studying acrylamide-based polymers for chemical enhanced oil recovery.* Oil & Gas Science and Technology–Revue d'IFP Energies nouvelles, 2012. **67**(6): p. 887-902.
85. Vargas-Vasquez, S. and L. Romero-Zerón, *A review of the partly hydrolyzed polyacrylamide Cr (III) acetate polymer gels.* Petroleum science and technology, 2008. **26**(4): p. 481-498.
86. Al-Muntasheri, G.A., *Conformance control with polymer gels: what it takes to be successful.* Arabian Journal for Science and Engineering, 2012. **37**(4): p. 1131-1141.
87. Seright, R.S., A. Campbell, and P. Mozley. *Stability of partially hydrolyzed polyacrylamides at elevated temperatures in the absence of divalent cations*. in *SPE International Symposium on Oilfield Chemistry*. 2009. Society of Petroleum Engineers.
88. Moradi-Araghi, A. and P.H. Doe, *Hydrolysis and precipitation of polyacrylamides in hard brines at elevated temperatures.* SPE Reservoir Engineering, 1987. **2**(02): p. 189-198.
89. Willhite, G.P. and R.S. Seright, *Polymer flooding*. 2010: Society of Petroleum Engineers.
90. Luo, J., Y. Liu, and P. Zhu, *Polymer solution properties and displacement mechanisms.* Enhanced Oil Recovery-Polymer Flooding; Shen, P.-P., Liu, Y.-Z., Liu, H.-R., Eds, 2006: p. 1-72.
91. Abidin, A., T. Puspasari, and W. Nugroho, *Polymers for enhanced oil recovery technology.* Procedia Chemistry, 2012. **4**: p. 11-16.
92. Virgen-Ortíz, J.J., et al., *Polyethylenimine: a very useful ionic polymer in the design of immobilized enzyme biocatalysts.* Journal of Materials Chemistry B, 2017. **5**(36): p. 7461-7490.
93. Kobayashi, S., *Ethylenimine polymers.* Progress in Polymer Science, 1990. **15**(5): p. 751-823.
94. Antonietti, L., et al., *Core− shell-structured highly branched poly (ethylenimine amide) s: synthesis and structure.* Macromolecules, 2005. **38**(14): p. 5914-5920.
95. Reddy, B., et al. *Recent advances in organically crosslinked conformance polymer systems*. in *SPE International Symposium on Oilfield Chemistry*. 2013. Society of Petroleum Engineers.
96. Suh, J., H.-j. Paik, and B.K. Hwang, *Ionization of Poly (ethylenimine) and Poly (allylamine) at Various pH' s.* Bioorganic Chemistry, 1994. **22**(3): p. 318-327.
97. Boussif, O., et al., *A versatile vector for gene and oligonucleotide transfer into cells in culture and in vivo: polyethylenimine.* Proceedings of the National Academy of Sciences, 1995. **92**(16): p. 7297-7301.
98. Seow, W.Y., et al., *Oxidation as a facile strategy to reduce the surface charge and toxicity of polyethyleneimine gene carriers.* Biomacromolecules, 2013. **14**(7): p. 2340-2346.

99. Yurlova, L.Y., A. Kryvoruchko, and B. Yatsik, *Impact of polyethyleneimine on utrafiltration extraction of Cr (VI) from contaminated waters.* Journal of Water Chemistry and Technology, 2014. **36**(3): p. 115-119.
100. Hammache, S., et al., *Comprehensive study of the impact of steam on polyethyleneimine on silica for CO2 capture.* Energy & Fuels, 2013. **27**(11): p. 6899-6905.
101. Janchitraponvej, B. and W. Brown, *Stable conditioning shampoo having a high foam level containing a graft copolymer of polyethylenimine and silicone as a conditioner*, 1998, Google Patents.
102. Allison, J.D. and J.D. Purkaple, *Reducing permeability of highly permeable zones in underground formations*, 1988, Google Patents.
103. Al-Muntasheri, G.A., *Polymer gels for water control: NMR and CT scan studies.* 2008.
104. Al-Muntasheri, G.A., et al. *Investigation of a high temperature organic water shutoff gel: reaction mechanisms*. in *SPE International Improved Oil Recovery Conference in Asia Pacific*. 2005. Society of Petroleum Engineers.
105. Al-Muntasheri, G.A., H.A. Nasr-El-Din, and I.A. Hussein, *A rheological investigation of a high temperature organic gel used for water shut-off treatments.* Journal of Petroleum Science and Engineering, 2007. **59**(1-2): p. 73-83.
106. Al-Muntasheri, G.A., et al., *Viscoelastic properties of a high temperature cross-linked water shut-off polymeric gel.* Journal of Petroleum Science and Engineering, 2007. **55**(1-2): p. 56-66.
107. Deolarte, C., et al., *Successful combination of an organically crosslinked polymer system and a rigid-setting material for conformance control in Mexico.* SPE Production & Operations, 2009. **24**(04): p. 522-529.
108. Liu, J. and R. Seright, *Rheology of gels used for conformance control in fractures.* SPE Journal, 2001. **6**(02): p. 120-125.
109. Zitha, P.L., et al., *Control of flow through porous media using polymer gels.* Journal of applied physics, 2002. **92**(2): p. 1143-1153.
110. El-Karsani, K.S.M., G.A. Al-Muntasheri, and I.A. Hussein, *Polymer systems for water shutoff and profile modification: a review over the last decade.* SPE Journal, 2014. **19**(01): p. 135-149.
111. El-Karsani, K.S., et al., *Gelation kinetics of PAM/PEI system.* Journal of Thermal Analysis and Calorimetry, 2014. **116**(3): p. 1409-1415.
112. El-Karsani, K.S., et al., *Gelation of a water-shutoff gel at high pressure and high temperature: rheological investigation.* SPE Journal, 2015. **20**(05): p. 1,103-1,112.
113. Al-Muntasheri, G.A., P.L.J. Zitha, and H.A. Nasr-El-Din. *Evaluation of a New Cost-Effective Organic Gel System for High Temperature Water Control*. in *International Petroleum Technology Conference*. 2007. International Petroleum Technology Conference.
114. Al-Muntasheri, G.A. and P.L. Zitha. *Gel under dynamic stress in porous media: new insights using computed tomography*. in *SPE Saudi Arabia section technical symposium*. 2009. Society of Petroleum Engineers.
115. Al-Muntasheri, G.A., P.L. Zitha, and H.A. Nasr-El-Din, *A new organic gel system for water control: a computed tomography study.* SPE Journal, 2010. **15**(01): p. 197-207.
116. Mohamed, A.I., et al., *DSC investigation of the gelation kinetics of emulsified PAM/PEI system.* Journal of Thermal Analysis and Calorimetry, 2015. **122**(3): p. 1117-1123.
117. Mohamed, A.I., et al., *Gelation of Emulsified Polyacrylamide/Polyethylenimine under High-Temperature, High-Salinity Conditions: Rheological Investigation.* Industrial & Engineering Chemistry Research, 2018. **57**(36): p. 12278-12287.
118. El Karsani, K.S., et al., *Impact of salts on polyacrylamide hydrolysis and gelation: New insights.* Journal of Applied Polymer Science, 2014. **131**(23).
119. Vasquez, J.E. and L.S. Eoff. *Laboratory development and successful field application of a conformance polymer system for low-, medium-, and high-temperature applications*. in *SPE Latin American and Caribbean Petroleum Engineering Conference*. 2010. Society of Petroleum Engineers.
120. Jia, H., et al., *Research on the gelation performance of low toxic PEI cross-linking PHPAM gel systems as water shutoff agents in low temperature reservoirs.* Industrial & Engineering Chemistry Research, 2010. **49**(20): p. 9618-9624.
121. Zhao, J.-Z., et al., *Influences of fracture aperture on the water-shutoff performance of polyethyleneimine cross-linking partially hydrolyzed polyacrylamide gels in hydraulic fractured reservoirs.* Energy & Fuels, 2011. **25**(6): p. 2616-2624.

122. Jia, H., et al., *New insights into the gelation behavior of polyethyleneimine cross-linking partially hydrolyzed polyacrylamide gels.* Industrial & Engineering Chemistry Research, 2012. **51**(38): p. 12155-12166.
123. Reddy, B., F. Crespo, and L.S. Eoff. *Water shutoff at ultralow temperatures using organically crosslinked polymer gels*. in *SPE Improved Oil Recovery Symposium*. 2012. Society of Petroleum Engineers.
124. Hashmat, M., et al. *Crosslinked polymeric gels as loss circulation materials: An experimental study*. in *SPE Kingdom of Saudi Arabia Annual Technical Symposium and Exhibition*. 2016. Society of Petroleum Engineers.
125. Taylor, K. and H. Nasr-El-Din. *Hydrophobically associating polymers for oil field applications*. in *Canadian International Petroleum Conference*. 2007. Petroleum Society of Canada.
126. Eoff, L., et al. *Development of a hydrophobically modified water-soluble polymer as a selective bullhead system for water-production problems*. in *International Symposium on Oilfield Chemistry*. 2003. Society of Petroleum Engineers.
127. Zhao, H., et al., *Using associated polymer gels to control conformance for high temperature and high salinity reservoirs.* Journal of Canadian Petroleum Technology, 2006. **45**(05).
128. Moradi-Araghi, A., D. Cleveland, and I. Westerman. *Development and evaluation of eor polymers suitable for hostile environments: II-Copolymers of acrylamide and sodium AMPS*. in *SPE International Symposium on Oilfield Chemistry*. 1987. Society of Petroleum Engineers.
129. Al-Muntasheri, G.A., et al. *Water Shut-off with polymer gels in a high temperature horizontal gas well: A success story*. in *SPE Improved Oil Recovery Symposium*. 2010. Society of Petroleum Engineers.
130. Vasquez, J.E., et al. *Organically crosslinked polymer system for water reduction treatments in mexico*. in *International Oil Conference and Exhibition in Mexico*. 2006. Society of Petroleum Engineers.
131. Jayakumar, S. and R.H. Lane. *Delayed Crosslink Polymer Flowing Gel System for Water Shutoff in Conventional and Unconventional Oil and Gas Reservoirs*. in *SPE International Symposium and Exhibition on Formation Damage Control*. 2012. Society of Petroleum Engineers.
132. Jayakumar, S. and R.H. Lane. *Delayed crosslink polymer gel system for water shutoff in conventional and unconventional oil and gas reservoirs*. in *SPE International Symposium on Oilfield Chemistry*. 2013. Society of Petroleum Engineers.
133. Hardy, M.A., *Method and compositions for reducing the permeabilities of subterranean zones*, 2001, Google Patents.
134. Guijiang, W., Yi Xiaoling, Wu Yingying, Feng Xinfang,Ouyang Jian, *A Novel Plugging Agent with Heat Tolerance and Salt Tolerance [J].* Petrochemical Technology, 2012. **2**.
135. van Eijden, J., et al. *Gel-cement, a water shut-off system: qualification in a Syrian field*. in *Abu Dhabi International Conference and Exhibition*. 2004. Society of Petroleum Engineers.
136. Eoff, L.S., et al., *Worldwide field applications of a polymeric gel system for conformance applications.* SPE Production & Operations, 2007. **22**(02): p. 231-235.
137. Peng, B., et al., *Applications of nanotechnology in oil and gas industry: Progress and perspective.* The Canadian Journal of Chemical Engineering, 2018. **96**(1): p. 91-100.
138. Fakoya, M.F. and S.N. Shah, *Emergence of nanotechnology in the oil and gas industry: Emphasis on the application of silica nanoparticles.* Petroleum, 2017. **3**(4): p. 391-405.
139. Cordova, M., et al., *Delayed HPAM gelation via transient sequestration of chromium in polyelectrolyte complex nanoparticles.* Macromolecules, 2008. **41**(12): p. 4398-4404.
140. Quiñones, J.P., H. Peniche, and C. Peniche, *Chitosan based self-assembled nanoparticles in drug delivery.* Polymers, 2018. **10**(3): p. 235.
141. Al-Muntasheri, G., H. Nasr-El-Din, and P. Zitha. *Gelation kinetics of an organically crosslinked gel at high temperature and pressure. SPE Paper 104071*. in *The First International Oil Conference and Exhibition in Mexico, Cancun, Mexico*. 2006.
142. van Eijden, J., et al. *Development and field application of a shallow perforation shut off system for HP-HT oil wells*. in *SPE European Formation Damage Conference*. 2005. Society of Petroleum Engineers.
143. Dalrymple, D., et al. *Shallow Penetration Particle-Gel System for Water and Gas Shut-Off Applications (Russian)*. in *SPE Russian Oil and Gas Technical Conference and Exhibition*. 2008. Society of Petroleum Engineers.

144. Hernandez Tapia, R., et al. *Successful water-shutoff case histories in a naturally fractured carbonate reservoir in offshore Mexico using an organically crosslinked polymer system with a modified tail-in*. in *SPE International Symposium and Exhibiton on Formation Damage Control*. 2010. Society of Petroleum Engineers.
145. Adewunmi, A.A., S. Ismail, and A.S. Sultan, *Investigation into the viscoelastic response at various gelation performance, thermal stability and swelling kinetics of fly ash reinforced polymer gels for water control in mature oilfields.* Asia-Pacific Journal of Chemical Engineering, 2017. **12**(1): p. 13-24.
146. Adewunmi, A.A., S. Ismail, and A.S. Sultan, *Crosslinked Polyacrylamide Composite Hydrogels Impregnated with Fly Ash: Synthesis, Characterization and Their Application as Fractures Sealant for High Water Producing Zones in Oil and Gas Wells.* Journal of Polymers and the Environment, 2018: p. 1-13.
147. Chen, L., et al., *Experimental investigation on the nanosilica-reinforcing polyacrylamide/polyethylenimine hydrogel for water shutoff treatment.* Energy & Fuels, 2018. **32**(6): p. 6650-6656.
148. Bach, T., et al. *Polymer sealant for unwanted gas in openhole gravel-pack completion*. in *SPE European Formation Damage Conference*. 2001. Society of Petroleum Engineers.
149. Mebratu, A., B. Nerland, and T. Kleppan. *Annular barrier re-establishment using a long-life, high-strength polymer gel system*. in *SPE International Symposium and Exhibition on Formation Damage Control*. 2004. Society of Petroleum Engineers.
150. Alqam, M., H. Nasr-El-Din, and J. Lynn. *Treatment of super-K zones using gelling polymers*. in *SPE International Symposium on Oilfield Chemistry*. 2001. Society of Petroleum Engineers.
151. Okasha, T., H. Nasr-El-Din, and W. Al-Khudair. *Abatement of water production from upper Permian gas wells in Saudi Arabia using a new polymer treatment*. in *SPE Middle East Oil Show*. 2001. Society of Petroleum Engineers.
152. Uddin, S., et al. *Lessons Learned from the First Openhole Horizontal Well Water Shutoff Job Using Two New Polymer Systems-A Case History from Wafra Ratawi Field, Kuwait*. in *Middle East Oil Show*. 2003. Society of Petroleum Engineers.
153. Beltagy, A.E., et al. *Offshore Coiled Tubing Interventions Maximized the Value of Watered Out Mature Fields Using Selective Water Shutoff Treatments With an Organic Crosslinked Polymer in a High Temperature Sour Well*. in *SPE/IATMI Asia Pacific Oil & Gas Conference and Exhibition*. 2015. Society of Petroleum Engineers.
154. Mercado, M., et al. *Successful High-Temperature, Water-Control Case Histories in Highly Naturally Fractured Carbonate Reservoirs*. in *SPE Annual Technical Conference and Exhibition*. 2010. Society of Petroleum Engineers.
155. Ortiz Polo, R.P., et al. *Field applications of low molecular-weight polymer activated with an organic crosslinker for water conformance in south mexico*. in *SPE Annual Technical Conference and Exhibition*. 2004. Society of Petroleum Engineers.
156. Civan, F., et al., *Laboratory and theoretical evaluation of gelation time data for water-based polymer systems for water control.* Petroleum Science and Technology, 2007. **25**(3): p. 353-371.
157. Simjoo, M., et al., *Polyacrylamide gel polymer as water shut-off system: preparation and investigation of physical and chemical properties in one of the Iranian oil reservoirs conditions.* Iranian Journal of Chemistry and Chemical Engineering (IJCCE), 2007. **26**(4): p. 99-108.
158. Sydansk, R.D., *A newly developed chromium (III) gel technology.* SPE Reservoir Engineering, 1990. **5**(03): p. 346-352.
159. Sydansk, R.D. and P.A. Argabright, *Conformance improvement in a subterranean hydrocarbon-bearing formation using a polymer gel*, 1987, Google Patents.
160. Stavland, A., et al. *In-depth water diversion using sodium silicate–Preparation for single well field pilot on Snorre*. in *IOR 2011-16th European Symposium on Improved Oil Recovery*. 2011.
161. Romero-Zeron, L.B., F.M. Hum, and A. Kantzas, *Characterization of crosslinked gel kinetics and gel strength by use of NMR.* SPE Reservoir Evaluation & Engineering, 2008. **11**(03): p. 439-453.
162. Li, D.C., Z. ZHANG Gui Cai, and F. Lin, *Studies on Influencing Factors for Formation of Aqueous Polyacrylamide/Formaldehyde Gel [J].* Oilfield Chemistry, 2001. **1**: p. 008.
163. You, Q., et al., *The Effect of Hydrogen Sulfide Concentration on Gel as Water Shutoff Agent.* Oil & Gas Science and Technology–Revue d'IFP Energies nouvelles, 2013. **68**(2): p. 355-361.

164. Liu, Y., et al., *New insights into the hydroquinone (HQ)–hexamethylenetetramine (HMTA) gel system for water shut-off treatment in high temperature reservoirs.* Journal of industrial and engineering chemistry, 2016. **35**: p. 20-28.
165. Wang, J., A.M. AlSofi, and A.M. AlBoqmi. *Development and evaluation of gel-based conformance control for a high salinity and high temperature carbonate*. in *SPE EOR Conference at Oil and Gas West Asia*. 2016. Society of Petroleum Engineers.
166. Al-Anazi, M., et al. *Laboratory evaluation of organic water shut-off gelling system for carbonate formations*. in *SPE European Formation Damage Conference*. 2011. Society of Petroleum Engineers.
167. Mokhtari, M. and M.E. Ozbayoglu. *Laboratory investigation on gelation behavior of xanthan crosslinked with borate intended to combat lost circulation*. in *SPE Production and Operations Conference and Exhibition*. 2010. Society of Petroleum Engineers.
168. McCool, C.S., X. Li, and G.P. Wilhite, *Flow of a polyacrylamide/chromium acetate system in a long conduit.* SPE Journal, 2009. **14**(01): p. 54-66.
169. Haiyang, Y., et al., *Dynamic gelation of HPAM/Cr (III) under shear in an agitator and porous media.* Oil & Gas Science and Technology–Revue d'IFP Energies nouvelles, 2015. **70**(6): p. 941-949.
170. Riihimaki, T.A. and S. Middleman, *The effect of shear rate on the kinetics of gelation.* Macromolecules, 1974. **7**(5): p. 675-680.
171. Ono, K. and K. Murakami, *Kinetics of gelation of aqueous poly (methacrylic acid) solutions under shear stress.* Journal of Polymer Science: Polymer Letters Edition, 1977. **15**(8): p. 507-511.
172. Winter, H.H., *Can the gel point of a cross-linking polymer be detected by the G'–G "crossover?* Polymer Engineering & Science, 1987. **27**(22): p. 1698-1702.
173. Grattoni, C.A., et al., *Rheology and permeability of crosslinked polyacrylamide gel.* Journal of colloid and interface science, 2001. **240**(2): p. 601-607.
174. Niţă, L.E., et al., *In situ monitoring the sol–gel transition for polyacrylamide gel.* Rheologica acta, 2007. **46**(5): p. 595-600.
175. Tung, C.Y.M. and P.J. Dynes, *Relationship between viscoelastic properties and gelation in thermosetting systems.* Journal of applied polymer science, 1982. **27**(2): p. 569-574.
176. Winter, H.H. and M. Mours, *Rheology of polymers near liquid-solid transitions*, in *Neutron spin echo spectroscopy viscoelasticity rheology*. 1997, Springer. p. 165-234.
177. Kakadjian, S., O. Rauseo, and F. Mejias. *Dynamic rheology as a method for quantify gel strength of water shutoff systems*. in *SPE International Symposium on Oilfield Chemistry*. 1999. Society of Petroleum Engineers.
178. te Nijenhuis, K., A. Mensert, and P.L. Zitha, *Viscoelastic behaviour of partly hydrolysed polyacrylamide/chromium (III) gels.* Rheologica acta, 2003. **42**(1-2): p. 132-141.
179. Bryan, J., A. Kantzas, and C. Bellehumeur. *Viscosity predictions for crude oils and crude oil emulsions using low field NMR*. in *SPE Annual Technical Conference and Exhibition*. 2002. Society of Petroleum Engineers.
180. Thomas, L., *Interpreting unexpected events and transitions in DSC results.* Technical publication TA-039, TA Instruments, 2010.
181. Michael, F.M., et al., *Enhanced Polyacrylamide Polymer Gels Using Zirconium Hydroxide Nanoparticles for Water Shutoff at High Temperatures: Thermal and Rheological Investigations.* Industrial & Engineering Chemistry Research, 2018. **57**(48): p. 16347-16357.
182. Zhao, G., et al., *Study on formation of gels formed by polymer and zirconium acetate.* Journal of sol-gel science and technology, 2013. **65**(3): p. 392-398.
183. Zhu, D., et al., *Effect of different phenolic compounds on performance of organically cross-Linked terpolymer gel systems at extremely high temperatures.* Energy & Fuels, 2017. **31**(8): p. 8120-8130.
184. Zhu, D., et al., *Terpolymer gel system formed by resorcinol–hexamethylenetetramine for water management in extremely high-temperature reservoirs.* Energy & Fuels, 2017. **31**(2): p. 1519-1528.
185. Jia, H. and H. Chen, *Using DSC technique to investigate the non-isothermal gelation kinetics of the multi-crosslinked Chromium acetate (Cr3+)-Polyethyleneimine (PEI)-Polymer gel sealant.* Journal of Petroleum Science and Engineering, 2018. **165**: p. 105-113.
186. Singhal, R., S. Sachan, and J. Rai, *Study of cure kinetics of polyacrylamide hydrogels by differential scanning calorimetry.* 2002.
187. Vera-Graziano, R., et al. *Characterization of acrylic dental polymers*. in *Macromolecular Symposia*. 1999. Wiley Online Library.

188. Masuelli, M.A., *Mark-houwink parameters for aqueous-soluble polymers and biopolymers at various temperatures.* 2014.
189. Sorbie, K., *Polymer-Improved Oil Recovery, 115 Glasgow.* Scotland: Blackie & Son, 1991: p. 126-163.
190. Milas, M., M. Rinaudo, and B. Tinland, *The viscosity dependence on concentration, molecular weight and shear rate of xanthan solutions.* Polymer Bulletin, 1985. **14**(2): p. 157-164.
191. Rodriguez, L., et al. *Monitoring Thermal and Mechanical Stability of Enhanced Oil Recovery (EOR) Acrylamide Based Polymers (PAM) Through Intrinsic Viscosity (IV) Determination Using a New Capillary Rheology Technique*. in *SPE EOR Conference at Oil and Gas West Asia*. 2016. Society of Petroleum Engineers.
192. McCarthy, K., C. Burkhardt, and D. Parazak, *Mark–Houwink–Sakurada constants and dilute solution behavior of heterodisperse poly (acrylamide-co-sodium acrylate) in 0.5 M and 1M NaCl.* Journal of applied polymer science, 1987. **33**(5): p. 1699-1714.
193. von Harpe, A., et al., *Characterization of commercially available and synthesized polyethylenimines for gene delivery.* Journal of Controlled Release, 2000. **69**(2): p. 309-322.
194. Wu, W.B., et al. *Preparation and Application of Hydrophobically Associating Cationic Polyacrylamide*. in *Advanced Materials Research*. 2011. Trans Tech Publ.
195. Rodriguez, L., et al., *A New Thermally Stable Synthetic Polymer for Harsh Conditions of Middle East Reservoirs: Part II. NMR and Size Exclusion Chromatography to Assess Chemical and Structural Changes During Thermal Stability Tests*, in *SPE Improved Oil Recovery Conference*2018, Society of Petroleum Engineers: Tulsa, Oklahoma, USA. p. 15.
196. Feng, Y., et al., *Hydrophobically associating polyacrylamides and their partially hydrolyzed derivatives prepared by post-modification. 1. Synthesis and characterization.* Polymer, 2002. **43**(7): p. 2055-2064.
197. Leung, W., D. Axelson, and J. Van Dyke, *Thermal degradation of polyacrylamide and poly (acrylamide-co-acrylate).* Journal of Polymer Science Part A: Polymer Chemistry, 1987. **25**(7): p. 1825-1846.
198. Guerrero, S.J., P. Boldarino, and J.A. Zurimendi, *Characterization of polyacrylamides used in enhanced oil recovery.* Journal of applied polymer science, 1985. **30**(3): p. 955-967.
199. Nedel'ko, V., et al., *The thermal degradation of branched polyethylenimine.* Polymer Science USSR, 1975. **17**(7): p. 1697-1703.
200. Gomes, M.P. and M. Costa, *Determination of the critical concentration of partially hydrolyzed polyacrylamide by potentiometry in an acidic medium.* Journal of applied polymer science, 2013. **128**(3): p. 2167-2172.
201. Rodd, A., D. Dunstan, and D. Boger, *Characterisation of xanthan gum solutions using dynamic light scattering and rheology.* Carbohydrate polymers, 2000. **42**(2): p. 159-174.
202. Cuvelier, G. and B. Launay, *Concentration regimes in xanthan gum solutions deduced from flow and viscoelastic properties.* Carbohydrate polymers, 1986. **6**(5): p. 321-333.
203. Benchabane, A. and K. Bekkour, *Rheological properties of carboxymethyl cellulose (CMC) solutions.* Colloid and Polymer Science, 2008. **286**(10): p. 1173.
204. Al Hashmi, A., et al., *Rheology and mechanical degradation of high-molecular-weight partially hydrolyzed polyacrylamide during flow through capillaries.* Journal of Petroleum Science and Engineering, 2013. **105**: p. 100-106.
205. Lopes, L. and B. Silveira, *Rheological Evaluation of HPAM fluids for EOR Applications.* 2014.
206. Silveira, B., L. Lopes, and R. Moreno, *Rheological approach of HPAM solutions under harsh conditions for EOR applications.* Int. J. Eng. Technol. IJET-IJENS, 2016. **16**(03).
207. Desbrieres, J., *Viscosity of semiflexible chitosan solutions: influence of concentration, temperature, and role of intermolecular interactions.* Biomacromolecules, 2002. **3**(2): p. 342-349.
208. Jouenne, S., et al. *Universal Viscosifying Behavior of Acrylamide-based Polymers Used in EOR-Application for QA/QC, Viscosity Predictions and Field Characterization*. in *IOR 2019–20th European Symposium on Improved Oil Recovery*. 2019.
209. Meeuw, H., V. Wisniewski, and B. Fiedler, *Frequency or Amplitude?—Rheo-Electrical Characterization of Carbon Nanoparticle Filled Epoxy Systems.* Polymers, 2018. **10**(9): p. 999.
210. Boudjema, F., B. Khelidj, and M. Lounis. *Dynamical properties of the brain tissue under oscillatory shear stresses at large strain range*. in *Journal of Physics: Conference Series*. 2017. IOP Publishing.
211. Eckmann, B., et al. *Measuring the rheological properties of bituminous binders final results from the round robin test of the BNPÉ/P04/GE1 Working Group (France)*. 2012.

212. Zandraa, O., et al., *Properties of guar gum-Dead sea salt (GG-DSS) medicated gel.* International Journal of Pharmacy and Pharmaceutical Sciences, 2015.
213. Risica, D., et al., *Rheological properties of guar and its methyl, hydroxypropyl and hydroxypropyl-methyl derivatives in semidilute and concentrated aqueous solutions.* Polymer, 2010. **51**(9): p. 1972-1982.
214. Jia, H., et al., *Evaluation of polyacrylamide gels with accelerator ammonium salts for water shutoff in ultralow temperature reservoirs: Gelation performance and application recommendations.* Petroleum, 2016. **2**(1): p. 90-97.
215. Lockhart, T.P. and P. Albonico, *New chemistry for the placement of chromium (III)/polymer gels in high-temperature reservoirs.* SPE Production and Facilities (Society of Petroleum Engineers);(United States), 1994. **9**(4).
216. Vossoughi, S., *Profile modification using in situ gelation technology—a review.* Journal of Petroleum Science and Engineering, 2000. **26**(1-4): p. 199-209.
217. Broseta, D., et al., *Shear effects on polyacrylamide/chromium (III) acetate gelation.* SPE Reservoir Evaluation & Engineering, 2000. **3**(03): p. 204-208.
218. Koohi, A.D., et al., *Rheological characteristics of sulphonated polyacrylamide/chromium triacetate hydrogels designed for water shut-off.* Iran. Polym. J, 2010. **19**(10): p. 757-770.
219. Calvet, D., J.Y. Wong, and S. Giasson, *Rheological monitoring of polyacrylamide gelation: Importance of cross-link density and temperature.* Macromolecules, 2004. **37**(20): p. 7762-7771.
220. Hatzignatiou, D.G., N.H. Giske, and A. Stavland, *Polymers and Polymer-Based Gelants for Improved Oil Recovery and Water Control Applications in Naturally Fractured Chalk Formations*, in *SPE Bergen One Day Seminar*2016, Society of Petroleum Engineers: Grieghallen, Bergen, Norway. p. 23.
221. Park, I.H. and E.-J. Choi, *Characterization of branched polyethyleneimine by laser light scattering and viscometry.* Polymer, 1996. **37**(2): p. 313-319.
222. Broseta, D., et al. *Rheological screening of low-molecular-weight polyacrylamide/chromium (III) acetate water shutoff gels*. in *SPE/DOE improved oil recovery symposium*. 2000. Society of Petroleum Engineers.
223. Lenji, M.A., et al., *Numerical modeling and experimental investigation of inorganic and organic crosslinkers effects on polymer gel properties.* Journal of Petroleum Science and Engineering, 2018. **160**: p. 160-169.
224. Zhao, G., et al., *The use of environmental scanning electron microscopy for imaging the microstructure of gels for profile control and water shutoff treatments.* Journal of applied polymer science, 2014. **131**(4).
225. Box, G.E. and K.B. Wilson, *On the experimental attainment of optimum conditions.* Journal of the Royal Statistical Society: Series B (Methodological), 1951. **13**(1): p. 1-38.
226. Montgomery, D.C., *Design and analysis of experiments*. 2017: John wiley & sons.
227. Myers, R.H., D.C. Montgomery, and C.M. Anderson-Cook, *Response surface methodology: process and product optimization using designed experiments*. 2016: John Wiley & Sons.
228. Bezerra, M.A., et al., *Response surface methodology (RSM) as a tool for optimization in analytical chemistry.* Talanta, 2008. **76**(5): p. 965-977.
229. Carley, K.M., N.Y. Kamneva, and J. Reminga, *Response surface methodology*, 2004, Carnegie-Mellon Univ Pittsburgh Pa School of Computer Science.
230. Baş, D. and I.H. Boyacı, *Modeling and optimization I: Usability of response surface methodology.* Journal of food engineering, 2007. **78**(3): p. 836-845.
231. Cavazzuti, M., *Optimization methods: from theory to design scientific and technological aspects in mechanics*. 2012: Springer Science & Business Media.
232. Taavitsainen, V.-M.T., *Experimental optimization and response surfaces.* Chemometrics in Practical Applications, 2012: p. 91-138.
233. Dejaegher, B. and Y. Vander Heyden, *Experimental designs and their recent advances in set-up, data interpretation, and analytical applications.* Journal of pharmaceutical and biomedical analysis, 2011. **56**(2): p. 141-158.
234. Croarkin, C., et al., *NIST/SEMATECH e-handbook of statistical methods.* NIST/SEMATECH, July. Available online: http://www. itl. nist. gov/div898/handbook, 2006.
235. Salehi, M.B., et al., *Study of salinity and pH effects on gelation time of a polymer gel using central composite design method.* Journal of Macromolecular Science, Part B, 2012. **51**(3): p. 438-451.

236. Box, G. and D. Behnken, *Simplex-sum designs: a class of second order rotatable designs derivable from those of first order.* The Annals of Mathematical Statistics, 1960. **31**(4): p. 838-864.
237. Doehlert, D.H., *Uniform shell designs.* Applied statistics, 1970: p. 231-239.
238. Ferreira, S.L., et al., *Doehlert matrix: a chemometric tool for analytical chemistry.* Talanta, 2004. **63**(4): p. 1061-1067.
239. Sautour, M., et al., *Application of Doehlert design to determine the combined effects of temperature, water activity and pH on conidial germination of Penicillium chrysogenum.* Journal of applied microbiology, 2001. **91**(5): p. 900-906.
240. Bosque-Sendra, J.M., et al. *Optimization of analytical methods by using Doehlert's designs*. in *Analytical Proceedings including Analytical Communications*. 1995. Royal Society of Chemistry.
241. Moghadam, A.M., et al., *Effect of nanoclay along with other effective parameters on gelation time of hydro polymer gels.* Journal of Macromolecular Science, Part B, 2012. **51**(10): p. 2015-2025.
242. Baghban Salehi, M., et al., *Effect of Process Variable on the Gelation Time of Sulfonated Polyacrylamide Nanocomposite Hydrogel.* Journal of Dispersion Science and Technology, 2014. **35**(5): p. 663-671.
243. Singh, R. and V. Mahto, *Study of the polymer concentration and polymer/crosslinker ratio effect on gelation time of a novel grafted polymer gel for water shutoff using a central composite design method.* Polymers for Advanced Technologies, 2016. **27**(2): p. 204-212.
244. ABEDI, L.M., et al., *Gelation time of hexamethylenetetramine polymer gels used in water shutoff treatment.* 2012.
245. Amir, Z., I. Mohd Saaid, and B. Mohamed Jan, *An Optimization Study of Polyacrylamide-Polyethylenimine-Based Polymer Gel for High Temperature Reservoir Conformance Control.* International Journal of Polymer Science, 2018. **2018**.
246. Vieira, S. and R. Hoffmann, *Estatística experimental*. 1989: Atlas.
247. Nikrooz, B. and M. Zandrahimi, *Optimization of process variables and corrosion properties of a multi layer silica sol gel coating on AZ91D using the Box–Behnken design.* Journal of sol-gel science and technology, 2011. **59**(3): p. 640.
248. Deghmoum, A., D. Tiab, and A. Mazouzi, *Relative permeability in dual porosity porous media.* Journal of Canadian Petroleum Technology, 2001. **40**(12).
249. Derringer, G. and R. Suich, *Simultaneous optimization of several response variables.* Journal of quality technology, 1980. **12**(4): p. 214-219.
250. Truong, N., et al., *Microstructure of acrylamide-acrylic acid copolymers: 1. As obtained by alkaline hydrolysis.* Polymer, 1986. **27**(3): p. 459-466.
251. Kulicke, W.-M. and H.-H. Hörl, *Preparation and characterization of a series of poly (acrylamide-co-acrylates), with a copolymer composition between 0–96.3 mol-% acrylate units with the same degree and distribution of polymerization.* Colloid and Polymer Science, 1985. **263**(7): p. 530-540.
252. Rabiee, A., M.E. Zeynali, and H. Baharvand, *Synthesis of high molecular weight partially hydrolyzed polyacrylamide and investigation on its properties.* Iranian Polymer Journal, 2005. **14**(7): p. 603.
253. Wagner, G.E., et al., *Monitoring fast chemical processes by reaction-interrupted excitation transfer (ExTra) NMR spectroscopy.* Chemical Communications, 2019. **55**(83): p. 12575-12578.
254. Kantorowski, E.J., et al., *NMR-Based Kinetic Experiments for Undergraduate Chemistry Laboratories*, in *NMR Spectroscopy in the Undergraduate Curriculum*. 2013, ACS Publications. p. 211-228.
255. Zell, M., et al. *Monitoring Chemical Reactions in Real Time with NMR Spectroscopy*. in *Small Molecule NMR Conference, Portland, OR, September*. 2010.
256. Baït, N., et al., *Hydrogel nanocomposites as pressure-sensitive adhesives for skin-contact applications.* Soft Matter, 2011. **7**(5): p. 2025-2032.
257. Cherifi, N., et al., *Diffusion-ordered spectroscopy NMR DOSY: an all-in-one tool to simultaneously follow side reactions, livingness and molar masses of polymethylmethacrylate by nitroxide mediated polymerization.* Polymer Chemistry, 2016. **7**(33): p. 5249-5257.
258. Kavakka, J.S., I. Kilpeläinen, and S. Heikkinen, *General chromatographic NMR method in liquid state for synthetic chemistry: polyvinylpyrrolidone assisted DOSY experiments.* Organic letters, 2009. **11**(6): p. 1349-1352.
259. Morris, G.A., *Diffusion-ordered spectroscopy.* eMagRes, 2007.
260. Huo, R., et al., *Assessment of techniques for DOSY NMR data processing.* Analytica chimica acta, 2003. **490**(1-2): p. 231-251.

261. Li, W., et al., *Application of 1H DOSY for facile measurement of polymer molecular weights.* Macromolecules, 2012. **45**(24): p. 9595-9603.
262. Swift, T., et al., *The pH-responsive behaviour of poly (acrylic acid) in aqueous solution is dependent on molar mass.* Soft Matter, 2016. **12**(9): p. 2542-2549.
263. Pearson, D., et al., *Viscosity and self-diffusion coefficient of linear polyethylene.* Macromolecules, 1987. **20**(5): p. 1133-1141.
264. Cross, J., *Anionic surfactants: analytical chemistry*. Vol. 73. 1998: CRC Press.
265. Cheng, Y., et al., *Generation-dependent encapsulation/electrostatic attachment of phenobarbital molecules by poly (amidoamine) dendrimers: evidence from 2D-NOESY investigations.* European journal of medicinal chemistry, 2009. **44**(5): p. 2219-2223.
266. Khoukh, A., *Apport de la RMN diffusionnelle à l'étude des systèmes polymères: extrémités de chaîne, contrôle des architectures et auto-assemblage*, 2014, Pau.
267. Abraham, R.J. and M. Mobli, *Modelling 1H NMR spectra of organic compounds: theory, applications and NMR prediction software*. 2008: John Wiley & Sons.
268. Burgess, R.R. and M.P. Deutscher, *Guide to protein purification*. 2009: Academic Press.